Rare Earths

Rare Earths

Science, Technology, Production and Use

Jacques Lucas
Emeritus Professor
University of Rennes, France

Pierre Lucas
Professor
Materials Science and Engineering Department,
University of Arizona

Thierry Le Mercier
Head of the Solvay research group dedicated to
Advanced Inorganic Materials
Solvay Research & Innovation, Auvervilliers Research Center
52, rue de la Haie Coq, 93308 Auvervillers Cedex

Alain Rollat
Technology Development Manager
Solvay Rare Earth Systems
La Rochelle, France

William Davenport
Professor Emeritus
University of Arizona
Tucson, Arizona

ELSEVIER
AMSTERDAM • BOSTON • HEIDELBERG • LONDON • NEW YORK • OXFORD
PARIS • SAN DIEGO • SAN FRANCISCO • SINGAPORE • SYDNEY • TOKYO

Elsevier
Radarweg 29, PO Box 211, 1000 AE Amsterdam, Netherlands
The Boulevard, Langford Lane, Kidlington, Oxford OX5 1GB, UK
225 Wyman Street, Waltham, MA 02451, USA

Copyright © 2015 Elsevier B.V. All rights reserved.

No part of this publication may be reproduced or transmitted in any form or by any means, electronic or mechanical, including photocopying, recording, or any information storage and retrieval system, without permission in writing from the publisher. Details on how to seek permission, further information about the Publisher's permissions policies and our arrangements with organizations such as the Copyright Clearance Center and the Copyright Licensing Agency, can be found at our website: www.elsevier.com/permissions.

This book and the individual contributions contained in it are protected under copyright by the Publisher (other than as may be noted herein).

Notice
Knowledge and best practice in this field are constantly changing. As new research and experience broaden our understanding, changes in research methods, professional practices, or medical treatment may become necessary.

Practitioners and researchers must always rely on their own experience and knowledge in evaluating and using any information, methods, compounds, or experiments described herein. In using such information or methods they should be mindful of their own safety and the safety of others, including parties for whom they have a professional responsibility.

To the fullest extent of the law, neither the Publisher nor the authors, contributors, or editors, assume any liability for any injury and/or damage to persons or property as a matter of products liability, negligence or otherwise, or from any use or operation of any methods, products, instructions, or ideas contained in the material herein.

ISBN: 978-0-444-62735-3

British Library Cataloguing in Publication Data
A catalogue record for this book is available from the British Library

Library of Congress Cataloging-in-Publication Data
A catalog record for this book is available from the Library of Congress

For information on all Elsevier publications
visit our web site at store.elsevier.com

ELSEVIER
Book Aid
International
Working together
to grow libraries in
developing countries
www.elsevier.com • www.bookaid.org

Contributors

Alain Rollat
Technology Development Manager, Solvay Rare Earth Systems, La Rochelle, France
Chapters 2, 4 & 5

Jacques Lucas
Emeritus Professor, University of Rennes, France
Chapters 8, 12, 13, 14 & 17

Pierre Lucas
Professor, Materials Science and Engineering Department, University of Arizona
Chapters 8, 12, 13, 14 & 17

Thierry Le Mercier
Head of the Solvay research group dedicated to Advanced Inorganic Materials, Auvervilliers, France
Chapters 8, 12, 15 & 16

William Davenport
Professor Emeritus, University of Arizona, Tucson, Arizona
Chapters 1, 2, 3, 6, 7, 9, 10, 11, 18 & 19

Preface

This book arose from a lecture, *Rare Earths*, presented to University of Arizona materials science students by Professor Jacques Lucas, our lead author. The lecture was also attended by Professors Pierre Lucas and Bill Davenport, coauthors.

Jacques, Pierre, and Bill quickly decided to expand the lecture into a book, a decision soon approved by Elsevier BV, Amsterdam. These authors were then joined by Alain Rollat and Thierry Le Mercier, rare earth experts working respectively for Solvay Rare Earth Systems (La Rochelle, France) and Solvay Research and Innovation (Aubervilliers, France).

The objective of our book is to describe rare earth occurrence, extraction, atomic structure, technology, applications, use, and recycle at the start of 2014. To achieve this objective we have visited many industrial rare earth facilities, mine-to-product. Our visits included:

Solvay Rare Earth Systems: refinery and formulation plant, La Rochelle, France
Solvay Rare Earth Systems: refinery and formulation plant, LiYang, China
Solvay Rare Earth Systems: formulation plant, Baotou, China
Solvay Rare Earth Systems: formulation plant, Anan, Japan
Solvay Rare Earth System: photonics laboratory, Aubervilliers, France
Arnold Magnetic Technologies: manufacturing plant, Rochester, New York
Umicore Autocat: catalytic converter manufacturing plant, Tulsa, Oklahoma
BASF Battery Materials, Ovonic: Ni-MH battery plant, Rochester Hills (Detroit), Michigan
Molycorp Metals and Alloys: rare earth metal production plant, Tolleson (Phoenix), Arizona
Phoenix Automotive Core: automobile catalyst recycle plant, Phoenix, Arizona
Mountain Pass: rare earth mine, Mountain Pass, California
Advalue Photonics Inc.: rare earth doped laser manufacture, Tucson, Arizona
Advanced Materials Research Institute: catalysis research center, Ploemeur, France
Guangzhou Magtrust Magnets Group Co.: magnet manufacture, Guangzhou, China
Shin Etsu Rare Earth Magnets Research Center: new rare earth magnet development, Japan

We thank the personnel at these facilities for their kindness in showing us around their plants and for answering any and all of our questions.

We also thank Christine McElvenny and Sharmila Vadivelan of Elsevier for so kindly helping us to get our undisciplined manuscript into book form—and Margaret Davenport, who proofread all our work.

A brief note about units. We have used SI-based units throughout except °C for temperature and pascals and bar (1×10^5 Pa) for pressure. Bar has been especially useful in our thermodynamic calculations because it is very close in value to the old standard atmosphere unit.

Rare earths are among the most interesting and useful of the earth's elements. We are delighted to present them to you.

Jacques Lucas
Rennes, France

Pierre Lucas
Tucson, Arizona

Thierry Le Mercier
Aubervilliers, France

Alain Rollat
La Rochelle, France

William Davenport
Tucson, Arizona

CHAPTER

Overview

1

This book defines rare earths as those elements that are between lanthanum and lutetium on the atomic chart, that is,

lanthanum, La
cerium, Ce
praseodymium, Pr
neodymium, Nd
promethium, Pm
samarium, Sm
europium, Eu
gadolinium, Gd
terbium, Tb
dysprosium, Dy
holmium, Ho
erbium, Er
thulium, Tm
ytterbium, Yb
lutetium, Lu.

They are also called lanthanides. In nature, they occur with yttrium (Y) and scandium (Sc), which some authors refer to as rare earths. We discuss these elements, but do not refer to them as rare earths.

Lanthanum through samarium account for ~98% of rare earths-in-ore, Fig. 1.1. Europium through lutetium account for the remainder (Dent, 2012).

The isotopes of promethium are all radioactive with short half-lives. Promethium is never found in nature.

The objective of this chapter is to summarize these rare earths in terms of their properties, uses, occurrence, and extraction—in preparation for our book's detailed chapters.

1.1 EXPLOITED PROPERTIES

Rare earth elements are always used in combination with other elements. Examples are as follows:

Rare Earths. http://dx.doi.org/10.1016/B978-0-444-62735-3.00001-2

FIG. 1.1

Rare earth oxides. Left to right are gadolinium oxide, samarium oxide, neodymium oxide, praseodymium oxide, lanthanum oxide, and cerium oxide.

Photo by Peggy Greb, US Department of Agriculture (public domain).

(a) as oxides in automobile exhaust pollution abatement catalysts
(b) alloyed with transition metals (Ni, Co, Mn) and hydrogen in rechargeable battery electrodes
(c) alloyed with magnesium to increase its high temperature strength and decrease its flammability
(d) alloyed with transition metals (Fe, Co) to make the world's strongest permanent magnets
(e) doped into glass to give specific, reproducible wavelength laser output light and
(f) doped into compounds, glasses, and polymers for use in luminescent products, for example, lights and screens.

The uniqueness of rare earth properties for many of these uses is a consequence of their blocked 4f electron orbitals.

1.2 USES

Table 1.1 shows world rare earth consumption in 2012. Cerium, lanthanum, and neodymium were by far the most consumed. The combined consumption of the highest atomic number rare earths (holmium, erbium, thulium, ytterbium, and lutetium) is <1 kilotonne per year.

Table 1.2 shows recent world rare earth consumption by application. Magnets, catalysts, polishing powder, and rechargeable batteries top the list. Other consumptions are smaller but technologically important.

Table 1.1 Estimate of 2012 World Consumption of Rare Earths

Element	Atomic Number	Estimated 2012 World Consumption of Contained Rare Earth Element (Kilotonnes)
Lanthanum	57	22
Cerium	58	39
Praseodymium	59	05
Neodymium	60	16
Samarium	62	2
Europium	63	00.2
Gadolinium	64	1
Terbium	65	00.4
Dysprosium	66	02
Holmium	67	<1
Erbium	68	<1
Thullium	69	<1
Ytterbium	70	<1
Lutetium	71	<1

Rare earths are consumed in many forms, for example, as alloys, ceramics, compounds (e.g., oxides), and glasses as shown in Table 1.2. None is used as a structural metal.
Gambogi (2013) and author estimates.

Table 1.2 Estimate of Rare Earth Consumption by Use

Application	Percent of World Rare Earth Element Consumption
Permanent magnets	20
Optical materials polishing powder	16
Fluid petroleum cracking catalyst	12
Automobile gaseous pollution abatement catalyst	7
Rechargeable battery electrodes	10
Metallurgy, for example, rare earth-magnesium alloys	9
Phosphors	8
Glass additives	6
Ceramics	5
Other	7

Permanent magnets, catalysts, polishing powders, and rechargeable battery electrodes are the largest applications.
Gambogi (2013), Gschneidner (2011), Goonan (2011), and author estimates.

1.3 OCCURRENCE

Rare earths occur mainly in bastnasite $(RE)FCO_3$ [where RE = rare earth elements] and monazite $(RE)PO_4$ ores (Jones et al., 1996). The ores typically contain 5-15 mass % rare earth elements.

About 90% of mined rare earths come from these minerals (Gupta and Krishnamurthy, 2005): 70% from bastnasite and 20% from monazite. A considerable percentage of monazite also occurs in beach sand deposits, mostly in India.

A growing source of rare earth elements are rare earth cation adsorption clays, particularly in subtropical Asia, mainly China. These clays consist of rare earth cations adsorbed on clay (often muscovite) particles. The rare earth cations are easily removed from these ores by ion exchange with ammonium chloride solutions. However, the ores contain only 0.2-0.3 mass% rare earth elements, so large amounts of ore must be treated per tonne of recovered rare earth elements.

Rare earth mines are mapped in Chapter 2.

1.4 MINES AND MINING

Most rare earth ores are found on or near the earth's surface. They are mined by surface (open pit) methods, Fig. 1.2.

Open pit mining (Figs. 1.2 and 3.1) entails the following:

(a) removing worthless overburden from atop the ore body (Hartman and Mutmansky, 2002)
(b) blasting and removing ore from a central location on the ore body surface
(c) building roads for bringing ore up to the surface and over to the rare earth element extraction plants
(d) gradually deepening and widening the mine by blasting, ore removal, and road building

until the ore body is fully exploited.

Of course, the ore body is not uniform in rare earth concentration. Some of the blasted material is low-grade waste—it is trucked to a storage site. Only high-grade "ore" is sent to the rare earth extraction plants. This and ore fragmentation are detailed in Chapter 3.

1.5 RARE EARTH [RE] EXTRACTION

The ore from open pit mining contains the following:

(a) rare earth minerals, mostly bastnasite $(RE)FCO_3$ and monazite $(RE)PO_4$ intermingled with

FIG. 1.2

Mountain Pass open pit mine, Mountain Pass, California (35.5° N; 115.5° W). A truck is being loaded at the bottom of the pit (center-left). Roads for trucking ore up out of the pit are noticeable. This mine started production in 1952. It closed in 2002 but reopened in 2012. The world's largest mine (also open pit) is the Bayan Obo mine in Inner Mongolia, China (41.8° N; 110.0° E). It is reported to (i) be producing ~100 kilotonnes of rare earth elements per year and to (ii) have a reserve of 40 megatonnes of rare earths in ore (Qifan et al., 2010).

Photo courtesy Molycorp, Inc.

(b) other minerals, for example, calcite ($CaCO_3$), dolomite ($CaCO_3$:$MgCO_3$), and barite ($BaCO_3$).

Extraction of pure individual rare earth products (e.g., CeO_2) from this mineral mix entails (Fig. 1.3) the following:

(a) isolating the ore's rare earth minerals (mostly bastnasite and monazite) into a concentrate, mostly by froth flotation, Fig. 1.3;

then, using bastnasite as an example,

(b) 600 °C sulfuric acid baking, then water leaching

(c) solid/liquid separation and disposal of solids

(d) precipitation of Ca and Fe compound impurities and disposal of solids

(e) purification of the resulting solution by solvent extraction

(f) separation of the pure rare earth solution into individual rare earth solutions (also by solvent extraction)

(g) compound precipitation

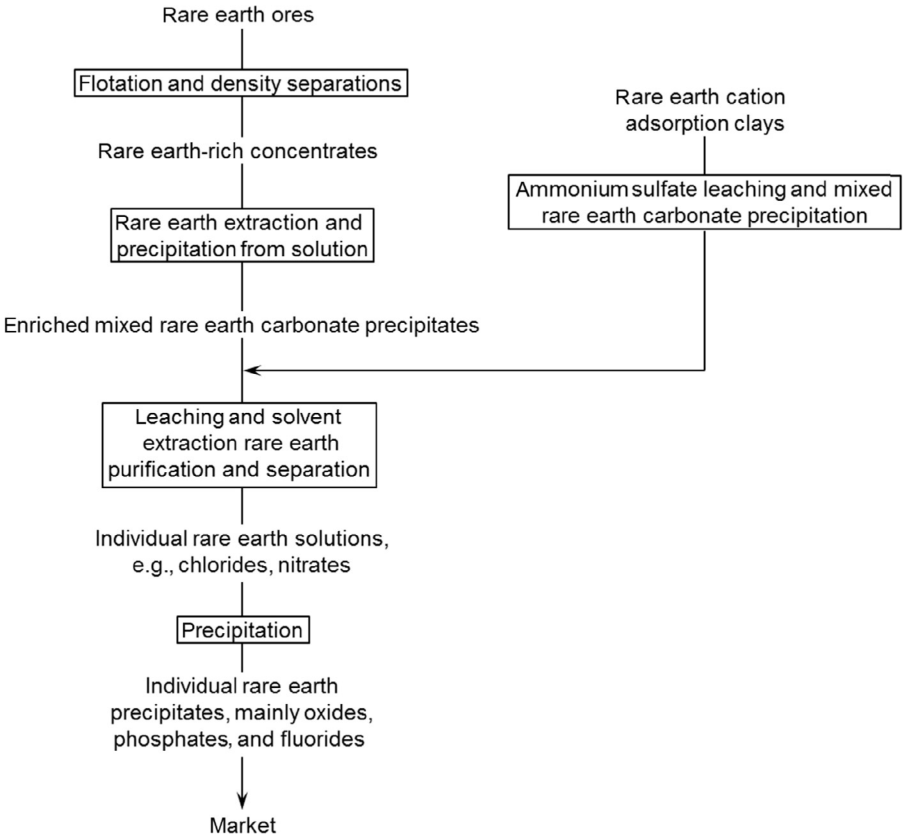

FIG. 1.3

Schematic flowsheet for producing pure marketable rare earth products from rare earth ores and rare earth cation adsorption clays. Magnetic separations are also used near the top of the flowsheet. The processes are continuous.

(h) thermal heating of these compounds to make marketable oxides, phosphates, and fluorides.

This process and several variations are detailed in Chapters 4 and 5.

1.6 METAL PRODUCTION

About half of rare earth consumption requires production of pure rare earth metal as an intermediate raw material. Examples of the uses of rare earth metal are in permanent magnet alloys, rechargeable battery electrodes, and magnesium alloys.

Rare earth metals are produced by reducing them from rare earth oxides, chlorides, and fluorides. Two techniques are used:

(a) high-temperature fused salt electrowinning
(b) high temperature reduction with very strong reductants such as lanthanum and calcium.

These techniques are detailed in Chapters 6 and 7.

1.7 RARE EARTH USES

The preceding sections have described how rare earths are produced. The following sections summarize their major uses, Table 1.2.

1.7.1 Rare earth metals in magnet alloys

Rare earth metal-transition metal alloy magnets are the strongest in the world (Fig. 1.4). Examples are as follows:

(a) neodymium-iron-boron magnets, for example,
$Nd_2Fe_{14}B$

FIG. 1.4

Surface mounted samarium-cobalt magnets on the rotor portions of three different motors.

Photo courtesy of Steve Constantinides, Arnold Magnetic Technologies.

(b) samarium-cobalt magnets, for example,
$SmCo_5$
Sm_2Co_{17}.

The strong magnetic fields exerted by these materials allow miniaturization of electric motors and generators, because tiny rare earth magnets exert strong forces. Modern automobiles, for example, use up to 100 magnets, mostly in motors (e.g., wiper motors), and some in sensors (e.g, fluid-level sensors) and actuators (Fig. 1.5).

Neodymium-iron-boron magnets are the strongest at ambient temperatures, but their strength falls with increasing temperature, Fig. 1.6. Samarium-cobalt magnets are not quite so strong at ambient temperatures, but their strength is not much reduced by increasing temperature.

Rare earth metal-transition metal magnets are made by

(a) producing molten magnet alloy from pure rare earth and transition metals
(b) rapidly solidifying (quenching) the alloy
(c) decrepitation and fine grinding of the solidified alloy
(d) compacting the fine particles into useful shapes (powder metallurgy)
(e) magnetizing the shaped products in a powerful electromagnetic field.

Magnets are the largest users of rare earths, Table 1.2.

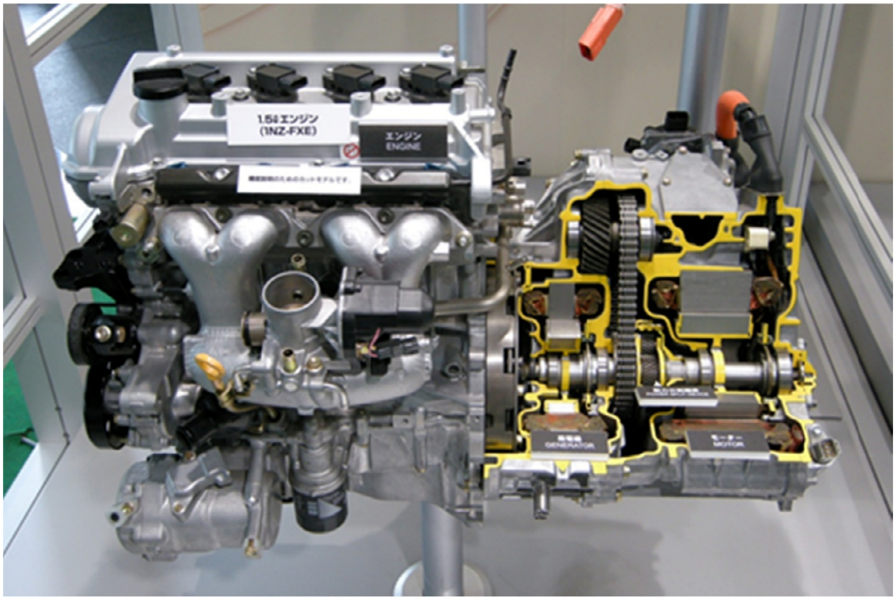

FIG. 1.5

Toyota Prius gasoline engine (left), generator (center), and electric drive motor (right) The electric drive motor is a big user of rare earth metal-transition metal permanent magnets.

Photograph (public domain).

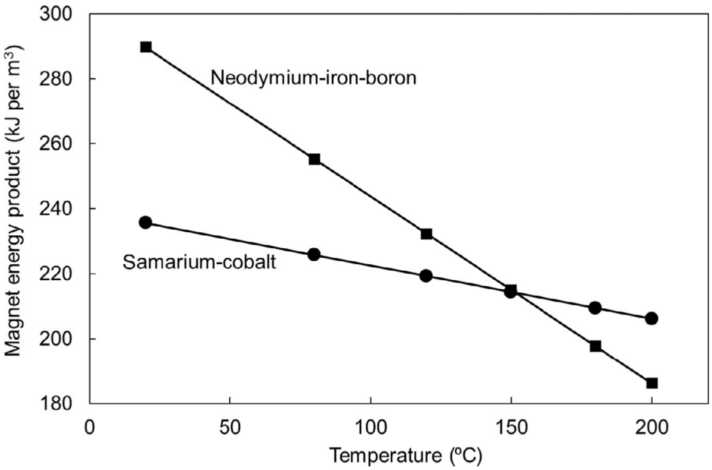

FIG. 1.6

Strength of Nd-Fe-B magnets versus Sm-Co magnets. Nd-Fe-B magnets are stronger at ambient temperatures. Sm-Co magnets are stronger at high temperatures, for example, near an internal combustion engine or rocket motor.

Data courtesy Steve Constantinides, graph drawn by William Davenport.

1.7.2 Rare earths in rechargeable battery electrodes

Rare earth rechargeable batteries are widely used in hybrid automobiles, Fig. 1.7.

One of the battery's electrodes is a metal hydride alloy, for example,

$$\mathrm{La_{5.7}Ce_{8.0}Pr_{0.8}Nd_{2.3}Ni_{59.2}Co_{12.2}Mn_{6.8}Al_{5.2}(H)}$$

FIG. 1.7

High power Ni-rare earth-H battery module for Toyota NHW20 Prius. The cutaway shows many rectangular NiMH batteries arranged in series. One model of the Prius uses 168 Ni-rare earth-H cells to give a total of ∼20 kW of power @ ∼200 V. Public domain photograph.

where the numbers are the atomic% of each element (excluding hydrogen). In use, these electrodes release their hydrogen into an electrolytic solution where it is oxidized to $H_2O(\ell)$ plus an electron, thereby providing the battery's electrical current and power.

The product $H_2O(\ell)$ is readily reduced and its hydrogen reabsorbed when the battery is recharged by an external electrical energy source, for example, an automobile generator. So the battery is *rechargeable*.

Like rare earth magnets, these electrodes are made from pure metals by powder metallurgy techniques.

1.7.3 Rare earth automobile exhaust pollution abatement catalysts

Rare earth oxides, specifically ceria (CeO_2), are used to minimize pollution from automobile exhaust gases. They work together with platinum, palladium, and rhodium to

(a) oxidize CO(g) and HC(g) to innocuous CO_2(g) and H_2O(g)
(b) reduce nitrogen oxides [e.g., NO(g)] to innocuous N_2(g).

The role of the platinum group metals is to catalyze (speed up) the oxidation and reduction reactions.

The role of the ceria is to provide a stable, predictable oxygen concentration in the catalytic converter even as driving conditions change.

Figure 1.8 shows a recent catalyst converter. The chapter on catalysts describes how it is made, how it is used, and how efficient it is at preventing unwanted CO(g), HC(g), and NO(g) pollution.

1.7.4 Glass polishing powders

Rare earth oxide polishing powder accounts for about 16% of rare earth use. Cerium oxide (ceria) is far and away the most used. It is used for polishing various grades of glass—from television screen glass to liquid crystal display glass.

The advantages of CeO_2 in this application are as follows:

(a) it is only slightly harder than glass, ~6.5 versus 6 mhos for glass
(b) it is readily made: by precipitating cerium hydroxide from aqueous solution, then calcining it to cerium oxide
(c) it reacts chemically with glass—dissolving protuberances and smoothing the glass.

Ceria particle size is controlled by adjusting solution pH and temperature.

A uniform, small powder size is absolutely necessary to prevent scratches and, hence, light scattering from the glass. The more critical the application, for example, glass fiber data transmission, the smaller and more uniform the polishing powder particles must be.

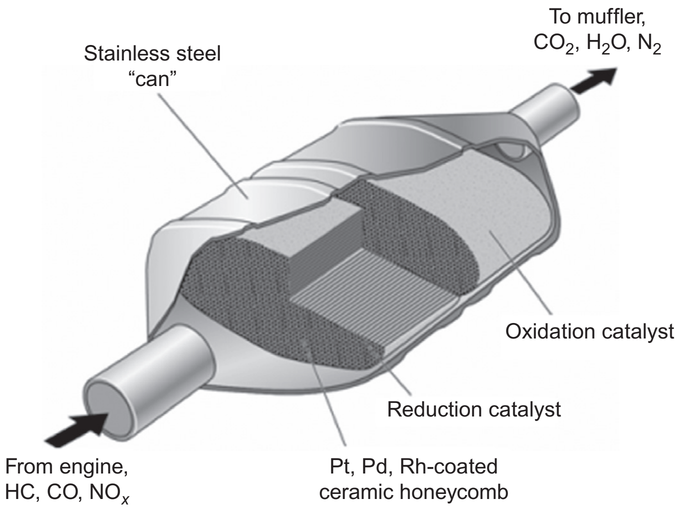

FIG. 1.8

Catalytic converter for converting unhealthful CO(g), C_mH_n(g), and NO_x(g) gasoline engine-out gases to innocuous CO_2(g), H_2O(g), and N_2(g) tail pipe exit gases (Crundwell et al., 2011). The converter consists of a channeled ceramic support block inside a stainless steel shell. The channel walls are covered with dried and heat-treated alumina-ceria/zirconia-platinum group metal dispersion layer(s). Automobile converters are typically 0.3 m long and 0.1 m in diameter. New automobiles have two to six converters.

1.7.5 Luminescent and phosphorescent uses

Rare earths are used extensively in lasers, optical amplifiers, and luminescent products (fluorescent lamps, light emitting diodes, liquid crystal, and plasma displays [televisions]).

1.8 RARE EARTH RECYCLING (FIG. 1.9)

2013 saw a strong push toward increasing recycling of end-of-use rare earth objects. Examples are recycling of the following:

(a) rechargeable Ni-rare earth-hydrogen batteries
(b) fluorescent lamp rare earth phosphor powders
(c) rare earth-transition metal magnet manufacturing waste (swarf).

New targets for recycling are rare earth automobile catalysts (already being recycled for their platinum group metals) and end-of-life rare earth magnets.

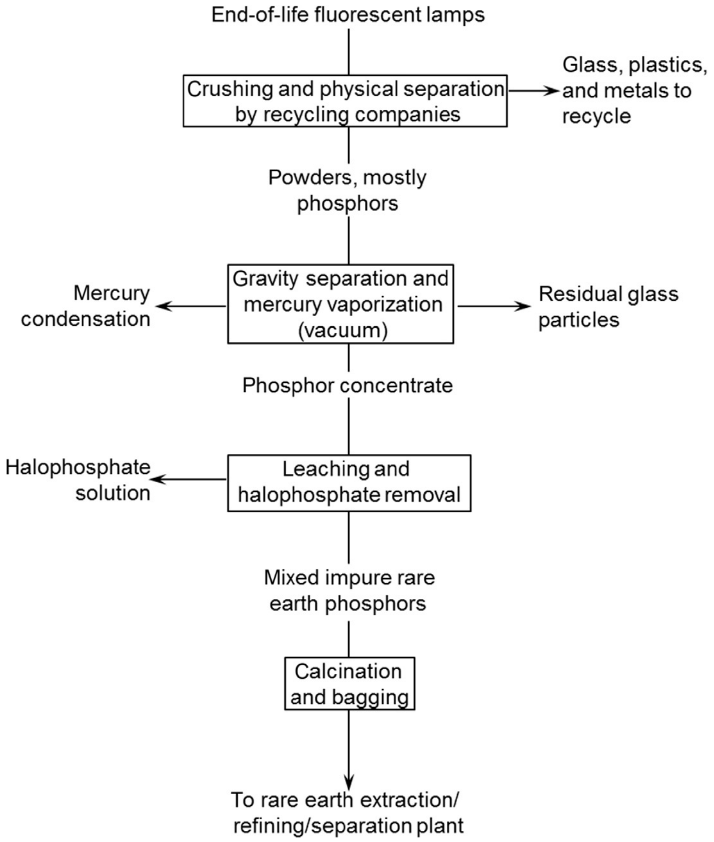

FIG. 1.9

Schematic flowsheet for recycling rare earth phosphors. It consists mainly of gravity separation, hydrometallurgical extraction, and solvent extraction/separation/purification.

Recycling has the following advantages:

(a) It slows depletion of our natural resources.
(b) It uses up to 90% less energy than rare earth-from-ore production, that is, it avoids mining, concentration, and smelting (Vanbellen and Chintinne, 2007).
(c) It avoids rare earth-from-ore extraction waste products.
(d) It slows the use of landfills.

1.9 SUMMARY

In 2014, ~90% of rare earth production originates in the mines of Inner Mongolia, China. The rare earth concentration in these ores is 5-15 mass%. The principal rare earth mineral in these deposits is bastnasite $(RE)FCO_3$ [where RE = rare earths].

High purity (99.9 mass%) rare earth compounds (e.g., oxides) are produced from these ores by the following method:

physical concentration (e.g., flotation)
leaching
solution purification by solvent extraction
rare earth separation by solvent extraction
individual rare earth compound precipitation
calcination of these compounds to form marketable oxides, phosphates, and fluorides.

About 40% of rare earth production is used in metallic form—for making magnets, battery electrodes, and alloys. Metals are made from the above compounds by (i) high-temperature fused salt electrowinning and (ii) high temperature reduction with metallic reductants, for example, calcium or lanthanum.

Production/consumption of rare earths is $\sim$100 kilotonnes per year. Rare earths are mainly used in the following:

- magnets (up to 100 magnets per new automobile)
- catalysts (automobile emission and petroleum cracking)
- glass polishing powders for television screens and glass data storage disks
- rechargeable batteries (especially for hybrid cars)
- photonics (luminescence, fluorescence and light amplification devices).

Magnets and photonics are expected to grow significantly over the next few years.

References

Crundwell, F.K., Moats, M.S., Ramachandran, V., Robinson, T.G., Davenport, W.G., 2011. Extractive Metallurgy of Nickel, Cobalt and Platinum-Group Metals. Elsevier, Oxford, England, 399.

Dent, P.C., 2012. Rare earth elements and permanent magnets. J. Appl. Phys. 111, 07A721 (published on line, 6 pages).

Gambogi, J., 2013. Rare Earths. USGS Geological Survey, Mineral Commodity Summaries, January 2013, USGS, Reston, VA.

Goonan, T.G., 2011. Rare Earth Elements – End Use and Recyclability. USGS Scientific Investigations Report 2100-5094, USGS, Reston, VA.

Gschneidner, K.A., 2011. The rare earth crisis-the supply/demand situation for 2010–2015. In: Material Matters, vol. 6, number 2. Aldrich Materials Science Sigma-Aldrich Corporation, Milwaukee, WI, USA, pp. 32–35. Retrieved on July 30, 2013 from, http://www.sigmaaldrich.com/technical-documents/articles/material-matters/the-rare-earth-crisis.html.

Gupta, C.K., Krishnamurthy, N., 2005. Extractive Metallurgy of Rare Earths. CRC Press, Boca Raton, FL.

Hartman, H.L., Mutmansky, J.M., 2002. Introductory Mining Engineering, second ed. Wiley, New York.

Jones, A.P., Wall, F., Williams, C.T., 1996. Rare Earth Minerals: Chemistry, Origin and Ore Deposits. Chapman and Hall, London, UK.

Qifan, W., Hua, L., Chenghui, M., Shunpin, Z., Zinhua, Z., Shenqing, X., Hongyan, W., 2010. The use and management of NORM residues in processing Bayan Obo ores in China. Paper Presented at 6th International Symposium on Naturally Occurring Radioactive Materials, Marrakech, March 22–26, 2010. Recovered on August 13, 2013 from http://qu-wifan.eu-norm.org.

Vanbellen, F., Chintinne, M., 2007. “Extreme Makeover”: UPME’s Hoboken plant. In: Dusseldorf, European Metallurgical Conference 2007, GDMBpp. 1–9.

Suggested Reading

Goode, J.R., Moloveanu, G., Rayat, M.S., 2012. Rare Earths 2012. Metsoc of CIM, Montreal, QC.

Gupta, C.K., Krishnamurthy, N., 2005. Extractive Metallurgy of Rare Earths. CRC Press, Boca Raton, FL.

Zhang, X., Du, H., Wang, X., Miller, J.D., 2013. Surface chemistry considerations in the flotation of rare-earth and other semisoluble salt minerals. Miner. Metall. Proc.. 30 (1), 24–37.

CHAPTER

Rare Earth Production, Use and Price

2

This chapter describes the sources, production, uses, and prices of rare earths. World production of rare earth elements is ∼100 kilotonnes per year, Fig. 2.1. In order of decreasing consumption, the rare earths are as follows:

cerium (Ce)
lanthanum (La)
neodymium (Nd)
praseodymium (Pr)
samarium (Sm)
gadolinium (Gd)
dysprosium (Dy)
erbium (Er)
terbium (Tb)
europium (Eu)
ytterbium (Yb)
holmium (Ho)
thulium (Tm)
lutetium (Lu)

excluding promethium (Pm), which is radioactive. Consumption of individual rare earths is reported in Tables 1.1 and 1.2.

Neodymium and dysprosium are often in short supply. There are two reasons for this:

(a) They are critical components in Fe-(Nd,Dy)-B high-strength permanent magnets.
(b) The demand for these magnets is growing rapidly as hybrid and electric vehicles are coming into increasing use (Constantinides, 2012).

Dysprosium, especially, is often in short supply because (i) it is present in low concentration in most ores and (ii) it is indispensable for improving the high-temperature strength (i.e., near internal combustion engines and other heat sources) of Fe-(Nd, Dy)-B magnets.

Cerium and samarium are often in excess supply, as are holmium, erbium, thulium, and ytterbium.

However, lanthanum is likely to be in short supply because of its huge use in petroleum refining catalysts.

Rare Earths. http://dx.doi.org/10.1016/B978-0-444-62735-3.00002-4

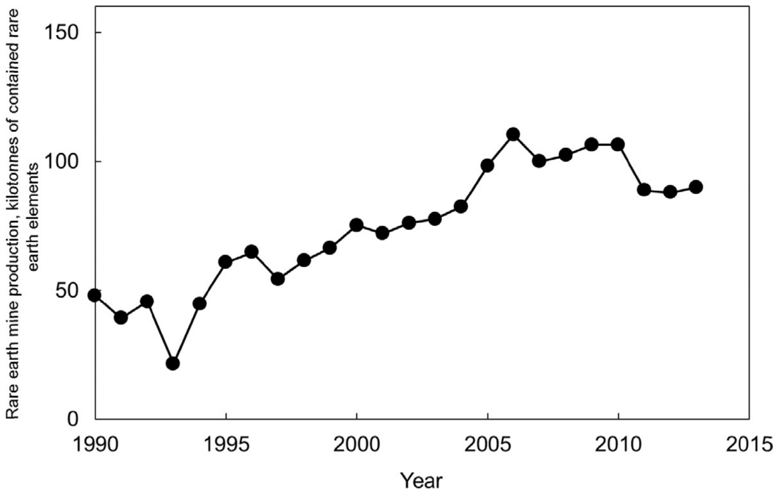

FIG. 2.1

Estimated annual world rare earth mine production from 1990 to 2013 (kilotonnes of contained rare earth elements). The information is from Goonan (2011) with additional information from Gambogi (2013). Growth seems to have slowed since about 2006. However, there may be an additional 10-20 kilotonnes of unreported illegal Chinese mine production not included in this graph.

2.1 CHAPTER OBJECTIVES

The objectives of this chapter are to detail the following:

(a) rare earth use
(b) the forms in which rare earths are used, for example, metal
(c) annual production, consumption, and price
(d) major rare earth sources around the world.

2.2 FORM OF USE

Rare earths are mainly used as follows:

(a) In metallic form, for example, in permanent magnet alloys, rechargeable battery electrodes, and magnesium alloys (~45%)
(b) As oxides, for example, in polishing powders, catalysts, glasses, and luminescent and optical materials (~35%)
(c) As chloride, nitrate, phosphate, and other compounds for petroleum catalysts, fluorescent lamps, light emitting diodes, and other uses (~20%).

Of course, quantity is not everything. Some applications, for example, medical lasers, use small amounts of rare earths, but the rare earth components are essential for safe, effective surgery. An example is a neodymium-doped aluminum garnet laser, which was used to safely remove a film from one of the authors' eyes. A second example is ytterbium-doped fiber lasers, which are fast becoming more prominent in medical and industrial applications. Organic gadolinium compounds are also used for magnetic resonance imaging.

2.3 DETAILED USES

Table 2.1 describes the major uses of individual rare earths in 2013. The items in bold are critical uses.

Table 2.1 Significant Uses of Rare Earth Metals

Element	Use
Lanthanum	**Petroleum fluid cracking catalyst**
	Ethanol reforming catalyst
	Nickel-metalhydride rechargeable battery electrodes
	Hydrogen storage alloys, $LaNi_5$
	Optical
	High refractive index lenses
	Heavy metal fluoride glasses
	Fiber optics
	Night vision goggles
	Phosphors
	Fluorescent lamps
	X-ray intensifying screens
	Reductant for making samarium, europium, thullium, and ytterbium metals (some in mischmetal)
Cerium	**Catalysts**
	Ceria and ceria/zirconia automotive pollution reduction catalysts
	Petroleum cracking catalysts
	Water purification
	Glass additives
	Decolorizer
	Ultra-violet light absorption
	Polishing media: **ceria for polishing**:
	Glass
	Precision glass lenses
	Glass display panels
	Liquid crystal displays
	Glass magnetic memory disks
	Silicon wafers

Continued

Table 2.1 Significant Uses of Rare Earth Metals—cont'd

Element	Use
	Ce-stabilized ZrO_2 Structural ceramics Synthetic gems (pale yellow) Phosphors Fluorescent lamps Scintillation counters Light-emitting diodes **Ductile iron processing** (**increases ductility**) Sputtering targets Superconductors **Nickel-metalhydride rechargeable battery electrodes**
Praseodymium	**Cheap substitute for some Nd in Nd-Fe-B permanent magnets** Pr-stabilized ZrO_2 synthetic gems (light green) Coloring agents Glass—light green Ceramic tile—yellow Scintillators for X-ray tomography Glass blower and welder goggles (with neodymium) In ceria and ceria-zirconia catalysts **Nickel-metalhydride rechargeable battery electrodes**
Neodymium	**Nd-Fe-B high strength permanent magnets** **In electric motors and generators** **In actuators** **In computer hard drive spindles** **In direct drive wind turbines** **In cell phones and iPods** Lasers (e.g., Nd-doped yttrium aluminum garnet lasers for eye surgery) Metal halide lamps Nd-stabilized ZrO_2 synthetic gems (pink/purple) Coloring agent Pink to purple glass Glass blower and welder goggles (with praseodymium)
Samarium	**Sm-Co high strength**, **high operating temperature permanent magnets** Glass coloring agent (light yellow) Phosphors Monitors, television screens Catalysts (e.g., for decomposition of plastics, dechlorination of pollutants)
Europium	**Red phosphors** **Television screens** **Fluorescent lamps** Blue phosphors $SrAl_2O_4$:Eu:Dy afterglow materials Light-emitting diodes (red)

Table 2.1 Significant Uses of Rare Earth Metals—cont'd

Element	**Use**
Gadolinium	**Host for phosphors** **Scintillators for X-ray tomography** **Magnetic resonance imaging contrast agents** **X-ray intensifying screens** Yttrium gadolinium garnets for Communications (radio frequencies) and phase shifters, tuners, filters, radar Optical lenses Magnetic refrigeration (research)
Terbium	**Phosphors** (**green**) **Fluorescent lamps** **Monitors and television screens** **Light-emitting diodes** X-ray intensifying screens **Terfenol-D** ($\mathbf{(Tb_{0.3}Dy_{0.7})Fe_2}$) **magnetostrictive alloy** Occasionally in Nd-Fe-B magnets for raising magnet operating temperature) Light-emitting diodes (green)
Dysprosium	**Included in Nd-Fe-B permanent magnets to raise operating temperature and coercivity** Phosphors Metal halide lamps **Terfenol-D** ($\mathbf{(Tb_{0.3}Dy_{0.7})Fe_2}$) **magnetostrictive alloy**
Holmium	Metal halide lamps In lasers, for example, in holmium-doped yttrium aluminum garnet lasers for kidney stone fragmentation
Erbium	**Optical fiber signal amplifiers** Lasers, for example, in erbium-doped yttrium aluminum garnet lasers for scar removal Glass coloring agent (pink) Er-stabilized ZrO_2-synthetic gems (pink)
Thullium	X-ray intensifying screens Metal halide lamps In lasers, for example, thullium-doped yttrium aluminum garnet lasers for prostate tumor vaporization
Ytterbium	Optical lenses Pressure sensors Lasers Portable X-ray machines Atomic clock
Lutetium	Lasers Host for scintillator detectors and X-ray phosphors Optical lenses Red phosphor in light-emitting diodes **In cerium-doped lutetium oxyorthosilicate detectors for positron emission tomography**

From Gschneidner (2011) and author estimates.

2.4 RARE EARTH PRICES

Figures 2.2–2.14 show recent prices of rare earths. Most of the prices are for 99% pure metal, in US dollars per kilogram loaded for shipping. A few are for 99% pure oxides, priced in Chinese renminbi per kilogram (domestic Chinese prices). On January 6, 2014, 1 renminbi was worth ~0.17 US$.

There is no formal open market for rare earths. The prices are determined entirely by supply and demand between buyers and sellers.

Several conclusions can be drawn from the price graphs.

1. Prices for all rare earths rose from 2008, peaked in 2011, and have been falling ever since.
2. Lanthanum and cerium are quite cheap, <150 US$ per kg at their peak, and in February 2014, below 15 US$ per kg.
3. Dysprosium is 100 times more costly than lanthanum and cerium, 3000-5000 US$ at its peak and in February 2014, around 700 US$ per kg.

The cheapness of lanthanum and cerium is mostly due to their large supply. The costliness of dysprosium is due to (i) the large demand for it in permanent magnets and (ii) its low concentrations in ore.

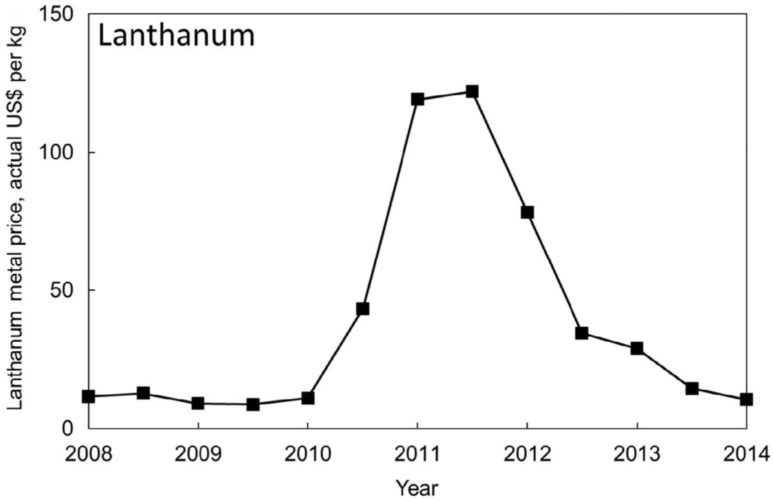

FIG. 2.2

Recent price estimates for 99% pure lanthanum metal. Notice the peak price in 2011 and the subsequent rapid price decline. Notice also lanthanum's low price relative to other rare earths, for example, europium, terbium, and dysprosium. Rare earth prices are negotiated between buyers and sellers. The prices here are representative of these negotiated prices.

Data courtesy of Alain Rollat, Solvay Rare Earth Systems.

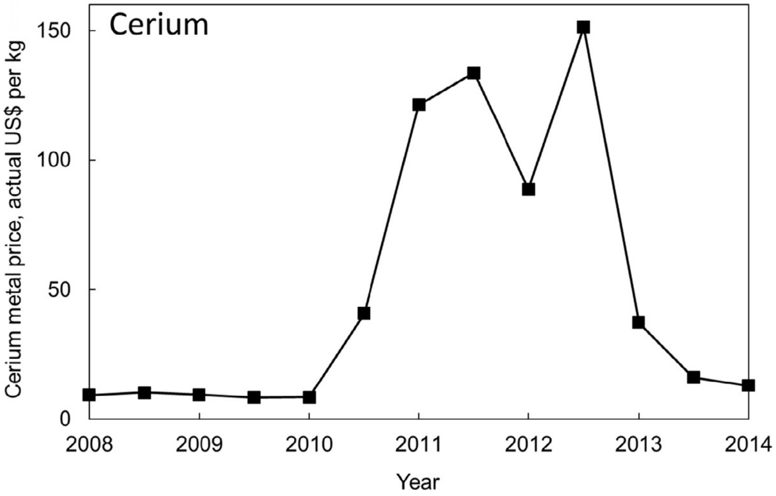

FIG. 2.3

Recent price estimates for 99% pure cerium metal. Notice the peak price in 2012 and the subsequent rapid price decline. Notice also cerium's low price relative to many rare earth metals.

Data courtesy of Alain Rollat, Solvay Rare Earth Systems.

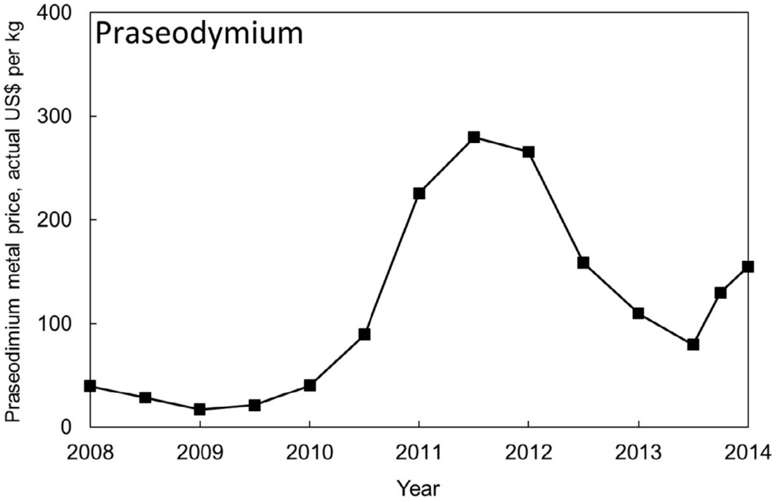

FIG. 2.4

Recent price estimates for 99% pure praseodymium metal. Notice the peak price in 2011 and the subsequent rapid price decline. Notice also praseodymium's intermediate price relative to other rare earth metals.

Data courtesy of Alain Rollat, Solvay Rare Earth Systems.

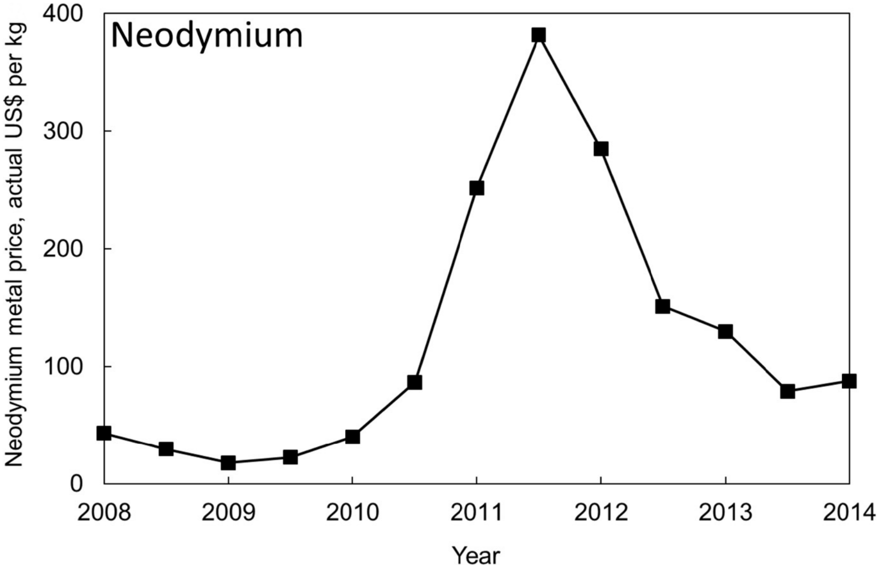

FIG. 2.5

Recent price estimates for 99% pure neodymium metal. Notice the peak price in 2011 and the subsequent rapid price decline. Notice also neodymium's intermediate price relative to other rare earth metals.

Data courtesy of Alain Rollat, Solvay Rare Earth Systems.

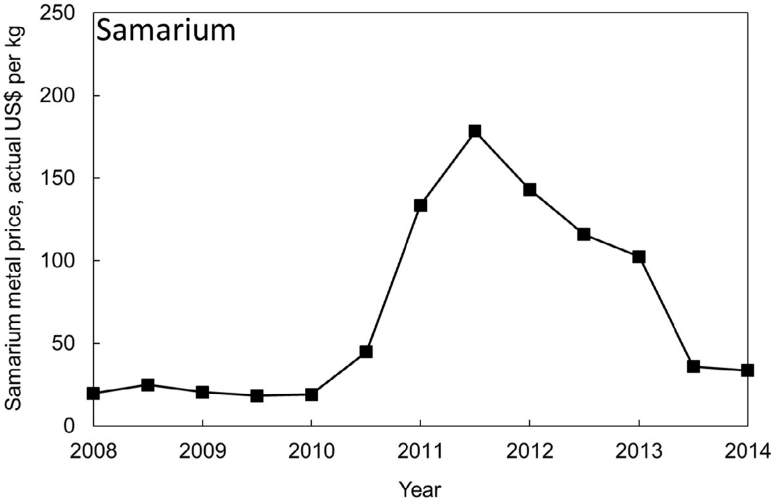

FIG. 2.6

Recent price estimates for 99% pure samarium metal. Notice the peak price in 2011 and the subsequent rapid price decline. Notice also samarium's relatively low price relative to other rare earth metals.

Data courtesy of Alain Rollat, Solvay Rare Earth Systems.

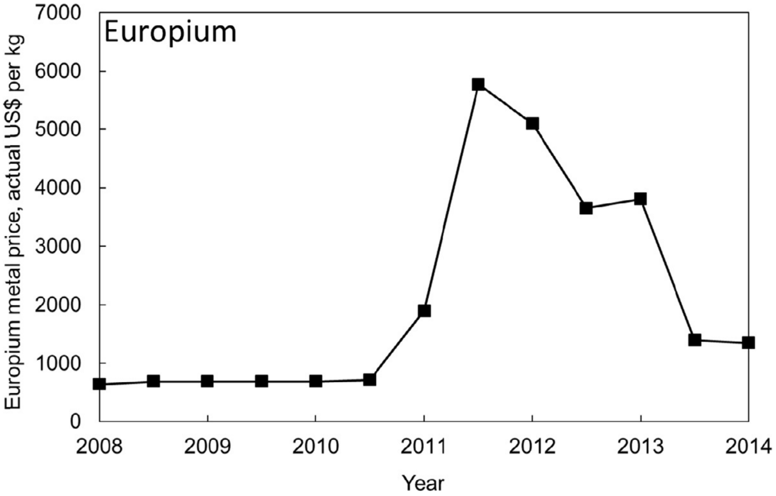

FIG. 2.7

Recent price estimates for 99% pure europium metal. Notice the peak price in 2011 and the subsequent rapid price decline. Notice also europium's high price relative to other rare earth metals.

Data courtesy of Alain Rollat, Solvay Rare Earth Systems.

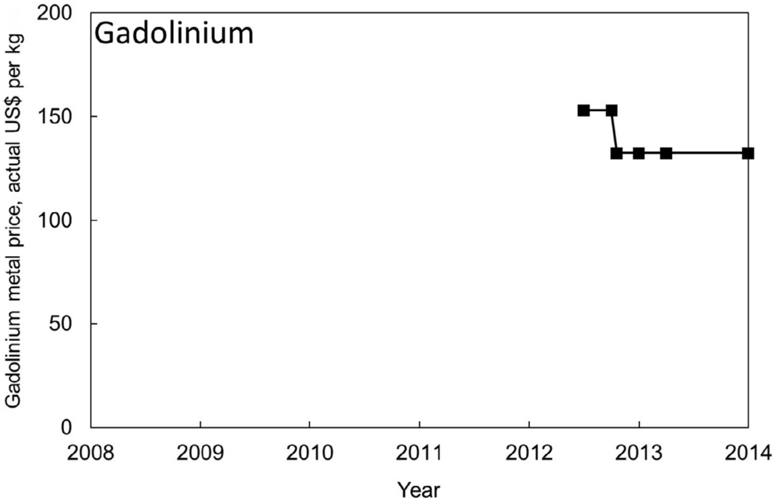

FIG. 2.8

2012 and 2013 price estimates for 99% pure gadolinium metal. The few available points are due to gadolinium's infrequent sales.

Data courtesy of Alain Rollat, Solvay Rare Earth Systems.

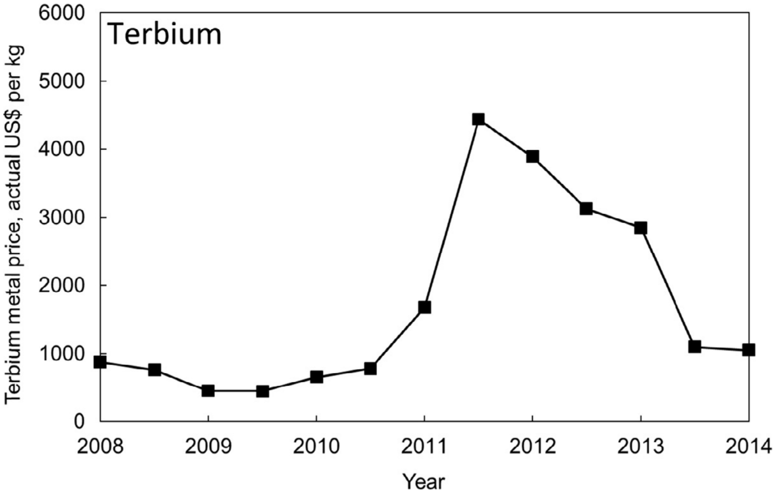

FIG. 2.9

Recent price estimates for 99% pure terbium metal. Notice the peak price in 2011 and the subsequent rapid price decline. Note terbium's high price relative to other rare earth metals.

Data courtesy of Alain Rollat, Solvay Rare Earth Systems.

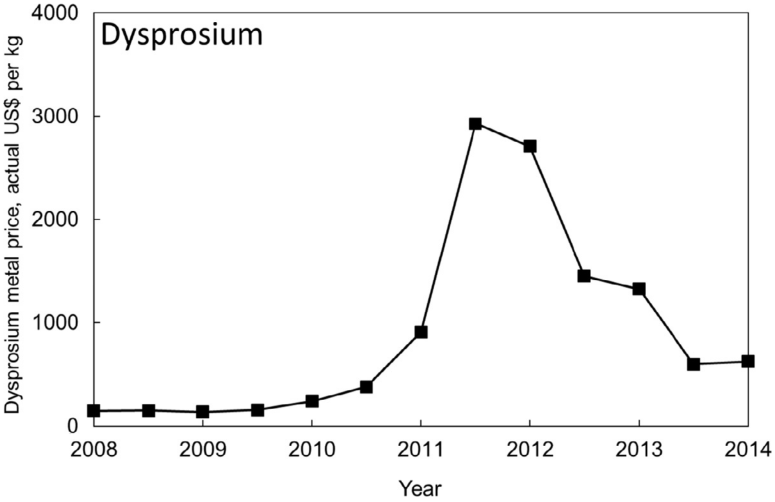

FIG. 2.10

Recent price estimates for 99% pure dysprosium metal. Notice the peak price in 2011 and the subsequent rapid price decline. Notice also dysprosium's high price relative to other rare earth metals.

Data courtesy of Alain Rollat, Solvay Rare Earth Systems.

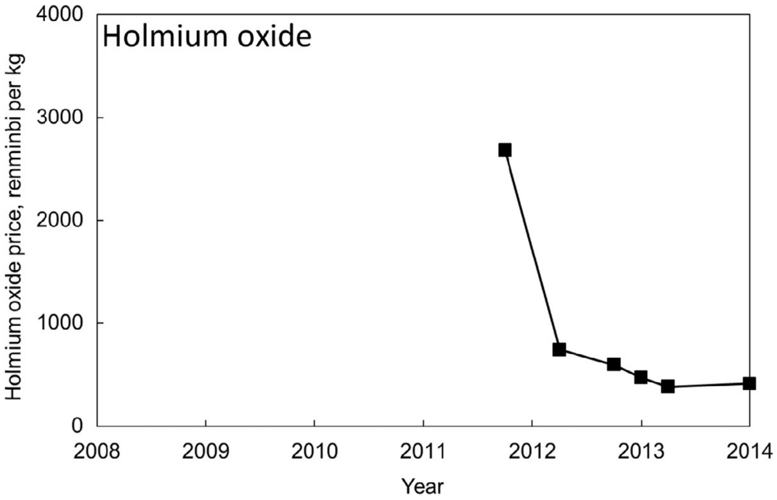

FIG. 2.11

Recent Chinese domestic price estimates for 99% pure holmium oxide. Holmium is seldom sold in metallic form because most of its uses are in glasses, lasers, and ceramics. Notice the typical price decline after 2011.

Data courtesy of Alain Rollat, Solvay Rare Earth Systems.

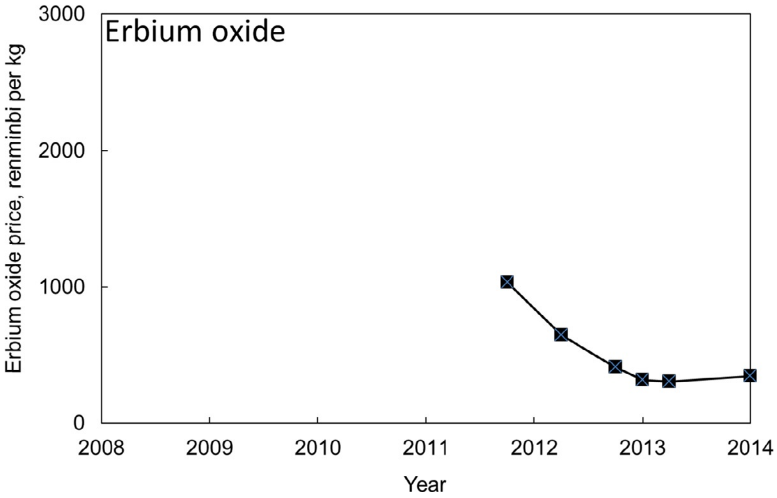

FIG. 2.12

Recent Chinese domestic price estimates for 99% pure erbium oxide. Erbium is seldom sold in metallic form because most of its uses are in glasses, lasers, and ceramics. Notice the price decline after 2011.

Data courtesy of Alain Rollat, Solvay Rare Earth Systems.

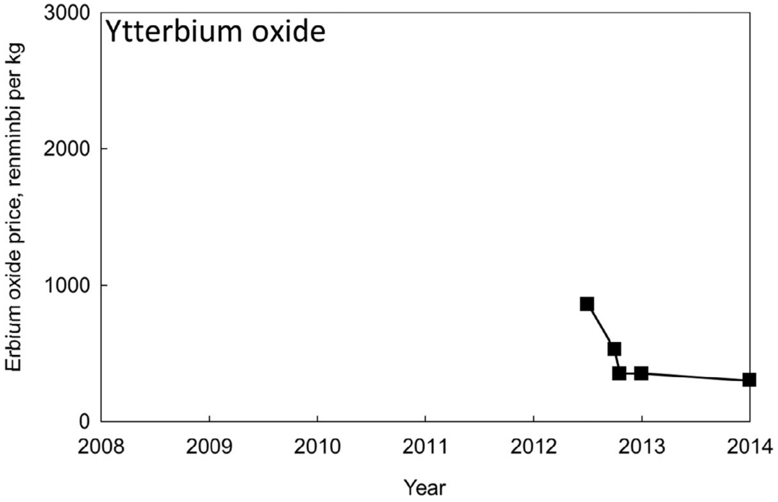

FIG. 2.13

Recent Chinese domestic price estimates for 99% pure Ytterbium oxide. Ytterbium is seldom sold in metallic form because most of its uses are in glasses, lasers, and ceramics. Notice the price decline during 2012.

Data courtesy of Alain Rollat, Solvay Rare Earth Systems.

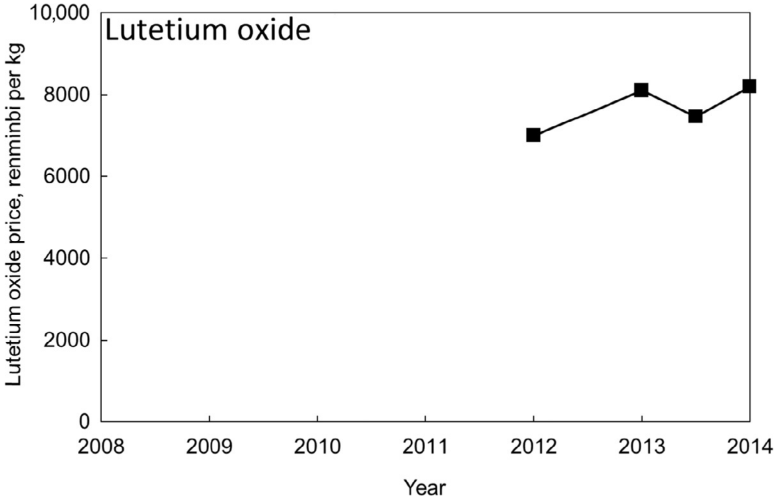

FIG. 2.14

Recent price estimates for 99% pure lutetium oxide. Lutetium is seldom sold in metallic form because most of its uses are in glasses, lasers, and ceramics.

Data courtesy of Alain Rollat, Solvay Rare Earth Systems.

2.4.1 Comparison with platinum group metals

The rare earth price behavior mimics the price behavior of platinum and rhodium—2 years later (2008 peaks for Pt and Rh, 2011 peaks for rare earths). In both cases,

- **(a)** the price rise was caused by increasing demand without a commensurate increase in supply (the rare earth supply might have been artificially curtailed)
- **(b)** the price fall was due to a decreasing demand (perhaps due to substitution) and a flat or increasing supply.

2.5 MINING RARE EARTHS

Table 2.2 describes rare earth mining around the world. In 2013, China

- **(a)** dominated rare earth mining (~90%) and
- **(b)** had about 50% of the rare earth ore reserves.

However, other countries are stepping up mine production, see Chapter 3.

2.5.1 Locations

The map in Fig. 2.15 pinpoints producing rare earth mines. They are listed in Table 2.3. In addition, there are rare earth mining projects in every continent but Antarctica. These projects will be added to future editions of this book, as they come into production. The dominance of south Asia is notable.

Table 2.2 Estimates of 2012 World Rare Earth Element Production and Rare Earth Reserves

Country	Mine Production of Rare Earth Elements (Kilotonnes)	Reserves of Rare Earth Elements (Megatonnes)
China	75	44
USA	1	13
Australia (mined and concentrated in Australia, extracted in Malaysia)	1	1
India	3	2
Other		33

Gamogi reports his data as rare earth oxide masses. We have multiplied his rare earth oxide masses by 0.8 to get rare earth element masses.
From Gambogi (2013) and author estimates.

FIG. 2.15

The world's rare earth producing mines, 2013. Table 2.3 gives details. One extraction plant (Kuantan, Malaysia: E) is also shown. Yet-to-produce mine projects are not shown. They will be included in future editions of this book.

Author estimates.

Table 2.3 Identity of Fig. 2.15's Pinpointed Mines

Number in Fig. 2.15	Property Name	Estimated 2012 Rare Earth Production (Kilotonnes Rare Earth Elements per Year)
1	Bayan-Obo, China	65
2	Rare earth cation clays, China	10
3	Mount Weld, Western Australia	1 (2013)
4	Vizag, Andhra Pradesh, India	Not available
5	Manavalakurichi, Tamil Nadu, India	Not available
6	Chavara, Kerala, India	Not available
7	Lovozerskoy, Russia	3
8	Mountain Pass, California	1
E	Kuantan, Malaysia (extraction plant)	1 (2013)

Production estimates are also given.
Gambogi (2013) and author estimates.

2.6 SUMMARY

Rare earths occur around the world but are mostly mined and extracted in China. Mining in other countries (e.g., Australia, India, and USA) is increasing—but slowly.

Prices of all rare earths peaked in 2011. They have fallen ever since. This has had a discouraging effect on new mining projects.

Rare earths have a myriad of uses. Their major uses (tonnage-wise) are in the following:

magnets
catalysts
polishing powders
rechargeable batteries

They also have many minor uses, small in tonnage but huge in significance—for example, in medical lasers, data transmission fiber amplifiers, and a myriad of other uses.

References

Constantinides, S., 2012. The Demand for Rare Earth Materials in Permanent Magnets. Retrieved on August 13, 2013 from, http://www.arnoldmagnetics.com/Content1.aspx?id=4828, This website contains two articles: this one and COM 2012. Both are useful.

Gambogi, J., 2013. Rare Earths. USGS Geological Survey, Mineral Commodity Summaries, January 2013, USGS, Reston, VA.

Goonan, T.G., 2011. Rare Earth Elements – End Use and Recyclability. USGS Scientific Investigations Report 2100-5094, USGS, Reston, VA.

Gschneidner, K.A., 2011. The rare earth crisis-the supply/demand situation for 2010–2015. In: Material Matters, vol. 6, number 2. Aldrich Materials Science Sigma-Aldrich Corporation, Milwaukee, WI, USA, pp. 32–35. Retrieved on July 30, 2013 from, http://www.sigmaaldrich.com/technical-documents/articles/material-matters/the-rare-earth-crisis.html.

CHAPTER

Mining and Rare Earth Concentrate Production

3

This chapter describes rare earth (RE) mining and concentration. Its objectives are as follows:

(a) to discuss the three main types of rare earth ore deposits
(b) to indicate how these ores are mined and prepared for subsequent rare earth element extraction.

3.1 RARE EARTH DEPOSITS

There are three main types of rare earth mineral deposits:

(a) surface hydrothermal and carbonitite igneous deposits of bastnasite [(RE)CO_3F] and monazite [(RE)PO_4] in iron hydroxide and carbonate host rock (Kanazawa and Kamitimi, 2006)
(b) monazite [(RE)PO_4]-rich placer deposits in ocean and river beach sands (Moustafa and Abdelfattaha, 2010; Rao and Misra, 2009)
(c) weathered rare earth cation adsorption clays in subtropical South East Asia, mostly China (Bao and Zhao, 2008; Moldoveanu and Papangelakis, 2013).

3.2 IGNEOUS DEPOSITS

The largest sources of rare earth elements are igneous deposits of bastnasite and monazite. They account for more than 90% of rare earth element production: ~70% from bastnasite and 20% from monazite. By far the world's largest bastnasite-monazite deposit is at the Bayan Obo mine in Inner Mongolia (Kanazawa and Kamitani, 2006).

Smaller deposits are those near Laverton, Western Australia (Lynas, 2013a) and Las Vegas, Nevada (Pradip and Fuerstenau, 2013).

Ore from these deposits typically contains 5-15 mass% rare earth elements. The concentrates from mining and concentrating these ores typically contain 30-50 mass % rare earth elements. **It is these concentrates that are sent to a chemical plant for rare earth extraction, purification, and separation**, see Chapters 4 and 5.

Rare Earths. http://dx.doi.org/10.1016/B978-0-444-62735-3.00003-6

FIG. 3.1

Rare earth mine near Laverton, Western Australia. Notice the 55-m-deep open pit mine. The road into and out of the mine is at the bottom of the photograph.

Photograph courtesy of Gloria Rodgers, Lynas Corporation, Inc.

3.3 MINING

Mining of these deposits is done by open pit methods, see Fig. 3.1. Material is blasted from the pit walls and trucked up to the surface for upgrading and further processing.

Two types of material are distinguished in the pit—rare earth-rich ore and rare earth-lean waste. They are trucked up separately. The ore is sent forward for concentration and then for chemical rare earth element extraction. The waste is sent to a waste dump.

The ore and waste are often distinguished *in-pit* by hand-held portable X-ray fluorescence analyzers (Thermo, 2013).

3.4 EXTRACTING RARE EARTH ELEMENTS FROM MINED ORE

Rare earth elements are extracted from igneous ore by the following methods:

(a) producing a rare earth-rich concentrate by discarding most of the ore's worthless waste mineral particles, see this chapter

(b) extracting rare earth elements from this concentrate's bastnasite [$(RE)CO_3F$] and monazite [$(RE)PO_4$] particles, mostly by leaching, see Chapter 4

(c) producing a carbonate precipitate from (b)'s pregnant leach solutions

(d) sending the carbonate precipitate to a refinery where it is leached in aqueous chloride or nitrate solutions

(e) purifying, then separating the resulting rare earth ion solutions into individual pure rare earth ion solutions, mostly by computer-controlled solvent extraction, see Chapter 5
(f) precipitating individual pure rare earth compounds (e.g., oxides, phosphates) from these pure solutions
(g) using these compounds as-is; reducing them to metals; or making them into other useful compounds.

3.5 CONCENTRATE PRODUCTION

The concentration of rare earth minerals in rare earth ores is too low for immediate leaching/extraction. The ore's large quantity of waste minerals would interfere with leaching and would take too much equipment, materials handling, reagents, energy, and time.

This problem is minimized by physically removing worthless minerals from trucked-up ore by crushing, grinding, and froth flotation, see Figs. 3.2–3.5. This process is referred to as concentration. It removes about 70% of the ore's *waste* minerals.

The waste-removal process entails the following procedure:

(a) breaking the ore finely enough so that its rare earth minerals are liberated from its waste minerals
(b) collecting the rare earth minerals by froth flotation
(c) discarding the waste minerals in an underflow stream.

Magnetic separations are also used.

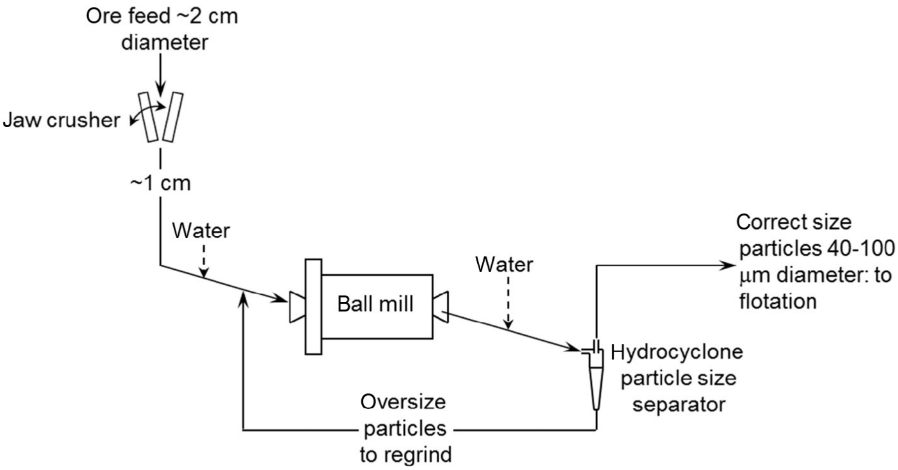

FIG. 3.2

Schematic flowsheet for producing rare earth mineral particles and waste mineral particles. These mineral particles are then separated by froth flotation, as shown in Fig. 3.3. The ball mill contains steel balls. The mill rotates continuously, causing these steel balls to cascade onto the ore, grinding it to a very fine size. The cyclone sends oversize particles back for more grinding. The process is continuous.

Flowsheet drawn by William Davenport.

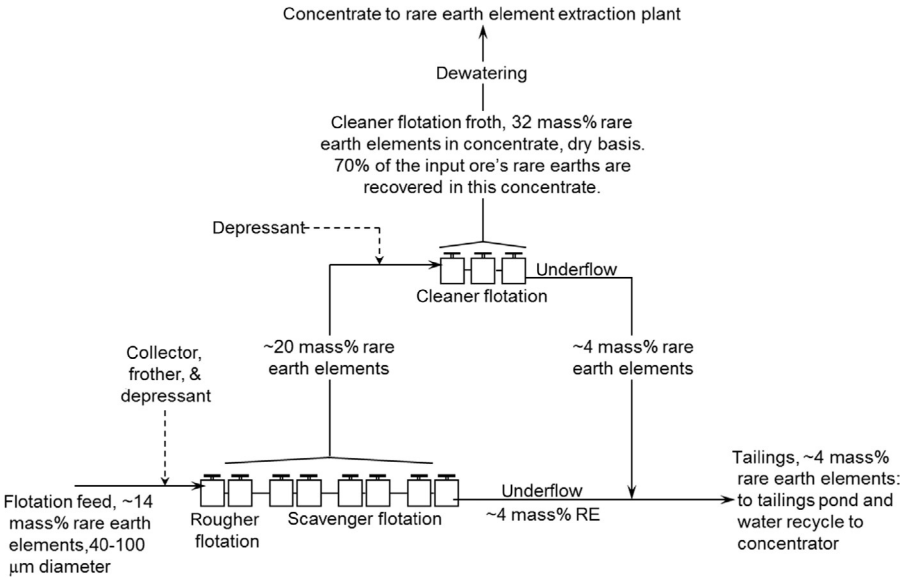

FIG. 3.3

Schematic flowsheet for floating rare earth mineral particles from waste mineral particles. The feed is finely ground ore-water slurry, pH ~ 9. The products are (i) rare earth mineral-rich *concentrate* and (ii) rare earth-lean waste tailings. The process is continuous. Figures 3.4 and 3.5 show a schematic flotation cell and a rising air bubble with attached water-repellent mineral particles. The process is continuous.

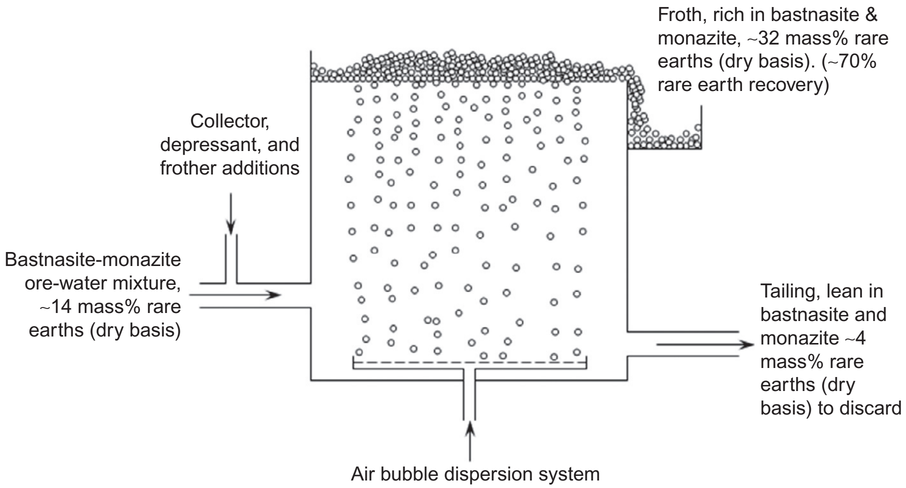

FIG. 3.4

Schematic of froth flotation cell. Ore-water slurry enters the cell, lower left. Collector is added to make rare earth minerals attach to the rising bubbles. Depressant is added to make waste minerals sink. Air bubbles are injected throughout the bottom. Frother causes the rare earth mineral particle-covered bubbles to form a froth, which overflows the cell, top right. The cells are cubic or cylindrical.

Crundwell et al., 2011.

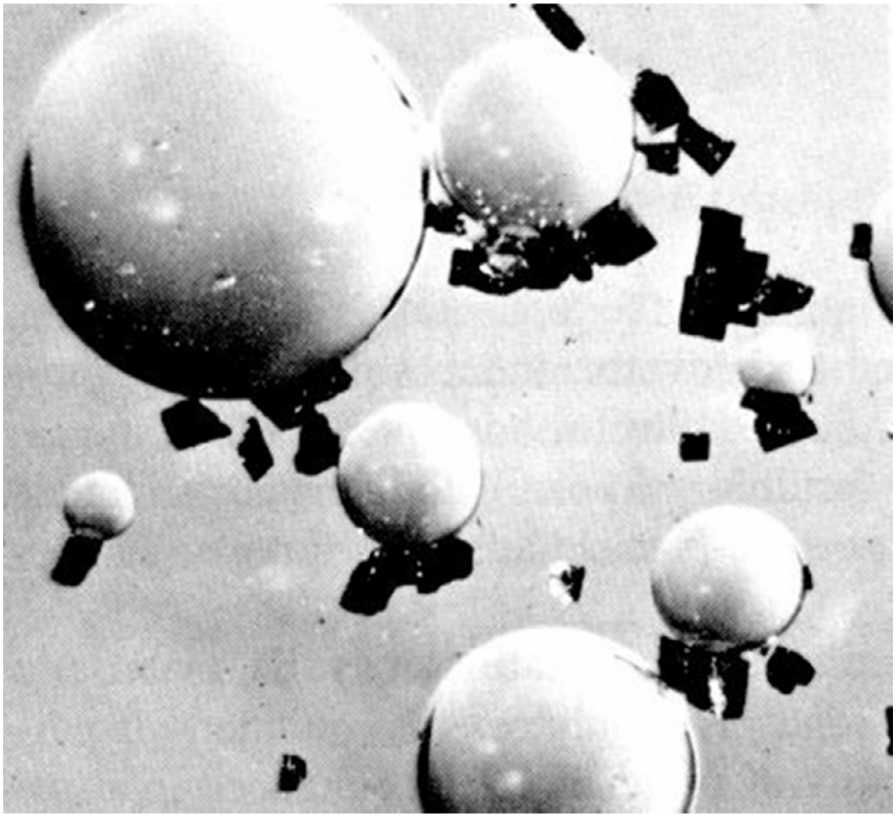

FIG. 3.5

Air bubbles rising in an ore particle-water slurry. Water-repellent minerals attach to rising bubbles and float. Water-*avid* particles do not attach—they sink (Crundwell et al., 2011).

The ore breaking is done by crushing, grinding, and cycloning (controlling particle size), see Fig. 3.2. The optimum particle size for rare earth froth flotation feed is 40-100 μm diameter (Lynas, 2013b; Pradip and Fuerstenau, 2013). Choice and control of particle size are discussed by Crundwell et al. (2011) and Schlesinger et al. (2011).

3.6 FROTH FLOTATION

The objective of froth flotation is to separate rare earth mineral particles from waste mineral particles. It does so by floating the rare earth mineral particles from ore-water slurry, while leaving the waste mineral particles behind in the slurry, see Fig. 3.3.

The process is continuous. It entails the following:

(a) preparing a ground ore particle-water slurry ~35 mass% solids in the slurry
(b) passing the slurry through a series of flotation cells

Table 3.1 Chemicals Used in Bastnasite-Monazite Flotation

Chemical	Purpose	Quantity (kg Per Tonne of Ore)
Tall oil (fatty acid)	Fatty acid bastnasite collector	0.35
Soda ash, Na_2CO_3	Waste mineral depressant	~3
Sodium fluosilicate	Waste mineral depressant	0.4
Ammonium lignin sulfonate	Waste mineral depressant	~3
Methyl isobutyl carbinol	Frother	
Flotation Conditions		
Slurry density	35 mass% solids in feed	
pH	~9	
Ore particle diameter	40-100 μm	

Alkyl hydroxamate is more selective than tall oil (Cytec, 2005). It is replacing tall oil in new applications.
The quantities are approximate.
Table prepared from author estimates and conference discussions.

(c) blowing small (~1 mm diameter) air bubbles up through the slurry
(d) creating chemical and physical conditions in the slurry whereby
  (i) rare earth mineral particles attach to the rising bubbles
  (ii) waste minerals do not attach so that they underflow the cell.

Zhang et al. (2013) report that hydroxamate collectors, dissolved in ore-water slurries, make bastnasite and monazite particles water-repellent. This causes the particles to be floated when they collide with rising air bubbles, see Figs. 3.4 and 3.5.

The ore's gangue minerals (e.g., hydroxides, carbonates) are not influenced by hydroxamates, so they do not attach to the rising bubbles. Flotation of these minerals is further suppressed by adding soda ash (Na_2CO_3), sodium fluosilicate (Na_2SiF_6), and/or ammonium lignin sulfonate depressants (Pradip and Fuerstenau, 2013). Table 3.1 gives details.

One other chemical is added to the ore particle-water slurry. It is frother, which creates a strong but short-lived air bubble froth that flows over the lip of the flotation cells, see Fig. 3.4. Methyl isobutyl carbinol is a commonly used frother (Pradip and Fuerstenau, 2013).

3.7 FLOTATION PRODUCT

The principal product of flotation is rare earth-rich overflow froth. It typically contains ~75 mass% water, most which is removed before the froth (now called concentrate) is shipped to chemical plants for rare earth extraction, purification, and separation, see Chapters 4 and 5.

The water is removed by overflowing it from froth settlers and filters. It is then recycled to the grinding circuit, see Fig. 3.3.

The second product is the rare earth-lean underflow slurry, called tailings. It is sent to a tailings pond where the water is drained. This water is also recycled to the grinding circuit. Most ore concentrators are designed for zero water discharge.

3.7.1 Flotation summary

Flotation is an effective way of preparing bastnasite-monazite ores for subsequent rare earth element extraction. Per tonne of rare earth element production, flotation confers the following advantages:

(a) It reduces the cost of shipping raw materials from the mine to a rare earth element extraction plant
(b) It simplifies leaching and decreases the amount of leach residue that has to be filtered and removed in the rare earth element extraction plant
(c) It minimizes the quantity of residue that has to be stored at the rare earth element extraction plant
(d) It decreases the capital and operating costs of concentrate leaching and rare earth recovery.

3.8 RARE EARTH BEACH SANDS

About 5% of the world's rare earth element production comes from monazite [(RE)PO_4)]-bearing high density beach sand deposits (Gambogi et al., 2013; Kanazawa and Kamitani, 2006; Fig. 3.6).

Other commercial dense minerals in the deposits are zircon $ZrSiO_4$ and rutile TiO_2. The high density sand deposits were formed by millions of years of (i) rock decomposition and (ii) river and wave forces.

Most beach sand monazite production comes from India, see Table 3.2. India has operated several plants for many years and is now constructing more to satisfy the world's need for additional rare earth production (Rao and Misra, 2009; Watanabe and Suzuki, 2012).

Figure 3.7 sketches a flowsheet for producing monazite concentrate from high-density beach sand. It is based on high-monazite-grade Indian beach sands.

Beach sand is dredged from the high-density sand deposits. Its high- and low-density components are then separated by gravity methods including spiral concentrators (Wills and Napier-Munn, 2006).

The high-density mineral material is then

(a) dried in a fluid bed dryer, and then
(b) separated into individual high-density minerals by magnetic, electrostatic, and density separations (Gupta and Krishnamurthy, 2005; Wills and Napier-Munn, 2006).

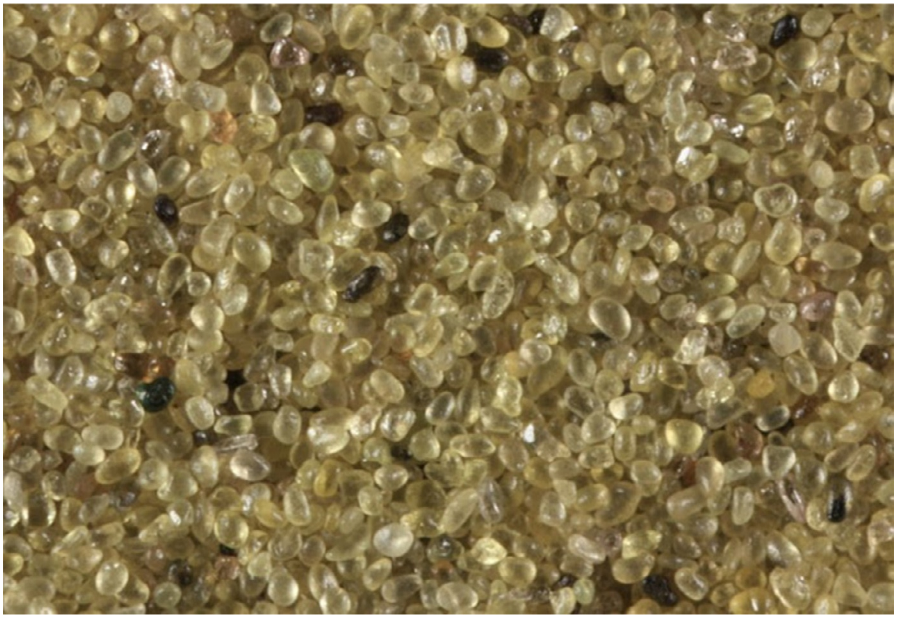

FIG. 3.6

Natural monazite sand particles (Sandatlas, 2012). They are about 100 μm in diameter.

Photograph courtesy Siim Sepp (www.sandatlas.org).

Table 3.2 Estimated Production of Monazite Concentrate from High-Density Beach Sands—*Tonnes of Contained Rare Earth Elements per Year* (Gambogi et al., 2013)

Country	2007	2008	2009	2010	2011
Brazil	230	200	180	150	150
India	3000	3000	3000	3100	3100
Malaysia	400	140	15	370	360
Vietnam	840	840	720	190	220
Total	4500	4200	3900	3800	3800

The numbers are approximate. Gambogi reports his data in tonnes of monazite concentrate per year. We have multiplied his tonnes of concentrate by 0.6 to obtain our rare earth element tonnes. India is the leading producer, followed by Vietnam. Many other countries have high density beach sands, for example, South Africa.

The resulting monazite concentrate is 97 mass% monazite mineral. Over 80% of the monazite in the initial dredged sand feed is recovered in the monazite concentrate.

This concentrate is now sent to chemical plants for rare earth extraction, purification, and separation, see Chapters 4 and 5.

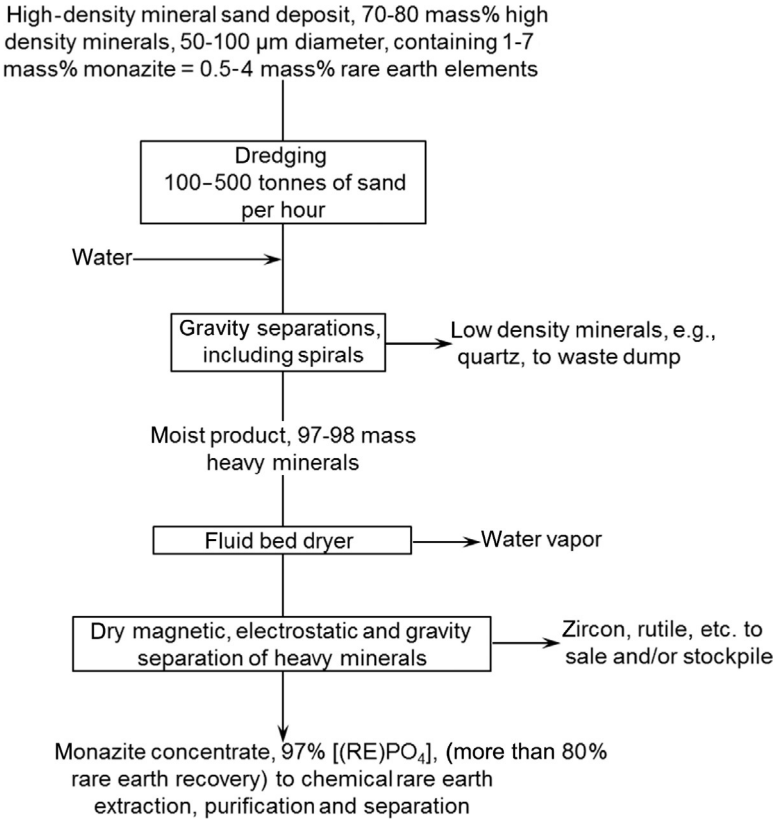

FIG. 3.7

Schematic flowsheet for recovering rich monazite concentrate from high density beach sand. Rare earth (RE) recovery to concentrate is more than 80%. Concentrate grade is 97 mass% $(RE)PO_4$ (~60 mass% rare earths). The concentrate is sent to a chemical rare earth element extraction/purification/separation plant. An advantage of monazite $[(RE)PO_4]$ is that it is environmentally easier to leach than bastnasite $[(RE)CO_3F]$, because it does not contain fluorine.

Drawing by William Davenport.

3.9 RARE EARTH CATION ADSORPTION CLAYS

The preceding sections describe igneous and beach sand rare earth ores. This section describes an upcoming rare earth source – rare earth cation adsorption clays. In 2014, they are expected to account for about 12 kilotonnes of rare earth element production per year.

These rare earth-rich clays contain 0.1-0.3 mass% rare earth elements, see Table 3.3 (Moldoveanu and Papangelakis, 2013). They were formed over millions

Table 3.3 Rare Earth Contents of Two Rare Earth Ion Adsorption Clay Ores (Moldoveanu and Papangelakis, 2013)

Element	Ore#1	Ore#2
Lanthanum	0.007	0.098
Cerium	0.006	0.020
Praseodymium	0.003	0.019
Neodymium	0.012	0.069
Samarium	0.004	0.018
Europium	0.000	0.001
Gadolinium	0.015	0.013
Terbium	0.004	0.002
Dysprosium	0.026	0.010
Holmium	0.005	0.002
Erbium	0.038	0.025
Thulium	0.004	0.002
Ytterbium	0.016	0.003
Lutetium	0.002	0.000
Total rare earth elements	*0.142*	*0.282*
Yttrium	0.157	0.047

Note the rather high concentrations of high-atomic-number (heavy) rare earth elements.

of years by natural leaching of rare earth-bearing granite rock—by warm tropical rain (1.5 m per year, 40 ºC) and vegetation acids. This natural leaching is continuing even today.

The advantages of these clay deposits are as follows:

(a) the deposits are soft and on the surface, so they are easily mined or *in situ* leached
(b) the clay particles are very fine (~5 μm diameter), so they do not require grinding before leaching
(c) their adsorbed rare earth ions are easily recovered by leaching (Moldoveanu and Papangelakis, 2013).

Their disadvantage is that their rare earth element concentrations are considerably lower (0.1-0.3 mass%) than those of igneous deposits (5-15 mass%) and beach sand deposits (0.5-4 mass%).

These low concentrations mean that much more ore must be treated per tonne of rare earth production and much more waste is left behind.

Rare earth concentrations vary through the ion adsorption clay deposits (Bao and Zhao, 2008). This might be used to maximize (i) overall rare earth recovery or (ii) recovery of specific high-price rare earths, for example, terbium, see Chapter 2.

3.10 DEPOSIT STRUCTURE

The precursors for rare earth ion adsorption clay deposits are

(a) granite (especially muscovite-bearing granite) rocks

that contain

(b) easily solubilized rare earth minerals, for example, doverite [$Ca(RE)(CO_3)_2F$].

Doverite is a particularly important precursor mineral because it contains relatively large quantities of expensive, high-atomic-number rare earth elements (i.e., Tb, Dy, and Lu). It transfers these expensive elements to rare earth ion adsorption clays during natural leaching (BaO and Zhao, 2008; Fig. 3.8).

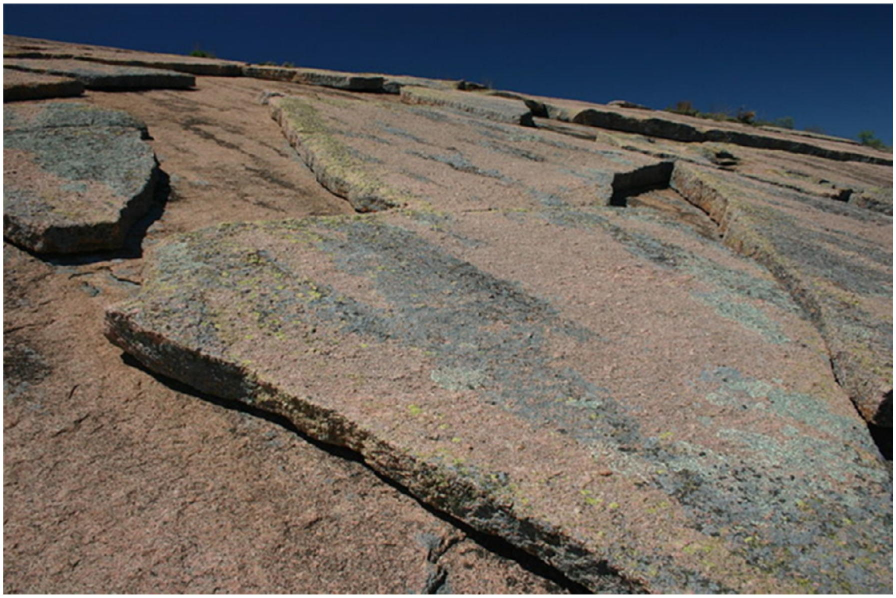

FIG. 3.8

Exfoliation of granite because of weathering (Exfoliation, 2005). This is the first step in clay formation. It continues over millions of years until the rock has become 5 μm-diameter mineral particles. The process is fastest in subtropical regions with high rainfalls (1.5 m per year) and warm temperatures (~40 °C).

Photo courtesy of Wikipedia.org (Creative Commons License).

3.11 ION ADSORPTION CLAY FORMATION

Rare earth ion adsorption clays are formed by millions of years of

(a) trickling warm vegetative acid through granite rock, causing the granite to exfoliate and eventually form fine (~5 μm diameter) clay particles, for example, muscovite [$KAl_2(AlSi_3O_{10})(F,OH)_2$] particles (Muscovite, 2013; Fig. 3.9).

(b) leaching of some rare earth mineral particles, for example, doverite, by reactions such as

$$\underset{\text{doverite}}{2\left[\mathrm{Ca(RE)(CO_3)_2F}\right](s)} + \underset{\text{natural tannic acid}}{6H^+(aq) + 6(\text{tannin})^-(aq)} + \underset{\text{oxygen from air}}{1.5O_2(g)}$$

$$\rightarrow \underset{\text{leached doverite}}{2\left[\mathrm{Ca(H_2O)_{1.5}(CO_3)_2F}\right](s)} + \underset{\text{rare earth cation}}{2RE^{3+}(aq)} + \underset{\text{tannic acid anion}}{6(\text{tannin})^-(aq)} \qquad (3.1)$$

(c) adsorption of the newly released rare earth cations on muscovite clay particles.

(c)'s adsorption step is promoted by the presence of electrically charged surfaces on muscovite (and similar clay minerals), Tong (2000). Positive ions such as Tb^{3+} are

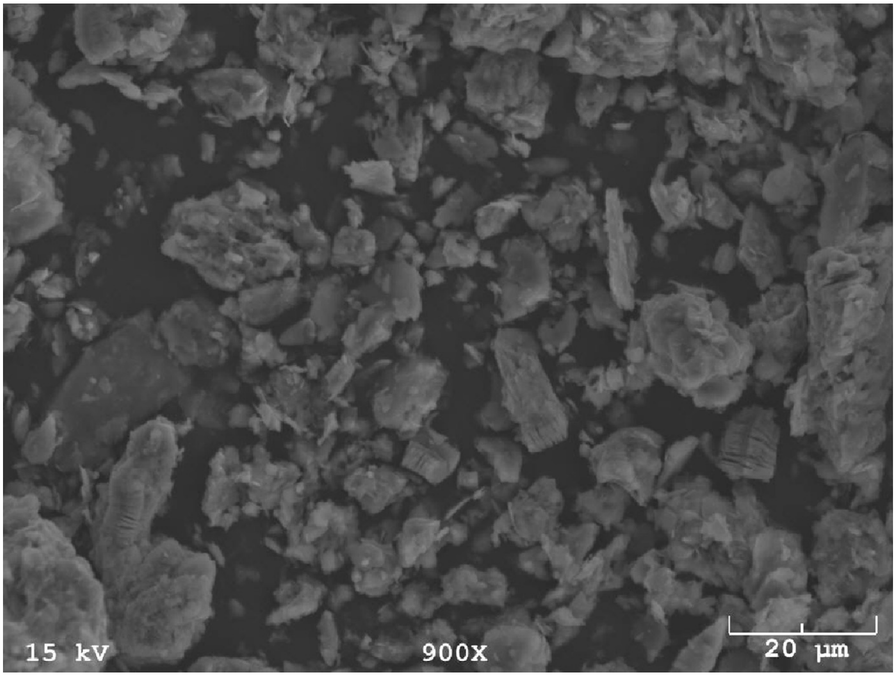

FIG. 3.9

Rare earth adsorption clay. The clay particles are all <20 μm in diameter.

Photograph courtesy of Vladimiros Papangelakis, University of Toronto.

attracted to muskovite's negatively charged surface while the companion negative ions (e.g., tannic acid anions) are attracted to muskovite's positively charged surfaces.

The negatively charged surfaces with their adsorbed rare earth cations may be represented by the formula:

$$\left[\mathrm{KAl_2(AlSi_3O_{10})(F,OH)_2}\right]_a \cdot b(\mathrm{RE})^{3+}$$

where *a* and *b* indicate that the surfaces adsorb variable numbers of rare earth cations (Moldoveanu and Papangelakis, 2013).

3.12 COMMERCIAL LEACHING OF THE CLAYS

The most common methods of leaching rare earth cation adsorption clays are *heap* and *in situ* leaching, using

> aqueous ammonium sulfate lixiviant, pH 3-4, ambient temperature, and pressure.

The reactions are represented by

$$\underbrace{\left[\mathrm{KAl_2(AlSi_3O_{10})(F,OH)_2}\right]_a \cdot b(\mathrm{RE})^{3+}(s)}_{\text{clay particles with adsorbed rare earth cations}} + \underbrace{3b\mathrm{NH_4^+}(aq) + 1.5b\mathrm{SO_4^{2-}}(aq)}_{\text{aqueous ammonium sulfate solution}}$$

$$\rightarrow \underbrace{\left[\mathrm{KAl_2(AlSi_3O_{10})(F,OH)_2}\right]_a \cdot 3b\mathrm{NH_4^+}(s)}_{\text{clay particles with adsorbed ammonium cations}} + \underbrace{b(\mathrm{RE})^{3+}(aq) + 1.5b\mathrm{SO_4^{2-}}(aq)}_{\text{aqueous rare earth sulfate solution}} \quad (3.2)$$

Other monovalent ions, for example, $\mathrm{Na^+}$ also work, but $\mathrm{NH_4^+}$ has the following advantages:

(a) aqueous ammonium sulfate is readily available and inexpensive
(b) it extracts rare earth ions very efficiently, yielding up to 90% extraction.

Divalent ions have also been tried but they tend to be less effective (Moldoveanu and Papangelakis, 2012).

$\mathrm{SO_4^{2-}}$ is chosen as the lixiviant anion because it is the most practical from the cost and environmental points of view. $\mathrm{Cl^-}$ could also be used, but it is harmful to the environment.

3.13 INITIAL RARE EARTH OXIDE PRODUCTION

Rare earth oxide production from rare earth ion adsorption clay entails the following:

(a) clarifying the product leach solution
(b) reacting the clarified solution with ammonium bicarbonate (ambient temperature and pressure) to form rare earth carbonates, that is,

$$\underbrace{\mathrm{(RE)_2(SO_4)_3(aq)}}_{\text{product leach solution}} + \underbrace{\mathrm{3NH_4HCO_3(s)}}_{\text{ammonium bicarbonate}} \rightarrow \underbrace{\mathrm{(RE)_2(CO_3)_3(s)}}_{\text{carbonate precipitate}} + \underbrace{\mathrm{3[NH_4HSO_4](aq)}}_{\text{ammonium bisulfate solution}} \quad (3.3)$$

These carbonates are now sent to chemical plants for rare earth extraction, purification, and separation, see Chapters 4 and 5 (Fig. 3.10).

FIG. 3.10

Oxalate product from extraction of rare earths from cation adsorption clays. It contains about 20 mass% rare earth elements, with quite high concentrations of expensive high-atomic-number (heavy) rare earth elements. Photograph courtesy of Professor Atsushi Shibayama, Akita University. This product is roasted to rare earth oxide, which is sent to chemical plants for rare earth extraction, purification, and separation. Oxalate precipitation has now been largely replaced by carbonate precipitation.

3.14 SUMMARY

Rare earth elements occur mainly in bastnasite-monazite igneous ores, monazite beach sands, and rare earth cation adsorption clays. They are all mined by surface mining techniques.

Bastnasite-monazite igneous ores are concentrated by froth flotation removal of waste rock before being sent to chemical rare earth leaching/purification/separation plants for pure individual rare earth compound production.

Monazite beach sands are upgraded by gravity/electrostatic/magnetic waste rock removal techniques before being sent to a rare earth leaching/purification/separation plant for individual pure rare earth compound production.

Rare earths are recovered from cation adsorption clays by (i) aqueous ammonium sulfate leaching; (ii) rare earth carbonate precipitation, and sometimes (iii) precipitate oxidation. The resulting oxides are then sent to a chemical rare earth leaching/purification/separation plant for pure individual rare earth compound production.

The final products after all these steps are individual rare earth precipitates, for example, oxides, phosphates, and fluorides. They are used in this form (e.g., cerium oxide polishing powder), reduced to metals, or made into other useful compounds, for example, nitrates.

References

Bao, Z., Zhao, Z., 2008. Geochemistry of mineralization with exchangeable REY in the weathering crusts of granitic rocks in South China. Ore Geol. Rev. 33, 519–535.

Crundwell, F.K., Moats, M.S., Ramachandran, V., Robinson, T.G., Davenport, W.G., 2011. Extractive Metallurgy of Nickel, Cobalt and Platinum-Group Metals. Elsevier, Oxford, England.

Cytec, 2005. Using Cytec's Alkyl Hydroxamate Collectors to Improve Flotation Results. Retrieved on August 13, 2013 from, https://www.cytec.com/specialty-chemicals/PDFs/Mineralprocessing/AHXCollectorsToImproveFlotationResults.pdf.

Exfoliation, 2005. Exfoliation Joint. Retrieved on August 13, 2013 from, http://en.wikipedia.org/wiki/Exfoliation_(geology).

Gambogi, J., Jackson, M.L., Miller, L.D., 2013. Thorium [advance release]. 2011 Minerals Yearbook. U.S. Geological Survey, Washington, DC, Retrieved on August 13, 2013 from http://minerals.usgs.gov/minerals/pubs/commodity/thorium/myb1-2011-thori.pdf.

Gupta, C.K., Krishnamurthy, N., 2005. Extractive Metallurgy of Rare Earths. CRC Press, Boca Raton, FL.

Kanazawa, Y., Kamitani, M., 2006. Rare earth minerals and resources in the world. J. Alloys Compd. 408–412, 1339–1343.

Lynas, 2013a. Mount Weld. Retrieved on August 13, 2013 from, http://www.lynascorp.com/Pages/mount-weld.aspx.

Lynas, 2013b. Concentration Plant. Retrieved on August 13, 2013 from, http://www.lynascorp.com/SiteCollectionDocuments/Fact%20Sheets/Concentration_Plant.pdf.

Moldoveanu, G.A., Papangelakis, V.G., 2012. Recovery of rare earth elements adsorbed on clay minerals: I. Desorption mechanism. Hydrometallurgy. 117–118, 71–78.

Moldoveanu, G.A., Papangelakis, V.G., 2013. Recovery of rare earth elements adsorbed on clay minerals: II. Leaching with ammonium sulfate. Hydrometallurgy. 131–132, 158–166.

Moustafa, M.I., Abdelfattah, N.A., 2010. Physical and chemical beneficiation of the Egyptian beach monazite. Resour. Geol. 60, 288–299.

Muscovite, 2013. Muskovite. Retrieved on August 13, 2013 from, http://en.wikipedia.org/wiki/Muscovite.

Pradip, Fuerstenau, D.W., 2013. Design and development of novel flotation reagents for the beneficiation of Mountain Pass rare-earth ore. Miner. Metall. Process. 30 (1), 1–9.

Rao, N.S., Misra, S., 2009. Sources of monazite sand in southern Orissa Beach placer, eastern India. J. Geol. Soc. India. 74, 357–362.

Sandatlas, 2012. Monazite. Retrieved on August 13, 2013 from, http://www.sandatlas.org/2012/02/monazite.

Schlesinger, M., King, M.J., Sole, K.C., King, M., Davenport, W.G., 2011. Extractive Metallurgy of Copper, fifth ed. Elsevier, Oxford, England.

Thermo, 2013. Portable XRF Analyzers. Retrieved on August 13, 2013 from, http://www.niton.com/en/mining.

Tong, W.K., 2000. Introduction to Clay Minerals and Soils. Retrieved on August 13, 2013 from, http://www.oakton.edu/user/4/billtong/eas100/clays.htm.

Watanabe, C., Suzuki, I., 2012. Japan signs deal with India on rare earth production, supply. Bloomberg News. Retrieved on August 13, 2013 from http://www.bloomberg.com/news/2012-11-16/japan-signs-deal-with-india-on-rare-earth-production-supply.html.

Wills, B.A., Napier-Munn, T., 2006. Mineral Processing Technology. Butterworth-Heinemann, Oxford, UK.

Zhang, X., Du, H., Wang, X., Miller, J.D., 2013. Surface chemistry considerations in the flotation of rare-earth and other semisoluble salt minerals. Miner. Metall. Eng. 30 (1), 24–37.

Suggested Reading

Government of India, 2012. Indian Rare Earths Limited. Retrieved on August 13, 2013 from, http://www.irel.gov.in/scripts/Mining_Mineral.asp.

CHAPTER

Extracting Rare Earth Elements from Concentrates

4

Chapter 3 describes production of two physical concentrates:

- **(a)** bastnasite-monazite flotation concentrates and
- **(b)** monazite beach sand concentrates

This chapter describes how these materials are made into mixed rare earth-rich chemical concentrates—ready for purification, rare earth element separation, and marketable product preparation. Its objectives are to describe

- **(a)** today's industrial rare earth minerals,
- **(b)** the principal methods of treating these minerals to produce soluble mixed rare earth precipitate—ready for subsequent rare earth purification and separation (Fig. 4.3), and
- **(c)** radioactive element removal.

Figs. 4.1 and 4.2 show an example of rare earth extraction feed and product. Chapter 5 describes how material shown in Fig. 4.2 is purified and made into marketable individual rare earth products (e.g., mostly oxides).

4.1 INDUSTRIAL RARE EARTH MINERALS

Rare earth elements are present in many different types of minerals, for example phosphates, carbonates, fluorocarbonates, silicates, polymetallic oxides, and fluorides. However, only a few of them are being exploited, Table 4.1.

Three main criteria are important in assessing the applicability of a given mineral to industrial rare earth production:

- **(a)** mineral type (phosphate, carbonate, etc.), which determines the extraction technique that must be used,
- **(b)** rare earth content of the mineral, which determines how much ore must be mined and processed per ton of product rare earth element, and
- **(c)** the amount of each rare earth (e.g., lanthanum, dysprosium) in the final product, which determines final product sales price (basket value).

Rare Earths. http://dx.doi.org/10.1016/B978-0-444-62735-3.00004-8

FIG. 4.1

Monazite flotation concentrate. It is a starting material for rare earth element extraction, Fig. 4.3. It contains ~30 mass% rare earth elements, dry basis. Its treatment is described in Fig. 4.3.

Photograph courtesy of Alain Rollat.

FIG. 4.2

Mixed rare earth carbonate precipitate. It is the final product of the extraction processing described in this chapter. It is also the feed to refinery/rare earth separation plant shown in Chapter 5. It contains about 95 mass% rare earth carbonates and 5 mass% impurity carbonates, dry basis.

Photograph courtesy of Alain Rollat.

Table 4.1 Formulae of Major Minerals Containing Rare Earths

Mineral	Formula	Type	REO Max (%)	Type of REE
Apatite[a]	$(Ca,Ce)_5\{(P,Si)O_4\}_3(F,Cl,OH)$	Phosphate	12	LRE
Bastnasite[a]	$(Ce,La,Y)(CO_3)F$	Carbonate	75	LRE
Churchite[b]	$YPO_4\cdot 2H_2O$	Phosphate	44	HRE
Eudialyte[b]	$Na_{15}Ca_6(Fe,Mn)_3Zr_3(Si,Nb)Si_{25}O_{73}(OH,Cl,H_2O)_5$	Silicate	10	LRE+HRE
Fergusonite[b]	$(Y,Er,U,Th)(Nb,Ta,Ti)O_4$	Oxide	46	LRE+HRE
Laterite (ionic clays)[c]	(Al,Si)Ox,RE	Alimino silicate	0.2	HRE
Loparite[a]	$(Na,Ca,Y,Ce)(Nb,Ti)O_3$	Oxide	34	LRE
Monazite[a]	$(Ce,La,Pr,Nd,Th,Y)PO_4$	Phosphate	71	LRE
Pyrochlore[d]	$(Na,Ca,Ce)_2Nb_2O_6F$	Oxide	6	LRE
Xenotime[c]	YPO_4	Phosphate	62	HRE
Yttrosynchisite[c]	$(Ce,Y)FCO_3$	Carbonate	50	LRE+HRE

REO, rare earth oxide; LRE, low atomic number (light) rare earths; HRE, high atomic number (heavy) rare earths.

[a] *Minerals that have already been mined for low atomic number (light) rare earth elements.*

[b] *Minerals that are being considered for new high atomic number (heavy) rare earth elements mining projects.*

[c] *Minerals that have already been mined for high atomic number (heavy) rare earth elements.*

[d] *Minerals that are being considered for new low atomic number (light) rare earth elements mining projects.*

Item (c) arises because rare earth prices vary considerably from element to element, Chapter 2. In early 2014, for example, the price of 99 mass% pure lanthanum oxide was ~US$6 per kilogram while the price of 99 mass% pure dysprosium oxide was ~US$475 per kilogram.

Table 4.2 shows the distribution of individual rare earths (plus yttrium) in several rare earth deposits around the world.

4.2 INDUSTRIAL RARE EARTH EXTRACTION

The starting points for rare earth extraction are the concentrates described at the beginning of this chapter. The objective of rare earth extraction is to get the rare earth elements of these concentrates into a product that can be purified and separated into individual high purity rare earth elements.

Table 4.2 Rare Earth Distribution in Rare Earth Deposits Around the World, Where REO Is the Total Rare Earth Oxide

	Typical Low Atomic Number Minerals Compositions			**Typical High Atomic Number Minerals Compositions**			
Bearing mineral	**Bastnasite**	**Monazite**	**Apatite**	**Ionic clay**	**Xenotime**	**Eudyalite**	**Fergusonite**
Chemical composition	Fluorocarbonate	Phosphate	Phosphate	Aluminosilicate	Phosphate	Silicate	Oxide
Deposit	Bayan Obo	Steenkampskraal	Kola	Xun Wu	Lofdal	Kipawa	Thor Lake
Country	China	South Africa	Russia	China	Namibia	Canada	Canada
La_2O_3/REO	26.9%	21.6%	26.0%	30.0%	1.3%	14.6%	14.9%
CeO_2/REO	50.9%	46.6%	47.0%	3.0%	2.4%	29.5%	32.6%
Pr_6O_{11}/REO	5.0%	5.0%	4.0%	7.0%	0.2%	3.5%	4.1%
Nd_2O_3/REO	15.2%	16.7%	15.0%	26.4%	0.9%	13.4%	16.5%
Sm_2O_3/REO	1.2%	2.5%	1.7%	5.1%	0.8%	3.0%	3.7%
Eu_2O_3/REO	0.2%	0.1%	0.5%	0.7%	0.6%	0.4%	0.5%
Gd_2O_3/REO	0.3%	1.6%	1.5%	4.2%	3.9%	3.0%	3.8%
Tb_4O_7/REO	<0.1%	<0.1%	0.1%	0.7%	1.2%	0.5%	0.6%
Dy_2O_3/REO	0.1%	0.7%	0.2%	2.9%	8.9%	3.4%	3.5%
Ho_2O_3/REO	<0.1%	<0.1%	<0.1%	0.4%	2.0%	0.8%	0.7%
Er_2O_3/REO	<0.1%	<0.1%	<0.1%	1.4%	6.1%	2.5%	1.7%
Tm_2O_3/REO	<0.1%	<0.1%	<0.1%	0.3%	0.9%	0.4%	0.2%
Yb_2O_3/REO	<0.1%	<0.1%	<0.1%	1.1%	5.8%	2.3%	1.4%
Lu_2O_3/REO	<0.1%	<0.1%	<0.1%	0.2%	0.8%	0.3%	0.2%
Y_2O_3/REO	0.2%	5.0%	3.0%	17.3%	64.2%	22.3%	15.7%

The following sections describe the rare earth extraction processes used for the most important industrial minerals shown in Table 4.1—that is bastnasite, monazite, and xenotime.

4.3 EXTRACTION FROM MONAZITE AND XENOTIME ORES

Monazite ((Ce,La,Pr,Nd,Th,Y)PO_4) is a low atomic number (light) rare earth (plus thorium) phosphate mineral. Monazite and bastnasite are currently the two most exploited light rare earth minerals.

Xenotime is a high atomic number (heavy) rare earth (plus thorium) phosphate mineral. It was the main source of high atomic number rare earths until China's recent exploitation of its rare earth cation adsorption clays.

These minerals are treated by leaching as described in the next three subsections. This in spite of the fact that they have very different crystal structures

monazite is monoclinic and
xenotime is tetragonal.

Two leaching processes are used—depending on rare earth mineral concentrations in the concentrate feed:

(a) Caustic soda leaching is used for concentrates containing above ~70-80 mass% rare earth minerals.

(b) Sulfuric acid leaching is used for concentrates containing below ~70 mass% rare earth minerals. Sulfuric acid is cheaper than caustic soda, so it is used when reagent consumption is large.

4.3.1 Caustic soda leaching

Caustic soda leaching of monazite entails reacting the concentrate feed with aqueous caustic soda solution in an autoclave or open tank at 140-180 °C.

The equivalent pressure in the autoclave is 0.5-5 bar above ambient pressure.

The reactions are represented (RE, rare earth elements) by:

$$\underset{\text{in concentrate feed}}{(RE)PO_4(s)} + \underset{\substack{\text{supersaturated aqueous}\\ \text{caustic solution}}}{3NaOH(aq)} \xrightarrow{140\text{-}180\,°C} \underset{\substack{\text{byproduct sodium}\\ \text{phosphate solution}}}{Na_3PO_4(aq)} + \underset{\substack{\text{solid rare earth}\\ \text{hydroxide product}}}{(RE)(OH)_3(s)} \tag{4.1}$$

The solid rare earth hydroxide product is then sent to the purification/rare earth separation plant for aqueous hydrochloric acid releaching and rare earth purification/separation/product precipitation (Fig. 4.3 where "rare earth hydroxide product" is called "mixed rare earth chemical concentrate").

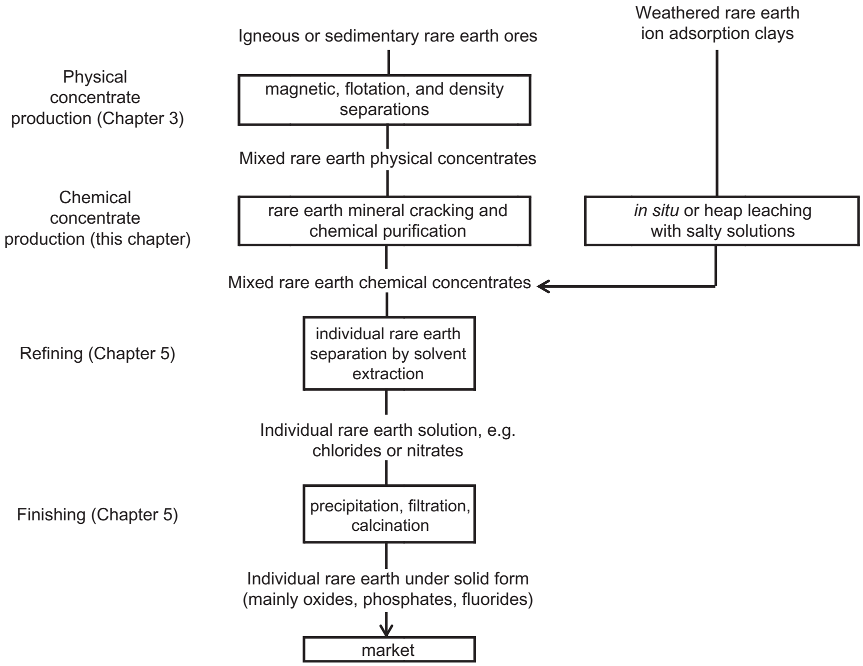

FIG. 4.3

Schematic flowsheet showing rare earth concentrate production (top, this chapter) and rare earth purification/separation/product preparation (bottom, Chapter 5).

Monazite always contains thorium as well as rare earth elements. Thorium's phosphate also reacts with aqueous caustic soda by the reaction:

$$\underset{\text{in concentrate feed}}{Th_3(PO_4)_4(s)} + \underset{\substack{\text{aqueous caustic}\\\text{solution}}}{12NaOH(aq)} \xrightarrow{140\text{-}180^\circ C} \underset{\substack{\text{byproduct sodium}\\\text{phosphate solution}}}{4Na_3PO_4(aq)} + \underset{\substack{\text{solid thorium}\\\text{hydroxide product}}}{3Th(OH)_4(s)} \tag{4.2}$$

This thorium product is subsequently removed from the system by hydrochloric acid leaching, selective precipitation, and solvent extraction.

Xenotime leaching is much the same as described by Reaction (4.2). However, xenotime is somewhat more difficult to leach—so that it is leached at a higher temperature and with a higher Na(OH)/mineral ratio.

The above leaching is sometimes combined with grinding. Grinding minimizes hydroxide layer formation on the mineral surfaces, thereby increasing leaching rate and efficiency. This grinding entails

(a) mixing the feed concentrate with caustic solution and
(b) grinding the resulting slurry in a small ball mill.

4.3.2 Advantages of caustic soda leaching

Caustic soda leaching has three major advantages:

- **(a)** The rare earths and thorium hydroxide products are easily prepared for solvent extraction purification and rare earth separation—by hydrochloric or nitric acid leaching.
- **(b)** Sodium phosphate can be sold as a byproduct.
- **(c)** The chemical reactions do not produce any liquid wastes, Reaction (4.1).

4.3.3 Acid baking process

Low grade monazite and xenotime concentrates are usually not leached by the above-described caustic soda method for economic reason. This is because non-rare earth minerals will also react with caustic soda and therefore consume an expensive chemical reagent.

These concentrates are usually treated by sulfuric acid baking, for example in Lynas Corporation's new leach plant in Gebeng, Malaysia.

The leaching (so-called acid baking) is done in rotating kilns, Fig. 4.4.

The reactions are (RE, rare earth elements)

$$\underset{\text{in concentrate feed}}{2(\mathrm{RE})\mathrm{PO}_4(\mathrm{s})} + \underset{\substack{\text{aqueous sulfuric}\\ \text{acid solution}}}{3\mathrm{H}_2\mathrm{SO}_4(\mathrm{aq})} \xrightarrow{200\text{-}500\,^\circ\mathrm{C}} \underset{\substack{\text{byproduct phosphoric}\\ \text{acid solution}}}{2\mathrm{H}_3\mathrm{PO}_4(\mathrm{aq})} + \underset{\substack{\text{solid rare earth}\\ \text{product}}}{(\mathrm{RE})_2(\mathrm{SO}_4)_3(\mathrm{s})} \tag{4.3}$$

$$\underset{\text{in concentrate feed}}{\mathrm{Th}_3(\mathrm{PO}_4)_4(\mathrm{s})} + \underset{\substack{\text{aqueous sulfuric}\\ \text{acid solution}}}{6\mathrm{H}_2\mathrm{SO}_4(\mathrm{aq})} \xrightarrow{200\text{-}500\,^\circ\mathrm{C}} \underset{\substack{\text{byproduct phosphoric}\\ \text{acid solution}}}{4\mathrm{H}_3\mathrm{PO}_4(\mathrm{aq})} + \underset{\substack{\text{solid thorium}\\ \text{sulfate}}}{3\mathrm{Th}(\mathrm{SO}_4)_2(\mathrm{s})} \tag{4.4}$$

and dehydration of phosphoric acid:

$$\underset{\substack{\text{byproduct phosphoric}\\ \text{acid}}}{2\mathrm{H}_3\mathrm{PO}_4(\mathrm{aq})} \xrightarrow{200\text{-}500\,^\circ\mathrm{C}} \underset{\substack{\text{pyrophosphoric}\\ \text{acid}}}{\mathrm{H}_4\mathrm{P}_2\mathrm{O}_7(\mathrm{aq})} + \underset{\text{water vapor}}{\mathrm{H}_2\mathrm{O}(\mathrm{g})} \tag{4.5}$$

Sulfuric acid evolves sulfur oxide gases during the process. These must be efficiently treated for environmental reasons.

As with caustic soda leaching, the reagent to mineral ratio is usually higher for xenotime treatment than for monazite treatment.

The baked kiln product is leached in water to produce impure rare earth sulfate solution. This solution is

- **(a)** purified by several steps of pH adjustment and precipitation/filtration and
- **(b)** sent to solvent extraction for purification, rare earth separation, and marketable product precipitation.

FIG. 4.4

Lynas Corporation's sulfuric acid baking kilns at Gebeng, Malaysia.

Photo courtesy of Alain Rollat.

4.4 BASTNASITE LEACHING

Bastnasite is a low atomic number (light) rare earths fluorocarbonate with thorium as an impurity. In 2013, it is by far the main source of low atomic number rare earth elements—as a byproduct of the iron ore mine at Bayan Obo, Inner Mongolia. The following three sections describe rare earth extraction from bastnasite ore.

4.4.1 Roast-hydrochloric acid leach process

The roast-hydrochloric acid leach process was pioneered and used by Molycorp, Inc., to recover rare earth elements from its Mountain Pass, California mine. It was used until the mid-1990s but is now obsolete.

The process entailed

(a) calcining bastnasite concentrate at 600-700 °C in air—thereby removing fluorine gas and oxidizing the concentrate's cerium to Ce^{4+},

(b) leaching the calcined product with hydrochloric acid to give an impure rare earth chloride solution, and

(c) purification of the solution by selective precipitation. Removal of radioactive impurities was particularly important at this stage.

The main chemical reactions were (RE, rare earths)

$$2CeFCO_3(s)\text{in concentrate feed} + \underset{\text{water}}{H_2O(l)} + \underset{\text{in air}}{0.5O_2(g)} \xrightarrow{600\text{-}700\,^\circ C} \underset{\text{cerium oxide}}{2CeO_2(s)} + \underset{\text{carbon dioxide}}{2CO_2(g)} + \underset{\text{gaseous hydrofluoric acid}}{HF(g)} + \underset{\text{steam}}{H_2O(g)} \tag{4.6a}$$

$$\underset{\text{in concentrate feed}}{3(RE)FCO_3(s)} + \underset{\text{water}}{H_2O(l)} \xrightarrow{600\text{-}700\,^\circ C} \underset{\text{rare earth oxide}}{(RE)_2O_3(s)} + \underset{\text{rare earth oxyfluoride}}{(RE)OF(s)} + \underset{\text{carbon dioxide}}{3CO_2(g)} + \underset{\substack{\text{hydrofluoric}\\\text{acid}}}{2HF(g)} \tag{4.6b}$$

$$\underset{\text{rare earth oxide}}{(RE)_2O_3(s)} + \underset{\text{rare earth oxyfluoride}}{(RE)OF(s)} + \underset{\substack{\text{hydrochloric}\\\text{acid}}}{9HCl(aq)} \xrightarrow{60\text{-}80\,^\circ C} \underset{\substack{\text{rare earth chloride}\\\text{solution}}}{3(RE)Cl_3(aq)} + \underset{\text{water}}{4H_2O(aq)} + \underset{\substack{\text{aqueous}\\\text{hydrofluoric}\\\text{acid solution}}}{HF(aq)} \tag{4.7}$$

The impure cerium oxide from Reaction (4.6a) was valorized after some physical treatments as a polishing powder.

The chloride solution from Reaction (4.7) was then sent to solution purification and on to solvent extraction purification/separation/product precipitation.

The main problem with this process was that the impure cerium still contains some radioactive thorium. This problem led Molycorp, Inc., to design a completely new bastnasite concentrate leach process based on caustic soda, described in the following section.

4.4.2 Caustic soda leaching

Caustic soda leaching of bastnasite concentrate is represented by the reactions:

$$\underset{\text{in concentrate feed}}{(RE)FCO_3(s)} + \underset{\substack{\text{supersaturated aqueous}\\\text{caustic solution}}}{3NaOH(aq)} \xrightarrow{120-130\,^\circ C} \underset{\substack{\text{solid rare earth}\\\text{product}}}{(RE)(OH)_3(s)} + \underset{\text{aqueous solution}}{NaF(aq) + Na_2CO_3(aq)} \tag{4.8}$$

After cooling, the rare earth hydroxide is removed from the product solution, and then dissolved into hydrochloric acid, that is:

$$\underset{\substack{\text{solid rare earth}\\\text{hydroxide}}}{(RE)(OH)_3(s)} + \underset{\substack{\text{hydrochloric}\\\text{acid}}}{3HCl(aq)} \rightarrow \underset{\text{rare earth chloride solution}}{(RE)Cl_3(aq) + 3H_2O(aq)} \tag{4.9}$$

Radioactive thorium chloride is also dissolved by the hydrochloric acid. It is removed from the solution as thorium hydroxide ($Th(OH)_4$). Barium chloride and sodium sulfate are also added to co-precipitate radium as radium/barium sulfate.

The rare earth chloride solution is then sent to solvent extraction for purification/rare earth separation and precipitation of marketable compounds, mostly oxides, phosphates, and fluorides.

The advantages of this process are

(a) fluorine is removed as sodium fluoride in aqueous solution thereby avoiding complex processing of gaseous hydrofluoric acid,
(b) solid waste production is minimized, and
(c) thorium and radium are efficiently removed.

4.4.3 Sulfuric acid baking

Sulfuric acid baking is popular in China because it is cheaper than caustic soda leaching. It is represented by the reactions:

$$\underset{\text{in concentrate feed}}{2(\mathrm{RE})\mathrm{FCO}_3(s)} + \underset{\text{sulfuric acid}}{3\mathrm{H}_2\mathrm{SO}_4(l)} \xrightarrow{200\text{-}500\,^\circ\mathrm{C}} \underset{\substack{\text{product rare earth}\\ \text{sulfate}}}{(\mathrm{RE})_2(\mathrm{SO}_4)_3(s)} + \underset{\substack{\text{hydrofluoric}\\ \text{acid gas}}}{2\mathrm{HF}(g)} + 2\mathrm{CO}_2(g) + 2\mathrm{H}_2\mathrm{O}(g) \tag{4.10}$$

and

$$\underset{\substack{\text{impurity in}\\ \text{concentrate feed}}}{\mathrm{Th}_3(\mathrm{FCO}_3)_4(s)} + \underset{\text{sulfuric acid}}{6\mathrm{H}_2\mathrm{SO}_4(l)} \xrightarrow{200\text{-}500\,^\circ\mathrm{C}} \underset{\substack{\text{solid thorium}\\ \text{sulfate}}}{3\mathrm{Th}(\mathrm{SO}_4)_2(s)} + \underset{\substack{\text{hydrofluoric}\\ \text{acid gas}}}{4\mathrm{HF}(g)} + 4\mathrm{CO}_2(g) + 4\mathrm{H}_2\mathrm{O}(g) \tag{4.11}$$

They are carried out at 200-500 °C in an acid-resistant brick lined furnace.

The product sulfates are then dissolved in water to give an impure sulfate solution. The solution is purified by pH adjustment with several steps of precipitation/filtration until it is pure enough to obtain a pure sulfate precipitate for sending to:

(a) solvent extraction purification and rare earth separation and
(b) precipitation of marketable carbonate precipitates.

The process is cheaper than caustic soda extraction so that it is quite popular in China. However,

(a) it requires complex gas treatment to capture (i) hydrofluoric acid gas and (ii) sulfur oxide gas from sulfuric acid decomposition/evaporation and
(b) it generates a large amount of solid wastes (gypsum—$CaSO_4 \cdot 2H_2O$) after carbonate precipitation or solvent extraction, for example:

$$(\mathrm{RE})_2(\mathrm{SO_4})_3(\mathrm{s}) + 3\mathrm{Na_2CO_3}(\mathrm{aq}) \rightarrow (\mathrm{RE})_2(\mathrm{CO_3})_3(\mathrm{s}) + 3\mathrm{Na_2SO_4}(\mathrm{aq}) \tag{4.12}$$

In fact in these conditions, the rare earths don't precipitate as pure carbonates, but as a mixture of carbonates and double sulfates then

$$\mathrm{Na_2SO_4}(\mathrm{aq}) + 3\mathrm{H_2O}(\mathrm{l}) + \mathrm{CaO}(\mathrm{s}) \rightarrow \mathrm{CaSO_4{\cdot}2H_2O}(\mathrm{s}) + 2\mathrm{NaOH}(\mathrm{aq}) \tag{4.13}$$

4.5 RARE EARTH CATION ADSORPTION CLAYS

Rare earth cation adsorption clays are discussed in Section 3.9, mostly from the ore formation and mining points of view. This section discusses them mainly from the extraction point of view.

Since the mid-1990s, most of the world's high atomic number (heavy) rare earth elements (e.g., Tb, Dy, and Y) have been produced from China's rare earth cation adsorption clays. The rare earths in these clays are present as trivalent cations (e.g., $\mathrm{Tb^{3+}}$, $\mathrm{Dy^{3+}}$, $\mathrm{Y^{3+}}$) that are electrically bonded to the clays' surface hydroxyl groups. The principal clays are muscovite and kaolinite.

This unique structure allows direct leaching of the clays by ionic solutions, specifically ammonium sulfate solutions. The process is represented by the equation (RE, rare earth elements):

$$\underset{\text{ore}}{2[(\mathrm{Al, Si})\mathrm{O}_x(\mathrm{OH^-})_3,(\mathrm{RE})^{3+}]} + \underset{\text{lixiviant}}{3[(\mathrm{NH_4}^+)_2, \mathrm{SO_4}^{2-}]}$$

$$\rightarrow \underset{\text{solid waste}}{2[(\mathrm{Al, Si})\mathrm{O}_x(\mathrm{OH^-})_3,3\mathrm{NH_4}^+]} + \underset{\text{product solution}}{2(\mathrm{RE})_2(\mathrm{SO_4})_3} \tag{4.14}$$

The product solution is then reacted with ammonium bicarbonate to produce rare earth carbonates, that is

$$(\mathrm{RE})_2(\mathrm{SO_4})_3(\mathrm{aq}) + 3\mathrm{NH_4HCO_3}(\mathrm{s}) \rightarrow \underset{\text{carbonate precipitate}}{(\mathrm{RE})_2(\mathrm{CO_3})_3(\mathrm{s})} + \underset{\text{ammonium bisulfate solution}}{3[(\mathrm{NH_4})\mathrm{HSO_4}](\mathrm{aq})} \tag{4.15}$$

The solid carbonates are then sent forward to:

(a) releaching,
(b) solvent extraction purification,
(c) solvent extraction rare earth separation, and
(d) rare earth product (e.g., oxides, phosphates, fluorides) precipitation.

4.5.1 Leaching methods

Historically, Chinese operations used heap leaching (Fig. 4.5) to treat the rare earth cation adsorption clays. This process consists of excavating the clay layer from the soil and putting it on a liner. Then the clays are sprinkled with the leaching solution and the leachate is recovered on the liner.

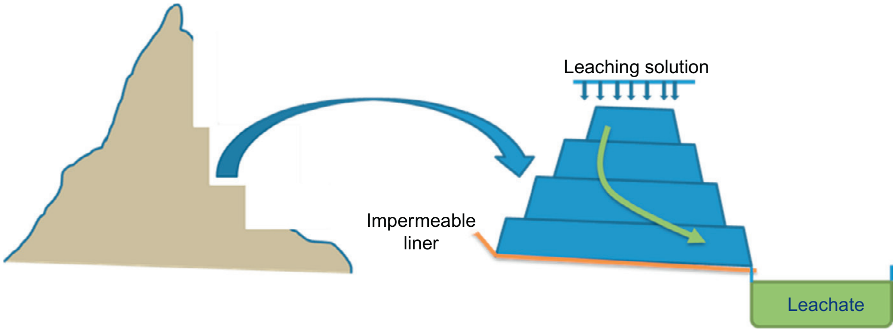

FIG. 4.5

Heap leaching of rare earth cation adsorption clays. The leaching solution is ammonium sulfate. Great care must be taken to avoid leakage of the product solution into the environment.

Drawing by Alain Rollat.

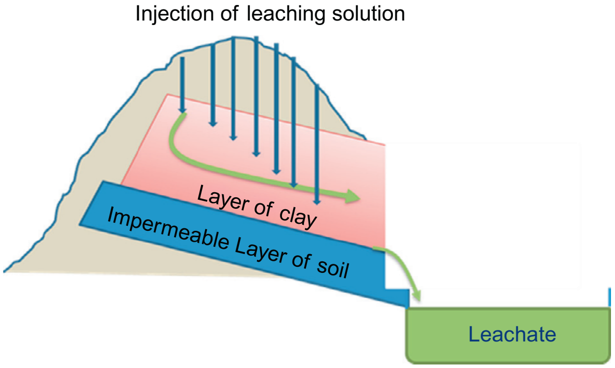

FIG. 4.6

In situ leaching of rare earth cation adsorption clays. The leaching solution is ammonium sulfate. Few deposits have a completely impermeable soil layer so that great care must be taken to avoid leakage of leachate into the environment.

Drawing by Alain Rollat.

In situ leaching (Fig. 4.6) is also being used. This process consists of injecting the ammonium sulfate solution directly in the deposit through holes which sink into the clays. Obviously, in this case the topography, the water table, and the global geology of the deposit are of first importance and not all deposits can be treated with this process.

Both, however, can be damaging to the environment—especially in high-rainfall tropical and subtropical regions—and Chinese authorities are supporting works aiming to design more sustainable processes.

4.6 LOPARITE

Loparite is a complex oxide of rare earths, niobium, tantalum, and titanium, for example (Na,Ca,Y,Ce)(Nb,Ta,Ti)O_3. Rare earths (and Nb, Ta, and Ti) are recovered from this mineral in Solikamsk (Urals), using ore from Lovoserskoye, Kola peninsula.

Even if this process is used only in Russia, its description is interesting because it shows how a process can be designed to take advantage of a specific situation, for example chlorine availability.

The basic idea of the Russian scientists who developed this process was to take advantage of chlorine availability in the Ural Mountains, Fig. 4.7.

The process called carbochlorination

- **(a)** uses this chlorine to convert all of loparite's metallic elements to chlorides at high temperature,
- **(b)** volatilizes then condenses the chlorides that are gaseous at high temperature,
- **(c)** separates the condensed liquid metal chlorides by distillation based on their different vapor pressures, and
- **(d)** recovers the nonvolatile chlorides at the bottom of the distillation column.

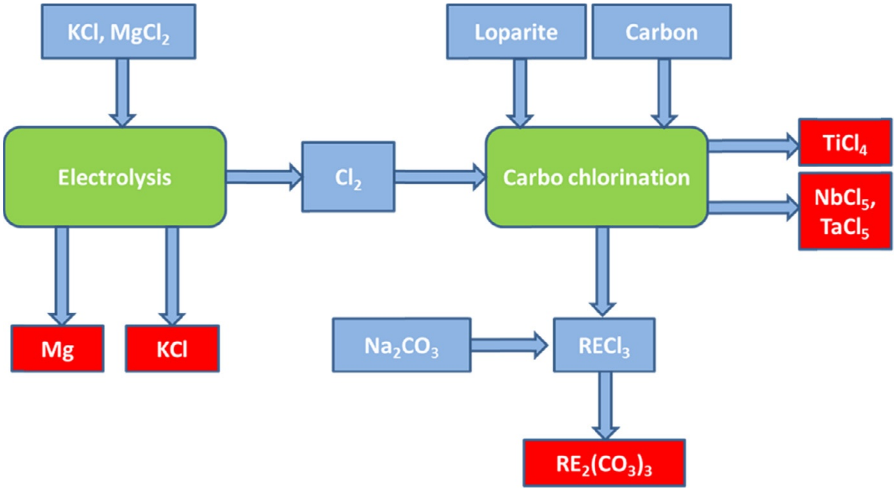

FIG. 4.7

Schematic flowsheet for carbochlorination of loparite rare earths, Nb, Ta, Ti ore (flowsheet prepared by Alain Rollat). The process is carried out in Solikamsk (Urals) using ore from Lovoserskoye, Kola Peninsula. The rare earth carbonate product is sent to Sillamae, Estonia, and to Kazakhstan for rare earth purification, separation, and marketable product (e.g., rare earth oxides, rare earth metals) precipitation.

The vapor pressures of the metal chlorides are

$$TiCl_4 > NbCl_5 > TaCl_5 > ThCl_4, FeCl_3, AlCl_3 > (RE)Cl_3, RaCl_2$$

so that the rare earth chlorides are obtained from the bottom of the distillation column. These rare earth chlorides are then:

(a) purified by chemical purification,
(b) reacted with sodium carbonate to form carbonates, and
(c) shipped to Estonia and Kazakhstan for solvent extraction purification and separation into individual rare earth solutions.

Carbochlorination has been developed for other metals. In France for example, Cezus, a subsidiary of the French nuclear company, Areva, uses this process for zirconium purification.

4.7 APATITE

Apatite ($Ca_{10}(PO_4)_6(OH,F,Cl)_2$) is the most common mineral for phosphates production, particularly for fertilizers and phosphoric acid. Apatite can be igneous or sedimentary. Almost all apatite ores contain rare earth elements, but igneous apatite has a higher concentration than sedimentary apatite. Another important difference is that igneous apatite contains less uranium than sedimentary apatite (Table 4.3).

Even if the rare earth concentration is low (i.e., less than 1 mass% rare earth elements), the huge quantity of apatite ore being treated for phosphate fertilizer production leads to a large extraction of rare earths.

There are two main processes used for apatite attack: sulfuric acid leaching and nitric acid leaching, described in the following section.

4.7.1 Sulfuric acid leaching

Sulfuric acid leaching is by far the most used method of treating apatite ores—and the only one aiming to produce phosphoric acid. The main chemical reaction is

Table 4.3 Rare Earth Contents of Igneous Apatite and Sedimentary Apatite Ores (Solvay Data)

Type	**Igneous Apatite**			**Sedimentary Apatite**			
Origin	**Kola**	**Foskorite**	**Pyroxenite**	**Morocco**	**Togo**	**Florida**	**Bucraa**
REE (ppm)	7400	4900	7300	630	870	550	300
U (ppm)	<5	<5	<5	110	100	<5	65

Igneous apatites contain more rare earths and less uranium than sedimentary apatites.
REE, rare earth elements; ppm, parts per million by mass.

$$\begin{aligned}&\underset{\text{apatite}}{Ca_{10}(PO_4)_6(OH, F, Cl)_2}(s) + 10\underset{\text{sulfuric acid}}{H_2SO_4}(aq) + 20H_2O(l)\\&\rightarrow 10\underset{\text{phosphogypsum}}{CaSO_4(2H_2O)(s)} + \underset{\text{impure phosphoric acid}}{6H_3PO_4(aq) + 2H(OH, F, Cl)(aq)}\end{aligned} \tag{4.16}$$

During this reaction, 70-90% of the rare earth elements end up in the product phosphogypsum with 10-30% going to the acid solution (called green acid).

The green acid is (i) used directly as fertilizers or (ii) purified further to produce pure phosphoric acid.

Thus, depending on the type of process used, rare earth element recovery can be done from primary gypsum, green acid, secondary gypsum, or pure acid.

Most Russian fertilizer producers use sulfuric acid leaching to process their apatite ores. It is estimated that more than 200 million tons of phosphogypsum are stored in Russia (2012) and that this stockpile is growing by ~30 million tons per year. This stockpile averages ~0.5 mass% rare earth elements so that the total rare earth quantity in the stockpile is about a million ton.

This huge source of recoverable rare earths has led to considerable research into suitable recovery processes including leaching, filtration, precipitation, ion exchange, and solvent extraction.

In 2014, this stockpile remains a resource awaiting utilization.

4.7.2 Nitric acid leaching

Nitric acid leaching process is used only by fertilizer producers. While this process is used much less than sulfuric acid leaching, it has several advantages for rare earths recovery. The main one is that mixed rare earth nitrate solutions can be separated into individual rare earth nitrate solutions directly by solvent extraction.

This process was used in the 1990s by Norsk Hydro (now Yara International ASA). Norsk Hydro was one of the world's largest producers of nitrogen-phosphorus-potassium (NPK) fertilizers.

Since this process directly produces rare earth nitrates, it is particularly well adapted to refineries that use nitrate solvent extraction.

This is why the rare earth nitrates produced in Glomfjord, Norway, were sent to Rhone-Poulenc's La Rochelle (France) refinery for individual rare earth production.

4.8 NEW PROCESSES FOR OTHER RARE EARTH MINERALS INCLUDING SILICATES

Many new projects outside of China have three characteristics that make them different from the above processes:

(a) they are based on unconventional minerals, for example

eudyalite	$Na_4(Ca,Ce)_2(Fe,Mn,Y)ZrSi_8O_{22}(OH,Cl)_2$
pyrochlore	$(Na,Ca,Ce)_2Nb_2O_6F$
fergusonite	$(Y,Er,U,Th)(Nb,Ta,Ti)O_4$

(b) their ores contain very small rare earth-bearing mineral particles difficult to separate from the other minerals and do not permit efficient rare earth concentrate production, and

(c) they are based on polymetallic ores, which means that processing must purify not only rare earths, but also for example niobium, tantalum, zirconium, and uranium.

Sulfuric acid leaching is the usual proposed process—but with more complicated flowsheets than today's commercial processes. The next section describes two of these proposed processes.

4.8.1 Thor Lake, Northwest territories, Canada (Avalon process, Fig. 4.8)

The Thor Lake deposit (Avalon Rare Metals, Inc.) is very complex. It contains

zirconium mineral:	63-66 mass% zirconium silicate (zircon),
rare earth minerals:	3-5 mass% fergusonite; 0.7-4 mass% bastnasite; 1.5-4.4 mass% synchysite; 5.2-9 mass% monazite; 12-20 mass% allanite,
niobium, tantalum	~4 mass% columbite.

The target is to recover rare earth elements *and* Nb, Ta, and Zr.

The process includes

(a) alkali ($CaCO_3$-Na_2CO_3) leaching,
(b) mixed rare earth precipitation, and
(c) sulfuric acid leaching of the rare earth precipitate

to produce a final rare earth-rich product that is sent forward to leaching, purification, rare earth separation, and marketable rare earth product precipitation.

This process (see Fig. 4.8a and b) seems quite complex. In 2013, Avalon was still working on its simplification and improvement.

4.8.2 Dubbo, New South Wales, Australia (Alkane Resources, Ltd.)

Alkane Resources' deposit near Dubbo, Australia, contains

zirconium	eudialyte and armstrongite,
rare earths	eudialyte, calcian, bastnasite, and ancylite,
niobium and tantalum:	natroniobite.

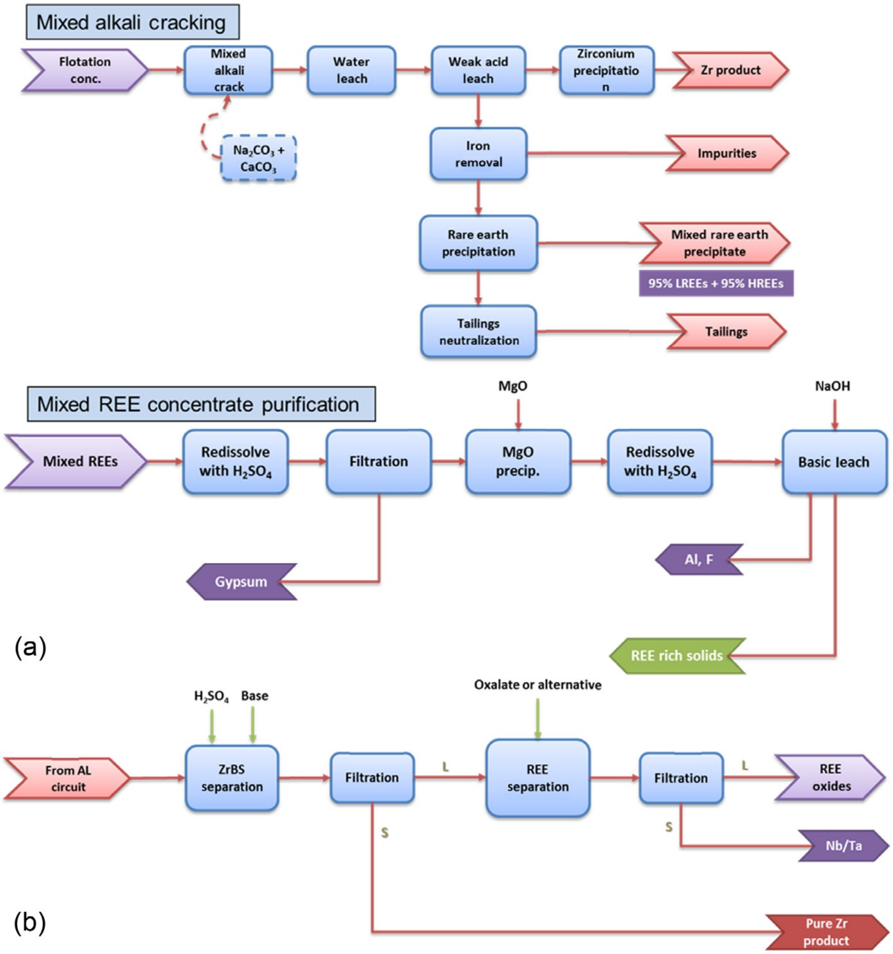

FIG. 4.8

(a) Avalon process for recovering rare earths, Nb, Ta, and Zr from Thor Lake ore, part 1 (used by permission of Avalon Rare Metals, Inc.). (b) Avalon process for producing pure rare earth oxides, Zr, and a mixed Nb/Ta product, part 2 (used by permission of Avalon Rare Metals, Inc.). The target of this second part is to recover the rare earths that have followed the Zr during weak acid leaching.

Like Thor Lake, the objective of treating this ore is to recover rare earth elements *and* Nb, Ta, and Zr. Fig. 4.9 sketches a flowsheet of the process. It shows that the initial process is sulfuric acid leaching followed by several filtration and solvent extraction steps.

Also noticeable is two rare earth precipitate streams—a high atomic number (heavy) rare earth stream and a low atomic number (light) rare earth stream. However, the efficiency of this division should be very low, and it is unlikely that this first pre-separation step simplifies the rare earth separation step by solvent extraction.

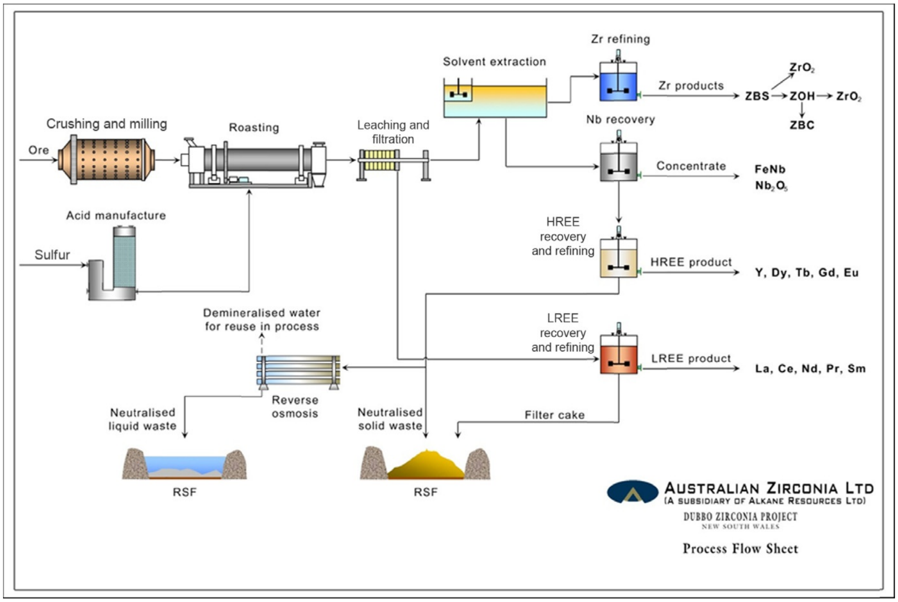

FIG. 4.9

Flowsheet for extracting rare earth elements from Dubbo (Australia) rare earths, niobium, tantalum, zirconium ores (flowsheet used by permission of Alkane Resources Ltd.). The process is in the development stage (2014).

4.9 THE KEY QUESTION OF RADIOACTIVE IMPURITIES REMOVAL

All rare earth deposits contain radioactive minerals, even if the concentration is low. So all rare earth extraction plants must be able to separate radioactive elements from their products. Well-established processes exist for removing these elements. But they must be evaluated for any proposed flowsheet at the start of any commercial rare earth mining/extraction venture.

The next section describes the radioactive elements that are found in rare earth ores. Subsequent sections describe how these radioactive elements are isolated and removed during rare earth production.

4.9.1 The radioactive families

Three natural radioactive isotopes are found with rare earth minerals: ^{232}Th, ^{238}U, and ^{235}U.

Two key points about these isotopes are

(a) during the rare earth extraction each member of the above radioactive families will be liberated from the host mineral. So the radioactive family members will not be at equilibrium anymore (radioactive family breakage). Each member of the family will have its own chemical behavior. So radioactive element removal must consider not only the family fathers, that is ^{232}Th, ^{238}U, and ^{235}U, but also the family daughters

(b) after radioactive family breakage, each radioelement will have a new concentration in the rare earth extraction products depending on its own half-life and on its own chemical behavior.

In practice, all radioelements with half-lives of more than 1 month must be considered. Typically, the main radioelements that must be considered are

$$\begin{aligned}&^{232}\text{Th family}: && ^{232}\text{Th}, ^{228}\text{Ra}, ^{228}\text{Th},\\ &^{238}\text{U family}: && ^{238}\text{U}, ^{234}\text{U}, ^{230}\text{Th}, ^{226}\text{Ra}, ^{210}\text{Pb},\\ &^{235}\text{U family}: && ^{235}\text{U}, ^{227}\text{Ac}.\end{aligned}$$

In terms of chemistry, it means that the behavior of five different chemical elements must be considered: uranium, thorium, radium, actinium, and lead. All the isotopes of each of these elements exhibit the same chemical behavior.

4.9.2 Thorium and uranium removal

Thorium and uranium are removed by (i) chemical processes (e.g., precipitation and filtration steps) or by (ii) solvent extraction.

Chemical processing is more common. It is based on the fact that the hydroxides of thorium and uranium precipitate at lower pHs than rare earth hydroxides. After caustic soda leaching of monazite, for example, re-dissolution of rare earth hydroxides in aqueous hydrochloric acid (Section 4.3.1) is carried out with careful pH control. Typically, both thorium and uranium are insoluble at pH 3, where rare earth elements are soluble.

Also, during solvent extraction, uranium and thorium are much more complexed by the organic extractant than rare earth elements. So a specific uranium and thorium extraction section can be placed ahead of the rare earth extraction sections.

4.9.3 Radium removal

Radium is an alkaline earth element. Like all alkaline earth elements and in particular the heaviest ones, its sulfate is insoluble. Its concentration in rare earth aqueous solutions is very small (1 Bq of ^{226}Ra is equivalent to 2.7×10^{-9} g and 1 Bq of ^{228}Ra is equivalent to 9.9×10^{-12} g), so that it must be co-precipitated with another element with an insoluble sulfate, for example barium. A representative reaction is

$$\underset{\substack{\text{radioactive}\\\text{impurity}}}{RaCl_2(aq)} + \underset{\substack{\text{added}\\\text{co-precipitant}}}{BaCl_2(aq)} + \underset{\substack{\text{added sulfate}\\\text{source}}}{2Na_2SO_4(aq)} \rightarrow \underset{\substack{\text{radium barium}\\\text{co-precipitate}}}{(Ra, Ba)SO_4(s)} + \underset{\text{in solution}}{4NaCl(aq)} \quad (4.17)$$

4.9.4 Lead removal

Lead is a member of the heavy metals group. Like all the heavy metals, its sulfide is insoluble. The classical way to remove lead is to precipitate lead sulfide. The reaction is

$$\underset{\text{in solution}}{\mathrm{PbCl_2(aq)}} + \underset{\text{sulfur source}}{\mathrm{Na_2S(s)}} \rightarrow \underset{\text{precipitate}}{\mathrm{PbS(s)}} + \underset{\text{in solution}}{\mathrm{2NaCl(aq)}} \tag{4.18}$$

4.9.5 Actinium removal

The chemistry of actinium is very close to the chemistry of rare earth elements, particularly to the chemistry of lanthanum. So actinium cannot be removed from rare earth elements by precipitation.

Actinium is always removed by solvent extraction.

4.9.6 Thorex radioactive element removal process

In the 1980s, the Rhone-Poulenc Company's La Rochelle refinery developed a process for separating all the radioactive elements in its monazite concentrate feed from its rare earth products—the Thorex process, Fig. 4.10.

It is based on tributyl phosphate's (TBP's) selectivity for radioactive elements in nitrate medium. The order of selectivity is

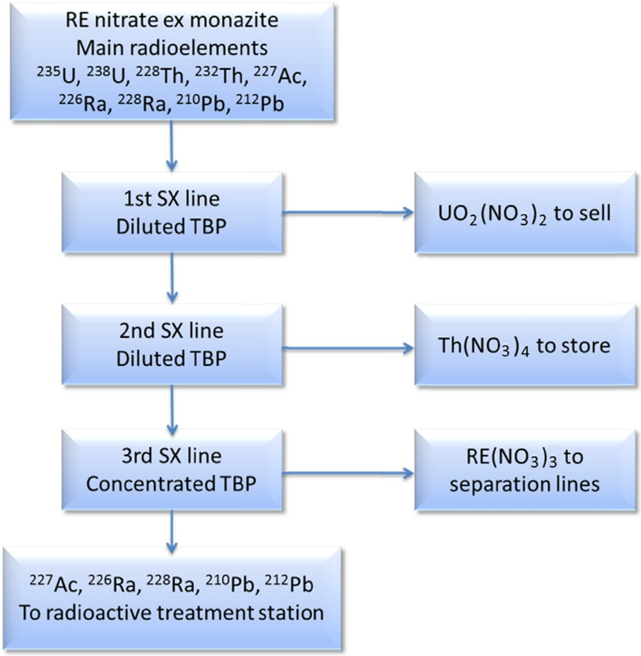

FIG. 4.10

Thorex process for removing radioactive elements during rare earth extraction from monazite (flowsheet prepared by Alain Rollat). It was used in the La Rochelle (France) refinery. TBP, tributyl phosphate; RE, rare earth elements.

$$UO_2{}^{2+} > Th^{4+} > RE^{3+} > Ac^{3+} > Pb^{2+} > Ra^{2+}$$

An interesting property of TBP is that it can extract both uranium and thorium with a high loading of UO_2^{2+} and Th^{4+} and with easy downstream organic solvent regeneration.

4.10 SUMMARY

The main industrial minerals used for rare earth production are

> bastnasite and monazite for low atomic number rare earths (La, Ce, Pr, Nd) and xenotime and rare earth cation adsorption clays for high atomic number rare earths (Sm, Eu, Gd, Tb, Dy, Ho, Er, Tm, Yb, Lu, and Y).

Bastnasite, monazite, and xenotime are all processed by caustic soda leaching or sulfuric acid roasting.

Rare earth cation adsorption clays are processed quite differently. Ammonium sulfate solution is sprayed onto the ore—thereby directly producing rare earth ions (RE^{3+}) in aqueous solution.

Other minerals are now under investigation for rare earth production, especially those containing high atomic number (heavy) rare earth elements. Examples are eudyalite and fergusonite, which also contain Zr, Nb, and Ta.

All rare earth deposits contain radioactive elements. This requires that

(a) processes be developed to remove radioactive elements during rare earth extraction and

(b) radioactive waste storage facilities exist.

Finally, whatever the rare earth extraction process is employed, its final concentrate (solution or precipitate) must be compatible with the next steps: rare earth element purification and separation by solvent extraction, Chapter 5.

Suggested Reading

Chi, Ruan, Tian, Jun, 2008. Weathered Crust Elution-Deposited Rare Earth Ores. Nova Science Publishers, New York.

Lokshin, E.P., Tareeva, O.A., 2010. Recovery of lanthanides from extraction phosphoric acid produced by the dihydrate process. Russ. J. Appl. Chem. 83 (6), 951–957.

Roskill Information Services Ltd., 2011. Rare Earths & Yttrium: Market Outlook to 2015. Roskill Information Services Ltd., London.

CHAPTER 5

Rare Earths Purification, Separation, Precipitation and Calcination

The products of rare earth cracking processes mentioned in Chapter 4 are quite pure rare earth concentrates, mainly oxides and carbonates, Fig. 5.1.

This chapter describes how these rare earth concentrates are

- **(a)** leached,
- **(b)** purified,
- **(c)** separated into individual high purity rare earth solutions, and
- **(d)** precipitated as individual pure rare earth oxides, phosphates, and fluorides

ready for

- **(a)** use in the applications using rare earth salts and oxides: catalysts, phosphors, polishing powders, etc.
- **(b)** reduction to metal for the applications using rare earth metals: magnets, batteries, etc.

The lixiviant used to leach rare earth carbonate feed that is mentioned in Fig. 5.1 depends on the aqueous medium used in the refinery. A chloride medium refinery uses hydrochloric acid

$$\underset{\text{carbonate precipitate}}{RE_2(CO_3)_3(s)} + \underset{\substack{\text{hydrochloric}\\\text{acid}}}{6HCl(aq)} \rightarrow \underset{\substack{\text{rare earth chloride}\\\text{aqueous solution}}}{2RECl_3(aq)} + \underset{\text{carbon dioxide}}{3CO_2(g)} + \underset{\text{water}}{3H_2O(aq)} \tag{5.1}$$

where RE is the rare earths in Fig. 5.1 feed.

The nitrate medium refinery uses nitric acid, that is

$$\underset{\text{carbonate precipitate}}{RE_2(CO_3)_3(s)} + \underset{\substack{\text{nitric}\\\text{acid}}}{6HNO_3(aq)} \rightarrow \underset{\substack{\text{rare earth nitrate}\\\text{aqueous solution}}}{2RE(NO_3)_3(aq)} + \underset{\text{carbon dioxide}}{3CO_2(g)} + \underset{\text{water}}{3H_2O(aq)} \tag{5.2}$$

The precipitate feed dissolves easily in a stirred tank under atmospheric conditions.

The impurities in the resulting pregnant solution are then removed by selective precipitation or solvent extraction. The result is a clear, filtered rare earth solution.

Three separation processes have been used to separate the RE ions in these solutions. They are

- **(a)** selective crystallization,
- **(b)** ion exchange, and
- **(c)** solvent extraction.

Rare Earths. http://dx.doi.org/10.1016/B978-0-444-62735-3.00005-X

FIG. 5.1

Mixed rare earth carbonate precipitate. It is the final product of cracking processes described in Chapter 4. It is also the feed to this chapter's refinery/rare earth separation plant. It contains usually more than 95 mass% rare earth carbonates and less than 5 mass% impurity carbonates, dry basis.

Photograph courtesy of Alain Rollat.

In 2014, solvent extraction is far and away the most used process.

This chapter concentrates on solvent extraction. It mentions selective crystallization and ion exchange.

Its main objective is to show how:

(a) individual pure rare earth element solutions from 99% to 99.999% pure depending on their eventual application

are made from:

(b) the above-mentioned clear, filtered rare earth solution.

5.1 SELECTIVE CRYSTALLIZATION

Rare earth separations were initially based on selective crystallization of individual rare earth-sodium double sulfates. The reactions are represented by

$$\underbrace{2\mathrm{RE}^{3+}(\mathrm{aq}) + 3\mathrm{SO_4}^{2-}(\mathrm{aq})}_{\text{leach solution}} + \underbrace{2\mathrm{Na}^{+}(\mathrm{aq}) + \mathrm{SO_4}^{2-}(\mathrm{aq})}_{\text{precipitation agent}} \rightarrow \underbrace{2\left[(\mathrm{RE},\mathrm{Na})(\mathrm{SO_4})_2\right](\mathrm{s})}_{\text{solid precipitate}} \tag{5.3}$$

where RE is rare earths.

Separation of individual rare earths one from the other is based on the fact that the water solubility of rare earth-sodium double sulfates increases across the atomic chart, from lanthanum to lutetium.

These solubilities are represented by

$$(\mathrm{La, Na})(\mathrm{SO_4})_2 < (\mathrm{Ce, Na})(\mathrm{SO_4})_2 < \cdots < (\mathrm{Yb, Na})(\mathrm{SO_4})_2 < (\mathrm{Lu, Na})(\mathrm{SO_4})_2$$

The differences in solubility are small so that selective crystallization (i) has a low productivity and (ii) is inefficient. It is no longer used on an industrial scale for high purity individual rare earths production.

It was first replaced by ion exchange (next section) and then permanently by solvent extraction, Section 5.3.

5.2 ION EXCHANGE

Ion exchange, as it applied to rare earth element separation, entailed

(a) leaching rare earth precipitates shown in Fig. 5.1,
(b) pumping the resulting leach solution through sulfonic resin-filled ion exchange columns—thereby fixing all the rare earth ions (RE^{3+}) on the sulfonic resin beads,
(c) sequentially removing the fixed rare earth ions from the column by eluting them with ethylene diamine tetraacetic acid (EDTA) or another aminopolyacetic acid complexant (HEDTA, DCTA TTHA), and
(d) precipitating rare earth compounds from the individual rare earth solutions as described in Section 5.4.

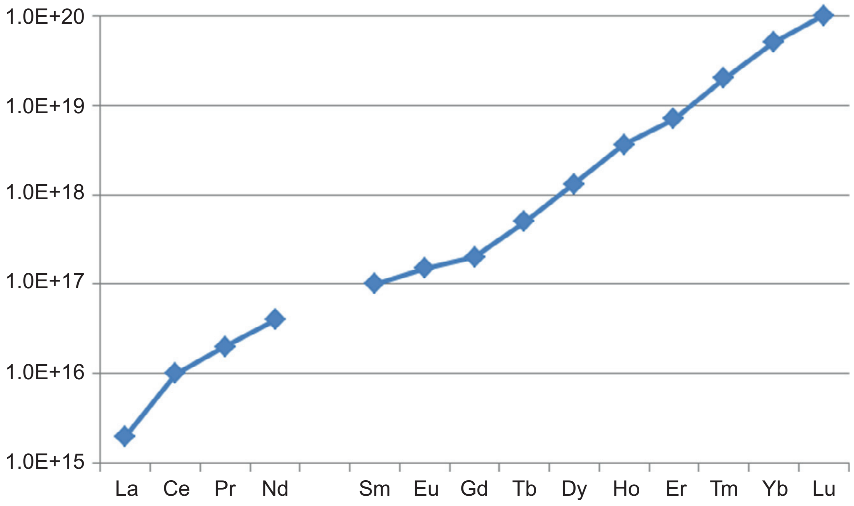

FIG. 5.2

Stability constants of EDTA with rare earth ions. The stability constant is represented by $K(\mathrm{RE_1}) = ([\mathrm{RE_1HL}][\mathrm{H^+}]^3)/([\mathrm{RE_1}^{3+}][\mathrm{H_4L}])$ and is expressed in $(\mathrm{M/L})^2$

The success of the separation is based on the increasing strength of rare earth-EDTA complexes across the rare earth series, from lanthanum to lutetium (Fig. 5.2).

Despite its high selectivity, ion exchange had several disadvantages:

- low yields,
- low productivity, and
- environmental difficulties with toxic solutions.

It has been almost completely replaced by solvent extraction, described in the following section.

5.3 SOLVENT EXTRACTION (RYDBERG ET AL., 2007)

In 2014, almost all industrial rare earth separations are based on solvent extraction, specifically:

China (all)
Solvay (La Rochelle, France) (Fig. 5.3)
Lynas (Gebeng, Malaysia)
Silmet/Molycorp (Sillamae, Estonia)
Molycorp (USA)

FIG. 5.3

Rare earth purification/separation plant in La Rochelle, France. It leaches intermediate products like that in Fig. 5.1. It then uses solvent extraction to (i) purify the resulting rare earth aqueous solution and then (ii) separate it into pure individual rare earth solutions. Finally, it precipitates pure rare earth products and calcines them for production of polishing powders, phosphors, and catalysts, Section 5.4. The plant is operated by Solvay Rare Earth Systems.

Photograph courtesy of Alain Rollat.

5.3.1 Solvent extraction process—how to get pure rare earths from a mixed rare earth solution

The separation of a mixed rare earth solution into pure individual rare earth solution is done step by step. Each separation step is performed in specific equipment called solvent extraction battery (see Section 5.3.2).

Each solvent extraction battery is able to separate one group of rare earths into two subgroups (or a mixture of two rare earths into two pure individual rare earths).

Thus, the production of pure lanthanum, pure cerium, pure praseodymium, and pure neodymium solutions from a mixed rare earth solution will need the following steps (Fig. 5.4):

- Separation of light rare earths (LRE) from heavy rare earths (HRE)
- Separation of dydimium (mixture of Pr + Nd) from La + Ce
- Separation of La from Ce
- Separation of Nd from Pr

Then the mixture of HREs coming out of the first solvent extraction battery is separated into pure individual HRE solutions by the same way (Fig. 5.5).

As it has been explained in the preceding text, each solvent extraction battery is able to separate one group of rare earths into two subgroups.

For example, the fourth solvent extraction battery in Fig. 5.4 is able to separate a mixture containing 25% Pr + 75% Nd into pure Pr and pure Nd. The purity of each individual rare earth can be as high as required by the application. Typical Nd purity for magnet application is 99.9%, but for some specific applications like laser, Nd needs to be as pure as 99.999%. The purity of Nd will depend on the number of stages and on the operational parameters, like reflux flow rate (see the following text).

The full separation of Nd from Pr will require three sections of the solvent extraction battery.

- *Extraction*: In this section the aqueous Pr + Nd solution coming from the previous battery is fed countercurrently with the solvent. The target of this section is to get the Pr as pure as possible, in other words to extract all the Nd. The aqueous phase coming out of this section is a pure Pr solution. So the solvent coming out of this section contains all the Nd, but also a part of Pr (Fig. 5.6).
- *Washing (or scrubbing or reflux)*: The target of this section is to remove all the Pr from the solvent coming from the extraction section. This can be achieved by sending countercurrently to the loaded solvent an aqueous phase containing pure Nd. Thus, the Pr in the solvent will be replaced by Nd from the scrubbing solution. Then, the solvent coming out of the washing section is pure in Nd. The aqueous phase coming out of the washing section remains in the battery and is mixed with feed solution (Fig. 5.7).
- *Stripping (or back extraction or regeneration)*: The target of this section is to recover Nd into aqueous solution and therefore to be able to recycle the solvent back to the extraction section. Then, the solvent coming out of the regeneration

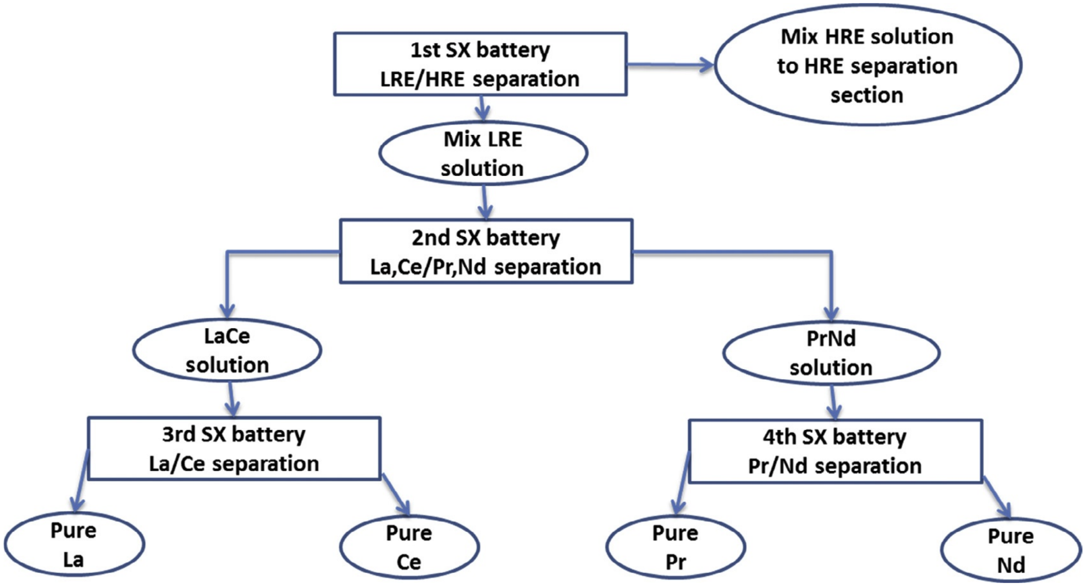

FIG. 5.4

Schematic flowsheet for producing individual pure low atomic number (light) element aqueous solutions. Individual high atomic number (heavy) element solutions are made as shown in Fig. 5.5. LRE, low atomic number (light) rare earth elements. HRE, high atomic number (heavy) rare earth elements.

Drawing by Alain Rollat.

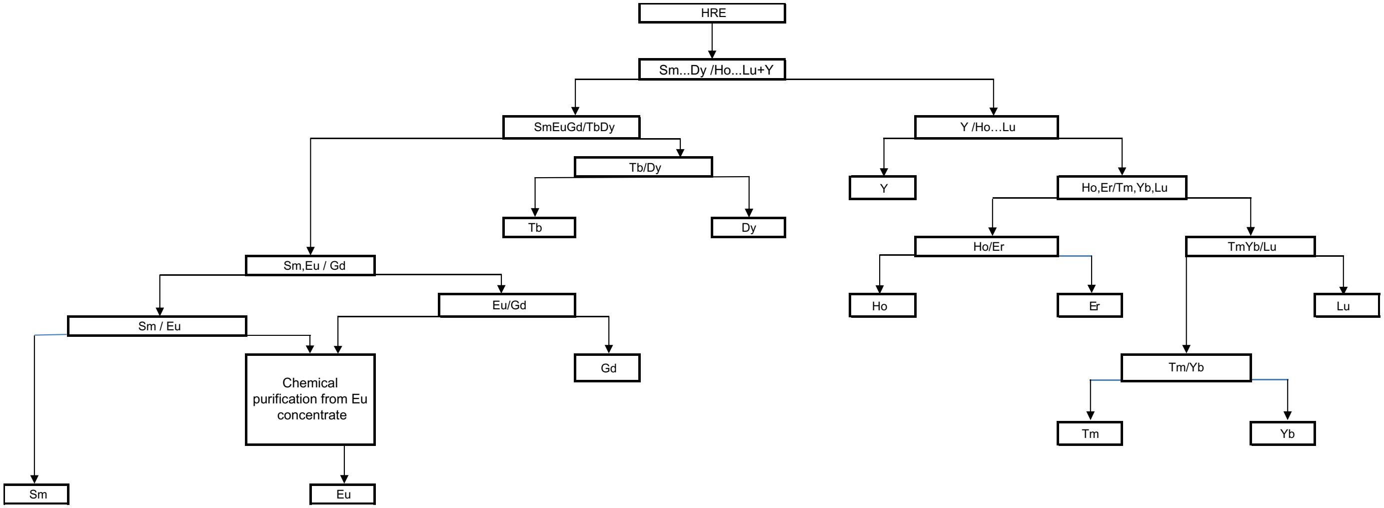

FIG. 5.5

Schematic flowsheet for producing individual pure high atomic number (heavy) element aqueous solutions from high atomic number (heavy) rare earth element (HRE) aqueous solution feed.

Drawing by Alain Rollat.

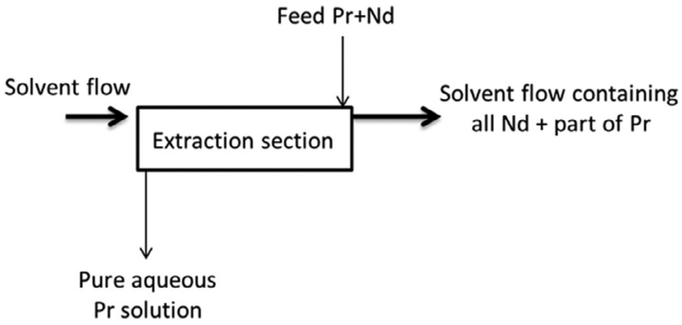

FIG. 5.6

Schematic flowsheet for extraction section.

Drawing by Alain Rollat.

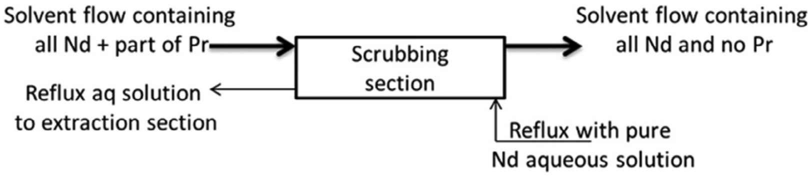

FIG. 5.7

Schematic flowsheet for scrubbing section.

Drawing by Alain Rollat.

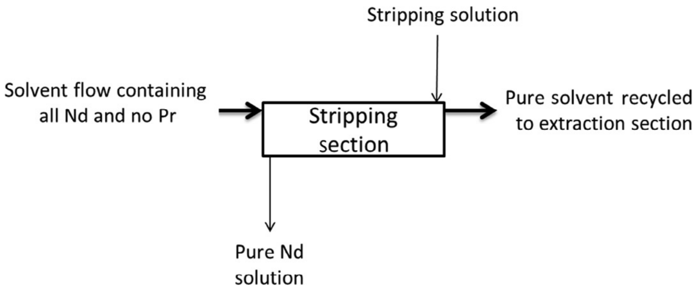

FIG. 5.8

Schematic flowsheet for stripping section.

Drawing by Alain Rollat.

section does not contain any Nd and the aqueous phase coming out of this section is the production of pure Nd (Fig. 5.8).

Thus, the global schematic flowsheet of Pr/Nd separation is a combination of the three sections above as it is shown in Fig. 5.9.

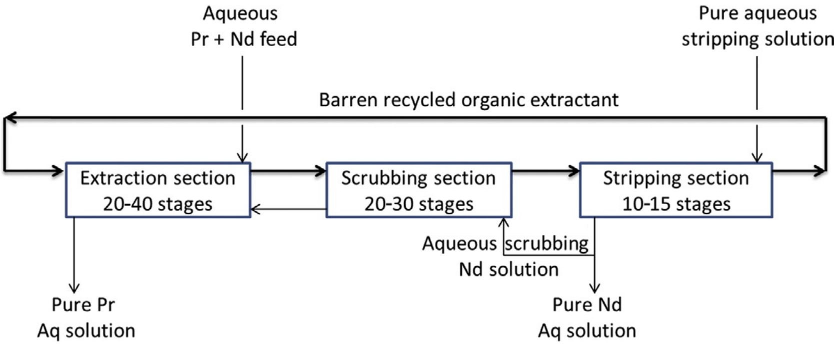

FIG. 5.9

Schematic flowsheet for producing pure praseodymium (Pr) aqueous solution and pure neodymium (Nd) aqueous solution from a mixture of Pr + Nd feed solution. The (Pr + Nd) feed solution has been purified by solvent extraction before it is fed into this rare earth separation battery. The process is continuous.

Drawing by Alain Rollat.

The way per which these three sections are carried out (concentration of aqueous RE solutions, composition of the stripping solution, etc.) depends on the chemistry of the extraction and so on the type of organic molecule which is used as solvent and this will be explained further (see Section 5.3.3).

5.3.2 The industrial solvent extraction equipment—mixer-settlers

Industrially, RE separation processes are all done in specific equipment called battery of mixer-settlers. The elementary effect of one mixer-settler is weak, but when repeated with countercurrent flows the purification of each RE can be achieved at purity as high as 6 N (99.9999%). A battery of mixer-settlers consists of a series of such equipment in which the aqueous and the organic phases circulate countercurrently in a continuous manner. The organic phase is simply the carrier of the RE and is not consumed during the process (Figs. 5.10 and 5.11).

The size of one mixer-settler depends on the capacity of the unit. Obviously, the mixer-settlers of the upstream batteries treating the main flows are bigger than the downstream ones.

The biggest batteries for RE industry can have a volume as big as 60 m^3 for only one mixer-settler. But this size is unusual. A typical size is more in the range of 500 L to 4 m^3 per mixer-settler (Fig. 5.12).

5.3.3 The chemistry of solvent extraction and the solvent choice

All the rare earth separation plants use batteries of mixer-settlers, but they do not use the same solvents. Thus, the key questions are: What is the chemistry of this process and how it works?

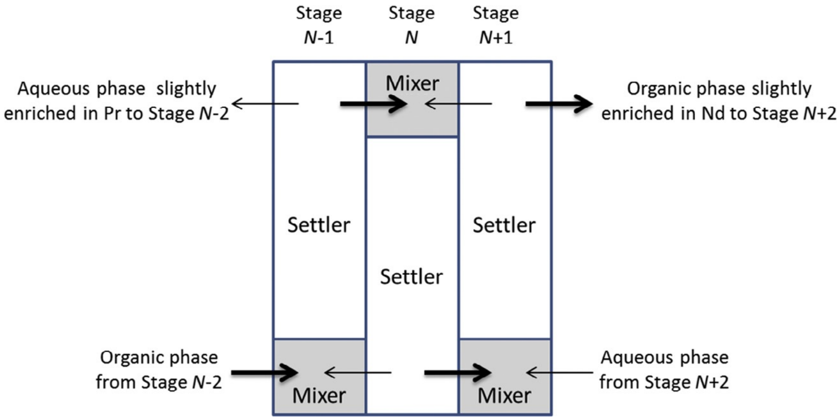

FIG. 5.10

Simplified schematic of a rare earth solvent extraction mixer-settlers. The drawing shows the flow pattern inside three mixer-settlers with a slight enrichment of Nd in the organic phase coming out from the stage $N+1$.

Drawing by Alain Rollat.

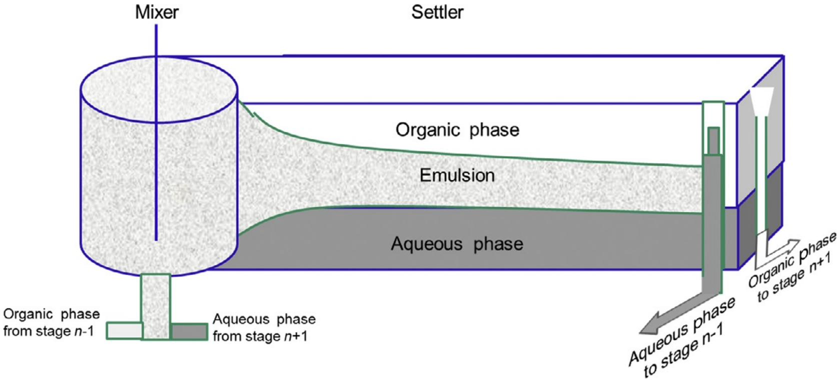

FIG. 5.11

Simplified schematic of a rare earth solvent extraction mixer-settler. The figure shows the flows pattern into one mixer-settler.

Drawing by Alain Rollat.

Indeed the heart of the solvent extraction process is the solvent itself and depending on the type of organic molecule used as solvent, the economics of the process will be different.

In order to assess the various solvents, three criteria must be taken into account. Two criteria will impact the capital expenditure (CAPEX):

- *Selectivity*. For a given separation, the higher the selectivity, the lower the number of stages.

FIG. 5.12

Rare earth solvent extraction battery in La Rochelle, France (photo courtesy of Alain Rollat, Solvay Rare Earth Systems). The mixer-settlers are connected in series—with the aqueous and organic phases moving countercurrently (Fig 5.10).

- *Loading capacity*. The loading capacity of a solvent is defined as the maximum quantity of rare earths that this solvent can load. For a given production, the higher the loading capacity, the lower the size of a cell (mixer-settler).

And one criterion will impact the operational expenditure (OPEX):

- *Energy and chemical reagents consumption*. Depending on the extracting molecule one will have to consume more or less chemicals (acid and base) and energy.

(a) Selectivity

The classical oxidation degree being RE^{3+} for all the rare earths, the selectivity of trivalent rare earths among various extractants is the main criterion to be checked first (for separation using other oxidation degrees see Appendix 5.2)

Diethyl2hexyl phosphoric acid (HDEHP), ethyl2hexyl ethyl2hexyl phosphonic acid (H(EH)EHP), tributyl phosphate (TBP), Aliquat 336, and versatic acid are the classical extractants used in RE separation processes (see Table 5.1).

The selectivity of these extractants is reported in Fig. 5.13.

This figure shows the relative affinity of each extractant for all the rare earths. This is illustrated by the example:

Extractant: H(EH)EHP·Cl
Rare earth ions: La^{3+}, Ce^{3+}

Table 5.1 Chemical Formula of the Main Extractants used in Rare Earth Separation Processes

Usual Name	Chemical Name	Chemical Formula
TBP	Tributyl phosphate	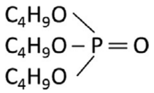
Aliquat 336	Quaternary ammonium salt with C_8 (octyl) and C_{10} (decyl) chains (C_8 predominating)	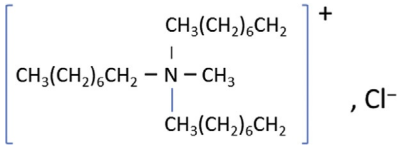
Versatic acid	Versatic 10 is a carboxylic acid containing a total of 10 carbon atoms	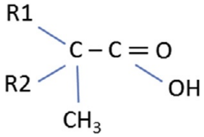
HDEHP	Di ethyl2hexyl phosphoric acid	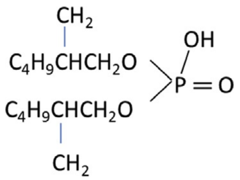
H(EH) EHP	Ethyl2hexyl,ethyl2hexyl phosphonic acid	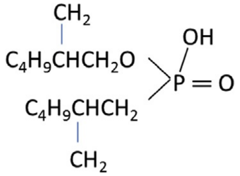

The partition coefficients are

$$\left[P\left(\mathrm{La}^{3+}\right)\right] = \left[\mathrm{La}^{3+}\right]_{\mathrm{organic}} / \left[\mathrm{La}^{3+}\right]_{\mathrm{aqueous}} = \sim 9 \times 10^{-6}$$

$$\left[P\left(\mathrm{Ce}^{3+}\right)\right] = \left[\mathrm{Ce}^{3+}\right]_{\mathrm{organic}} / \left[\mathrm{Ce}^{3+}\right]_{\mathrm{aqueous}} = \sim 1 \times 10^{-4}$$

and the separation factor of $\mathrm{Ce}^{3+}/\mathrm{La}^{3+}$ is

$$\left[P\left(\mathrm{Ce}^{3+}\right)\right] / \left[P\left(\mathrm{La}^{3+}\right)\right] = \left[1 \times 10^{-4}\right] / \left[9 \times 10^{-6}\right] = \sim 11$$

which shows that the solubility of Ce^{3+} in H(EH)EHP·Cl is ~11 times larger than the solubility of La^{3+}. This is a perfect separation coefficient for industrial rare earth separations.

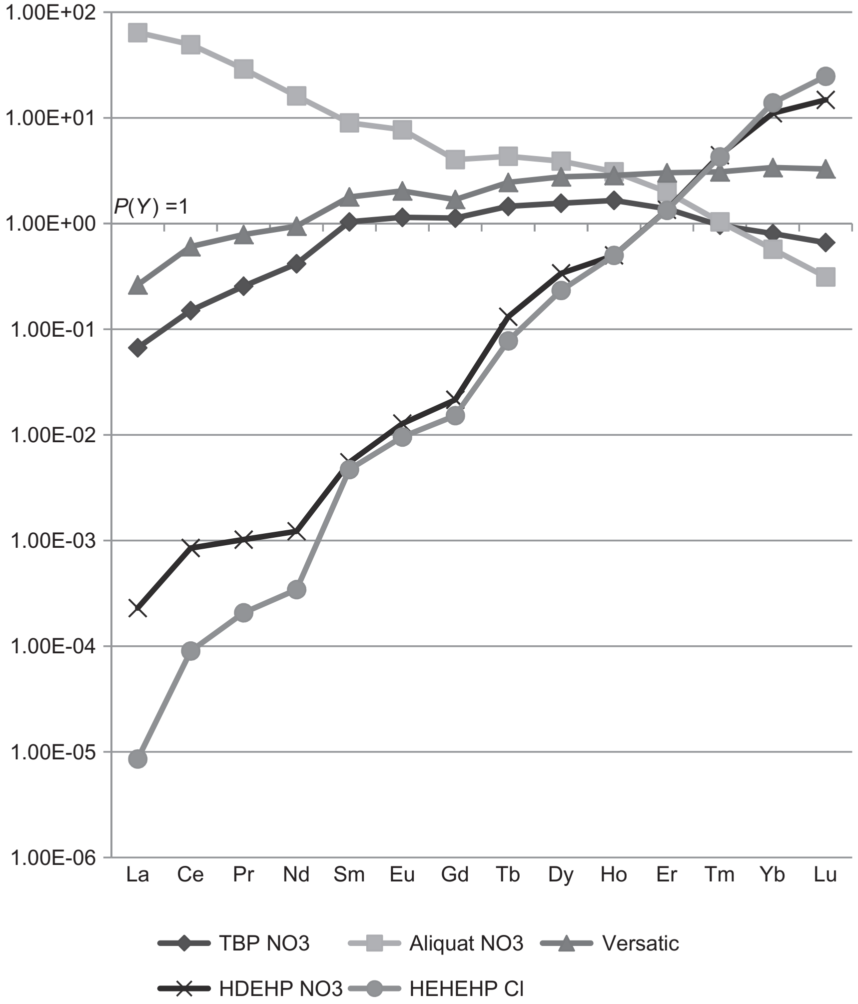

FIG. 5.13

Relative partition coefficients of RE^{3+}, that is, [$P(RE^{3+})$] with selected extractants (graph courtesy of Alain Rollat, Solvay Rare Earth Systems). The Y axis is equilibrium: $[RE^{3+}]_{organic}/[RE^{3+}]_{aqueous}$ distribution ratios for all the rare earth elements, where $[RE^{3+}]_{organic} = RE^{3+}$ concentration in the organic (extractant) phase and $[RE^{3+}]_{aqueous} = RE^{3+}$ concentration in the aqueous phase. The larger the difference of $P(RE^{3+})$ between two adjacent RE the more selective the extractant is.

H(EH)EHP gives the highest total difference of partition coefficients between rare earths: $P(Lu^{2+})/P(La^{3+}) > 10^6$. It is the most selective extractant along the lanthanide series. It can be used for all the rare earth separations.

Nevertheless, one must also note that TBP in nitrate medium can be used for La/Ce/Pr/Nd separation and Aliquat 336 in nitrate medium can also be used for some low atomic number (light) and high atomic number (heavy) rare earth separations.

(b) Loading capacity

The loading capacity of a solvent is defined as the maximum quantity of rare earths that this solvent can load. Two characteristics of the molecules will strongly impact this criterion:

  i. *Molecular weight*: For a given complex structure (number of organic ligands per rare earth cation) the lower the molecular weight, the higher the loading capacity.

  ii. *Viscosity*: The more viscous the extracting molecule, the more dilution is necessary. And the more diluted the extracting molecule the lower is loading capacity of the organic phase.

(c) Energy and chemical reagents consumption

The chemicals and energy consumption will depend on the extraction mechanisms. Indeed, the driving force of the extraction is linked to the modification of the chemical composition of the aqueous or organic media. All the solvents can be classified into three different types of extracting molecules: solvating agents, anion exchangers, and cation exchangers.

The chemical reaction involved during the extraction will determine how to act on the extraction (see Appendix 5.3).

i. Solvating agents or neutral extractants:

TBP is the most classical molecule of this type.

This type of extractant will consume steam (extraction section) and water (stripping section).

ii. Anion exchangers or basic extractants:

Salts of trilauryl methyl ammonium and of tricapryl methyl ammonium ($R_3CH_3N^+$, X^-) are typical molecules of this type, Aliquat 336 being of particular industrial importance.

Like solvating agents, this type of extractant will consume steam (extraction section) and water (stripping section).

iii. Cation exchangers or acidic extractants:

Ethyl2hexyl,ethyl2hexyl phosphonic acid (HEHEHP) is the most classical molecule of this type.

This type of extractant will consume basic chemicals (NaOH or NH_4OH) in the extraction section and acids (HCl or HNO_3) in the stripping section.

5.3.4 Chloride process vs. nitrate process

There are different ways to classify the solvent extraction processes, but the usual way is to distinguish between the chloride process and the nitrate process.

The advantages and drawbacks of the different extractants have been defined in Section 5.3.3

These advantages and drawbacks are summarized in Table 5.2.

Table 5.2 Advantages and Drawbacks of the Most Important Extractants for RE Separation

Class of Extractant/ Typical Molecule	Advantages	Drawbacks
Solvating agents/TBP	High loading capacity Low chemicals consumption	Can be used only in nitrate medium Interesting only for LRE High energy consumption
Anion exchangers/ Aliquat 336	Low chemicals consumption	Can be used only in nitrate medium High energy consumption Interesting only for some RE Low loading capacity
Cation exchangers/H (EH)EHP	Can be used for all RE separations	Very high chemicals consumption Low loading capacity

The best process does not exist. The choice will depend on specific criteria based on strategy of each company (privilege OPEX or CAPEX) and on specific local constraints (possibility to release NaCl, existing fertilizer market for NH_4NO_3 byproduct, etc.).

(a) The chloride process

The chloride process is the most widely used. In particular, all the Chinese plants use this process.

The main advantage of the chloride route is that the same solvent can be used for all the RE separations. Indeed, as it is shown in Fig. 5.13, ethyl2hexyl,ethyl2hexyl phosphonic acid (H(EH)EHP) which can be use in chloride medium is selective all along the lanthanide series.

Another interest of the chloride route is that, since the anion is chloride the liquid wastes is NaCl which in most of the cases can be released into the environment with low constraints.

Nevertheless, one of the main drawbacks of this route is its large HCl and NaOH consumptions.

(b) The nitrate process

The main RE producers using the nitrate route are Solvay in its La Rochelle plant in France and Molycorp in its Silmet plant in Estonia.

Solvay La Rochelle's plant is the only one able to separate all the rare earths using the nitrate route.

The advantage of the nitrate process is the lower operating costs compared to the chloride process. Indeed, with nitrate route both solvating and basic extracting molecules can be used and as it is shown in Table 5.2 the solvents based on these molecules consume almost no chemicals.

But, the design of a whole RE separation process in nitrate route needs to play with all the types of extractants and therefore is more complicated.

5.4 PURE RARE EARTH COMPOUND PRODUCTION

The individual pure rare earth solutions from the above separations are usually not marketable products. Indeed, unless for fuel cracking catalysis where the lanthanum chloride solution is directly used in the application, in all the other cases rare earths are sold and used in solid form—mostly oxides but also phosphates and fluorides.

The processes whereby chloride or nitrate rare earth solutions are transformed to marketable solids are referred to as finishing. It always entails (Figs. 5.14, 5.15, and 5.16)

FIG. 5.14

Precipitation of gadolinium oxalate. After filtration and calcination it will be gadolinium oxide ready for the market.

Photo courtesy of Alain Rollat.

FIG. 5.15

Filtered mixture of (La + Ce) fluoro hydroxide. After calcination and grinding it will be a polishing powder ready for the market.

Photo courtesy of Alain Rollat.

FIG. 5.16

Furnace for producing rare earth oxides from rare earth oxalates, hydroxides, and carbonates, Reactions (5.4), (5.6), and (5.8). The foreground shows the precipitated product as it enters the furnace. The furnace operates between 500 and 1000 °C depending on the oxide characteristics targeted.

Photograph courtesy of Alain Rollat.

(a) precipitation, whereby a precipitating agent (oxalic acid, ammonia, or ammonium—or sodium—bicarbonate) is added to a rare earth solution to precipitate an insoluble compound;
(b) filtration, which separates the new solid product from the now-barren aqueous solution;
(c) thermal treatment, which is calcination (chemical reaction) in the case of oxides and drying in the case of phosphates and fluorides.

All of these steps are critical in obtaining the particle sizes, specific surface areas, and morphologies required by rare earth compound consumers.

5.4.1 Oxides production

Oxides are the main marketable rare earth product. Oxide applications include

automotive catalysts,
polishing powders,
rare earth metal reduction starting materials,
red phosphors,
glasses and ceramics.

Five precipitating agents are used for oxides production: oxalic acid, ammonium/sodium hydroxides, and ammonium/sodium bicarbonates.

The oxalate precipitating reactions are represented by (RE = rare earths, $X = Cl^-$ or NO_3^-)

$$\underset{\substack{\text{purified rare}\\ \text{earth solution}}}{2\left(RE^{3+},3X^-\right)(aq)} + \underset{\substack{\text{oxalic acid solution}\\ \text{precipitation agent}}}{3(H_2C_2O_4)(aq)} \rightarrow \underset{\substack{\text{solid oxalate}\\ \text{precipitate}}}{RE_2(C_2O_4)_3(s)} + \underset{\text{waste water}}{6(H^+,X^-)(aq)} \tag{5.4}$$

then calcination

$$\underset{\text{oxalate precipitate}}{RE_2(C_2O_4)_3} \xrightarrow{900\text{–}1000\ ^\circ C} \underset{\text{marketable oxide}}{RE_2O_3(s)} + \underset{\text{carbon dioxide}}{6CO_2(g)} \tag{5.5}$$

The hydroxide precipitating reactions are represented by ($RE = $ rare earths, $X = Cl^-$ or $NO_3{}^-$)

$$\underset{\substack{\text{purified rare}\\ \text{earth solution}}}{\left(RE^{3+}, 3X^-\right)(aq)} + \underset{\substack{\text{ammonium hydroxide}\\ \text{solution precipitation}\\ \text{agent}}}{3\left(NH_4{}^+, OH^-\right)(aq)} \rightarrow \underset{\substack{\text{solid hydroxide}\\ \text{precipitate}}}{RE(OH)_3(s)} + \underset{\substack{\text{In nitrate medium}\\ NH_4NO_3\text{ is a marketable}\\ \text{byproduct solution}}}{3\left(NH_4{}^+, X^-\right)(aq)} \tag{5.6}$$

$NH_4{}^+$ ion can be replaced bt Na^+, then calcination

$$\underset{\text{hydroxide precipitate}}{2RE(OH)_3} \xrightarrow{600\text{–}900^\circ C} \underset{\text{marketable oxide}}{RE_2O_3(s)} + \underset{\text{water vapor}}{3H_2O(g)} \tag{5.7}$$

Bicarbonate precipitation is represented by

$$\underset{\substack{\text{purified rare}\\ \text{earth solution}}}{\left(RE^{3+}, 3X^-\right)(aq)} + \underset{\substack{\text{ammonium bicarbonate}\\ \text{solution precipitation}\\ \text{agent}}}{3(NH_4{}^+, HCO_3{}^-)(aq)} + \underset{\substack{\text{ammonium hydroxide}\\ \text{solution precipitation}\\ \text{agent}}}{3(NH_4{}^+, OH^-)(aq)}$$

$$\rightarrow \underset{\substack{\text{solid carbonate}\\ \text{precipitate}}}{RE_2(CO_3)_3(s)} + \underset{\substack{\text{In nitrate medium}\\ NH_4NO_3\text{ is a marketable}\\ \text{byproduct solution}}}{6(NH_4{}^+, X^-)(aq)} \tag{5.8}$$

NH^{4+} ion can be replaced by Na^+, then calcination

$$\underset{\text{hydroxide precipitate}}{RE_2(CO_3)_3} \xrightarrow{800\text{–}1000^\circ C} \underset{\text{marketable oxide}}{RE_2O_3(s)} + \underset{\text{carbon dioxide}}{3CO_2(g)} \tag{5.9}$$

Oxalate precipitation is used for high purity products. The choice between hydroxide and carbonate precipitation will depend on the physical characteristics important for the final application (particle size, surface area, porosity).

5.4.2 Phosphates production

Phosphates are important in luminescent products, mainly as LAP, that is, (La,Ce, Tb)PO_4, which is a green phosphor. LAP is obtained directly by

(a) blending the separation plant's pure La, Ce, and Tb in the right proportions,
(b) precipitating LAP from the blended solution by reactions like

$$\underset{\text{combined La+Ce+Tb rareearth solution}}{\left(RE^{3+}, 3X^-\right)(aq)} + \underset{\text{phosphoric acid}}{H_3PO_4(aq)} + \underset{\text{ammonium hydroxide}}{3\left(NH_4^+, OH^-\right)(aq)} \rightarrow \underset{\text{La+Ce+Tb phosphate LAP}}{RE(PO_4)_3(s)} + \underset{\text{byproduct solution}}{3\left(NH_4^+, X^-\right)(aq)} + 3H_2O \tag{5.10}$$

where RE in this case is a specified combination of La + Ce + Tb and X^- is Cl^- or NO_3^-.

The product $RE(PO_4)_3$ precipitate is filtered off and then heated. The phosphate remains a phosphate but with improved structure and morphology.

Solvay rare earth systems makes this product in La Rochelle (France) and Liyang (China).

5.4.3 Fluorides

Rare earth fluorides are used in rare earth electrowinning electrolytes, Chapter 6. These fluorides are precipitated from individual high purity rare earth solutions—using ammonium fluoride as the precipitation agent. The precipitation reaction (using neodymium as the example rare earth) is

$$\underset{\substack{\text{pure chloride or}\\\text{nitrate solution}}}{\left(Nd^{3+}, 3X^-\right)(aq)} + \underset{\substack{\text{ammonium fluoride}\\\text{precipitation agent}}}{3\left(NH_4^+, F^-\right)(aq)} \rightarrow \underset{\substack{\text{neodymium}\\\text{fluoride}}}{NdF_3(s)} + \underset{\text{barren solution}}{3\left(NH_4^+, X^-\right)(aq)} \tag{5.11}$$

Drying of the precipitate is done carefully to avoid formation of NdOF which can be detrimental to some applications.

5.5 SUMMARY

This chapter describes production of pure, marketable individual rare earth compounds from impure mixed rare earth carbonate precipitates shown in Fig. 5.1.

In 2014, virtually all rare earth purification and separations are done by solvent extraction. As applied to rare earths the purification/separations entail

(a) leaching impure mixed rare earth carbonate or oxide mentioned in Chapter 4,
(b) purifying the resultant solution by solvent extraction,
(c) producing individual pure rare earth solutions also by solvent extraction,
(d) precipitating rare earth compounds from these purified leach solutions,
(e) thermally treating these precipitated compounds to produce marketable oxides, phosphates, and fluorides.

The success of solvent extraction in separating rare earths is based on their different complex stabilities with organic extractants across the atomic chart.

APPENDIX 5.1 RARE EARTH SEPARATION SIMULATION

The design of solvent extraction rare earth separations (number of stages of each section, flow rates, etc.) is done by using in-house designed software to simulate the behavior of each rare earth along the solvent extraction battery (concentration of each rare earth in the aqueous phase and the organic phase for each stage).

This software is based on the chemical behavior and selectivity of specified solvents for each rare earth. From such simulations, the concentration of each rare earth at each stage can be obtained for the aqueous and organic phases. Then, using these concentration profiles, the control of the separation is done by checking what is called a ‘critical stage’. A critical stage is a stage where the concentration of a rare earth element drops or increases dramatically.

At its La Rochelle plant, Solvay typically has a full set of online analyzers, usually 3 per solvent extraction battery in order to follow carefully the rare earths concentrations in the critical stage. The output from these analyzers allows the operator to adjust his flowrates (e.g. scrubbing liquid flowrate in Fig. 5.5) to obtain his target individual rare earth concentrations.

APPENDIX 5.2 RARE EARTH SEPARATIONS USING SPECIFIC OXIDATION DEGREES

All rare earths exist as trivalent ion RE^{3+} in aqueous solution. However, it is possible to stabilize Ce^{4+} in nitrate medium and Eu^{2+} in chloride medium. If the chemical behavior of all the RE^{3+} is similar, the chemical behavior of Ce^{4+} and Eu^{2+} is very different from the others. This property can be used for rare earth separations.

Appendix 5.2.1 Cerium purification using Ce(IV) oxidation degree

Cerium IV can be obtained from cerium III by chemical oxidation or electrochemical oxidation. The chemical behavior of Ce(IV) is very different from those of trivalent rare earths. This difference has been used for facilitating the separation between Ce(IV) and RE(III).

Ce^{3+} is always between La^{3+} and Pr^{3+}, but Ce^{4+} is much more extractable than all RE^{3+} whatever the extractant. This difference can be very useful industrially. Indeed, cerium represents almost half of the RE in many ores. Therefore, the extraction of cerium first can be used to minimize the size of all the downstream batteries.

Mainly, two types of processes have been studied:

(a) extraction of Ce(IV) with TBP in nitrate solution

Ce^{4+} nitrate is readily extracted by TBP. The main drawback of this process is linked to the difficulty of the solvent regeneration. Indeed, the complex between $Ce(NO_3)_4$ and TBP is so strong that it is almost impossible to strip Ce^{4+} from the solvent. The only way is to reduce the Ce^{4+} to Ce^{3+} before (or during) the regeneration step.

(b) extraction of Ce(IV) with carboxylic acids

This process can be used in nitrate or sulfate solution. As with TBP, the selectivity between Ce^{4+} and RE^{3+} is very large.

The usefulness of carboxylic acid is that the partition coefficient can be easily changed by adjusting the acidity of aqueous phase so that cerium can be easily recovered as Ce^{4+}.

Appendix 5.2.2 Europium purification using Eu(II) oxidation degree

Europium can be stabilized as Eu^{2+} in chloride solution. Eu^{2+} can be obtained by chemical reduction with Zn° for example or by electrochemical reduction.

Then, separation of Eu^{2+} from RE^{3+} is done by chemical separations (precipitation, filtration) using the difference of solubility between the Eu^{2+} species and the corresponding RE^{3+} species or by solvent extraction.

Chemical reduction followed by precipitation is widely used particularly in China. For the chemical route, two types of insoluble compounds are commonly used:

- **(a)** *hydroxide*: The pH of precipitation of $Eu(OH)_2$ is much higher than those of $RE(OH)_3$. Then, from a solution containing Eu^{2+} and other RE^{3+}, it is possible to precipitate all the RE^{3+} while keeping Eu^{2+} in solution.
- **(b)** *sulfate*: The chemical behavior of Eu^{2+} is close to that of Sr^{2+} and in particular, its sulfate is very insoluble. Since the RE^{3+} sulfates are readily soluble, this difference can also be used for final europium purification by precipitating $Eu(SO_4)$ selectively from a solution containing Eu^{2+} and other RE^{3+}.

APPENDIX 5.3 CHEMICAL REAGENTS CONSUMPTION

From a mass transfer point of view, the separation of two rare earths (RE1 and RE2) by solvent extraction can be described as a three step process:

- **(a)** *extraction or loading*: during this step the global chemical reaction is the solvent loading: $RE1_{aq} \rightarrow RE1_{org}$
- **(b)** *RE separation*: during this step the global chemical reaction is the exchange between two RE, that is: $RE1_{org} + RE2_{aq} \rightarrow RE1_{aq} + RE2_{org}$
- **(c)** *stripping or back extraction or regeneration*: during this step the global chemical reaction occurring is the solvent unloading: $RE2_{org} \rightarrow RE2_{aq}$

The two steps that involve the highest chemical reagent consumption are extraction and stripping. During these two steps an important global mass transfer from one phase to the other occurs.

During RE separation, however, the composition of both phases is quite stable.

The reagents consumption is linked to the driving force of the chemical reactions involved in extraction and back extraction (stripping).

As described in Section 5.3, there are three main types of extraction mechanisms (solvation, anion exchange, and cation exchange).

The driving force is specific to each extraction mechanism.

Appendix 5.3.1 Solvation

The solvation reaction (using TBP as the example) is

$$\underset{\text{aqueous rare earth feed}}{RE^{3+}(aq) + 3NO_3{}^-(aq)} + \underset{\text{barren organic feed}}{3TBP(org)} \rightarrow \underset{\text{rare earth organic complex}}{\left[RE(NO_3)_3{,}3TBP\right](org)} \qquad (A5.3.1)$$

where RE^{3+} is the trivalent rare earth ion.

The equilibrium constant of this equation is

$$K = \left[RE(NO_3)_3{,}3TBP\right]_{org} / \left[RE^{3+}\right]_{aq} [NO_3{}^-]^3_{aq} [TBP]^3_{org}$$

The organic/aqueous distribution coefficient for Reaction (A5.3.1) is

$$P_{RE} = [RE]_{org}/[RE]_{aq} = \left[RE(NO_3)_3{,}3TBP\right]_{org} / \left[RE^{3+}\right]_{aq}$$

which in this case is given by

$$P_{RE} = K[NO_3{}^-]^3_{aq}[TBP]^3_{org}$$

During the extraction step, P_{RE} must be high. This can be achieved by increasing nitrate concentration (by evaporating water)—in which case extraction will consume energy (steam for evaporation).

And during stripping P_{RE} must be low. This can be achieved by decreasing nitrate concentration (by adding water), in which case stripping will consume water.

Appendix 5.3.2 Anion Exchange

The anion exchange reaction, using Aliquat 336 (quaternary ammonium) as the example, is

$$\underset{\text{aqueous rare earth feed}}{RE^{3+}(aq) + 3NO_3{}^-(aq)} + \underset{\text{barren organic feed}}{(R_3CH_3N^+{,}NO_3{}^-)(org)}$$

$$\rightarrow \underset{\text{rare earth organic complex}}{\left[R_3CH_3N^+{,}RE(NO_3)_4{}^-\right](org)} \qquad (A5.3.2)$$

where $RE^{3+}$is the trivalent rare earth ion.

The equilibrium constant of this equation is

$$K = \left[R_3CH_3N^+{,}RE(NO_3)_4{}^-\right]_{org} / \left(\left[RE^{3+}\right]_{aq}[NO_3{}^-]^3_{aq}[R_3CH_3N^+{,}NO_3{}^-]_{org}\right)$$

The organic/aqueous distribution coefficient is equal to

$$P_{RE} = [RE]_{org}/[RE]_{aq} = \left[R_3CH_3N^+{,}RE(NO_3)_4{}^- / \left(RE^{3+}\right)\right]_{aq}$$

from which

$$P_{RE} = K[NO_3{}^-]^3_{aq}[R_3CH_3N^+{,}NO_3{}^-]_{org}$$

Here the conclusions are the same as for solvation, that is

> During extraction P_{RE} must be high. This can be achieved by increasing nitrate concentration (by removing water), meaning that extraction will consume energy for vaporizing water.
> And during back (reverse) extraction, P_{RE} must be low. This can be achieved by decreasing nitrate concentration, by adding water.

Appendix 5.3.3 Cation Exchange

The reaction for cation exchange, using phosphonic acid (H(EH)EHP) as the example, is

$$RE^{3+}(aq) + 3H_2L_2(org) \rightarrow \left[RE(HL_2)_3\right]org + 3H^+(aq) \qquad (A5.3.3)$$

where

> H_2L_2 is the dimeric species of the phosphonic acid.
> RE^{3+} is the trivalent rare earth ion.

The equilibrium constant for this reaction is equal to

$$K = \left(\left[RE(HL_2)_3\right]_{org}[H^+]^3_{aq}\right) / \left(\left[RE^{3+}\right]_{aq}[H_2L_2]^3_{org}\right)$$

while its distribution coefficient is

$$P_{RE} = [RE]_{org}/[RE]_{aq} = \left[RE(HL_2)_3\right]_{org} / \left[RE^{3+}\right]_{aq}$$

from which

$$P_{RE} = K[H_2L_2]^3_{org}/[H^+]^3_{aq}$$

During extraction, P_{RE} must be high. This is achieved by lowering H^+ concentration, that is, by neutralizing with NaOH. And during the stripping, P_{RE} must be low which is possible by adding acid.

This acid consumption is the main drawback of acidic extractants like H(EH)EHP. Indeed, the higher the equilibrium constant, the higher the acid requirement.

Along the RE series the equilibrium constant of extraction increases from La^{3+} to Lu^{3+}, that is

$$La^{3+} < Ce^{3+} < \cdots < Ho^{3+} < Y^{3+} < Er^{3+} < \cdots < Yb^{3+} < Lu^{3+}$$

Consequently, purification of high atomic number (heavy) RE with these types of molecules requires a large quantity of acid—at considerable cost.

Reference

Rydberg, J., Cox, M., Musikas, C., Chopin, G.R., 2007. Solvent Extraction Principles and Practice, second ed., Revised and Expanded. CRC Press, Boca Raton, Florida.

CHAPTER

Production of Rare Earth Metals and Alloys—Electrowinning

6

The products of Chapter 5's rare earth separations are individual high purity rare earth oxides, phosphates, and fluorides. They are often used in this form, e.g., as:

automotive pollution-abatement catalysts (oxides)
fluorescent lamps (phosphates)
electrowinning electrolytes (fluorides).

However, many applications require that the oxides and fluorides be reduced to metals and alloys. Examples are

neodymium metal for Nd-Fe-B permanent magnets
samarium metal for Sm-Co permanent magnets
lanthanum, cerium, praseodymium, and neodymium for rechargeable battery electrodes
cerium for improving cast iron ductility.

About 40% of mined rare earth production is reduced to metals and alloys, including most of Nd, Sm, and Dy.

This chapter

(a) summarizes production of rare earth metals from their oxides and halides
(b) details fused-salt electrowinning of rare earth metals

while chapter 7

(a) details metallothermic rare earth metal production
(b) summarizes rare earth metal refining.

6.1 REDUCTION

Reduction is splitting a compound into its metal and nonmetal components. An industrial rare earth example of this is

$$\underset{\text{raw material}}{Sm_2O_3(s)} + \underset{\text{reductant}}{2La^\circ(\ell)} \xrightarrow{1200^\circ C} \underset{\text{slag}}{La_2O_3(s)} + \underset{\text{product metal}}{2Sm^\circ(g)} \tag{6.1}$$

for which we say *lanthanum metal is reducing samarium oxide to elemental samarium metal* (vapor in this case).

This is often referred to as metallothermic reduction because a metal is used as the *reductant*. It is detailed in Chapter 7.

Rare Earths. http://dx.doi.org/10.1016/B978-0-444-62735-3.00006-1

FIG. 6.1

Fused-salt (1050 °C) electrowinning cell for producing 99.9 mass% pure molten neodymium (see sign on wall). The central tungsten cathode is noticeable. It is surrounded by four submerged graphite anodes (Fig. 6.3).

Photo courtesy of Professor Toru Okabe, Tokyo University.

Rare earth compounds are too strongly bonded to be reduced by carbon or hydrogen. These *reductants* are never used to produce pure rare earth metals.

6.1.1 Electrowinning

Much of rare earth reduction is done by fused-salt electrowinning, e.g., Figs. 6.3 and 6.6

$$\underset{\substack{\text{dissolved in molten}\\ \text{halide salt solution}}}{\mathrm{Nd}^{3+}} + \underset{\substack{\text{electrons from external}\\ \text{direct current power source}}}{3e^{-}} \xrightarrow{1050\,^{\circ}\mathrm{C}} \underset{\text{molten metal}}{\mathrm{Nd}^{\circ}(\ell)} \tag{6.2}$$

It is analogous to aluminum molten salt electrowinning.

6.1.2 Industrial reduction

Industrial rare earth reduction employs both electrowinning and metallothermic reduction. Electrowinning produces the most metal. It can be operated continuously, except for “tapping.”

Metallothermic reduction is used for elements that cannot be electrowon, e.g., samarium. Samarium is critical for the manufacture of Sm-Co permanent magnets. It is made almost entirely by metallothermic reduction (Reaction (6.1)).

6.2 INDUSTRIAL RARE EARTH ELECTROWINNING

Rare earth metals cannot be electrowon from aqueous solutions because it requires:

a larger electrical potential
to dissociate:
dissolved rare earth compounds
than is required to dissociate water.

So, as electrolytic cell applied potential is gradually increased, it is water that decomposes first [to $H_2(g)$ and $O_2(g)$] rather than dissolved rare earth compounds.

As a consequence, all rare earth metal electrowinning uses molten halide salt electrolyte (Fig. 6.2). In this, they are like aluminum which is made exclusively by molten salt electrowinning.

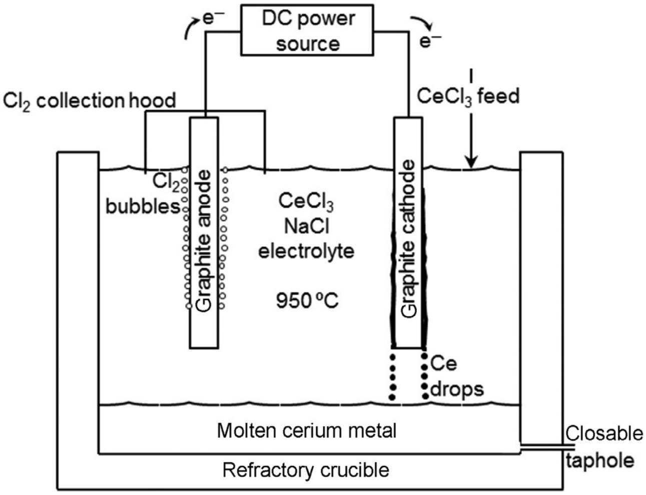

FIG. 6.2

Schematic electrolysis cell for electrowinning rare earth metals from purified chloride feed. Chlorine is continuously collected, purified and reused. The cell is operated above the melting temperatures of the electrolyte and metal, Table 6.1. It is heated by the electrowinning current. The process is continuous except for molten metal removal (tapping), which is intermittent. Its applied potential is ~10 volts and the current is 2-10 kiloamperes. An alternative arrangement is to have the cathode at the bottom of the cell. Chlorine production is a disadvantage. It has led to wide adoption of oxide feed-molten salt electrowinning, Section 6.4.

Drawing by William Davenport.

6.3 CHLORIDE ELECTROWINNING

The simplest type of rare earth metal electrowinning is chloride electrowinning (Fig. 6.2). It:

(a) charges solid anhydrous purified rare earth chloride powder (e.g., CeCl_3) to a 950 °C furnace
(b) dissolves the anhydrous chloride charge into a molten chloride (e.g., $\text{CeCl}_3\text{-NaCl}$) electrolyte
(c) applies a direct current potential between a graphite anode and a graphite cathode, both immersed in the electrolyte (Fig. 6.2).
(d) produces molten rare earth metal at the cathode and $\text{Cl}_2(g)$ at the anode.

The metal is denser than the electrolyte. It sinks to the bottom of the furnace where it is periodically:

(a) syphoned out of the furnace via a vacuum pipe
or
(b) drained out of the furnace through a submerged closable taphole.

Industrial molten salt electrowinning is always designed to produce *molten* metal. A molten product is easily tapped, poured, or syphoned from the electrowinning furnace. It allows almost continuous electrowinning.

6.3.1 Reactions

Figure 6.2's electrowinning reactions are represented by the following equations: *Dissolution*:

$$\underset{\substack{\text{anhydrous purified}\\ \text{cerium chloride feed powder}}}{\overset{30\,^\circ\text{C}}{2\text{CeCl}_3(s)}} \longrightarrow 2\text{Ce}^{3+} \underset{\text{dissolved in CeCl}_3\text{–NaCl electrolyte}}{\overset{950\,^\circ\text{C}}{+}} 6\text{Cl}^- \tag{6.3}$$

Electrowinning
At the cathode (Fig. 6.2):

$$\underset{\text{in molten electrolyte}}{2\text{Ce}^{3+}} + \underset{\substack{\text{electrons at the cathode surface}\\ \text{from DC electric power source}}}{6\text{e}^-} \xrightarrow{950\,^\circ\text{C}} \underset{\substack{\text{metal pool on}\\ \text{furnace bottom}}}{2\text{Ce}^\circ(\ell)} \tag{6.4}$$

At the anode:

$$\underset{\text{in molten electrolyte}}{6\text{Cl}^-} \xrightarrow{950\,^\circ\text{C}} \underset{\substack{\text{chlorine gas to}\\ \text{collection and re-use}}}{3\text{Cl}_2(g)} + \underset{\substack{\text{electrons to DC electrical power}\\ \text{source then back to the cathode}}}{6\text{e}^-} \tag{6.5}$$

for a total of:

$$\underset{\substack{\text{anhydrous purified}\\ \text{cerium chloride powder feed}}}{\overset{30\,^\circ\text{C}}{2\text{CeCl}_3(s)}} \longrightarrow \underset{\substack{\text{metal pool on}\\ \text{furnace bottom}}}{\overset{950\,^\circ\text{C}}{2\text{Ce}^\circ(\ell)}} + \underset{\substack{\text{chlorine gas to}\\ \text{collection and re-use}}}{\overset{950\,^\circ\text{C}}{3\text{Cl}_2(g)}} \tag{6.6}$$

6.3.2 Metal purity

Electrowinning's rare earth metal product is almost as pure as its rare earth chloride feed. It can be further purified (refined) as described in Sections 7.5–7.7.

6.3.3 Alloy electrowinning

Chloride molten salt electrowinning is also used to produce *mischmetal* alloy containing about:

25 mass% lanthanum
50 mass% cerium
5 mass% praseodymium
20 mass% neodymium.

It is made from anhydrous chloride powder of about the above metal proportions, i.e.,

$$\mathrm{La}:\mathrm{Ce}:\mathrm{Pr}:\mathrm{Nd} = 25:50:05:20$$

Chlorides like this precipitate naturally from bastnasite and monazite mineral leach solutions. However, the composition varies according to the composition of the original ore.

Production of the above described mischmetal is possible because La, Ce, Pr, and Nd chlorides all have about the same decomposition potential. So as the applied potential in Fig. 6.2 is increased, they all begin to dissociate to metal and gas at about the same voltage.

The mischmetal is used for metallothermic reduction and in rechargeable battery alloy electrodes. Increasingly, however, mischmetal is being replaced by high-purity lanthanum, cerium, praseodymium, and neodymium for making battery electrode alloys. Mischmetal is being relegated to fire-starter alloys.

6.3.4 Industrial status

Industrial chloride electrowinning started at the beginning of the twentieth century, mostly in China and Japan. It is still used in China for producing cerium metal and mischmetal alloy. Large (up to 50,000 ampere) electrolytic cells are used, producing several tons of metal or alloy per day.

However, the chloride process was discarded in Japan around 1975 in favor of oxide feed-fluoride electrolyte electrowinning. This is because:

(a) the oxide feed can be handled safely and easily
(b) production of halide gas is minimized.

6.4 OXIDE FEED—FLUORIDE MOLTEN SALT ELECTROWINNING

Oxide feed-molten fluoride salt electrowinning is used extensively for making neodymium metal and neodymium-iron alloys. These products are essential for making Nd-Fe-B permanent magnets, the world's strongest.

Neodymium electrowinning is very similar to aluminum metal electrowinning. Both processes:

(a) feed pure anhydrous oxide to a high temperature (950-1050 °C) electrolytic cell
(b) dissolve this oxide feed in molten fluoride electrolyte
(c) use carbon anodes
(d) heat the cell with the electrowinning electric current
(e) collect reduced metal at the bottom of the cell
(f) release oxygen and some carbon monoxide through the top of the cell.

A major difference is that neodymium electrowinning uses a metal (rather than carbon) cathode (Fig. 6.3). It is:

(a) tungsten or molybdenum, if the cathode product is neodymium metal (because tungsten and molybdenum don't melt or dissolve at ~1050 °C, Table 6.1)
(b) high-purity iron, if the product is to be neodymium-iron alloy.

The success of the process depends on:

(a) high-purity rare earth oxide feed
and
(b) an electrolyte from which the rare earth metal is the only one to electrodeposit.

In the present case, the first metal to deposit (as the cell's anode-cathode electrical potential is raised from zero) is neodymium, not the electrolyte's Li, Ca, and Ba.

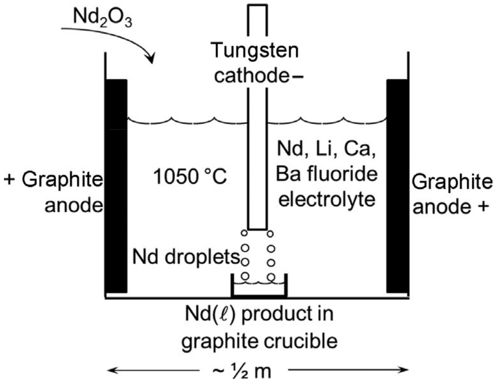

FIG. 6.3

Schematic of electrolytic cell for producing molten neodymium metal. The feed is pure Nd_2O_3. The product is pure molten neodymium metal. The electrolyte is molten Nd, Li, Ca, Ba, fluoride, 1050 °C. Nd-Fe alloy may be produced in this cell by replacing its inert tungsten cathode with a pure cast Fe cathode. The electrowinning is continuous. The solid charge is added as needed. The metal is removed by lifting out the submerged graphite crucible (Fig. 6.4) or by syphoning.

Drawing by William Davenport.

Table 6.1 Melting points of rare earth metals and four metals that are used in processing rare earth metals (Ames Laboratory, 2013)

Metal	Melting Point (°C)
Lanthanum	0920
Cerium	0795
Praseodymium	0935
Neodymium	1024
Samarium	1072
Europium	0826
Gadolinium	1312
Terbium	1356
Dysprosium	1407
Holmium	1461
Erbium	1529
Thulium	1545
Ytterbium	0824
Lutetium	1652
Iron	1538
Molybdenum	2620
Tantalum	3020
Tungsten	3420

6.4.1 Electrolytic cell

Figure 6.3 sketches an electrolytic cell for producing neodymium metal and alloys from purified oxide feed via molten fluoride electrolyte. The graphite anodes and metal cathode are notable.

Figures 6.1 and 6.4 through Fig. 6.6 show ~3000 ampere rare earth metal and alloy electrowinning furnaces. They are about 1 m × 1 m × 1 m (outside) with a 1/2 m diameter molten fluoride electrolyte bath inside. They produce about 100 kg of rare earth metal per day.

6.4.2 Electrolyte

The electrolyte for electrowinning neodymium-iron alloys and neodymium metal is made up of Nd, Li, Ca, and Ba fluorides. Its composition varies from production company to production company. The fluorides are made industrially by reacting oxides with ammonium bifluoride, NH_4FHF (Riedemann, 2011).

An industrial example is (Fig. 6.5):

Neodymium fluoride	60 mass%
Lithium fluoride	25 mass%
Calcium fluoride	10 mass%
Barium fluoride	5 mass%

FIG. 6.4

Photograph showing submerged metal-catching crucible being lifted out of an electrolyte bath. The molten rare earth metal will be poured into the mold, front. Notice that the central cathode has to be lifted out of the electrolyte for the tongs to reach the central submerged graphite crucible.

Photo courtesy of Professor Toru Okabe, Tokyo University.

FIG. 6.5

Photograph of rare earth metal and alloy electrowinning smelter. Notice the gas collection hood, above. The nearest furnace produces holmium-iron alloy (used in powerful magnets). Other products of the smelter are:

Dy-Fe alloy
Nd-Fe alloy
Nd-Pr alloy
99% Nd
99.9% Nd.

All are used in magnets.

Photograph courtesy of Professor Toru Okabe, University of Tokyo.

The electrolyte is chosen to have:

(a) a low melting point
(b) high solubility for neodymium oxide
(c) good stability, i.e., no extraneous reactions during electrowinning
(d) high ionic conductivity
(e) low viscosity
(f) reasonable corrosivity.

FIG. 6.6

Electrowinning furnace for producing molten dysprosium-iron alloys. Neodymium-iron alloys are made the same way. The central "rod bundle" is an iron cathode. It is encircled by graphite anodes (Fig. 6.3). The molten material is Dy, Li, Ca, Ba fluoride electrolyte, 1050 °C. A DC potential (~12 volts) is applied between anodes and cathode, causing (i) current (~3200 amperes) to flow and (ii) dysprosium to electrodeposit on the iron cathode. Molten Dy-Fe alloy then forms and drips down off the cathode. The circular opening is ~0.3 m diameter. The furnace operates continuously except when removing molten alloy product (Fig. 6.4).

Photo courtesy of Professor Toru Okabe, Tokyo University.

6.4.3 Reactions

Oxide feed-fluoride electrolyte electrowinning (with Nd as the example) proceeds by reactions like:

(a) dissolution of pure Nd_2O_3 powder into the electrolyte, i.e.:

$$\underset{\substack{\text{high purity anhydrous}\\ \text{oxide powder feed}}}{\overset{30\,^\circ\mathrm{C}}{2Nd_2O_3}} \longrightarrow 4Nd^{3+} \underset{\text{dissolved in electrolyte, }\sim 1050\,^\circ\mathrm{C}}{\overset{1050\,^\circ\mathrm{C}}{+}} 6O^{2-} \tag{6.7}$$

(b) metal reduction at cathode surface:

$$\underset{\substack{\text{dissolved in}\\ \text{molten electrolyte}}}{4\mathrm{Nd}^{3+}} + \underset{\substack{\text{electrons from DC}\\ \text{electrical power source}\\ \text{at cathode surface}}}{12\mathrm{e}^{-}} \xrightarrow{\sim 1050\,^{\circ}\mathrm{C}} \underset{\substack{\text{molten metal droplets}\\ \text{dripping from cathode}\\ \text{surface into submerged}\\ \text{graphite crucible}}}{4\mathrm{Nd}^{\circ}(\ell)} \tag{6.8}$$

(c) gas evolution at anode surfaces:

$$\underset{\substack{\text{dissolved in}\\ \text{molten electrolyte}}}{6\mathrm{O}^{2-}} \xrightarrow{\sim 1050\,^{\circ}\mathrm{C}} \underset{\substack{\text{oxygen evolving at}\\ \text{anode surfaces}}}{3\mathrm{O}_2(\mathrm{g})} + \underset{\substack{\text{electrons to the DC}\\ \text{electrical power source then}\\ \text{back to cathode surface}}}{12\mathrm{e}^{-}} \tag{6.9}$$

for a total of:

$$\underset{\substack{\text{high purity anhydrous}\\ \text{oxide powder feed}}}{\overset{30\,^{\circ}\mathrm{C}}{2\mathrm{Nd}_2\mathrm{O}_3(\mathrm{s})}} \longrightarrow \underset{\substack{\text{molten metal droplets}\\ \text{dripping from cathode}\\ \text{surface into submerged}\\ \text{graphite crucible}}}{\overset{\sim 1050\,^{\circ}\mathrm{C}}{4\mathrm{Nd}^{\circ}(\ell)}} + \underset{\substack{\text{oxygen evolving at}\\ \text{anode surfaces}}}{\overset{\sim 1050\,^{\circ}\mathrm{C}}{3\mathrm{O}_2(\mathrm{g})}} \tag{6.10}$$

Some carbon monoxide is inadvertently produced at the graphite anode surfaces—by the reaction:

$$\underset{\substack{\text{oxygen evolving at}\\ \text{anode surfaces}}}{\mathrm{O}_2(\mathrm{g})} + \underset{\text{graphite anodes}}{2\mathrm{C}(\mathrm{s})} \longrightarrow \underset{\substack{\text{formed at the}\\ \text{anode surfaces}}}{2\mathrm{CO}(\mathrm{g})} \tag{6.11}$$

This requires careful ventilation in the workplace.

Reactions 6.8 and 6.9 are driven by the cell's applied DC potential.

6.4.4 Neodymium-iron alloy production

Neodymium tends to self-combust in air. It must be handled very carefully. This risk is lowered by producing Nd-Fe alloy. This alloy is less combustible than Nd itself and is a useful starting material for neodymium-iron-boron magnets. Also it has a lower melting point than pure Nd (Fig. 6.7) so that alloy electrolysis can be operated cooler than pure metal electrolysis.

Neodymium-iron alloy is produced by replacing the insoluble cathode in Fig. 6.3 with a pure cast Fe cathode.

The newly electrowon neodymium at the cathode surface reacts with the Fe cathode to produce molten alloy which melts and drips into Fig. 6.3's submerged graphite crucible. The reaction is:

$$\underset{\substack{\text{electrodeposited}\\ \text{on Fe cathode}}}{\mathrm{Nd}^{\circ}(\ell)} + \underset{\text{cathode}}{\mathrm{Fe}(\mathrm{s})} \xrightarrow{\sim 1050\,^{\circ}\mathrm{C}} \underset{\substack{\text{molten alloy drops to}\\ \text{submerged graphite crucible}}}{\text{Nd-Fe alloy}(\ell)} \tag{6.12}$$

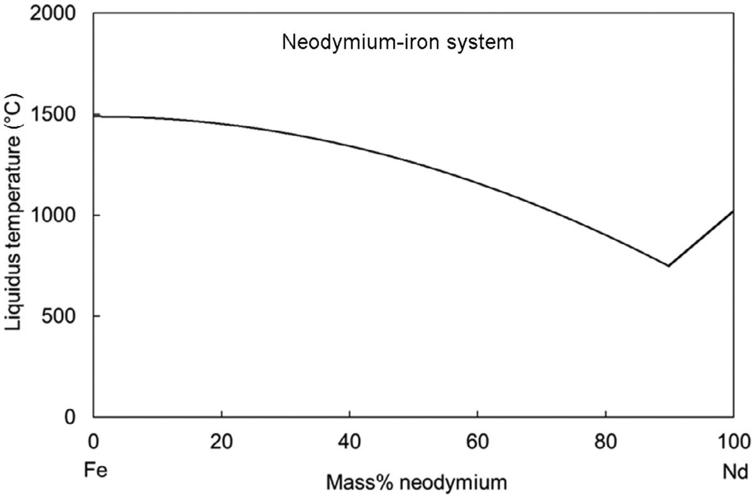

FIG. 6.7

Approximate liquidus line for Fe-Nd alloys, °C and mass%. The alloys are fully molten above the liquidus line. The information is based on Okamoto (2006), who gives concentration in atom percent. Electrowinning's product alloys typically contain 70-85 mass% Nd.

Data courtesy ASM International.

FIG. 6.8

Electrowon neodymium ingot, buffed and given an identification number. It is ~11 cm long across the top. Its purity is ~99.9 mass% Nd.

Photo courtesy of Randall Ice.

Typical alloy product contains ~80 mass% Nd, 20 mass% Fe, melting point ~900 °C. It is made into ~30% Nd magnet alloy by melting it along with pure Fe during magnet making.

Dysprosium-iron alloy is made in a similar way. Dysprosium increases the high temperature magnetic strength of Nd,(Dy),Fe,B permanent magnets (Constantinides, 2012).

6.4.5 Purity

Carefully electrowon Nd, Nd-Fe, and Dy-Fe alloys are better than 99.9 mass% pure. They need no further refining before magnet making. However, they and other magnet ingredients are always vacuum melted (hence purified) before being cast as magnet alloy (Sections 7.5–7.7).

6.5 NEODYMIUM ELECTRODEPOSITION RATE

Electrodeposition of neodymium from a molten salt bath may be represented by the reaction:

$$\underset{\substack{\text{dissolved in molten}\\ \text{halide salt solution}}}{\mathrm{Nd}^{3+}} + \underset{\substack{\text{electrons from external}\\ \text{direct current power circuit}}}{3\mathrm{e}^{-}} \xrightarrow{1050\,^{\circ}\mathrm{C}} \underset{\text{molten metal}}{\mathrm{Nd}^{\circ}(\ell)} \tag{6.2}$$

This equation indicates that three electrons are required to electrodeposit one atom of neodymium metal. It also indicates that the gram-equivalent mass of neodymium is:

$$\begin{aligned}(\text{gram-equivalent mass})_{\mathrm{Nd}} &= \frac{(\text{gram-molecular mass})_{\mathrm{Nd}}}{3\text{ electrons required to deposit one atom of Nd}}\\ &= \frac{144.2\,\mathrm{g}_{\mathrm{Nd}}}{3}\\ &= 48.1\,\mathrm{g}\end{aligned} \tag{6.13}$$

where gram-equivalent $\text{mass}_{\mathrm{Nd}}$ is the mass of neodymium (g) that is electrodeposited by 1 Faraday (97,500 coulombs) of electrical charge. This number is used in the following neodymium electrodeposition rate calculation.

6.5.1 Electrodeposition rate

Electrowinning furnaces are often rated in terms of their installed electrical current capability, amperes. The greater the installed current capability, the greater is the design rare earth metal production rate. This is shown by the following calculation, using neodymium as the example.

Table 6.2 Estimated industrial rare earth electrowinning current efficiencies

Element	Current Efficiency (%)
La	73
Pr	62
Nd	75
Gd	76
Tb	74
Dy	95

Table courtesy of Professor Osamu Takeda, Tohoku University, Japan.

Neodymium electrodeposition rate is given by the equation:

$$\text{Nd electrodeposition rate, g/s} = \frac{i \times \text{current efficiency}}{\text{Faraday's constant, F}} \times (\text{gram-equivalent mass})_{\text{Nd}} \tag{6.14}$$

where i = current, coulombs per second (amperes); current efficiency = % of total current that is actually being used to electrodeposit Nd° (i.e., not for side reactions); and Faraday's constant, F = charge (coulombs) required to electrodeposit one gram-equivalent mass of any metal ~96,500 coulombs per gram-equivalent mass.

Assuming a 75% current efficiency (Table 6.2) and a current of 1 coulomb per second (i.e., 1 ampere), the electrodeposition rate of neodymium metal is:

$$\begin{aligned}\text{Nd electrodeposition rate, g/s} &= \frac{1\ \text{coulomb per second} \times (75/100)\%}{96{,}500\ \text{coulombs per gram-equivalent mass}} \\ &\quad \times 48.1\ \text{g Nd per gram-equivalent mass} \\ &= 3.8 \times 10^{-4}\ \text{g/s}.\end{aligned} \tag{6.15}$$

With 8.64×10^4 s in a day this is equivalent to 33 g/day.

Thus a 3000 ampere furnace will produce 3000 times this much, i.e., 3000 × 33 g/day = 1×10^5 g/day or 100 kg of neodymium per day. This is equivalent to 0.10 tonnes per day × 365 days per year = ~40 tonnes per year.

The same deposition rate applies to electrolytic Nd-Fe alloy production, where the result would be 40 tons per year of *Nd-in-alloy*.

6.5.2 Metals and alloys made industrially by electrowinning

Metals and alloys commonly made by oxide feed/fluoride electrolyte electrowinning are:

La
Ce
Pr

Nd
Dy
La-Ce-Pr-Nd (mischmetal)
Nd-Fe
Nd-Dy
Nd-Pr
Dy-Fe
Pr-Nd-Fe
Nd-Dy-Fe
Ho-Fe

The remainder:

Sm
Eu
Gd
Tb
Tm
Er
Yb
Lu

are mostly made by metallothermic reduction (Chapter 7).

Cerium is made by both methods.

Samarium is never made by electrolytic reduction. Too much samarium vapor would be lost in the process (because of samarium's high vapor pressure).

6.6 SUMMARY

This chapter describes fused-salt rare earth metal electrowinning. The process entails:

(a) dissolving a rare earth compound (e.g., Nd_2O_3) in 1050 °C molten halide electrolyte
(b) passing direct electric current through the electrolyte from a graphite anode to a tungsten cathode
(c) consequently electrodepositing molten rare earth metal (e.g., neodymium) on the tungsten cathode.

The electrodeposited molten metal drips off the cathode into a small graphite collection crucible where it is collected, cast, and used.

This process is much like fused-salt electrowinning of aluminum, but on a much, much smaller scale.

Iron-rare earth alloys are also made by electrowinning—by replacing the tungsten cathode with an iron cathode. In this case, the newly deposited molten rare earth metal dissolves some of the iron cathode to produce molten iron-rare earth metal alloy.

The main advantage of electrowinning is that it is a semicontinuous process that is done at a moderate temperature (~1000 °C) and ambient pressure.

Its main competitor for rare earth metal production is metallothermic reduction (Chapter 7).

References

Ames Laboratory, 2013. What are the Rare Earths? Ames, Iowa. Retrieved on August 14, 2013 from www.ameslab.gov/dmse/rem/what-are-rare-earths.

Constantinides, S., 2012. The demand for rare earth materials in permanent magnets. In: Rare Earths. Met Soc of CIM, Montreal, QC, pp. 293–307.

Okamoto, H., 2006. Fe-Nd Phase Diagram, ASM Alloy Phase Diagrams Center, P. Villars, editor-in-chief: H. Okamoto and K. Cenzual, section editors: http://www1.asminternational.org/AsmEnterprise/APD, ASM International, Materials Park, OH, USA.

Riedemann, T.M., 2011. High Purity Rare Earth Metals Preparation. Ames Laboratory, US Department of Energy, Ames, IA. Retrieved on August 14, 2013 from, https://www.ameslab.gov/files/REM_presentation_ShortForm.pptx.

Suggested Reading

Constantinides, S., 2013. Rare earth elements in transportation. In: Rare Earth Elements. Met Soc of CIM, Montreal, QC, pp. 47–62.

Wang, C., Liu, Y., He, H., Gao, F., Liu, L., Chang, S., Guo, J., Chang, L., Ouyang, Y., 2013. Electrochemical behavior of cerium ion in molten LiCl-KCl. J. Rare Earths. 31 (4), 405–409.

CHAPTER

7

Metallothermic Rare Earth Metal Reduction

Chapter 6 describes rare earth metal electrowinning. This chapter describes metallothermic rare earth metal reduction, which is done by:

(a) high temperature-high vacuum lanthanum reduction of rare earth oxides to metal vapor and deposition of this vapor as pure solid metal on a cool surface (Fig. 7.1)

and:

(b) high temperature calcium reduction of rare earth fluorides to molten metal (Fig. 7.5).

Method (a) avoids hazardous preparation of fluoride compounds but it can only be used for metals with high vapor pressures. It is used to produce Sm, Eu, Tm, and Yb. Lanthanum is used for the reduction because it:

(a) is a strong reductant
(b) has a low vapor pressure (and therefore doesn't contaminate the reduction/deposition product)

Calcium reduction is used for all other rare earth metals, often in competition with electrowinning.

Carbon and hydrogen are never used for rare earth metal reduction. Their reducing power is too weak.

7.1 SAMARIUM REDUCTION

The metal most produced by lanthanum reduction is samarium. It is widely used in samarium-cobalt permanent magnets but it can't be electrowon (because of its high vapor pressure). Sm-Co magnets are the strongest in the world at high operating temperatures (~200 °C). They are especially useful in aerospace electric motors and high-temperature magnetic bearings.

All of the samarium in permanent magnets is produced by lanthanothermic reduction/vapor deposition.

The reduction reaction is:

$$\underset{\text{raw material}}{Sm_2O_3(s)} + \underset{\text{reductant}}{2La^\circ(\ell)} \xrightarrow{1200^\circ C} \underset{\text{slag}}{La_2O_3(s)} + \underset{\text{product metal vapor}}{2Sm^\circ(g)} \tag{7.1a}$$

Rare Earths. http://dx.doi.org/10.1016/B978-0-444-62735-3.00007-3

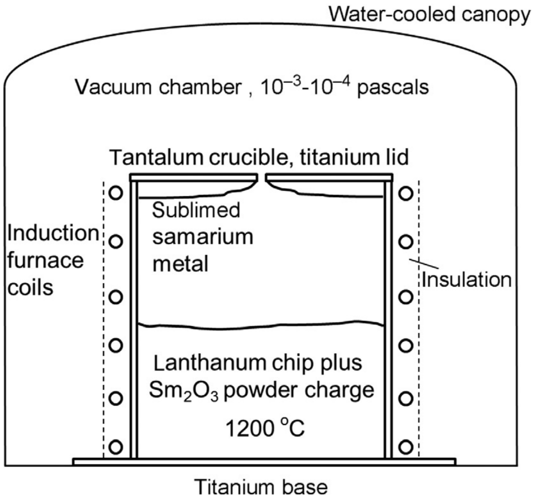

FIG. 7.1

Sketch of furnace for (i) La reduction of pure $Sm_2O_3(s)$ to samarium vapor followed by (ii) deposition of this samarium vapor as high purity solid samarium metal. The induction furnace, tantalum crucible, cooled deposition surface, and vacuum exit port are notable. The furnace operates at ~1200 °C and ~10^{-3}-10^{-4}pascal absolute pressure. Samarium recovery from Sm_2O_3 is ~90%.

Drawing by William Davenport.

Figure 7.1 is a sketch of an industrial furnace. It is cylindrical. Its key component is a tantalum crucible, 0.25 m diameter, 0.4 m tall, and 0.003 m thick. It is heated electrically by an induction coil. It produces up to 100 kg of vapor-deposited samarium per day.

A typical samarium production batch entails:

1. charging lanthanum metal or mischmetal chips (99.9% pure, flat, ~3 mm diameter) and samarium oxide powder (99.9% pure, ~40 μm diameter) into the crucible, 2/3 full, tamped
2. fitting and sealing the lid
3. purging the chamber with argon (twice) and then starting water cooling of the vacuum chamber
4. drawing a vacuum to 10^{-3}-10^{-4}pascal absolute in the vacuum chamber
5. turning on the induction furnace and gradually heating the crucible to ~1200 °C
6. turning off the furnace after a specified time
7. purging and filling the chamber with argon
8. removing the lid and chiseling off the dendritic samarium deposit (99.9% Sm, ~6 cm thick)
9. starting again with a cleaned, buffed, and acid (dilute HNO_3) washed crucible.

FIG. 7.2

La or mischmetal reduced, vapor-deposited samarium. The maximum dimension of the large piece is ~11 cm. Photo courtesy of Randall Ice. Fully dense samarium is made by vacuum melting and vacuum casting this dendritic product.

The dendritic samarium metal (Fig. 7.2) is usually melted in a vacuum furnace and then vacuum cast, giving a dense, high quality samarium ingot.

A batch of samarium production typically takes ~10 h and produces 20-40 kg of dendritic samarium metal. Samarium recovery from Sm_2O_3 is about 90%.

Europium, thulium, and ytterbium are also made this way, usually on a smaller scale and under considerably lower pressures, 10^{-5}-10^{-6}pascal absolute.

7.2 THERMODYNAMIC EXPLANATION

The Gibbs free energy change $\Delta_r G^\circ{}_{1473}$ for the reaction:

$$\underset{\substack{\text{pure anhydrous solid feed materials}\\ \text{La melting point} = 920^\circ\text{C}}}{Sm_2O_3(s) + 2La^\circ(l)} \xrightarrow{1200^\circ\text{C (1473 K)}} \underset{\text{solid product}}{La_2O_3(s)} + \underset{\text{vapor product}}{2Sm^\circ(g)} \tag{7.1b}$$

is +45 megajoules per kg-mole of Sm_2O_3 (Barin, 1993).

FIG. 7.3

Small-scale induction furnace for lanthanum reduction of high purity ytterbium and other high vapor pressure rare earth metals (europium, samarium, and thulium)(Riedemann, 2011). It operates at ∼1500 °C and 10^{-3}-10^{-4} pascal absolute pressure. Lanthanum metal chips reduce Yb_2O_3 powder in a tantalum crucible (hidden by the induction coil). The product is ytterbium vapor, which deposits as solid metal in a cool zone atop the furnace. Figure 7.4 shows the product ytterbium metal. The borosilicate glass furnace is ∼10 cm diameter, inside.

Photo courtesy Trevor Riedemann, Ames Laboratory, Ames Iowa.

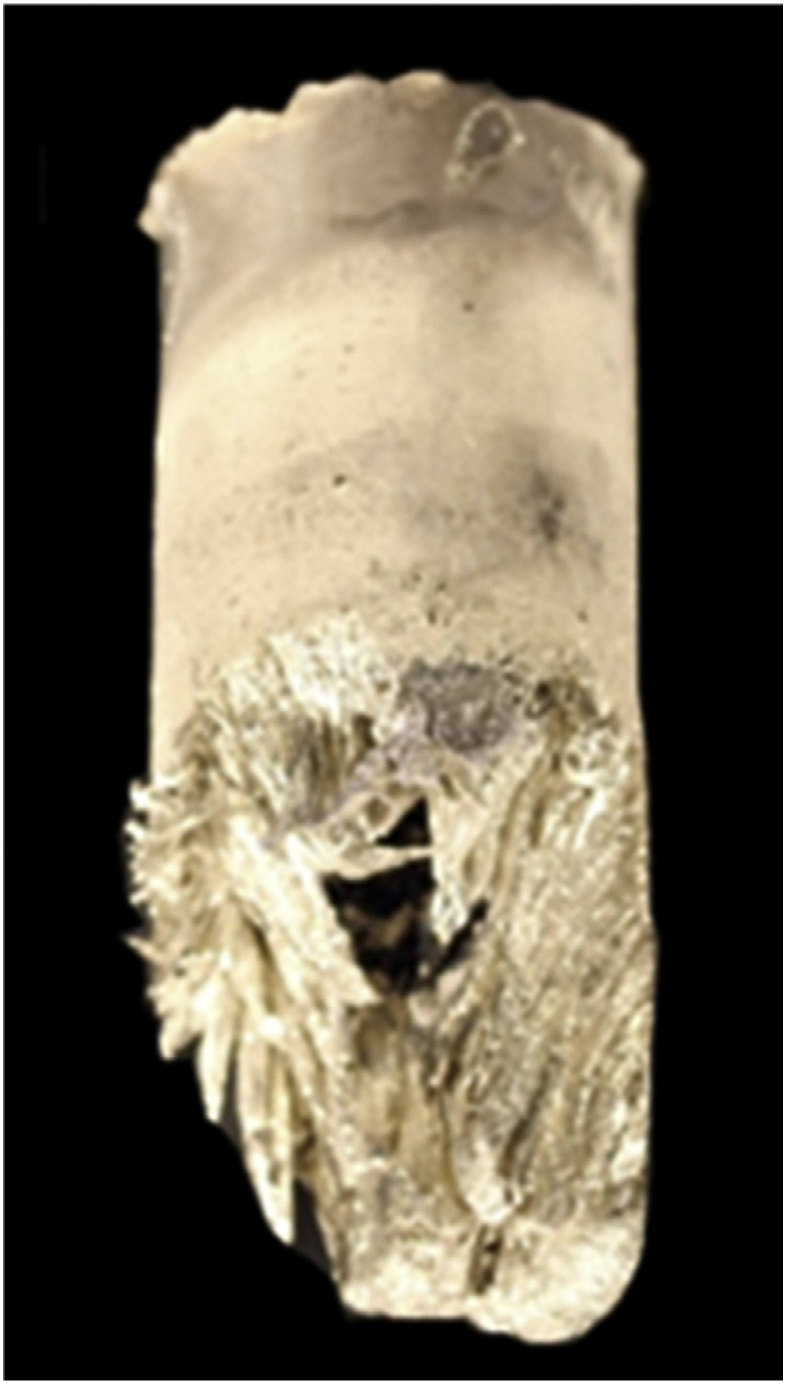

FIG. 7.4

Vapor-deposited ytterbium metal from the Fig. 7.3 furnace, 1 cm diameter and 5 cm long (Riedemann, 2011). As is, it contains 99.99 mass% Yb. It may be marketed in this form or remelted to make a dense ytterbium ingot.

Photo courtesy Trevor Riedemann, Ames Laboratory, Ames Iowa.

This free energy change is related to Reaction (7.1)'s equilibrium quantities by the equations:

$$K_E = \frac{a^E_{La_2O_3(s)} \times \left(a^E{}_{Sm^\circ(g)}\right)^2}{a^E_{Sm_2O_3(s)} \times \left(a^E{}_{La^\circ(\ell)}\right)^2} \tag{7.2}$$

and

$$K_E = e^{\left(\frac{-\Delta_r G^\circ{}_{1473}}{R \times 1473}\right)} \tag{7.3}$$

where

$\Delta_r G^\circ{}_{1473}$ = Gibbs free energy change (1473 K) for Reaction (7.1b), +45megajoules per kg-mole of $Sm_2O_3(s)$
K_E = equilibrium constant for Eqs. (7.2) and (7.3) at 1473 K, unitless
a^E = thermodynamic activity of each component, unitless
R = gas constant, megajoules per kg-mole of $Sm_2O_3(s)$ = 0.008314 MJ per kg-mole of $Sm_2O_3(s)$
1473 = reaction temperature, K

The activities of $La_2O_3(s)$, $Sm_2O_3(s)$, and $La^\circ(\ell)$ are all 1 because they are all present as pure phases in Fig. 7.1's crucible. This simplifies Eqs. (7.2) and (7.3) to:

$$K_E = \left(a^E_{Sm^\circ(g)}\right)^2 = e^{\left(\frac{-\Delta_r G^\circ{}_{1473}}{R \times 1473}\right)} \tag{7.4}$$

from which

$$\begin{aligned}\left(a^E_{Sm^\circ(g)}\right)^2 &= e^{\left(\frac{-(+45)}{0.008314 \times 1473}\right)} \\ &= 0.025\end{aligned} \tag{7.5}$$

Taking the square root of both sides gives:

$$a^E_{Sm^\circ(g)} = (0.025)^{1/2} = 0.16 \tag{7.6}$$

The activity of gases is defined as:

$$a^E_{Sm^\circ(g)} = \frac{P^E_{Sm^\circ(g)}}{1} \tag{7.7}$$

where

$P^E_{Sm^\circ(g)}$ = the equilibrium partial pressure (bar) of Sm°(g) in Fig. 7.1's crucible
1 = the standard state pressure (bar) of pure gas = 10^5pascal.

Equations (7.6) and (7.7) are combined to give:

$$a^E_{Sm^\circ(g)} = \frac{P^E_{Sm^\circ(g)}\,\text{bar}}{1\,\text{bar}} = 0.16$$

from which

$$\begin{aligned} P^{E}{}_{Sm^\circ(g)}\text{bar} &= a^{E}{}_{Sm^\circ(g)} \times 1\,\text{bar} \\ &= 0.16 \times 1\,\text{bar} \\ &= 0.16\,\text{bar} \\ &= 1.6 \times 10^{4}\,\text{pascal} \end{aligned} \tag{7.8}$$

This relatively high samarium pressure indicates that the reduction process can proceed quickly under a moderate vacuum of 10^{-3}-10^{-4}pascal absolute.

7.2.1 Lanthanum and tantalum vapor pressures

The other metals in the Fig. 7.1 furnace are lanthanum (excess reductant) and tantalum (crucible). They both have low vapor pressures:

Lanthanum (1200 °C): 10^{-4}pascal (Habermann and Daane, 1964)
Tantalum (1200 °C): 10^{-21}pascal (Edwards et al., 1951)

so they don't contaminate the vapor-deposited samarium.

The purity of the vapor-deposited samarium is typically 99.9 mass% Sm. It needs no further refining. During Sm-Co magnet making, it is:

(a) mixed with pure cobalt and minor components (e.g., Cu, Fe, Gd, Pr, Zr)
(b) melted under vacuum to produce the required magnet alloy (and remove some impurities)
(c) solidified quickly
(d) decrepitated and ground to very fine particles
(e) compacted into useful magnet shapes by powder metallurgy techniques
(f) magnetized quickly in a huge magnetic field (ZAP!).

7.3 REDUCTION OF RARE EARTH FLUORIDES WITH CALCIUM METAL

Calcium reduction of rare earth fluorides is typified by the reaction:

$$\underset{\text{mixed high purity feed}}{1.5\text{Ca}(\ell) + \text{GdF}_3(\ell)} \xrightarrow{1470^\circ\text{C (1743 K)}} \underset{\text{two immiscible liquids}}{1.5\text{CaF}_2(\ell) + \text{Gd}(\ell)} \tag{7.9}$$

for which $\Delta_r G^\circ{}_{1743K} = -120$ MJ per kg-mole of $\text{GdF}_3(\ell)$(Barin, 1993).

It is used for producing all low vapor pressure rare earth metals, often in competition with electrowinning.

The melting points of Reaction (7.9)'s reactants and products are:

Ca	~840 °C
GdF_3	~1230 °C
CaF_2	1418 °C
Gd°	1312 °C

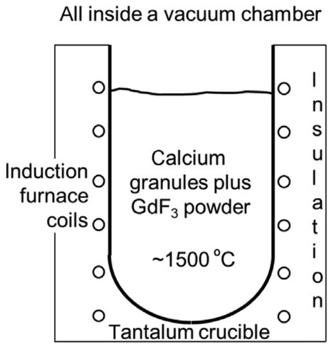

FIG. 7.5

Sketch of furnace for calcium reduction of gadolinium fluoride, ~1500 °C. The charge is made up of solid calcium metal granules ~3 mm diameter and solid gadolinium fluoride powder ~50 μm diameter, intimately mixed and tamped. The products are a molten gadolinium layer (bottom) and a calcium fluoride slag layer (top). These liquids are cast into a two-piece graphite mold, which is pulled apart after solidification, permitting easy separation of metal from slag. The purity of the gadolinium is improved by remelting several batches of gadolinium in this crucible under a strong vacuum ~10^{-4}pascal absolute. The crucible is ~0.25 m diameter × 0.4 m high. It produces ~15 kg of 99.9% pure gadolinium per batch. About 90% of the GdF_3's gadolinium is recovered as metal.

Drawing by William Davenport.

so, reduction to molten metal must be done at ~1470 °C to obtain fully liquid products.

Figure 7.5 sketches the inside of a reduction furnace and crucible. The tantalum crucible is initially full of mixed solid calcium metal granules and $GdF_3(s)$ powder feed. After the reaction is complete, the crucible contains two molten layers:

$$\begin{array}{l} CaF_2(\ell)\ (\text{specific gravity}\ \ 2.6)\ \text{on top} \\ Gd^{\circ}(\ell)\ (\text{specific gravity}\ \ 7.9)\ \text{below.} \end{array}$$

These layers are readily separated after cooling and solidification.

7.3.1 Operation

Industrial reduction entails:

- **(a)** drying and fluorinating gadolinium oxide (Section 6.4.2)
- **(b)** mixing and charging calcium metal chips and gadolinium fluoride powder to the tantalum crucible
- **(c)** purging the vacuum chamber with argon several times
- **(d)** closing up the vacuum chamber and drawing the vacuum down to ~10^{-4}pascal
- **(e)** slowly heating the mixture to ~1470 °C and holding for several hours under vacuum

(f) casting the crucible product into a two-piece graphite mold (also in the vacuum chamber)
(g) solidifying the products, pulling the mold apart and separating gadolinium metal (Fig. 7.6) from calcium fluoride slag
(h) remelting and vacuum casting several batches of gadolinium to remove volatile impurities.

The equipment is then cleaned, buffed, and acid washed. The process begins again.

The product from final step (h) can then be used as is or refined further as described in Sections 7.5–7.7.

FIG. 7.6

Gadolinium ingot from calciothermic reduction of gadolinium fluoride. Photo courtesy of Randall Ice. The largest diameter is ~13 cm. The ingot contains about 99.9 mass% Gd. The scratch marks are the result of physically separating this ingot from solid calcium fluoride slag above it.

Other metals that can be produced by calcium reduction are:

Lanthanum
Cerium
Praseodymium
Neodymium
Terbium
Dysprosium
Holmium
Erbium
Lutetium

many of them in competition with fused-salt electrowinning, particularly La, Ce, Pr, Nd, Dy, and Ho.

7.4 THERMODYNAMIC EXPLANATION

The equilibrium quantities and Gibbs free energy in Section 7.3 are related by the equations:

$$K_E = \frac{\left(a^E_{CaF_2(\ell)}\right)^{1.5} \times \left(a^E{}_{Gd^\circ(\ell)}\right)}{\left(a^E_{GdF_3(\ell)}\right) \times \left(a^E{}_{Ca^\circ(\ell)}\right)^{1.5}} \tag{7.10}$$

and

$$K_E = e^{\left(\frac{-\Delta_r G^\circ{}_{1743}}{R \times 1743}\right)} \tag{7.11}$$

where

$\Delta_r G^\circ{}_{1743}$ = Gibbs free energy change for Reaction (7.9), MJ per kg-mole of $GdF_3(\ell)$
K_E = equilibrium constant for Reaction (7.9) at 1743 K, unitless
a^E = equilibrium thermodynamic activity of each component, unitless
R = gas constant, MJ per kg-mole $GdF_3(l)$
  = 0.008314 MJ per kg-mole of $GdF_3(l)$
1743 = reaction temperature, K
$\Delta_r G^\circ{}_{1743}$ for Eq. (7.9) is:

$$-120\,\text{MJ per kg-mole of}\,GdF_3(\ell)$$

so

$$\begin{aligned} K_E^{1743} &= e^{\left(\frac{-(-120)}{0.008314 \times 1743}\right)} \\ &= 4 \times 10^3 \end{aligned} \tag{7.12}$$

7.4.1 Interpretation

The above large value of K_E^{1743} indicates that Reaction (7.9) goes to near completion. Assumptions that allow us to examine this are:

$a^E{}_{Gd^\circ(l)} = 0.98$(assumes that the reaction product is nearly pure liquid gadolinium)
$a^E{}_{Ca^\circ(l)} = 0.02$(impurity in molten gadolinium)
$a^E{}_{CaF2(l)} = 0.90$(slag is mostly $CaF_2(l)$)

which leads to

$$K_E = 4 \times 10^3 = \frac{\left(a^E_{CaF_2(\ell)}\right)^{1.5} \times a^E{}_{Gd^\circ(\ell)}}{a^E_{GdF_3(\ell)} \times \left(a^E{}_{Ca^\circ(\ell)}\right)^{1.5}} = \frac{(0.90)^{1.5} \times 0.98}{a^E_{GdF_3(\ell)} \times (0.02)^{1.5}} \tag{7.13}$$

or dividing both sides by 4×10^3 and multiplying both sides by $a^E_{GdF_3(\ell)}$

$$\begin{aligned} a^E_{GdF_3(\ell)} &= \frac{(0.90)^{1.5} \times 0.98}{4 \times 10^3 \times (0.02)^{1.5}} \\ &= 0.07 \end{aligned}$$

which indicates that most of the feed $GdCl_3(\ell)$ has reacted to $Gd^\circ(\ell)$.

The purity of the reduced gadolinium is ~99 mass% Gd. It is further purified by high temperature vacuum treatment Sections 7.5–7.7.

7.5 REFINING RARE EARTH METALS AND ALLOYS

The rare earth metals and alloys that are produced as described above are pure enough for most applications. This is because they are made carefully from pure raw materials. However, their purity can be improved further by (i) vacuum casting and (ii) vacuum vaporization.

Rare earth metals are also occasionally further purified by zone refining and other ultra-purification techniques. Details of these are given by Gupta and Krishnamurthy (2005).

7.6 VACUUM CASTING

Virtually all rare earth metals and alloys are purified by vacuum casting. The process entails melting the rare earth metal, holding it at temperature and then casting it—all under high vacuum ~0.1 pascal absolute.

High vapor pressure impurities vaporize under these conditions leaving behind an improved-purity product. Gases are also removed—by desorption from the molten metal.

The process is carried out during metal production and/or during product manufacture. For example, Nd, Dy, Fe, B magnet manufacturers:

(a) mix solid magnet alloy ingredients (e.g., high purity Nd-Fe alloy, Dy-Fe alloy, iron boride, Fe, Nd, Dy, Pr)
(b) melt and hold them under vacuum
(c) vacuum cast the molten product in a form that is convenient for magnet making (e.g., strip casting (Constantinides, 2012, 2013), rotating disc casting (Dent, 2012a,b) and ingot casting (Shin-Etsu, 2012).

Sm-Co magnets are made the same way with a mix of solid Sm, high purity Co, and minor quantities of high purity Cu, Fe, Gd, Pr, and Zr.

7.6.1 Lanthanum

Lanthanum is used in rechargeable battery electrode alloys. It has a low vapor pressure so that high vapor pressure impurities and gases are readily removed by vacuum melting/casting (Riedemann, 2011).

7.7 VAPORIZATION/VAPOR DEPOSITION

Purer rare earth metal can be made by vaporizing Section 7.6's as-cast product and

(a) depositing pure vaporized rare earth metal as a solid on cool surfaces above the vaporization furnace
(b) discarding the unvaporized impurities.

This is used by the Ames Laboratory (Riedemann, 2011) to purify Dy, Er, Gd, Ho, Lu, and Tb. It is not used for:

(a) Sm, Eu, Tm, and Yb, which have already been made by reduction/vaporization/deposition

or

(b) Ce, La, Nd, and Pr, which are purified by precipitating impurities from liquid rare earth metals near their solidification temperature (this is especially useful for eliminating tantalum that has absorbed from reduction's tantalum crucibles).

The vaporization/vapor-deposition process entails:

(a) holding the rare earth metal at high temperature and under high vacuum
(b) vaporizing the rare earth metal
(c) depositing pure rare earth metal vapor on cool surfaces above the holding furnace
(d) discarding the small remaining "butt" of very impure residue.

The result is a 99.9+% pure solid rare earth metal deposit.

7.8 SUMMARY

Metallothermic reduction is the reaction of a metal reductant with a rare earth oxide or halide to produce rare earth metal. Important examples are:

(a) reduction of samarium oxide with lanthanum to produce samarium metal
(b) reduction of gadolinium fluoride with calcium to produce gadolinium metal.

The process is always operated in batch mode so it is slow and expensive. However, it is the only way that samarium, europium, thulium, and ytterbium can be produced, because of their high vapor pressures. Electrowinning cannot be used because metal vapor losses would be excessive.

All the other rare earth metals can be produced by electrowinning or metallothermic reduction.

Electrowinning is probably the better process for producing large quantities of metal, e.g., neodymium. Metallothermic reduction is probably the better process for producing small quantities of metal (e.g., lutetium).

References

Barin, I., 1993. Thermochemical Data of Pure Substances. VCH Publishers, New York.

Constantinides, S., 2012. The demand for rare earth materials in permanent magnets. In: Rare Earths. Met Soc of CIM, Montreal, QC, pp. 293–307.

Constantinides, S., 2013. Rare earth elements in transportation. In: Rare Earths. Met Soc of CIM, Montreal, QC, pp. 47–62.

Dent, P.C., 2012a. Rare earth elements and permanent magnets. J. Appl. Phys. 111, 1–6.

Dent, P., 2012b. Rare earth permanent magnet supply chain and technology advances overview. In: Rare Earths. Met Soc of CIM, Montreal, QC, pp. 309–316.

Edwards, J.W., Johnston, H.L., Blackburn, P.E., 1951. Vapor pressure of inorganic substances. IV. Tantalum between 2624 and 2943 K. J. Am. Chem. Soc. 73 (1), 172–174.

Gupta, C.K., Krishnamurthy, N., 2005. Extractive Metallurgy of Rare Earths. CRC Press, Boca Raton, FL, 328–352.

Habermann, C.E., Daane, A.H., 1964. Vapor pressures of the rare-earth metals. J. Chem. Phys. 41, 2818–2827.

Riedemann, T.M., 2011. High Purity Rare Earth Metals Preparation. Ames Laboratory, US Department of Energy, Ames, IA. Retrieved on August 14, 2013, from, https://www.ameslab.gov/files/REM_presentation_ShortForm.pptx, Work at the Ames Laboratory was supported by the Department of Energy-Basic Energy Sciences under Contract No. DE-ACO2-07CH11358.

Shin-Etsu, 2012. Manufacturing process/sintering process. Tokyo. Retrieved on August 14, 2013 from, http://www.shinetsu-rare-earth-magnet.jp/e/masspro/

Suggested Reading

Gibson, K., 2001. Magnetic Refrigeration Successfully Tested. U.S. Department of Energy Research News, Washington, D.C. Recovered on August 14, 2013 from, http://www.eurekalert.org/features/doe/2001-11/dl-mrs062802.php.

Gupta, C.K., Krishnamurthy, N., 2013. Oxide reduction processes in the preparation of rare earth metals. Miner. Metall. Proc. 30 (1), 38–44.

Karsjen, S., 2013. Room-Temperature Magnetic Refrigeration. The Ames Laboratory, Ames, Iowa. Retrieved on August 14, 2013 from, http://www.ameslab.gov/files/MagFridge_Foundation.pdf.

Zhang, X., Miao, R., Chen, D., Wang, Z., Li, Z., Yan, S., Jin, X., 2013. Numerical simulation during vacuum sublimation purification of metal Tm(I): model foundation and validation. J. Rare Earths. 31 (2), 180–185.

CHAPTER

8

Rare Earth Electronic Structures and Trends in Properties

The rare earths occupy a unique position in the periodic table due to the progressive filling of internal atomic orbitals called 4f orbitals. The first member of the family Lanthanum (La) has an atomic number $Z=57$. The last member is Lutetium (Lu) with $Z=71$.

This homogeneous family is also called Lanthanides and the symbol Ln can be used instead of RE.

This chapter presents the physical properties associated with this peculiar electronic structure. The following points will be discussed:

- The electronic configuration of rare earths
- The oxidation state of rare earths
- The trends in rare earth properties
- The most common rare earth oxides

8.1 ELECTRONIC CONFIGURATION OF RARE EARTHS

8.1.1 Rare earths in the periodic table

Formally, the rare earths or lanthanides are the atoms with atomic number ranging from 58 (Ce) to 71 (Lu) in which the 4f orbitals are gradually filled from 1 to 14. These elements therefore belong to period number six on the periodic table as depicted on Fig. 8.1.

The period starts by filling the 6s orbitals with Cesium Cs, $Z=55$ and Barium Ba, $Z=56$. Obviously, the lanthanum is also considered as a rare earth despite that it has no 4f electron. In La, the 5d subshell is lower in energy than 4f, so that lanthanum has the electron configuration $[\mathrm{Xe}]6s^2 5d^1$. This electronic structure is similar to that of Y $[\mathrm{Kr}]5s^2 4d^1$ which is considered to be part of the rare earth family although it is much lighter $Z=39$. Note that, for the same reason, in some cases, scandium is also included in the rare earth family.

8.1.2 Electronic configurations of rare earth elements

One of the most unique and important aspects of the electronic structure of rare earths is the highly localized nature of the 4f electrons wave functions; they do not overlap with neighboring atoms, and are instead shielded by the 5s and 5p electrons.

Rare Earths. http://dx.doi.org/10.1016/B978-0-444-62735-3.00008-5

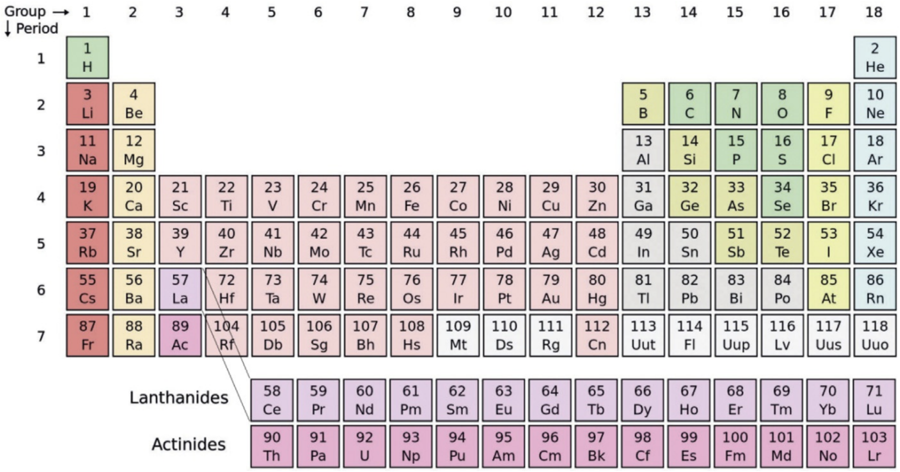

FIG. 8.1

Periodic table of the elements. For convenience, the Lanthanides (4f) and Actinides (5f) elements are extracted from their normal position in the table.

Courtesy of Dr. Thierry Le Mercier, Solvay Rare Earth Systems.

The radial distribution function of Fig. 8.2 shows that 4f electrons are indeed closer to the nucleus than 5s, 5p, and 6s electrons and are consequently buried within the electronic cloud.

As a result, rare earth ions in the solid state tend to have the same electronic structure as free ions since the 4f electrons are isolated from the influence of ligands and crystal field. This has a direct influence on the optical and magnetic properties of the corresponding solid.

As described in Chapter 15, external excitation can promote electron into empty 5d orbitals. In this case, rare earth ion environments (crystal fields) strongly influence the energy positioning of 5d orbitals (main applications are found for Ce^{3+} and Eu^{2+}).

The inset in Fig. 8.2 illustrates how the 4f shell is unfilled, yet has a smaller radius than the full 5s and 5p shells, which act as shielding electrons, while the 6s shell corresponds to delocalized bonding electrons.

This is further exemplified by the differences in sequence between the orbital size and orbital energy listed in Table 8.1. The electronic configuration listed according to the orbital energy shows a different sequence than the electronic configuration listed as a function of orbital size.

Consequently, the 4f shell has higher energy and can remain unfilled even though it has a smaller radius.

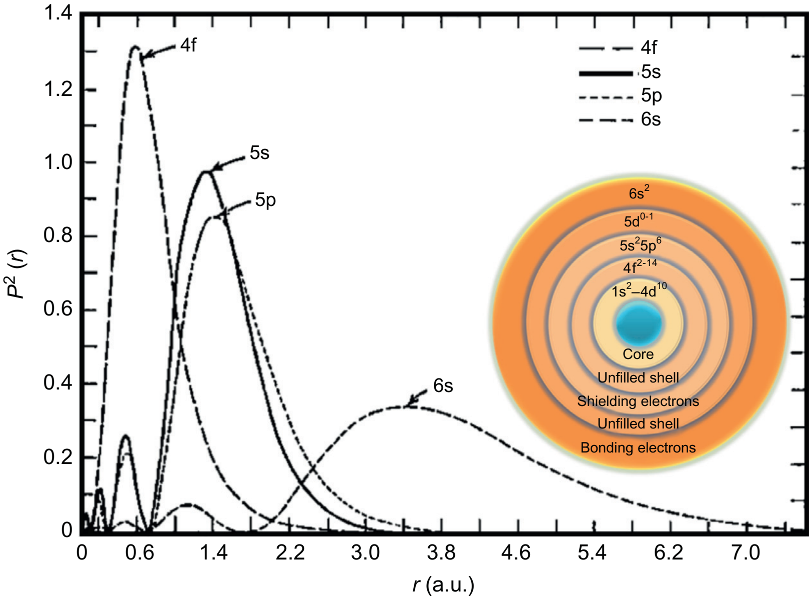

FIG. 8.2

Electronic radial distribution functions of the orbitals on a d$^+$ ion showing the electronic density as a function of distance from the nucleus. The inset is a simplified representation of the relative radius of each orbital.

Reproduced from Rivera, V.A.G., Ferri, F.A., Marega, E., Jr. 2012. Localized surface plasmon resonances: noble metal nanoparticle interaction with rare earth ions. In: Kim, K.Y. (Ed.), Plasmonics: Principles and Applications, pp. 283–312.

The relative energy of rare earth orbitals can be explained as follow: as protons are added to the nucleus, the 4f orbitals contract rapidly and become more stable than the 5d so that Ce has the electron configuration [Xe]6s^{2}4f^{1}5d^1. This effect gets stronger for Pr having the arrangement [Xe]6s^{2}4f^3 where the 5d orbital remains unfilled. All remaining rare earths have the configurations [Xe]6s^{2}4f^n with the notable exception of Gd where the added stability of the half-filled 4f shell is such that the next electron is added to the 5d orbital, Gd being [Xe]6s^{2}4f^{7}5d^1. The last lanthanide, Lu, where the 4f subshell is now filled, is predictably [Xe]6s^{2}5d^{1}4f^{14}.

Note that Ln^{n+} ions have the same electronic configuration as Ln$^{(n+1)+}$ ions. For example Eu^{2+} has the same configuration as Gd^{3+} ions.

The ground state electronic configurations shown in Table 8.1 define the number of unpaired electron spins which in turn defines the magnetic properties, and also the possible electronic transitions which in turn define the optical properties.

Any disruption to this electronic configuration will therefore affect the rare earth properties.

Table 8.1 Electronic Configuration of Isolated Rare Earth Atoms and Ions Listed According to the Energy of Each Orbital and According to the Spatial Extent (size) of Each Orbital

			Energy of Electronic Shells		**Size of Electronic Shells**
Z	**Element**		***Ln atom***	***Ln^{3+} ion***	***Ln atom***
54	Xenon	Xe	$[Kr]4d^{10}5s^{2}5p^{6}$	–	$[Kr]4d^{10}4f^{0}5s^{2}5p^{6}5d^{0}6s^{0}$
57	Lanthanum	La	$[Xe]6s^{2}5d^{1}4f^{0}$	$[Xe]4f^{0}$	$[Kr]4d^{10}4f^{0}5s^{2}5p^{6}5d^{1}6s^{2}$
58	Cerium	Ce	$[Xe]6s^{2}4f^{1}5d^{1}$	$[Xe]4f^{1}$	$[Kr]4d^{10}4f^{1}5s^{2}5p^{6}5d^{1}6s^{2}$
59	Prasedymium	Pr	$[Xe]6s^{2}4f^{3}5d^{0}$	$[Xe]4f^{2}$	$[Kr]4d^{10}4f^{3}5s^{2}5p^{6}5d^{0}6s^{2}$
60	Neodymium	Nd	$[Xe]6s^{2}4f^{4}5d^{0}$	$[Xe]4f^{3}$	$[Kr]4d^{10}4f^{4}5s^{2}5p^{6}5d^{0}6s^{2}$
61	Promethium	Pm	$[Xe]6s^{2}4f^{5}5d^{0}$	$[Xe]4f^{4}$	$[Kr]4d^{10}4f^{5}5s^{2}5p^{6}5d^{0}6s^{2}$
62	Samarium	Sm	$[Xe]6s^{2}4f^{6}5d^{0}$	$[Xe]4f^{5}$	$[Kr]4d^{10}4f^{6}5s^{2}5p^{6}5d^{0}6s^{2}$
63	Europium	Eu	$[Xe]6s^{2}4f^{7}5d^{0}$	$[Xe]4f^{6}$	$[Kr]4d^{10}4f^{7}5s^{2}5p^{6}5d^{0}6s^{2}$
64	Gadolinium	Gd	$[Xe]6s^{2}4f^{7}5d^{1}$	$[Xe]4f^{7}$	$[Kr]4d^{10}4f^{7}5s^{2}5p^{6}5d^{1}6s^{2}$
65	Terbium	Tb	$[Xe]6s^{2}4f^{9}5d^{0}$	$[Xe]4f^{8}$	$[Kr]4d^{10}4f^{9}5s^{2}5p^{6}5d^{0}6s^{2}$
66	Dysprosium	Dy	$[Xe]6s^{2}4f^{10}5d^{0}$	$[Xe]4f^{9}$	$[Kr]4d^{10}4f^{10}5s^{2}5p^{6}5d^{0}6s^{2}$
67	Holmium	Ho	$[Xe]6s^{2}4f^{11}5d^{0}$	$[Xe]4f^{10}$	$[Kr]4d^{10}4f^{11}5s^{2}5p^{6}5d^{0}6s^{2}$
68	Erbium	Er	$[Xe]6s^{2}4f^{12}5d^{0}$	$[Xe]4f^{11}$	$[Kr]4d^{10}4f^{12}5s^{2}5p^{6}5d^{0}6s^{2}$
69	Thulium	Tm	$[Xe]6s^{2}4f^{13}5d^{0}$	$[Xe]4f^{12}$	$[Kr]4d^{10}4f^{13}5s^{2}5p^{6}5d^{0}6s^{2}$
70	Ytterbium	Yb	$[Xe]6s^{2}4f^{14}5d^{0}$	$[Xe]4f^{13}$	$[Kr]4d^{10}4f^{14}5s^{2}5p^{6}5d^{0}6s^{2}$
71	Lutetium	Lu	$[Xe]6s^{2}4f^{14}5d^{1}$	$[Xe]4f^{14}$	$[Kr]4d^{10}4f^{14}5s^{2}5p^{6}5d^{1}6s^{2}$

4f orbitals have higher energy (remain unfilled) yet have smaller radius than 5s, 5p and 6s orbitals.
Courtesy of Jacques Lucas research group.

8.1.3 Focus on 4f energy levels

8.1.3.1 The 4f orbitals

The 4f electrons always have quantum number $n=4$ and $l=3$, but can have quantum number $m_l=3; 2; 1; 0; -1; -2; -3$ and $m_s=½; -½$. Hence, there are seven 4f orbitals as depicted in Fig. 8.3, each hosting up to two electrons. There are at the maximum 3432 energy levels for the f electrons. This huge number explains the complexity of classifying the 4f energy levels. This explains also the richness of rare earths especially in terms of optical properties

In a first approximation, the seven orbitals have the same energy and are called degenerated. This is the case when the orbitals are empty but available.

On the other hand, when the 4f orbitals become partially populated with electrons, the Coulombic and magnetic spin interactions between electrons leads to more or less stable configurations and lifts the degeneracy of the 4f levels.

8.1.3.2 Energy levels of 4f orbitals

Each electron in a rare earth atom is described by a wave function ψ which is a solution to the Schrödinger equation $H\psi = E\psi$ where E is the energy of the electron and H (the Hamiltonian) represents the sum of interactions experienced by the electron.

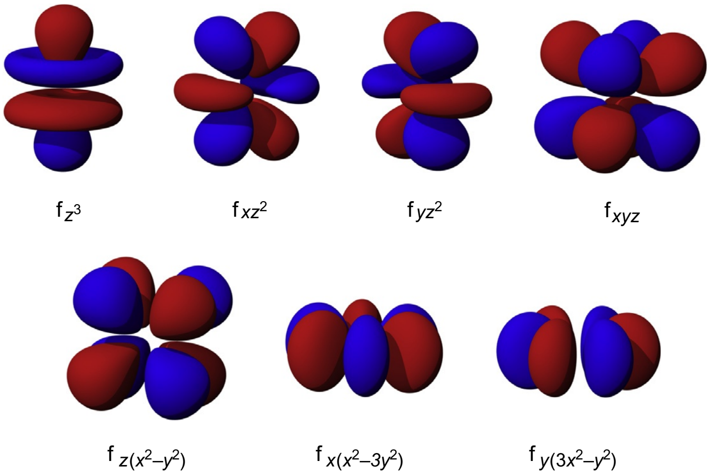

FIG. 8.3

The seven 4f orbitals pointing in different directions in space.

An electron experiences multiple interactions and the Hamiltonian can be written as:

$$H = H_o + H_{e-e} + H_{so} + H_{cf}$$

where:

- H_o is the attractive Coulomb interaction between the electrons and the nuclei. This enables classification of different configurations ns, np, 4f, 5d…
- $H_{e\text{-}e}$ is the repulsive Coulomb interaction between electrons and leads to spectroscopic terms $^{2S+1}\Gamma$.
- H_{so} is the interaction between the magnetic field generated by the orbiting electron and the magnetic moment of the electron due to its spin, also called spin-orbit coupling and leads to spectroscopic levels $^{2S+1}\Gamma_J$.

H_o is the same for all the 4f electrons and therefore leads to the same solution *E*, so that all the $4f^6$ electronic levels are degenerated as in Fig. 8.4.

The strength of the repulsive interaction $H_{e\text{-}e}$ depends on the shape and orientation of the orbital so that 4f electrons with different quantum numbers may yield different solutions *E* and lift the degeneracy of the $4f^6$ electronic levels as shown in Fig. 8.4.

The magnitude of H_{so} quantifies the alignment of the spin with the magnetic field generated by the circulating electron and also depends on the orbital type so that the spin-orbit coupling further lift the degeneracy of the electronic levels as shown in Fig. 8.4.

The three first terms of H (H_o $H_{e\text{-}e}$ and H_{so}) are sufficient to describe the free ion.

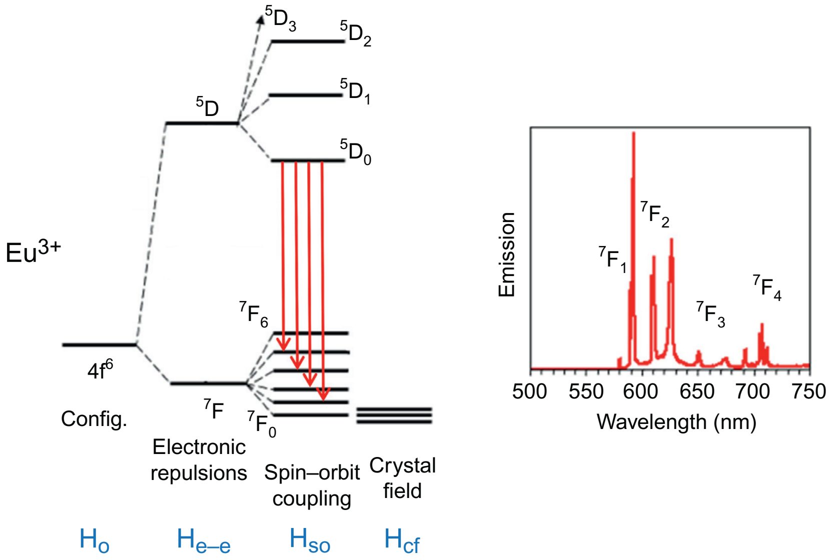

FIG. 8.4

Different contributions to the splitting of 4f^6 energy levels in an Eu^{3+} ion. The multiplicity of electronic levels leads to sharp optical transitions as shown by the emission spectra of Eu^{3+} ion doped in a YBO_3 crystal.

Courtesy of Dr. Thierry Le Mercier, Solvay Rare Earth Systems.

Finally, the disruption arising from the local ligand symmetry induces the crystal field effect which also lifts the degeneracy.

The splitting of electronic level is extremely rich and complex in rare earths due to the seven 4f orbitals. This electronic level multiplicity is crucial for the development of photoluminescent materials and laser active materials as is described in Chapters 15 and 17. Figure 8.4 illustrates the emission lines resulting from electronic transition between $^5D_0 \rightarrow {}^7F_n$ levels. The series of electronic transitions between these levels produces photons with distinct energy (or wavelength) as illustrated by the individual peaks on the emission spectrum of Fig. 8.5. The emission lines are very sharp as expected from the shielding of 4f-4f transitions, that is, the effect of the crystal field is negligible.

8.1.3.3 Spectroscopic terms

The energy levels illustrated in Fig. 8.5 are classified using "term symbols" labeled as $^{2S-1}L_J$. Where:

– S is the total spin quantum number: $S = \sum_i m_{S_i}$ with m_{S_i} the spin quantum number for electron i.

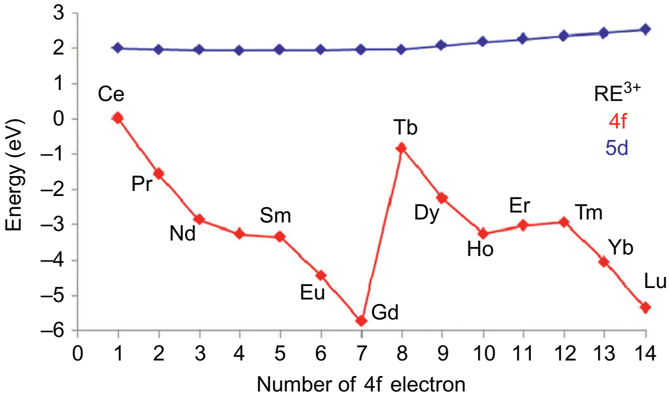

FIG. 8.5

Relative evolution of 4f (red) and 5d (blue) lowest energy levels belonging to Ln series. Note that the energy difference between 4f and 5d levels has been chosen arbitrarily.

Drawing has been done from data: Dorembos, P. 2003. J. Phys.: Condens. Matter 15: 8417–8434; Courtesy of Dr. Thierry Le Mercier, Solvay Rare Earth Systems.

– L is the total orbital quantum number: $L = \sum_i m_{l_i}$ with m_{l_i} the orbital quantum number for electron i.

– J is the total angular momentum quantum number: $J = S + L$, to, $S - L$

Letters are used instead of numbers for the notation of L, with S, P, D, G… corresponding to L=1, 2, 3, 4…

According to Hund's rule, the ground state is that with the highest S value and highest L value. For example, the ground state for Eu^{3+} ($4f^6$) represented below has L=3 and S=3 which corresponds to the ^7F term symbol.

m_l	3	2	1	0	–1	–2	–3
	↑	↑	↑	↑	↑	↑	

If the spin-orbit coupling is taken into account, the ^7F term splits into ^7F_J sublevels with J=6, 5, 4, 3, 2, 1, 0 as depicted in Fig. 8.4.

8.1.3.4 The 4f and 5d energy levels variation

Is it interesting to compare the evolution of 4f and 5d energy levels belonging to the lanthanide series (Fig. 8.5). The following remarks are true for all structures where the rare earths are included:

- The 5d levels have a relatively constant energy (around +0.5 eV from Ce to Lu).
- On the contrary, 4f fundamental levels show a dramatic variation, and a "famous" zig-zag curve is observed as shown in Fig. 8.5 for Ln^{3+} ions. The zig-zag

variation is always the same with minimum value of energy for n = 7 (Gd) et 14 (Lu). This variation is due to the relative strength of the spin-orbit coupling. The same variations are available for Ln^{2+} shifted towards higher energy (in this case the most stable 4f levels are found for Eu^{2+}). Note that the energy difference between 4f and 5d levels is strongly dependent on the host matrix.

8.1.3.5 Crystal field effects

The perturbation generated by the charge of neighboring ions in a solid can have an effect called the "crystal field effect."

The 4f orbitals are shielded from their environment, and are thus largely immune to these perturbations. Only very small modifications of the energy levels are observed (lower than 0.1 eV).

On the contrary, the 5d orbitals of rare earth ions are greatly disturbed by their environment. This includes the symmetry of the site, the nature of the ligand (oxygen, sulfide,...), the vibrations of the host lattice and the structural disorder (as in amorphous solids). Note that for RE ions, 5d orbitals are filled only after excitation of the 4f configuration. In this case, they are filled with only one electron. At the end, the number of 5d levels depends on the symmetry.

An example of crystal field effect is given in Fig. 8.6 for the case of $(Y,Ce)_3Al_5O_{12}$. In this material, the trivalent cerium ion is located on a site having D_2 symmetry (derived from cubic symmetry). The 5 orbitals 5d are spread out in five

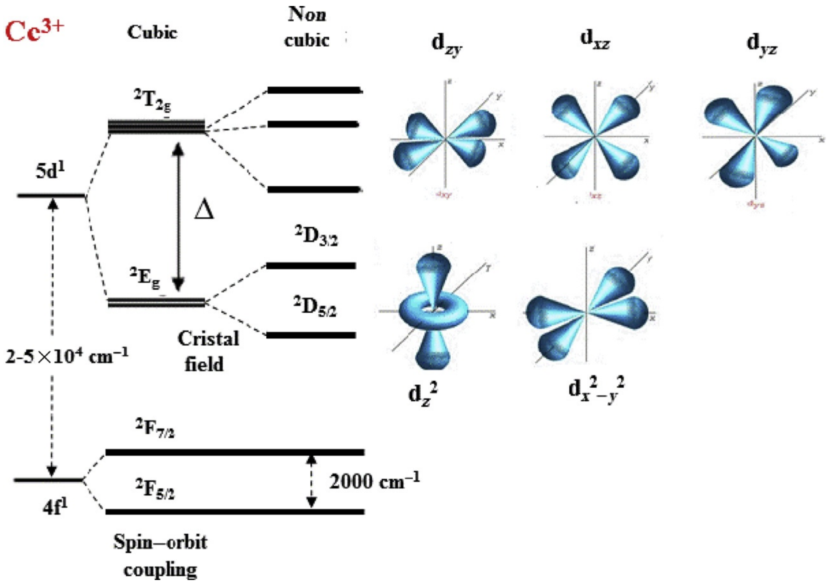

FIG. 8.6

Energy levels of Ce^{3+}in $Y_3Al_5O_{12}$.

Courtesy of Dr. Thierry Le Mercier, Solvay Rare Earth Systems.

different levels. Note that the fundamental 4f levels are not affected (as a first approximation) by the crystal field.

These effects have a direct impact on the optical properties of rare earth ions. For example, optical transitions between 4f-4f orbitals exhibit sharp and well defined energies, while optical transitions between 4f-5d exhibit broad emission energies. This is discussed in more detail in Chapter 15.

8.2 DEGREES OF OXIDATION OF RARE EARTHS

The chemistry of lanthanides is largely dominated by the degree of oxidation +III. While there are only two electrons on the outermost orbital $6s^2$, the lanthanides lose an additional 4f electron to form the triply charged Ln^{3+} ions. The loss of a third electron further contracts the 4f shell and stabilizes the ion.

Notable exceptions to the +III oxidation state are:

- Ce which can lose all four outer electrons to form a Ce^{4+} ion $[Xe]4f^0$. Similar behavior is observed with Pr^{4+} and Tb^{4+} (especially in oxides)
- Eu which can lose only two electrons to form $Eu^{2+}[Xe]4f^7$ due to the stabilization of the half-full 4f shell. Similar behavior is observed with $Sm^{2+}[Xe]4f^6$
- Yb which also loses only two electrons form $Yb^{2+}[Xe]4f^{14}$ due to the stabilization of the full 4f shell.

8.2.1 The metallic state

Bonding in rare earth metals is the result of strong interaction between the Ln^{3+} cationic cores and the $3N$ delocalized valence electrons, where N is the number of atoms.

Eu and Yb are two exceptions. They give only two electrons to the collective electron gas to stabilize the electronic structure $4f^7$ and $4f^{14}$ respectively.

One consequence is the lower melting point of Eu and Yb metal due to the weaker metallic bond as shown in Fig. 8.7.

Another consequence is the much larger atomic radius of Eu and Yb as shown on Fig. 8.8.

8.2.2 The ionic state

Rare earth ions are dominated by the trivalent Ln^{3+} with the exceptions of Ce^{4+}, Eu^{2+}, and Yb^{2+} and to a lesser degree Sm^{2+}.

For Ln^{3+} trivalent ions, Fig. 8.8 shows that the ionic radius decreases with increasing Z number. This effect is known as the "lanthanide contraction." It illustrates the internal character of the 4f orbitals which does not expand with the addition

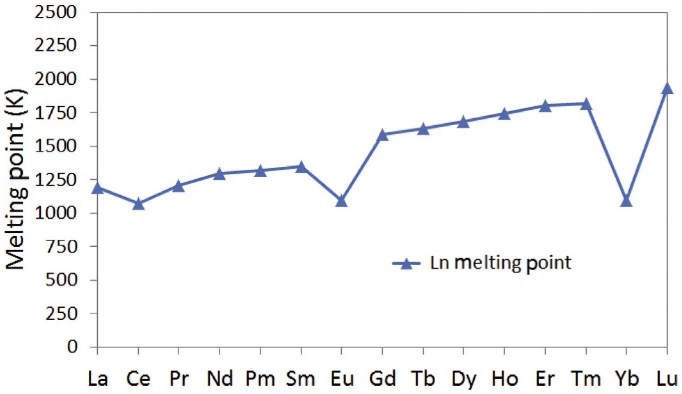

FIG. 8.7

Melting point of metallic lanthanides showing the abnormal behavior of divalent Eu and Yb.

Drawn by Pierre Lucas from public domain data.

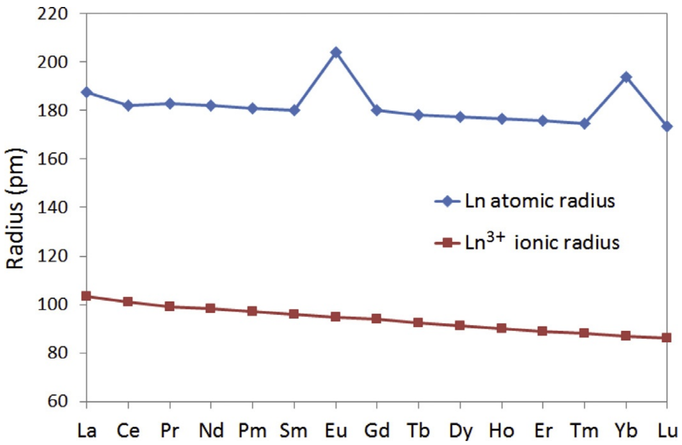

FIG. 8.8

Atomic and ionic radii of lanthanides.

Drawn by Pierre Lucas from public domain data.

of 4f electrons. These core-like electrons are dominated by the attraction of the increasingly charged nucleus and therefore contract with increasing atomic number.

Lanthanides are strong reductants with low standard redox potentials $E^o(Ln/Ln^{3+}) \approx -2.3$ V except for the two divalent elements Eu and Yb which are slightly less reducing due to their tendency to form divalent ions as depicted in Fig. 8.9.

Lanthanide metals should therefore be stored under controlled atmosphere in a glove box away from oxygen and moisture.

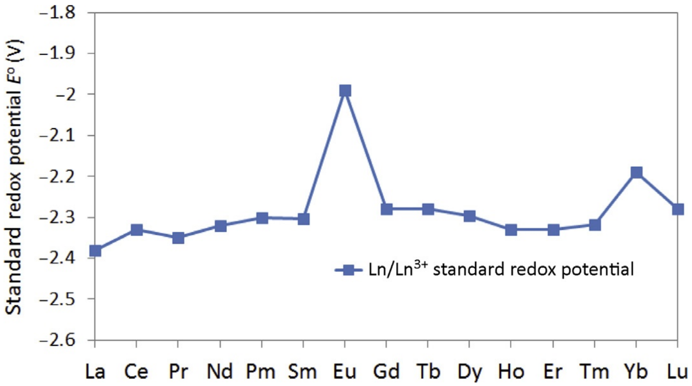

FIG. 8.9

Standard redox potential for the Ln/Ln^{3+} couple of lanthanides.

Drawn by Pierre Lucas from public domain data.

The Eu^{2+} oxidation state of europium is, for example, stabilized in phases where Eu substitutes for Ba, Sr or Ca. This is the case of (Ba, Eu)$MgAl_{10}O_{17}$. In this case, the Eu^{2+} state can be stable in air at room temperature, but is oxidized to Eu^{3+} if calcined at high temperature (>600 °C).

8.3 LANTHANIDES IN SOLUTION (IN WATER)

The behavior of Ln^{3+} lanthanide ions in solution is controlled by their size. The electric field around the triply charged Ln^{3+} ions increases when the size decreases. As a result, the enthalpy of hydration increases with atomic number (Fig. 8.10) so that Lu^{3+} complexes are more stable than the La^{3+} complexes.

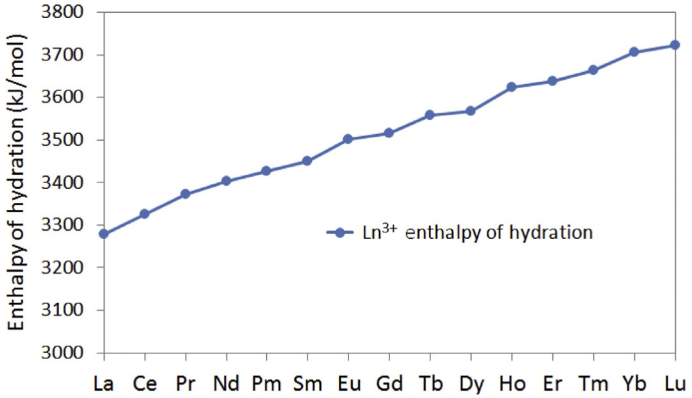

FIG. 8.10

Enthalpy of hydration for Ln^{3+} lanthanide ions.

Courtesy of Dr. Thierry Le Mercier, Solvay Rare Earth Systems.

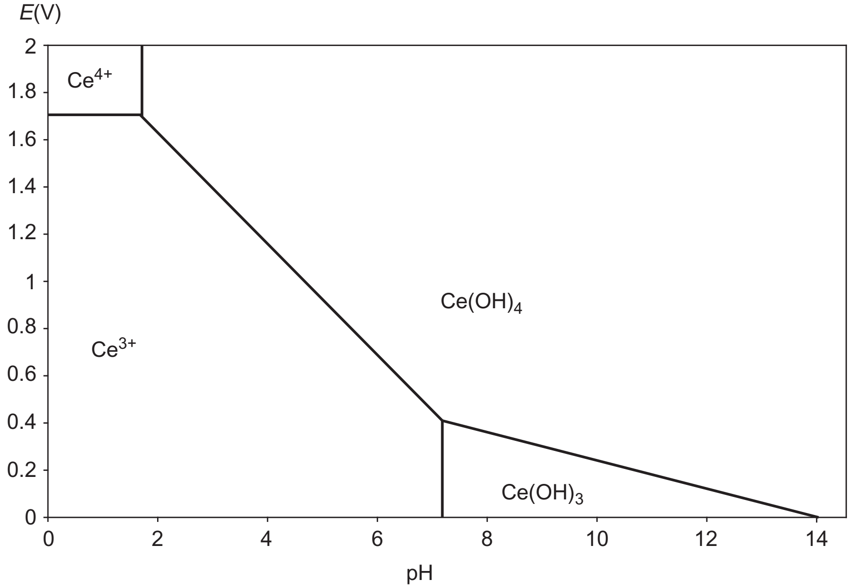

FIG. 8.11

Simplified diagram E-pH of cerium, $[Ce^{3+}]=0.01$ M.

Courtesy of C. Feral-Martin, Solvay.

This difference in behavior is critical for the separation and purification process of rare earth elements, as discussed in Chapter 5.

The first members of the lanthanide family have the largest size and form ninefold $[Ln(H_2O)_9]^{3+}$ hydrated complex ions in a tricapped trigonal prism configuration. While the smaller heavy Ln^{3+} are surrounded by only eight water molecules and form $[Ln\ (H_2O)_8]^{3+}$ ions in a square anti-prism configuration.

In water solution, the trivalent state Ln^{3+} is the generally observed ionic state in acidic conditions. In basic conditions, the rare earth salts are precipitated as hydroxides (or even oxides) of rare earths. Cerium is a special case. It can also exist as Ce^{4+}, in nitric conditions.

The Ce^{4+}/Ce^{3+} redox potential is 1.72 V, meaning that Ce^{3+} in solution (as ion, or as hydroxide) can be turned to the Ce^{4+} valence state by oxidation. This process can occur by adding an oxidizer or at a high temperature.

The redox behavior in water can be easily understood from the Pourbaix diagram as shown in Fig. 8.11.

8.4 COMMON RARE EARTH OXIDES

8.4.1 Non-stoichiometric oxides

Rare earth oxides are the most stable lanthanide compounds.

They are produced by calcination in air of almost any Lanthanide salts or hydroxides. They are refractory materials, for instance the melting point of La_2O_3 is $T_m=2315\ °C$.

Most of them have the formula Ln_2O_3 and are white or slightly colored.

Two of them, $PrO_{1.81}$ (Pr_6O_{11}) and $TbO_{1.75}$ (Tb_4O_7) are non-stoichiometric. They are mixed valence oxides and have a black color. Visible light is absorbed by the electrons transferring from Ln^{3+} to Ln^{4+} (by a hopping mechanism).

One exception is also the ceria oxide CeO_2 which is stable as well as some intermediate oxides CeOx with $1.5 \geq x \geq 2$. Refer to Chapter 12 on polishing (yellowish body color).

The Ln_2O_3 oxides exhibit three crystalline forms: A (hexagonal), B (monoclinic), and C (cubic) Ln_2O_3 which is a CaF_2 super-cell. Their respective domains of stability with atomic number and temperature are schematically represented in Fig. 8.12.

The structure of stoichiometric and non-stoichiometric oxides LnO_x ($1.5 \geq x \geq 2$) ranging from Ln_2O_3 to LnO_2 can be derived from the CaF_2 structure.

The structures are composed of edge-sharing LnO_8 cubes as depicted on Fig. 8.13. Each oxygen atom is common to four Ce atoms so that the formula of the 3D network is $CeO_{8/4}$ and the resulting stoichiometry is LnO_2. This is the case for the classic CeO_2 compound.

In the oxides Ln_2O_3 ($LnO_{1.5}$) each cube contains two oxygen vacancies. The elementary building units are deficient cubes $LnO_{6/2}$.

Their 3D connection gives the formula $LnO_{6/4} \rightarrow Ln_2O_3$ since each oxygen remains common to four RE.

The symmetry of the network changes with atomic number and temperature depending on the way the vacancies are ordered. This results in a distorted sixfold coordination for the type C, and distorted sevenfold coordination for type A and B.

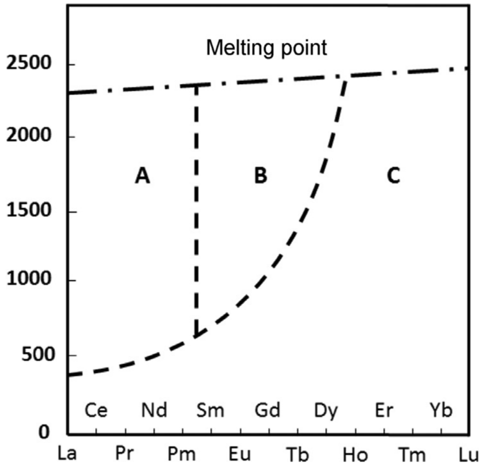

FIG. 8.12

Schematic representations of the domains of stability for the three crystalline forms of the Ln_2O_3 oxides versus atomic number and temperature. Type C is cubic, type B is monoclinic, type A is hexagonal. All three of them are related to the fluorite structure.

Courtesy of Jacques Lucas research group.

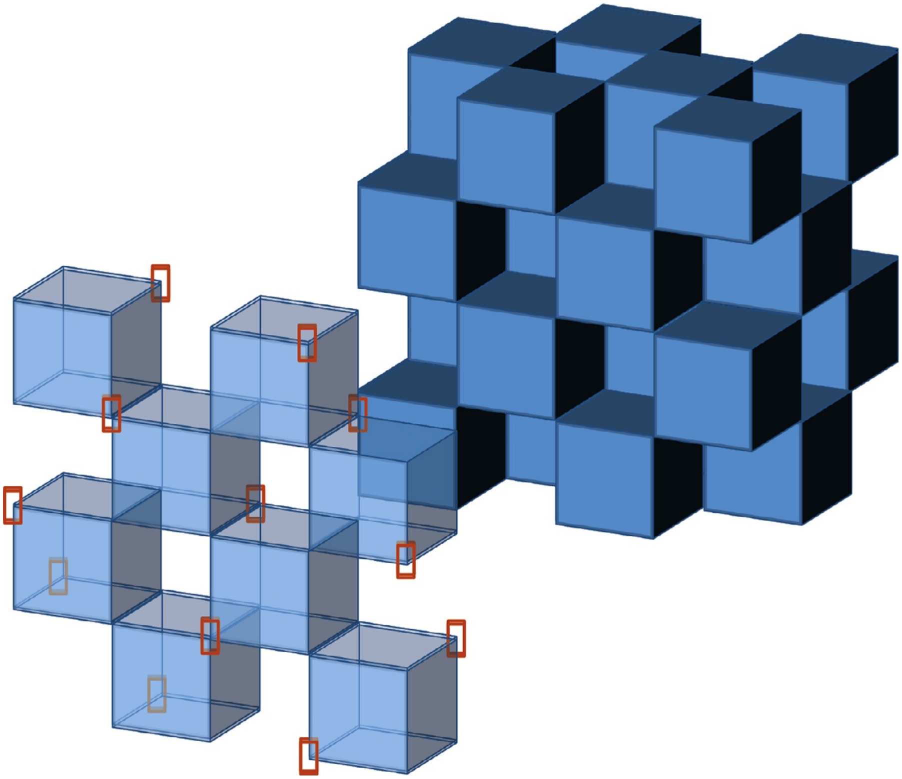

FIG. 8.13

Structure of LnO_x crystals derived from the CaF_2 structure type of CeO_2; PrO_2 or TbO_2. The building units are edge sharing LnO_8 cubes where each O atom is shared with 4 Ln. The structure of Ln_2O_3 is represented on the left as composed of oxygen deficient $LnO_{6/2}$ cubes. The ordering of the vacancies (red squares) depends on the atomic number of the rare earth and temperature and can lead to three types of superstructures A, B and C.

Courtesy of Jacques Lucas research group.

When the lanthanides Ln can have two oxidation states Ln^{3+} and Ln^{4+} such as Ce, Pr, or Tb, many complex crystalline phases exist between LnO_2 and Ln_2O_3.

These phases contain vacancies and mixed valences which result in the formula: $Ln^{4+}{}_{(1\text{-}x)}Ln^{3+}{}_{x}O_{(2-x)}\square_x$. They can contain up to 50/50% Ln^{4+}/Ln^{3+}.

Ordering of the vacancies leads to complicated crystal chemistry.

The mixed valence of these phases enables charge transfer, which leads to semiconductor properties and light absorption (color).

The vacancies also permit the capture and release of oxygen which has potential for solid electrolytes or catalysis as discussed in Chapter 9.

8.4.2 Yttrium aluminum garnet: YAG

The reaction of $3Y_2O_3+5\ Al_2O_3$ leads to the formation of a cubic materials $Y_3Al_5O_{12}$ having the cubic garnet structure. In this host, the Y^{3+} ions can be easily substituted by lanthanide ions such as Ce^{3+} or Nd^{3+}.

In this structure, two Al form AlO_6 octahedra while three other Al form AlO_4 tetrahedra. These tetrahedral and octahedral share corners to build the 3D framework represented on Fig. 8.14.

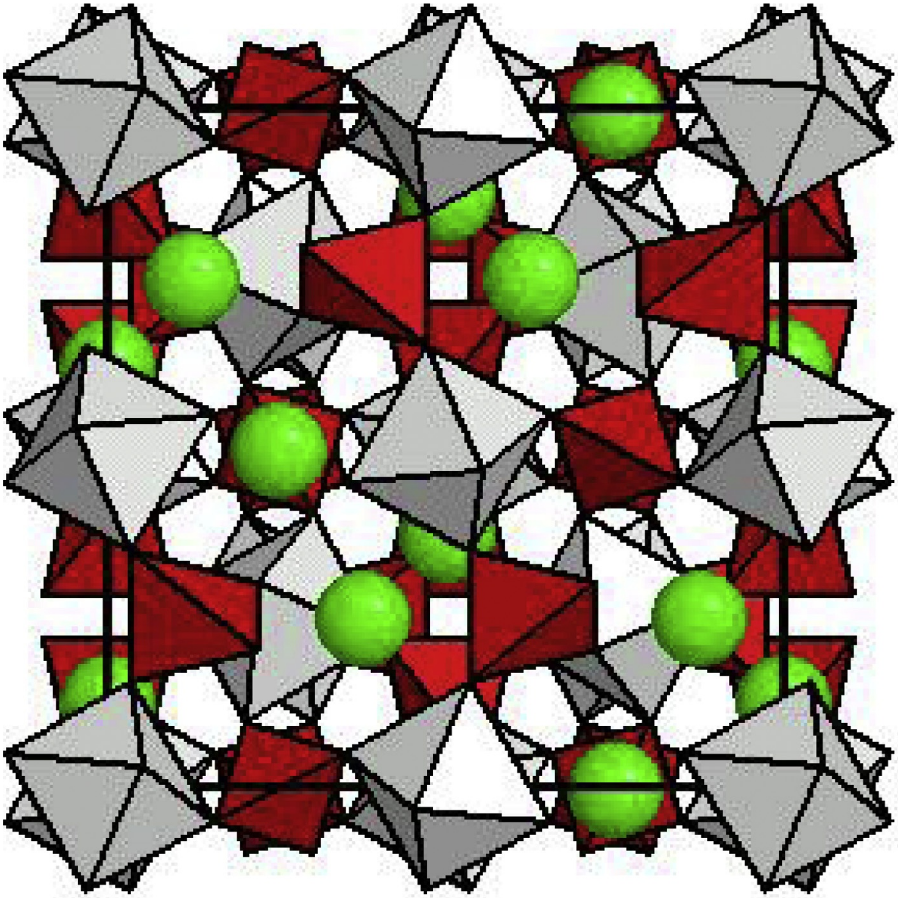

FIG. 8.14

Structure of the yttrium aluminum garnet: YAG, $Y_3Al_5O_{12}$ crystal. Green spheres represent the Y atoms which can be substituted by Ce or Nd. AlO_4 tetrahedra (red) and AlO_6 octahedra (grey) form the network.

Courtesy of Prof. Robert T. Downs, University of Arizona.

The Y atoms occupy a distorted site composed of eight oxygen atoms forming a dodecahedron. This crystallographic site generates a crystalline field which is very favorable for obtaining strong emission. Two industrial products are related to this Al Garnet:

- In the Nd^{3+} YAG Laser, Y^{3+} is substituted by less than 0.1% of Nd^{3+}: the Nd: YAG laser emits light in the infrared around 1.06 μm (see Chapter 17 on rare earth lasers). In addition to good optical quality, the YAG crystals have an excellent thermal conductivity. This is good for heat dissipation.
- Ce^{3+}YAG powders are used as phosphors for white light emitting diodes (LED) (see Chapter 16). A part of the blue light LED is converted by Ce^{3+} into yellow. The mixture of colors produces white light.

8.4.3 Phosphate RE: $LnPO_4$

Rare earth orthophosphates are important compounds. They are crystallized as two different structures: xenotime for heavy rare earths (Ln = Y, Tb-Lu) and monazite for light rare earths (Ln = La-Gd).

Monazite is one of the most common ores for rare earths. The general formula is (Ce, La, Th)PO_4. The structure is given in Fig. 8.15. In this material, isolated tetrahedral PO_4 are separated by LnO_9 polyhedra. Each oxygen is linked to two rare earth elements.

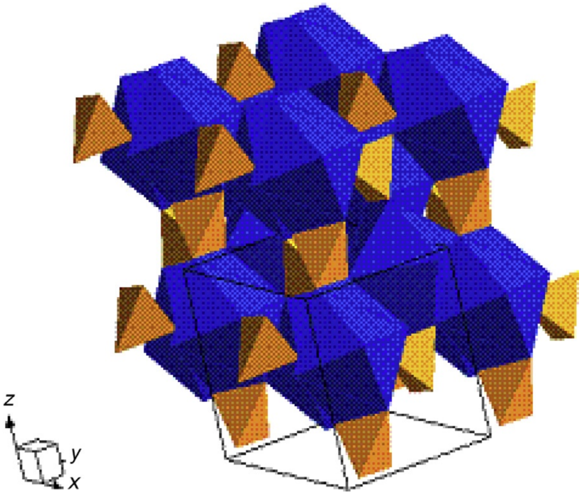

FIG. 8.15

Structure of the lanthanum phosphate $LaPO_4$ structure, monazite type. In blue LaO_9 polyhedra it can be substituted by Ce, Tb,.. In orange by PO_4 tetrahedra.

Courtesy of Dr. Thierry Le Mercier, Solvay Rare Earth Systems.

This structure is used as a green phosphor in trichromatic fluorescent lighting devices when the $LaPO_4$ host matrix is doped with Tb^{3+} and Ce^{3+} ions.

8.5 SUMMARY

Lanthanides are elements resulting from filling the 4f orbitals.

The 4f orbitals are partially filled yet they are buried below the 5s and 5p which shield them from the local environment.

The localized 4f orbitals are therefore not affected by the crystal field while the extended 5d are strongly affected.

As a result, the electronic structure of 4f levels in solids is similar to that of isolated ions.

The electronic structure controls the optical and magnetic properties of rare earth solids.

The atomic and ionic radii decrease with increasing atomic number due to the increasing attraction from the nuclei. This is called the “lanthanide contraction.”

Oxidation of lanthanides is dominated by the trivalent state Ln^{3+}.

The trends in atomic radius, melting point, and standard redox potentials show an anomaly for Eu and Yb due to their divalent nature.

Some lanthanide oxides can integrate mixed valences and oxygen vacancies.

$Y_3Al_5O_{12}$ (YAG) crystals can be doped with optically active Ce^{3+} and Nd^{3+} ions. They are widely used in lasers and solid state lighting applications.

The $LaPO_4$ type structure is an important RE ore. RE materials and derivatives are used in fluorescent lamps.

CHAPTER

Rare Earth Catalysts

9

Rare earths are used as catalysts to speed up many chemical reactions. The two most important are

- **(a)** lanthanum chloride and lanthanum nitrate petroleum-refining catalyst, which speeds up the production of gasoline and diesel from large molecule distillation residues
- **(b)** cerium oxide automobile emission reduction catalyst, which helps platinum, palladium, and rhodium to speed up conversion of
  - **(i)** unhealthful CO(g), gaseous hydrocarbons, and nitrogen oxides in automotive engine-out gases to:
  - **(ii)** innocuous CO_2(g), H_2O(g), and N_2(g) tailpipe gases

Other rare earth catalysts are

- **(a)** ceria and lanthana for speeding up hydrogen production, synthetic gas production, and ethylbenzene dehydrogenation,
- **(b)** neodymium versatates and organophosphates for speeding up organic polymerization (especially for polymerizing synthetic rubber precursors), and
- **(c)** samarium iodide, for speeding up plastics decomposition, polychlorinated biphenyls (PCBs) dechlorination, and ethanol dehydration and dehydrogenation.

9.1 CHAPTER OBJECTIVES

The objectives of this chapter are to describe and explain the role of rare earths in speeding up chemical reactions. Emphasis is placed on

- **(a)** oxidation of CO(g) and gaseous hydrocarbons to CO_2(g) and H_2O(g) in automotive catalytic converters,
- **(b)** reduction of gaseous nitrogen oxides to N_2(g) in automotive catalytic converters, and
- **(c)** production of gasoline and diesel fuel from petroleum distillation residues.

Rare Earths. http://dx.doi.org/10.1016/B978-0-444-62735-3.00009-7

9.2 AUTOMOTIVE CATALYTIC CONVERSION

All new cars and trucks use on-board catalytic converters (Fig. 9.1). Ceria is used in all of these catalytic converters. It is always partnered with palladium, platinum, and/or rhodium metal nanoparticle catalyst. Their usage is:

Palladium	60%
Platinum	30%
Rhodium	10%

Ruthenium, iridium, and osmium are not used because they tend to form volatile oxides.

In 2014, the ceria is mostly chemically combined with zirconia in ceria-zirconia solid solution particles.

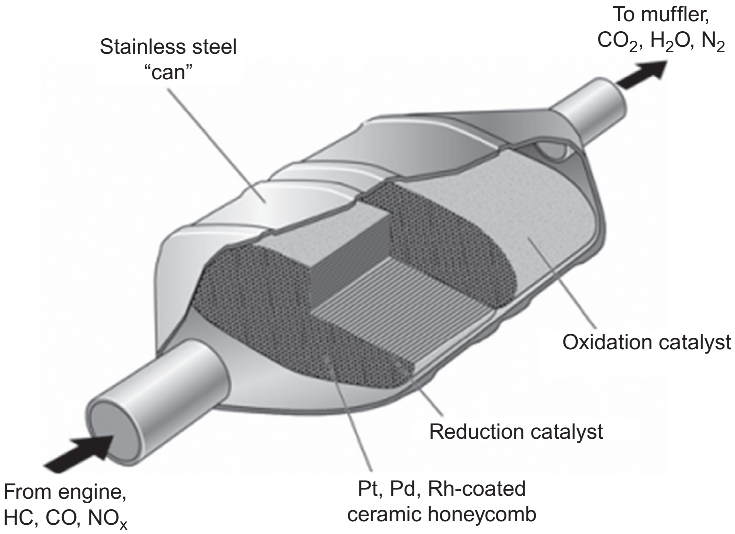

FIG. 9.1

Catalytic converter for converting unhealthful carbon monoxide, hydrocarbon, and nitrogen oxide to innocuous $CO_2(g)$, $H_2O(g)$, and $N_2(g)$ in tailpipe exit gases (Crundwell et al., 2011). Almost all converters consist of a channeled ceramic support block inside a stainless steel shell. The channel walls are covered with a solidified dispersion layer of alumina particles, ceria-zirconia particles, and Pd, Pt, Rh metal catalyst nanoparticles. Automobile converters are typically 0.3 m long and 0.1 m diameter. Engine-out gas residence time in a catalytic converter is ~0.02-0.1 seconds, depending on fuel consumption rate.

9.2.1 Platinum group metals versus rare earth oxides

As a general concept:

(a) the platinum group metal nanoparticles catalyze all the emission abatement reactions, e.g., Reaction (9.1)

while

(b) the rare earth oxides absorb and desorb $O_2(g)$ as needed to optimize (i) CO(g) and gaseous hydrocarbon oxidation and (ii) nitrogen oxide gas reduction.

Together, the Pt group metals and rare earth oxides give nearly 100% conversion of smog-forming gases to innocuous $CO_2(g)$, $H_2O(g)$, and $N_2(g)$.

The rare earth oxides are said to provide oxygen storage capacity.

9.2.2 Principal role

The principal role of these materials is to speed up the removal of unhealthful components from car-truck engine-out gas before it enters the environment.

The main unhealthful components are

(a) carbon monoxide, CO(g)
(b) gaseous hydrocarbons, $C_mH_n(g)$
(c) nitrogen oxides, $NO_2(g)$, NO(g), and $N_2O(g)$—collectively referred to as NO_x.

CO(g) is eliminated by oxidizing it to $CO_2(g)$. $C_mH_n(g)$ is oxidized to $CO_2(g)$ and $H_2O(g)$. Nitrogen oxides $NO_x(g)$ are eliminated by reducing them to $N_2(g)$.

Catalysts that simultaneously speed up these three reactions are called three-way catalysts. They convert 99+% of these unhealthful pollutants to innocuous tailpipe gases.

Automotive engines (especially diesel engines) also emit solid particulates. These are also unhealthful. Their removal from diesel engine-out gas is described in Section 9.12.

9.3 THE AUTOMOTIVE CATALYTIC CONVERTER

The automotive catalytic converter (Fig. 9.1) is always placed between

(a) the car-truck engine, where unhealthful engine-out gas is produced, and
(b) the tailpipe, where the vehicle's gaseous byproducts enter the environment.

The engine-out gas passes continuously through catalyst-coated gas channels inside the converter—where almost all of its unhealthful components are converted to innocuous gas.

9.3.1 Converter internal structure

Figure 9.1 is a sketch of an automotive catalytic converter. It consists of

(a) an external stainless steel shell with an opening at each end,
(b) inside, an extruded, multichannel ceramic block through which engine-out gas passes toward the tailpipe, and
(c) catalyst coatings on the channel walls (Fig. 9.2) where (i) CO(g) and C_mH_n(g) oxidation and (ii) NO_x reduction take place.

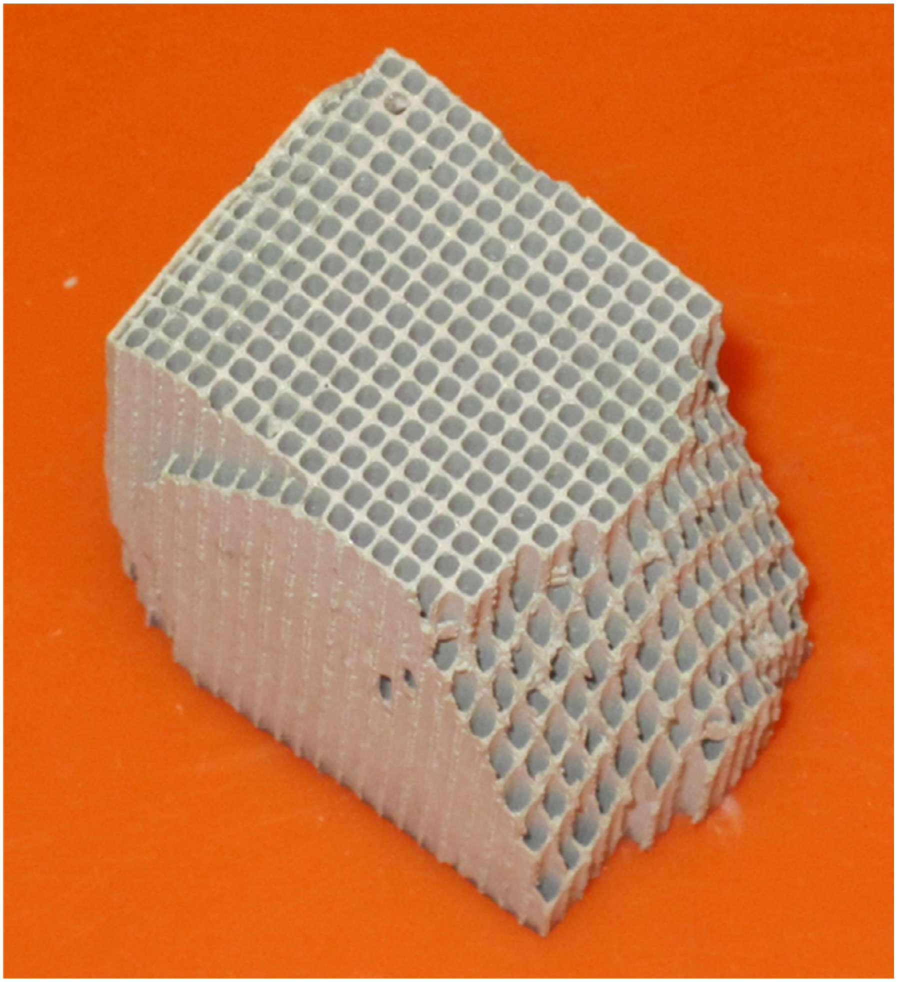

FIG. 9.2

Chunk of automobile emission reduction catalyst (from an end-of-use catalytic converter). The square channels are about 0.8 × 0.8 mm inside with 0.1 mm thick walls. They are as long as the catalytic converter (0.15-0.5 m). They are coated inside with a thin (~0.01 mm) layer of dried and heat-treated alumina particle, ceria-zirconia particle, Pd, Pt, Rh nanoparticle dispersion catalyst.

Photo by William Davenport.

There may be several separate, sequential ceramic blocks for separate oxidation and reduction. There may also be two converters—one near the hot engine (close coupled) for rapid catalyst heat-up and one further toward the tailpipe (underfloor). High-performance “muscle” cars have up to six catalytic converters.

9.3.2 Catalyst support platform

The catalyst support in 95+% of automotive catalytic converters is multichanneled, synthetic cordierite ($Al_4Mg_2Si_5O_{18}$) (Heck et al., 2009, p. 176). A few converters use Fe-Cr-Al alloy supports (Twigg, 2011). However, cordierite is the material of choice because it

(a) strongly holds and supports dried catalyst dispersion layers,
(b) has excellent high-temperature strength and durability up to 1200 °C,
(c) has a low coefficient of thermal expansion, $\sim 2 \times 10^{-6} (°C)^{-1}$, and
(d) resists damage when thermally shocked, e.g., during engine start-up.

The multichanneled blocks are made by

(a) squeezing (extruding) moist cordierite clay through a channel wall-shaped-perforated steel extrusion plate—thereby producing thousands of long, cordierite-walled open-faced channels in the extruded product (Fig. 9.2),
(b) cutting the new thin-walled, multichanneled extrusion into appropriate catalyst converter lengths, ~0.3 m, and
(c) drying and heat treating the resulting thin-walled multichannel blocks to obtain optimum physical properties and correct dimensionality.

The channels are usually square, ~1 × 1 mm, with 0.1 mm thick walls (Corning, 2013a,b,c). They provide a large channel area per square meter of frontal area with a low resistance to engine-out gas flow. Example catalyst block details are given in Table 9.2. The catalyst-coated blocks are designed to survive >150 000 km of travel. 250 000 km of travel is not uncommon.

9.3.3 Channel wall requirements

The cordierite channel walls must

(a) accept and hold particulate alumina-ceria/zirconia-platinum group metal dispersion coatings,
(b) have large surface areas,
(c) be strong, shock resistant, and wear resistant at all temperatures up to 1200 °C, and
(d) have (i) a low thermal mass, (ii) a low heat capacity, and (iii) a high thermal conductivity in order to heat up quickly during engine start-up.

Carefully mixed, extruded, dried, and heat-treated cordierite blocks efficiently meet these requirements.

Table 9.1 Engine-out Gas Compositions

Exhaust Component	Gasoline Stoichiometric Sparked Engine	Gasoline Direct Injection Lean-Burn Sparked Engine	Diesel Engine
Total gaseous hydrocarbons (volume%)	0.04-0.5	0.04-0.2	0.001-0.03
N_2 (volume%)	~70	~70	~70
CO_2 (volume%)	10-18	10-15	3-13
H_2O (volume%)	10-12	10-12	1-7
CO (volume%)	0.1-6	0.5-0.9	0.02-0.1
O_2 (volume%)	0.2-2	0.6-7	5-15
($N_2O+NO+NO_2$) (volume%)	0.01-0.4	0.08-0.2	0.02-0.1
Sulfur oxides (volume%)	0.002-0.006	0.001-0.005	0.001-0.01
Particulates (milligrams/m^3)			50-400
Temperature, (°C)	1100	900	700
Air-fuel ratio (kg/kg)	~14.7	~14.6	

Data from Martinez-Arias, A., Conesa, J.C., Fernandez-Garcia, M., Anderson, J.A., 2012. Reproduced under license (3330810966269) from John Wiley and Sons. The high level of particulates and oxygen in diesel engine-out gas are notable.

Table 9.2 Details of a Typical Converter Ceramic Block. The Block is Enclosed in a Stainless Steel Container (Fig. 9.1)

Material	Synthetic cordierite
Block shape	Circular or oval cylinder
Approximate ceramic block size	150 mm diameter × 300 mm long
Channels	
Frontal size	~1 × 1 mm square with 0.1 mm thick walls
Number per square centimeter of frontal area	50-100
Open frontal area (%)	70-80%

Table prepared by William Davenport from observations at Phoenix Autocores, Phoenix, Arizona.

9.4 CATALYST DEPOSITION

A catalyst company receives properly shaped, cut-to-length channeled cordierite blocks from a block manufacturer, e.g., Corning Incorporated, New York. The receiving company then applies catalyst dispersion layers to each block's channel walls.

9.4.1 Dispersion preparation

A catalyst dispersion consists basically of

water,
alumina (often stabilized with ~4 mass% lanthana) powder (~20 μm diameter),
ceria-zirconia (often stabilized with lanthana) powder (~20 μm diameter),
water-soluble Pt, Pd, and/or Rh nitrates,
sugar, to reduce the nitrates to metal-metal oxide crystallites, and
proprietary stabilizers such as $BaSO_4$ and lanthanum oxide.

As mixed, the dispersion is a non-Newtonian fluid, somewhat like dripless paint. Like dripless paint, it encourages a uniform thickness dispersion layers throughout Fig. 9.2's channels.

When solidified and heat treated, the platinum group nitrates are reduced to 1-2 nm diameter metal-metal oxide crystallites.

9.4.2 Dispersion application

The dispersion is applied to a cordierite block's channels by

(a) sucking the dispersion up into the channels (under vacuum) and
(b) sucking it back down again (under vacuum) after a prescribed length of time.

These proactive steps ensure a catalyst layer that is uniform and of prescribed thickness, ~0.01 mm.

9.4.3 Drying and heat treatment

The catalyst-coated blocks are dried, then heat treated at 300-600 °C to obtain the catalytic properties that are demanded by the carmaker, particularly catalyst adhesion. Heat treatment also includes reduction of the platinum group metal nitrates to metal-metal oxide nanoparticle size crystallites.

The Section 9.4.2 and 9.4.3 processes take place on a continuous conveyor, which moves each block through the above process steps and on to market.

9.4.4 Critical steps

Each of the above steps must be carried out exactly as specified to obtain optimum catalyst activity. It is essential, for example, that the precipitated platinum group metal particles are small (20-40 nm diameter), uniformly sized, and uniformly distributed in the ceria-zirconia layer.

It is also essential that the ceria-zirconia dispersion layer has exactly the right surface area, particle size distribution, and thermal stability.

Controlled deposition, precipitation, drying, and heat treatment achieve these goals.

9.4.5 Catalyst layer arrangements

The simplest catalytic converter blocks have a single catalyst layer along the whole length of the block's channels (Fig. 9.2). Somewhat more complicated is a block with two different layers of catalyst—e.g., a Pd-rich layer on the channel walls and Rh-rich layer on top of it.

Another arrangement is half the length covered with one catalyst (e.g., Pd-rich) and the other half covered with another catalyst (e.g., Rh-rich).

There are many commercial arrangements, all targeting 100% conversion of CO(g), H_mC_n(g), and NO_x(g) to innocuous gases.

9.5 AUTOMOTIVE CATALYSTS: PAST, PRESENT, AND FUTURE

Automotive emission abatement catalyst originally consisted of platinum group metal (Pt, Pd, Rh) catalyst nanoparticles on a porous particulate alumina dispersion substrate, both deposited onto the interior walls of ceramic (occasionally steel) support block channels. This was sufficient for CO(g) and gaseous hydrocarbon oxidation, but insufficient for simultaneous NO_x(g) reduction.

Efficient simultaneous (i) *oxidation* of CO(g) and gaseous hydrocarbons and (ii) *reduction* of NO_x(g) was made possible by adding ceria (cerium oxide) to Section 9.4.1's catalyst dispersion. Ceria is a so-called oxygen storage compound which rapidly absorbs and desorbs oxygen to maintain a constant oxygen-in-gas composition that maximizes CO(g), C_mH_n(g), and NO_x(g) conversion.

Oxygen storage was improved further by changing the ceria dispersion component to ceria-zirconia solid solution particles. Ceria-zirconia solid solutions store much more oxygen than ceria itself. They also further accelerate oxidation and reduction kinetics.

In 2014, lanthana is also included in the ceria-zirconia solid solution particles. It stabilizes the oxygen storage capacity for up to 250 000 km of engine operation.

9.6 CATALYTIC REACTIONS

The simplest automotive emission abatement reaction is

$$\overset{\text{unhealthful}}{CO(g)} \underset{\text{in engine-out gas}}{+} \overset{\text{from engine input air}}{0.5O_2(g)} \xrightarrow[\sim 1000^\circ C]{\text{Pt group metal catalyst}} \underset{\substack{\text{in innocuous catalytic}\\ \text{converter exit gas}}}{CO_2(g)} \tag{9.1}$$

Car-truck engines are operated with a high-enough air-fuel ratio, so that this reaction can always go to completion.

The equilibrium constant for this reaction is plotted in Fig. 9.3. It shows that CO_2(g) formation is strongly favored at all temperatures. The equilibrium constant is related to:

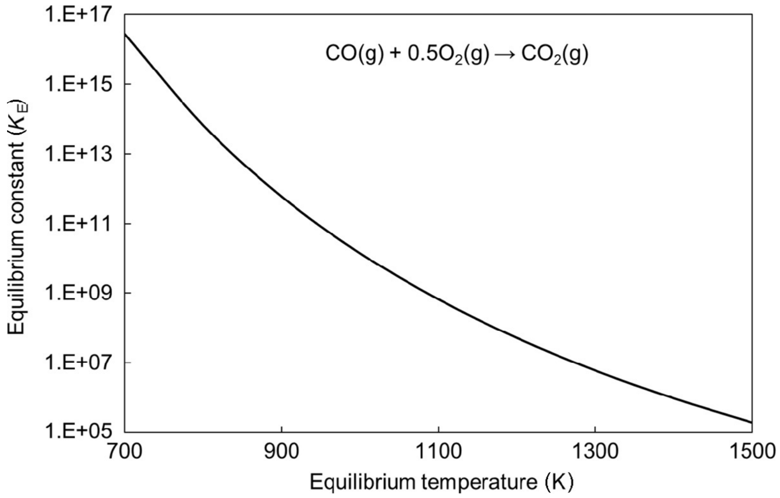

FIG. 9.3

Carbon monoxide oxidation equilibrium constant as a function of equilibrium temperature. It is large at all temperatures because the reaction's heat of reaction ($\Delta H_r°$) is very negative.

Graph calculated by William Davenport.

(a) equilibrium CO(g), O_2(g), and CO_2(g) concentrations
and:
(b) equilibrium pressure

by the equation:

$$K_E = \frac{X^E_{CO_2(g)}}{X^E_{CO(g)} \times \left(X^E_{O_2(g)}\right)^{0.5}} \times P_t^{-0.5} \tag{9.2}$$

where
X^E = the equilibrium volume fraction of each gas, P_t = total pressure at the catalytic converter exit = ~1 bar.

Specification that the catalytic converter exit gas pressure is ~1 bar simplifies Eq. (9.2) to

$$K_E = \frac{X^E_{CO_2(g)}}{X^E_{CO(g)} \times \left(X^E_{O_2(g)}\right)^{0.5}} \tag{9.3}$$

or

$$\frac{X^E_{CO_2(g)}}{X^E_{CO(g)}} = K_E \times \left(X^E_{O_2(g)}\right)^{0.5} \tag{9.4}$$

which shows clearly that the improved removal of CO(g) from engine-out gas is favored by a high engine-out oxygen concentration.

Unfortunately, a high-oxygen content has an adverse effect on nitrogen oxide reduction—so it must never be excessive.

9.7 CO(g) OXIDATION WITHOUT CATALYST (MINIMAL)

The above section describes equilibrium $CO(g) + 0.5O_2(g) \rightarrow CO_2(g)$ oxidation. This section describes its kinetics.

Engine-out gases pass rapidly through catalytic converters. Their residence times are typically 0.02-0.1 s. Achievement of near equilibrium CO(g) oxidation in these short times requires rapid, catalyst-assisted reactions.

9.7.1 Gas-gas oxidation kinetics

Without catalyst, gas oxidation reactions like $CO(g) + 0.5O_2(g) \rightarrow CO_2(g)$ oxidation are very slow. The slowness arises because $O_2(g)$ molecules must be split into O atoms, i.e.,

$$O_2(g) \xrightarrow{\text{high-energy dissociation (scission) reaction}} 2O(g) \tag{9.5}$$

before CO(g) oxidation

$$2CO(g) + 2O(g) \rightarrow 2CO_2(g) \tag{9.6}$$

can occur.

Reaction (9.5) is a high activation energy, homogeneous reaction that occurs slowly unless reaction temperature is extremely high.

So the situation before the invention of catalytic converters is very clear. All the CO(g), gaseous hydrocarbons, and $NO_x(g)$ in a car's engine-out gas were being released to the environment. This caused serious smog issues in Los Angeles and other cities.

9.8 EARLY CATALYTIC CONVERTER OBJECTIVES

The objectives of the early catalytic converters were to oxidize a car engine's exhaust CO(g) and gaseous hydrocarbons to innocuous $CO_2(g)$ and $H_2O(g)$. This was achieved mostly with:

(a) a channeled ceramic support block with its interior walls coated with an alumina particle-platinum group metal nanoparticle catalyst layer
(b) a slight excess of $O_2(g)$ in the engine-out gas.

With CO(g) oxidation and palladium as the example platinum group metal, the catalytic reactions were

(a) rapid formation of Pd-O complexes on the palladium nanoparticles

$$\underset{\text{in engine-out gas}}{O_2(g)} + \underset{\text{palladium nanoparticles}}{2Pd^{\circ}} \xrightarrow{\sim 1000^{\circ}C} \underset{\substack{\text{complexes on palladium} \\ \text{nanoparticle surfaces}}}{2(\text{Pd-O})} \tag{9.7}$$

(b) rapid reaction of CO(g) with these Pd-O complexes, i.e.,

$$\underset{\text{in engine-out gas}}{2\text{CO(g)}} + \underset{\substack{\text{active complexes}\\ \text{on palladium}\\ \text{nanoparticle surfaces}}}{2(\text{Pd-O})} \xrightarrow{\sim 1000^\circ\text{C}} \underset{\substack{\text{restored}\\ \text{palladium metal}}}{2\text{Pd}^\circ} + \underset{\substack{\text{in innocuous catalytic}\\ \text{converter exit gas}}}{2\text{CO}_2\text{(g)}} \tag{9.8}$$

which add to

$$\underset{\text{in engine-out gas}}{2\text{CO(g)} + \text{O}_2\text{(g)}} \xrightarrow[\sim 1000^\circ\text{C}]{\text{Pt group metal catalyst}} \underset{\text{in innocuous catalytic converter exit gas}}{2\text{CO}_2\text{(g)}} \tag{9.9}$$

or, dividing by two

$$\underset{\text{in engine-out gas}}{\text{CO(g)} + 0.5\,\text{O}_2\text{(g)}} \xrightarrow[\sim 1000^\circ\text{C}]{\text{Pt group metal catalyst}} \underset{\text{in innocuous catalytic converter exit gas}}{\text{CO}_2\text{(g)}} \tag{9.1}$$

which is the overall CO(g) oxidation reaction.

Thus palladium catalysis replaces slow homogeneous O_2(g) scission with rapid heterogeneous Pd-O complex formation (Eq. 9.7).

In practice, progress of the above catalytic converter reactions entails

(a) rapid passage of hot engine-out gas through cordierite block channels,
(b) convection and diffusion of O_2(g) to the catalyst's Pt group metal particle surfaces—where it quickly adsorbs,
(c) rapid reaction of the adsorbed O_2(g) to form active Pd-O complexes,
(d) convection and diffusion of CO(g) to the active Pd-O sites and rapid formation of CO_2(g) at these sites, and
(e) rapid desorption of CO_2(g) from the palladium particle surfaces and convection-diffusion into the converter exit (tailpipe) gas.

9.9 GASEOUS HYDROCARBON OXIDATION

Oxidation of engine-out gas's gaseous hydrocarbons (Table 9.3) proceeds much like CO(g) oxidation. The overall reaction is

$$\underset{\text{in engine-out gas}}{(\text{C}_m\text{H}_n)\text{(g)} + (m + 0.25n)\text{O}_2\text{(g)}} \xrightarrow[1000^\circ\text{C}]{\text{Pt group metal catalyst}} \underset{\substack{\text{in innocuous catalytic}\\ \text{converter exit gas}}}{m\text{CO}_2\text{(g)} + (0.5n)\text{H}_2\text{O(g)}}. \tag{9.10}$$

The equilibrium constant for this reaction is also very large because hydrocarbon compounds are very weak [as compared to CO_2(g) and H_2O(g)] at elevated temperatures.

Table 9.3 Representative Sparked Gasoline Engine-Out Hydrocarbon Gas Composition

Hydrocarbon Group	Mass%
Aromatics	46
Olefins	27
Paraffins (C_{5+})	12
Methane	7
Paraffins (C_2-C_4)	5
Other	3

Data courtesy of John Noonan, Umicore.

The catalyzed gaseous hydrocarbon oxidation mechanism is

$$\underset{\substack{\text{in engine-out}\\ \text{gas}}}{(\mathrm{C}_m\mathrm{H}_n)(\mathrm{g})} + \underset{\substack{\text{active complex on}\\ \text{palladium nanoparticles}}}{(2m+0.5n)(\text{Pd-O})} \xrightarrow{\sim 1000\,^\circ\mathrm{C}} \underset{\substack{\text{restored palladium}\\ \text{metal}}}{(2m+0.5n)\mathrm{Pd}^\circ} + \underset{\substack{\text{in innocuous catalytic}\\ \text{converter exit gas}}}{m\mathrm{CO}_2(\mathrm{g}) + (0.5n)\mathrm{H}_2\mathrm{O}(\mathrm{g})}. \tag{9.11}$$

As with CO(g) oxidation, completion of these reactions benefits from a slight excess of O_2(g) in the engine-out gas.

9.10 COLD START-UP

The reactions in Sections 9.8 and 9.9 are fastest when the car engine's exhaust gas is at its normal driving temperature, ~1000 °C. The reactions are sluggish at cold engine start-up, leading to CO(g) and gaseous hydrocarbons in the car's tailpipe gas. However, they benefit somewhat from (Pd-O) complexes remaining at engine turn-off.

Moreover, it was discovered that ceria (CeO_2) particles in the catalyst layer accelerated cold start-up CO(g) and gaseous hydrocarbon oxidation. The ceria was thought to produce additional (Pd-O) complexes by reactions like:

$$\underset{\substack{\text{at ceric oxide-platinum}\\ \text{group metal interfaces}}}{3\mathrm{CeO}_2(\mathrm{s}) + 2\mathrm{Pd}^\circ(\mathrm{s})} \rightarrow \underset{\substack{\text{cerous oxide in}\\ \text{cerous-ceric oxide mixture}}}{\mathrm{Ce}_3\mathrm{O}_4(\mathrm{s})} + \underset{\substack{\text{active Pt group}\\ \text{metal-oxygen complexes}}}{2(\text{Pd-O})} \tag{9.12}$$

Ceria has been included in automobile catalyst ever since (now in the form of lanthana-stabilized ceria-zirconia solid solution particles).

Rapid cold-start catalysis is also enhanced by placing the catalytic converter as close as possible to a car's engine. This increases catalyst heat-up speed. Heat-up is also accelerated by minimizing catalytic converter mass (e.g., by using thin cordierite channel walls).

Some car manufacturers electrically heated the catalytic converter at the turn of the starter key. Modern catalytic converter technology has made this obsolete. Nevertheless, rapid catalyst heat-up is still a key factor in minimizing automobile pollution.

9.11 NITROGEN OXIDE (NO_X(g)) REDUCTION

Automotive catalytic converters were initially designed to oxidize toxic CO(g) and gaseous hydrocarbons to innocuous CO_2(g) and H_2O(g). However, it soon became clear that engine-out nitrogen oxides (NO_2(g), NO(g), and N_2O(g)) were also contributing to smog formation. The simplest reaction for reducing these nitrogen oxide gasses is

$$\underset{\text{in engine-out gas}}{(2x)CO(g)+2NO_x(g)} \rightarrow \underset{\text{in tailpipe gas}}{(2x)CO_2(g)+N_2(g)}. \qquad (9.13)$$

The equilibrium extent of this reaction is indicated in Fig. 9.4.

9.11.1 Required gas composition

For maximum conversion, the engine-out gas must have exactly the stoichiometric concentrations of O_2(g), CO(g), C_mH_n(g), and NO_x(g).

Too little O_2 will result in CO(g) and C_mH_m(g) in the tailpipe gas.

Too much O_2 will result in NO_x(g) in the tailpipe gas.

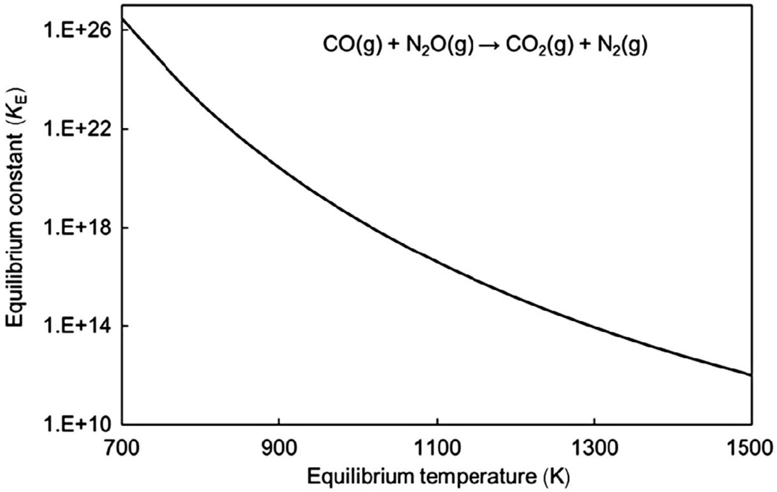

FIG. 9.4

Equilibrium constant for N_2O(g) reduction by CO(g) as a function of temperature. The equilibrium constant is very large at all temperatures indicating that even the tiniest amount of CO(g) will drive N_2O(g) reduction to completion. This is because CO_2(g) is a much more strongly bonded compound than N_2O(g). The kinetics of this reaction are discussed below.

Graph calculated by William Davenport.

9.11.2 Engine air-fuel ratio control

An operating automotive engine is computer controlled (using oxygen sensors) to give near-complete CO(g), C_mH_n(g), and NO_x(g) conversion.

However, the computer control is not perfect so that the air-fuel ratio varies slightly as driving conditions change. These variations move CO(g), C_mH_n(g), and NO_x(g) conversion away from their optima.

Fortunately, this effect is minimized by the catalytic converter's particulate ceria-zirconia dispersion layer, which

(a) quickly desorbs oxygen into the catalytic converter gas when the air-fuel ratio is too low

(b) quickly adsorbs oxygen from the converter input gas when the air-fuel ratio is too high

thus maintaining (i) the optimum oxygen content in the catalytic converter and (ii) maximum CO(g), C_mH_n(g), and NO_x(g) conversion.

Ceria's oxygen desorption reaction is represented by

$$\underset{\text{ceric oxide}}{3CeO_2(s)} \rightarrow \underset{\text{cerous oxide}}{Ce_3O_4(s)} + \underset{\text{atomic oxygen}}{2O} \tag{9.14}$$

which provides atomic oxygen for rapid CO(g) and C_mH_n(g) oxidation.

The oxygen may also go to an active platinum group metal-oxygen reaction site, i.e.,

$$\underset{\substack{\text{at ceric oxide platinum}\\ \text{group metal interface}}}{3CeO_2(s) + 2Pd^{\circ}(s)} \rightarrow \underset{\substack{\text{cerous oxide in cerous-ceric}\\ \text{oxide mixture}}}{Ce_3O_4(s)} + \underset{\substack{\text{active Pt group}\\ \text{metal-oxygen complex}}}{2(\text{Pd-O})} \tag{9.15}$$

which provides Pd-O complexes for rapid CO(g) and C_mH_n(g) oxidation.

Oxygen absorption is represented by

$$\underset{\text{cerous oxide}}{Ce_3O_4(s)} + \underset{\text{oxygen in engine-out gas}}{O_2(g)} \rightarrow \underset{\text{ceric oxide}}{3CeO_2(s)}. \tag{9.16}$$

9.11.3 Optimum ceria-zirconia composition

Dried and heat-treated ceria-zirconia dispersion layers consist mainly of lanthanum-stabilized ceria-zirconia solid solution particles. A typical composition is 60 mass% zirconia, 40 mass% rare earths mostly ceria with La, Pr, Nd, and Y oxide dopants. Each automobile manufacturer has its own specifications and additives.

Lanthana is the best thermal stabilizer. It also favors a cubic structure, which encourages rapid O transport.

Yttria is the best cubic structure stabilizer, maximizing O transport rate.

Praseodymia is between the two and appears to promote rapid oxygen absorption-desorption, like Reaction (9.16).

All are designed to maximize CO(g), C_mH_n(g), and NO_x(g) conversion.

9.11.4 Optimum platinum group metal use

Car companies use many combinations of Pd, Pt, and Rh in their catalysts. The choice depends mainly on the company's engine control system and engine-out gas characteristics. In broad terms, however,

1. Palladium is the best catalyst for immediate, rapid reactions at cold start-up.
2. Platinum is particularly effective for gaseous hydrocarbon oxidation.
3. Rhodium is particularly effective for $NO_x(g)$ reduction.

Price also drives metal choice—but this is notoriously unpredictable (Johnson Matthey, 2013).

9.12 DIESEL ENGINE POLLUTION ABATEMENT SYSTEMS

A significant difference between sparked gasoline engine-out gas and diesel engine-out gas is that the latter contains a significant quantity of solid particulates (soot), Tables 9.1 and 9.4. This soot is harmful to fauna and flora. It must be prevented from reaching the environment.

The first step in lowering soot emission was to improve the diesel engines themselves—by introducing high-pressure fuel injection. This beneficially improved carbon combustion in the engine and reduced soot production by about 60%.

The second step was to develop systems by which the soot is held up in filters, where it has time to be oxidized to carbon dioxide (Fig. 9.5). The filters themselves may be coated with catalyst to speed up soot oxidation (Johnson Matthey, 2014).

9.12.1 Example soot elimination process

Figure 9.5a is a flow sheet of a diesel engine-out gas pollution abatement system. The abatement steps are as follows:

1. The diesel engine-out gas is oxidized to near completion as it passes through a platinum group metal catalyst-coated ceramic block (Fig. 9.2). The reactions are

Table 9.4 Composition of Solid Particulates (Soot) Produced by Automotive Diesel Engines

Item	Concentration in Soot (Mass%)
Dry carbon	43
Lubricant soluble organic	35
Fuel soluble organic	20
Other	2

Reproduced by permission of Imperial College Press from the book Supported Metals in Catalysts, edited by James A. Anderson and Marcos Fernandez Garcia, copyrighted by Imperial College Press 2012.

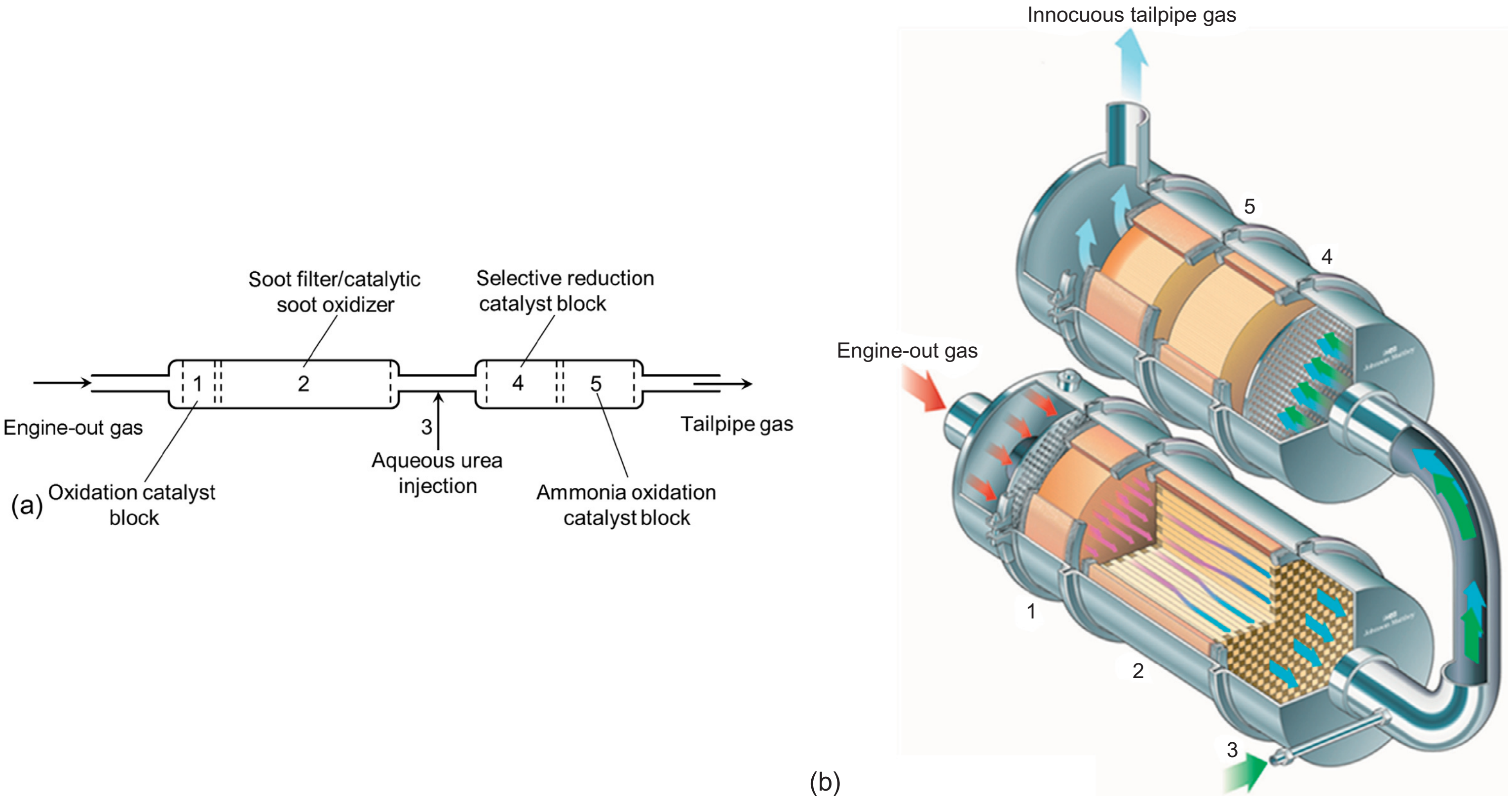

FIG. 9.5

(a) Schematic flow sheet for changing diesel engine-out CO(g), gaseous hydrocarbons, NO_x(g), and solid soot to innocuous tailpipe CO_2(g), H_2O(g), and N_2. The numbers correspond to the steps in Section 9.12.1. The system is detailed in Johnson Matthey (2014). It is shown as a straight line, but it can be bent between the 1,2 and 4,5 sections. Other emission-control companies use slightly different systems (Drawing by William Davenport). (b) Diesel engine emission reduction catalytic converter system. Figure 9.5a is a line drawing of this system. The numbers refer to those in Section 9.12.1. Note particularly soot filter 2. Half the filter's channels are open at the inlet end and closed at the outlet end. Half the channels are closed at the inlet end and open at the outlet end. So, the inlet gas must pass through the porous cordierite walls to escape the filter, trapping the soot in the cordierite *filter*. Image reproduced courtesy of Ann Macchia, Johnson Matthey. This is the arrangement with a vertical tailpipe. It would lie flat in a diesel car.

$$\overset{\text{unhealthful}}{\mathrm{CO(g)}} \underset{\text{in engine-out gas}}{+} \overset{\text{excess in engine input air}}{\mathrm{0.5O_2(g)}} \xrightarrow{\text{Pt group metal catalyst}} \underset{\text{in first catalyst block exit gas}}{\mathrm{CO_2(g)}} \tag{9.1}$$

$$\underset{\text{in engine-out gas}}{\overset{\text{unhealthful}}{(\mathrm{C}_m\mathrm{H}_n)\mathrm{(g)}} + \overset{\text{excess in engine input air}}{(m+0.25n)\mathrm{O_2(g)}}} \xrightarrow{\text{Pt group metal catalyst}} \underset{\text{n first catalyst block exit gas}}{m\mathrm{CO_2(g)} + (0.5n)\mathrm{H_2O(g)}} \tag{9.10}$$

and

$$\overset{\text{unhealthful}}{(\mathrm{NO_x})\mathrm{(g)}} \underset{\text{in engine-out gas}}{+} \overset{\text{excess in engine input air}}{(1\text{-}0.5x)\mathrm{O_2(g)}} \xrightarrow{\text{Pt group metal catalyst}} \underset{\text{in first catalyst block exit gas}}{\mathrm{NO_2(g)}}\ . \tag{9.17}$$

2. The diesel engine-out soot is caught in a long filter immediately downstream from catalyst block (1). The soot is oxidized in the filter to CO_2(g) and NO(g) by reactions like:

$$\underset{\text{soot entrapped in filter}}{\mathrm{C(s)}} + \underset{\text{in first catalyst block exit gas}}{\mathrm{2NO_2(g)}} \xrightarrow{\text{Pt group-coated filter}} \underset{\text{in filter exit gas}}{\mathrm{CO_2(g)} + \mathrm{2NO(g)}} \tag{9.18}$$

3. Urea aqueous solution is injected into the filter exit gas where it reacts to form gaseous ammonia, i.e.,

$$\underset{\text{injected urea}}{\mathrm{CO(NH_2)_2(aq)}} + \underset{\text{in filter exit gas}}{\mathrm{H_2O(g)}} \rightarrow \underset{\text{byproduct carbon dioxide}}{\mathrm{CO_2(g)}} + \underset{\mathrm{NH_3(g)}\text{ reductant}}{\mathrm{2NH_3(g)}} \tag{9.19}$$

4. The ammonia-enriched filter exit gas enters a second catalytic converter block (4) where NO(g) is reduced to N_2(g) by reactions like:

$$\underset{\text{ammonia reductant from urea injection}}{\mathrm{2NH_3(g)}} + \underset{\text{in filter exit gas}}{\mathrm{NO(g)} + \mathrm{NO_2(g)}} \xrightarrow[\text{Pt group metal catalyst}]{\text{selective catalytic reduction}} \underset{\text{in selective reduction catalyst block exit gas}}{\mathrm{3H_2O(g)} + \mathrm{2N_2(g)}} \tag{9.20}$$

5. Excess NH_3(g) from Reaction (9.20) is removed in a third catalyst block by reactions like:

$$\underset{\text{excess ammonia from Reaction (9.20)}}{\mathrm{2NH_3(g)}} + \underset{\text{in excess engine input air}}{\mathrm{1.5O_2(g)}} \xrightarrow{\text{platinum group metal catalyst}} \underset{\text{in innocuous tailpipe gas}}{\mathrm{3H_2O(g)} + \mathrm{N_2(g)}} \tag{9.21}$$

9.12.2 Tailpipe emission

The overall tailpipe products from the above described reactions are

(a) $CO_2(g)$ from Reactions (9.18) and (9.19),
(b) $H_2O(g)$ from Reactions (9.20) and (9.21), and
(c) $N_2(g)$ from Reactions (9.20) and (9.21).

$CO(g)$, $C_mH_n(g)$, $NO_x(g)$, and soot are nearly 100% eliminated.

Other catalyst manufacturers market similar soot oxidation systems.

9.13 CATALYTIC PETROLEUM CRACKING

Fluid catalytic petroleum cracking is an extremely important part of petroleum refining. It converts

(a) the high-boiling temperature (>340 °C), high molecular mass (200-600+ kg/kg-mole) residues from crude oil distillation

to

(b) gasoline, diesel, fuel oil, and other valuable products.

9.13.1 Cracking process

The cracking process breaks large hydrocarbon molecules into small molecules by vaporizing them at moderate temperatures (~540 °C) and pressures (~2.7 bar absolute) in contact with *powdered* zeolite catalyst. A simplified reaction is

$$\underset{\substack{\text{in catalytic fluid}\\ \text{petroleum cracking feed}}}{C_{16}H_{34}(g)} + \underset{\substack{\text{from zeolite}\\ \text{catalyst}}}{2H} \xrightarrow[535\,^{\circ}C]{\substack{\text{in a fluidized zeolite}\\ \text{catalyst powder reactor}}} \underset{\text{product gasoline}}{2C_8H_{18}(g)} \tag{9.22}$$

which breaks one C-C bond and makes two molecules of gasoline.

The main chemical reaction is breaking (scission) of carbon-to-carbon bonds, spurred on by the high temperature and pressure of the process.

World-wide, catalytic petroleum-cracking plants treat $\sim 10^9$ tonnes of feedstock per year and produce ~1/3 of the world's gasoline. Much of this production uses La (and some Ce) in its zeolite catalyst.

9.13.2 The catalyst

Petroleum-cracking catalyst contains

faujasite zeolite (zeolites are porous aluminosilicate minerals),
amorphous alumina,
silica sol (binder), and
kaolin filler (clay).

The faujasite is a molecular sieve consisting primarily of alumina and silica tetrahedrons. The structure contains holes which allow hydrocarbon molecules to enter its lattice. The catalytic sites in faujasite's lattice are provided by the alumina tetrahedrons where

(a) $H_2O(g)$ molecules in the vaporized petroleum are broken into OH^- and H^+ ions,
(b) OH^- ions are trapped at the alumina tetrahedron's acidic Al sites, and
(c) freed hydrogen reacts with C-C hydrocarbon bonds, *cracking* large hydrocarbon molecules into smaller gasoline molecules.

9.13.3 La and Ce in catalyst

Modern catalytic petroleum-cracking catalysts typically contain ~2.5 mass% (La + Ce) (Fig. 9.6). The La and Ce are added as cations by soaking the catalyst zeolites in La and Ce chloride (mostly) and nitrate solutions.

The role of the La and Ce ions in the faujasite is to maintain the catalytic activity of the alumina tetrahedrons during high temperature processing. The La and Ce ions exchange with faujasite's naturally occurring H_3O^+ and Na^+ ions as La^{3+} and Ce^{3+} to form a stronger *artificial* zeolite structure, which

(a) avoids high-temperature destruction (sintering) of the faujasite lattice
(b) keeps the active alumina tetrahedral sites available for catalysis.

La ions appear to be slightly better than cerium ions for petroleum cracking. Ce is used if it is significantly cheaper.

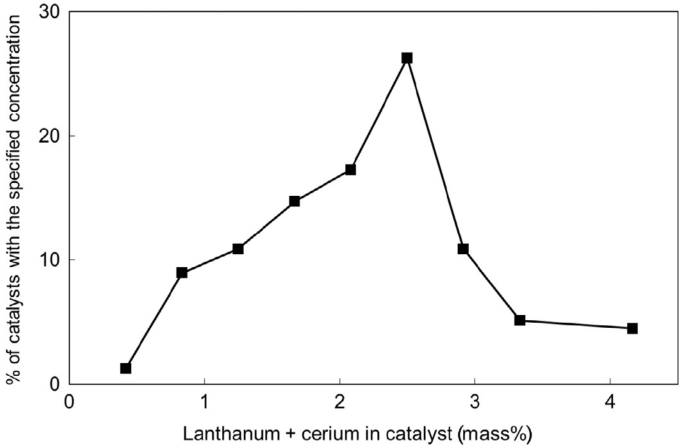

FIG. 9.6

La + Ce concentrations in industrial catalytic petroleum-cracking catalysts. 2.5% La + Ce is the most common. Most, but not all, petroleum-cracking plants use La + Ce in their catalyst.

Data kindly supplied by Solly Ismail, BASF.

9.14 QUANTITATIVE BENEFITS

Figure 9.7 demonstrates improved catalytic activity due to lanthanum and cerium in catalyst. It shows that high-value gasoline production increases with increasing lanthanum + cerium concentration in catalyst. This is of considerable economic benefit to petroleum producers-refiners.

A second benefit for some refineries is a commensurate decrease in liquid petroleum gas production (Fig. 9.8). Handling of petroleum gas is often a bottleneck in fluid catalyst petroleum-cracking plants.

9.14.1 Explanation

The increased gasoline production efficiency is due to

(a) more efficient carbon-to-carbon bond breaking (scission)

and

(b) more efficient hydrogen transfer to the cracked products, which avoids overcracking of 4-carbon gasoline molecules to 3-carbon molecules (e.g., propane, C_3H_8).

9.14.2 Hydrothermal stability

The high temperatures (>700 °C) in the catalyst regeneration section of fluid catalytic petroleum-cracking plants tend to cause sintering of the zeolite catalyst. This sintering

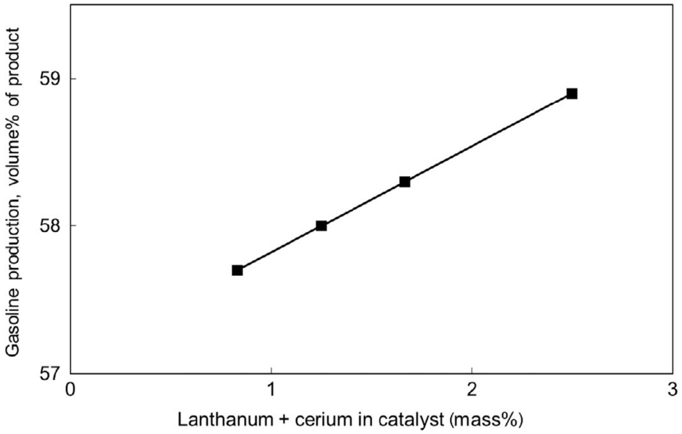

FIG. 9.7

Effect of % La + Ce in catalyst on the percentage of catalytic petroleum-cracking feed that is converted to gasoline. The increase in gasoline production is notable. Gasoline is the cracking plant's most valuable product. Its production is usually maximized.

Data kindly supplied by Solly Ismail, BASF.

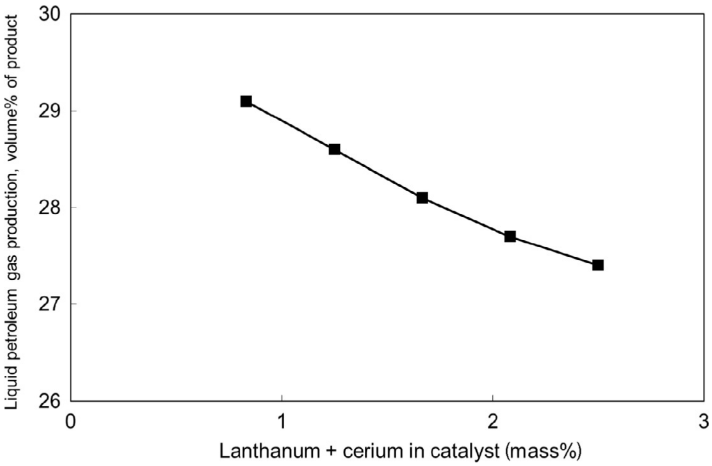

FIG. 9.8

Effect of La + Ce in catalyst on the percentage of catalytic petroleum-cracking plant feedstock that is converted to liquid petroleum gas. The decrease is notable. Handling of this product is often the bottleneck in a petroleum-cracking plant.

Data kindly supplied by Solly Ismail, BASF.

(a) reduces the activity of the catalyst

and

(b) increases the requirement for new (fresh) catalyst per tonne of feedstock.

The reduction of activity is due to a loss of active catalytic sites during sintering.

The presence of lanthanum and cerium ions in the catalyst minimizes sintering and lowers the need for new catalyst. Figure 9.9 shows the trade-off between lanthanum + cerium in catalyst and new catalyst requirement.

9.15 NEODYMIUM CATALYSTS

The main use of neodymium is in neodymium-iron-boron permanent magnets. However, it is also used as organic polymerization catalyst. Examples are dienes, styrene, propylene, and isoprene polymerization. Perhaps the most important application is production of butadienes, which are used in synthetic rubber tire production. The neodymium is used in the form of versatate solutions and organophosphate solutions.

9.16 SAMARIUM CATALYSTS

The main use of samarium is in samarium-cobalt permanent magnets. However, it is also used in compound form to speed up decomposition of plastics, dechlorination of PCBs, and dehydration and dehydrogenation of ethanol. Samarium iodide is a particularly useful compound in this regard.

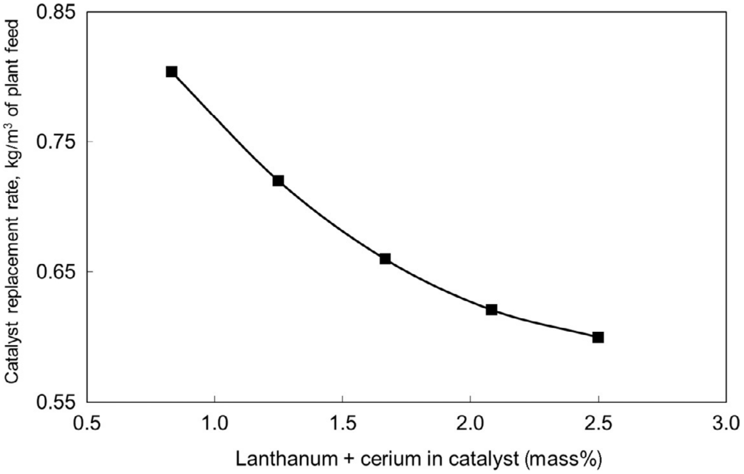

FIG. 9.9

Effect of La + Ce in catalyst on catalyst replacement requirement, where the replacement is to maintain constant catalytic activity. The decrease in replacement requirement with increasing La + Ce in catalyst is notable. Replacement requirement varies greatly for different feedstocks and plant-operating conditions. A representative value is 0.6 kg of new catalyst per cubic meter of cracking plant feed.

Data kindly supplied by Solly Ismail, BASF.

9.17 SUMMARY

The largest catalytic rare earth use is lanthanum ions and sometimes ceria ions in fluid petroleum-cracking catalysts. La^{3+} and Ce^{3+} ions exchange with H_3O^+ and Na^+ ions in zeolite catalysts to form strong zeolite catalyst structures, which

(a) minimize high-temperature destruction (sintering) of the cracking catalyst,
(b) increase cracking catalyst life, thereby:
(c) maximizing gasoline and diesel production.

Another critical use of rare earths in catalyst is in automotive catalytic converters. In this service, they help platinum, palladium, and rhodium to speed up conversion of unhealthful

$CO(g)$, $C_mH_n(g)$, $NO_x(g)$ and solid soot
in engine-out gas to
innocuous $CO_2(g)$, $H_2O(g)$, and $N_2(g)$

in tailpipe exhaust gas. With platinum group metal/ceria-zirconia catalysts, conversion to innocuous tailpipe gas is nearly 100% especially when the catalyst has reached its steady-state operating temperature (~1000 °C). The most important rare earth compounds for this application are cerium and lanthanum oxides.

Neodymium is used as an organic polymerization catalyst. Its principal use is for the polymerization of butadiene, which is used for synthetic rubber tire production. It is used in the form of Nd versatate solutions and Nd organophosphate solutions.

Samarium is also used as a catalyst, mostly as samarium iodide. It is used for speeding up decomposition of plastics and PCBs and for ethanol dehydration and dehydrogenation.

References

Bosch, 2014. Bosch Lambda Sensor Function. Retrieved from http://www.bosch-lambdasonde.de/en/lambdasonde_funktion.htm on March 7, 2014.

Corning, 2013a. Corning Celcor® Thin-Wall Substrates for Advanced Catalyst Converters. Corning Incorporated, Corning, NY. Retrieved on August 15, 2013 from, www.corning.com/WorkArea/downloadasset.aspx?id=6281.

Corning, 2013b. Corning Celcor® Ultrathin-Wall Substrates for Ultra-High Performance, Ultra-Low Emissions. Corning Incorporated, Corning, NY. Retrieved from, www.corning.com/WorkArea/downloadasset.aspx?id=6283.

Corning, 2013c. Corning Celcor® LFA Substrates for Reducing Diesel Engine Exhaust Emissions. Corning Incorporated, Corning, NY. Retrieved on August 15, 2013 from, www.corning.com/WorkArea/downloadasset.aspx?id=6285.

Heck, R.M., Farrauto, R.J., Gulati, S.T., 2009b. Catalytic Air Pollution Control, third ed. Wiley, Hoboken, NJ, 3–23 and 103–237.

Ismail, S., 2011. Fluid Catalytic Cracking (FCC) Catalyst Optimization to Cope with High Rare Earth Oxide Price Environment. BASF Corporation, Iselin, NJ. Retrieved on August 15, 2013, http://www.catalysts.basf.com/p02/USWeb-Internet/en_GB/function/conversions:/publish/content/microsites/catalysts/prods-inds/process-catalysts/BF-9626_US_REAL_Technical_Note.pdf BASF technical note, BASF Corporation, 25 Middlesex/Essex Turnpike, Iselin, NJ 08830.

Matthey, J., 2013. Platinum Group Metal Prices. Johnson Matthey PLC, Royston, England. Retrieved on August 15, 2013 from, http://www.platinum.matthey.com/pgm-prices/price-charts/.

Matthey, J., 2014. Diesel Emission Reduction System. *Google*: SCRT emission control system Johnson Matthey, *then press* SCRT Animation. Recovered February 12, 2014.

King, M.J., Davenport, W.G., Moats, M.S., 2013. Sulfuric Acid Manufacture. Elsevier Science Press, Oxford, England.

Martinez-Arias, A., Conesa, J.C., Fernandez-Garcia, M., Anderson, J.A., 2012. Supported metals in vehicle emission control. In: Anderson, J.A., Garcia, M.F. (Eds.), Supported Metals in Catalysis. second ed. Imperial College Press, London, England, 494, Chapter 10.

Oxygen Sensor, 2014. Retrieved from http://en.wikipedia.org/wiki/Oxygen_sensor on March 7, 2014.

Twigg, M.V., 2011b. Catalytic control of emissions from cars. Catal. Today. 163, 33–41.

Suggested Reading

Anderson, J.A., Garcia, M.F., 2012. Supported Metals in Catalysis, second ed. Imperial College Press, London.

BASF, 2012. FCC Refining Catalysts. BASF Corporation, Iselin, NJ. Retrieved on August 15, 2013 from, http://www.catalysts.basf.com/p02/USWeb-Internet/catalysts/en/content/microsites/catalysts/prods-inds/process-catalysts/refinery-catalysts.

Colwell, R., Jergenson, D., Hunt, D., Sudhakar, J., Udvari, E., 2012. Alternatives to rare earth in FCC operations. Refinery Operations. 3 (4), 1–7.

Crundwell, F.K., Moats, M.S., Ramachandran, V., Robinson, T.G., Davenport, W.G., 2011. Extractive Metallurgy of Nickel, Cobalt and Platinum-Group Metals. Elsevier, Oxford, England, 399.

Heck, R.M., Farrauto, R.J., Gulati, S.T., 2009a. Catalytic Air Pollution Control, third ed. Wiley, Hoboken, NJ.

Johnson, T.V., 2011. Diesel emissions in review. SAE Int. J. Engines. 4 (1), 143–157.

Mul, G., Moulijn, J.A., 2012. Preparation of supported metal catalysts. In: Anderson, J.A., Garcia, M.F. (Eds.), Supported Metals in Catalysis, second ed. Imperial College Press, London, England, Chapter 1.

Rothenberg, G., 2008. Catalysis. Wiley-VCH, Weinheim, Germany.

Trovarelli, A., 2002. Catalysis by Ceria and Related Materials. Imperial College Press, London.

Twigg, M.V., 2011a. Catalytic control of emissions from cars. Catal. Today. 163, 33–41.

APPENDIX 9.1 TAILPIPE GAS COMPOSITION CONTROL

Modern cars automatically and continuously control their fuel/air input quantities so as to minimize CO(g), C_mH_n(g) and NO_x(g) in their tailpipe exit gas. The control is based on an oxygen sensor between the engine and the catalytic converter, Fig. 9.10.

This system:

1. Senses the composition of the engine-out gas by means of the oxygen sensor, Fig. 9.10. This sensor then adjusts electric current to the electronic control unit, which in turn, modifies fuel injection pump speeds to maintain optimum engine-out gas composition.
2. As this control is not instantaneous, there is a risk of the catalytic converter feed gas being slightly rich in oxygen or slightly lean in oxygen.
3. It is this variation that is offset by the ceria and other rare earth oxides in the catalytic converter as described in Section 9.11.2.
4. There is a second oxygen sensor after the catalyst converter. It allows calculation of the amount of oxygen that is available in the catalyst rare earth oxides. This can be restored to a set point by running the engine either oxygen-rich or oxygen-lean for a specified period of time (controlled by the system's electronic control unit).

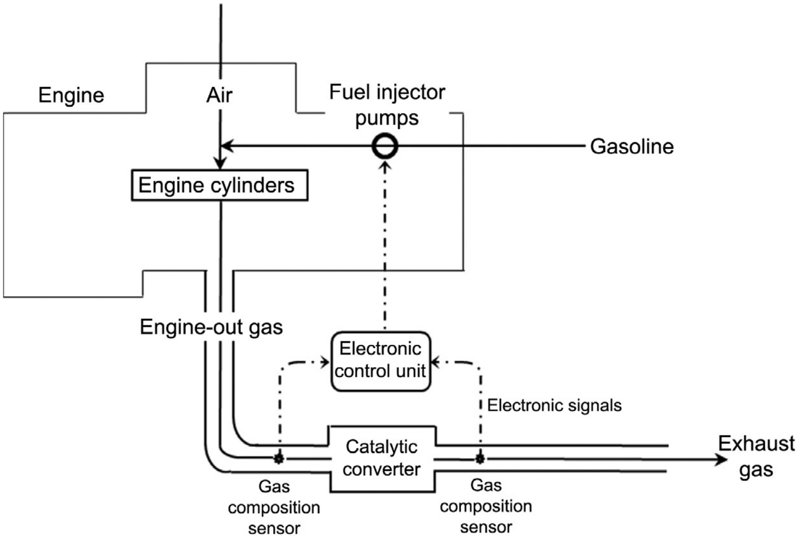

FIG. 9.10

Engine-out gas composition control system. Note the oxygen sensor between the engine and the catalytic converter. Together with the electronic control unit, it adjusts fuel injector pump speed to maintain a constant optimum engine-out gas composition. Minor deviations in engine-out (catalytic converter input) gas oxygen concentration are adjusted by ceria and other rare earth oxides in the catalytic converter, Section 9.11.2. Oxygen sensors and emission control systems are described by Oxygen Sensor (2014) and Bosch (2014).

CHAPTER

10

Rare Earths in Rechargeable Batteries

A rechargeable battery is a battery that:

(a) is used to power an electric motor or other device while the battery is discharging then:
(b) is electrically recharged when a specified amount of its chemical energy has been used by step (a).

In step (a), the battery's chemical energy is converted to electrical energy.

In step (b), electrical energy from an external power source, e.g., an automobile's electrical generator, is converted to chemical energy.

A modern battery of this type is the nickel-metal hydride rechargeable battery, Figs. 10.1a and 10.1b, Table 10.1. After initial electrical charging it contains:

(a) an alloy hydride electrode, containing mostly nickel and rare earth metals plus hydrogen
(b) a nickel oxyhydroxide (NiOOH) electrode
(c) liquid KOH, LiOH, $H_2O(\ell)$ electrolyte.

The battery provides power by oxidizing the alloy hydride electrode's hydrogen. The role of rare earth metals in the alloy hydride electrode is to provide adequate storage, rapid desorption, and rapid re-absorption of this hydrogen.

About 10% of the world's rare earth production is used in this application.

Many Ni-MH batteries are used to power hybrid vehicles. Major virtues of these batteries in this service is that they operate safely and last as long as the vehicle itself, i.e., 10+ years and 150,000+ kilometers (Electric, 2013). They are currently employed by ~10 million motor vehicles of all types and sizes. Major examples are motorcycles, cars, trucks, and buses. One of this writer's colleagues has driven his 2001 Toyota Prius hybrid car 350,000 km with perfect Ni-MH battery operation.

2013 saw about 2 million hybrid vehicles built and sold, including ~1.3 million Toyota hybrids, each with an Ni-MH electric drive motor (traction) battery.

Hybrid vehicles have several fuel efficiency/pollution minimization advantages. Examples are (Hybrid, 2013):

(a) reduction of fuel consumption/air pollution by shutting off the gasoline engine while the vehicle is stopped or traveling slowly

Rare Earths. http://dx.doi.org/10.1016/B978-0-444-62735-3.00010-3

(b) capturing a car's kinetic energy as battery chemical energy during braking
(c) minimizing drive train mass by combining the best attributes of a gasoline engine and an electric motor.

Other Ni-MH batteries

Figure 10.2 shows the extent of Ni-MH battery usage: button, cylindrical, and rectangular batteries. Worldwide sales of AA, AAA, C, D, and 9 volt consumer batteries are of the order of one billion per year.

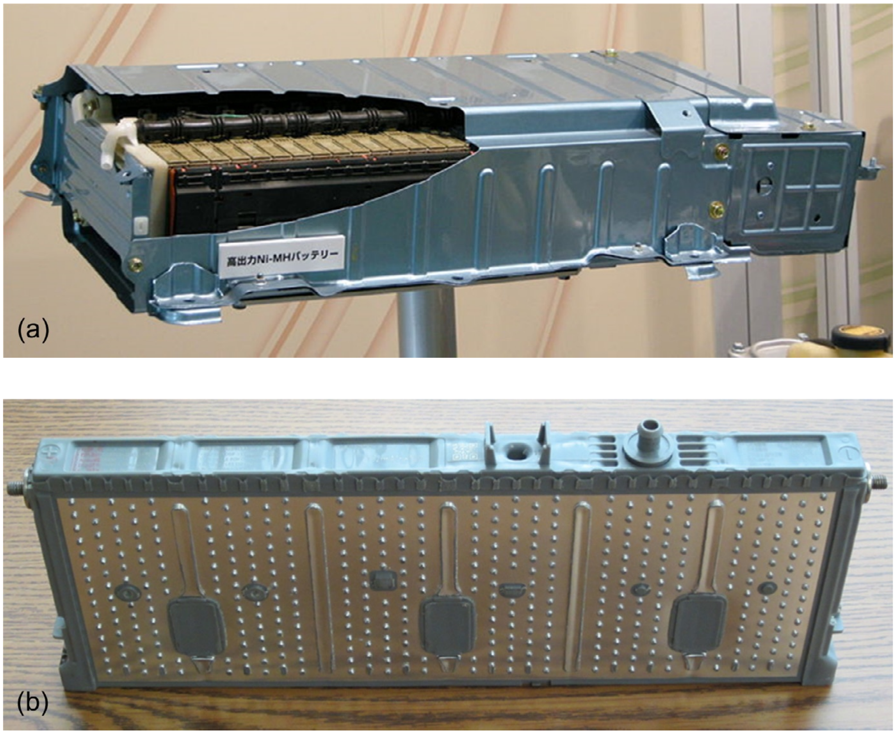

FIG. 10.1

(a) High power nickel-metal hydride (Ni-MH) battery pack for Toyota NHW20 Prius (Nickel, 2013). The cutaway shows many rectangular (prismatic) Ni-MH batteries arranged in series. Data for this type of pack are given in Table 10.1. One model of the Prius uses 168 Ni-MH cells (Fig. 10.2). They provide 20 kW of power @ 200 V. (Wikipedia Commons public domain photo in Nickel (2013). (b) Nickel-metal hydride battery from Fig. 10.1a's battery pack. It is about 0.3 m long. It contains six 1.2 V Ni-MH cells connected in series, left to right, for a total of 7.2 V. Figure 10.1a's battery pack contains 28 of these batteries also connected in series for a total of ~200 V. The interior of an Ni-MH cell is shown in Figs. 10.4 through 10.7.

Photo by William Davenport.

Table 10.1 Details of Toyota Prius Battery Pack

Automobile	Toyota Prius Hybrid
Battery type	Ni-MH
Shape	Rectangular (prismatic)
Battery life	Life-of-car
Cell potential (V)	1.2
Cells per battery	6
Batteries per pack	28
Total cells	168
Nominal pack electrochemical potential (V)	201.6
Charge (Ah)	6.5
Nominal energy storage (kWh)	1.31
Charge-discharge, % (state of charge)	82-38%, average 60%
Available energy storage (kWh)	~0.4
Battery pack location in vehicle	Behind back seat
Battery pack mass (kg)	~50
Battery pack lanthanum content	15-20 kg
Power, kW @ 50% battery discharge	20 kW
Cooling system	Blower motor and air ducting

The Prius has a gasoline engine and an electric motor, Fig. 1.5. It can be powered by its gasoline engine, its electric motor or by both in any proportion. The advantages of this arrangement are described by Hybrid (2013). The charged battery pack powers the electric motor. It is then recharged by a DC generator attached to the gasoline engine, Fig. 1.5. It is also rapidly recharged by the moving car's kinetic energy—during braking (Regenerative, 2013). Diesel engines are also used in hybrid vehicles (mainly buses), but less than gasoline engines.
Wikipedia, Toyota Prius creative commons share alike license

10.1 CHAPTER OBJECTIVES

The objectives of this chapter are to:

(a) describe Ni-MH battery construction and operation
(b) describe the role of rare earths in these batteries
(c) compare these batteries with their competitors (e.g., lithium ion batteries)
(d) discuss their future.

10.2 ADVANTAGES AND DISADVANTAGES OF Ni-MH BATTERIES

The advantages of Ni-metal hydride batteries are (Fetcenko and Koch, 2011):

(a) a long useful life
(b) safe operation

FIG. 10.2

Ni-MH rechargeable battery range.

Photo courtesy Mike Fetcenko, BASF Battery Materials—Ovonic.

FIG. 10.3

Nickel-metal hydride 'D' cell batteries connected in series. This form of battery pack is also used in motor vehicle battery packs.

Photo taken by William Davenport.

(c) rapid conversion of a car's kinetic energy to battery chemical energy during braking
(d) flexible battery capacities from 0.06 to 250 ampere hours of stored chemical energy
(e) large energy and power capacities per unit mass and unit volume
(f) flexible vehicle packaging (Figs. 10.1 and 10.3)
(g) efficient application to series and series-parallel power circuits

(h) availability as cylindrical and rectangular (prismatic) cells (Fig. 10.3)
(i) safe during use (discharging) and re-charging—including some tolerance to abusive over discharging and over recharging
(j) low maintenance
(k) wide operating temperature range (−30 to +70 °C)
(l) inexpensive charging with simple electronic control circuits
(m) environmentally acceptable, recyclable materials.

In 2014, Ni-MH batteries are used in virtually all hybrid vehicles. They are also used in some stationary electric power backup systems.

Their main disadvantage is that they store only about two-thirds as much energy per kilogram of battery as lithium ion batteries. The latter are used in almost all fully electric vehicles and in portable electric and electronic devices. However, at the time of writing, they don't seem to be as safe as Ni-MH batteries.

10.3 NI-MH BATTERY OPERATION

As constructed, an Ni-MH chemical cell consists of:

(a) a nickel-rare earth alloy electrode
and:
(b) a nickel hydroxide $Ni(OH)_2$ electrode
immersed in:
(c) $KOH\text{-}LiOH\text{-}H_2O(\ell)$ electrolyte, Fig. 10.4.

In this form, there is no electrical potential between the electrodes so the cell can't do any useful work, i.e.,:

$$\begin{aligned}\text{work (joules)} &= \text{current (amperes)} \times \text{electrical potential (volts)} \times \text{time (seconds)}\\ &= 0\end{aligned}$$

To do work, the electrochemical cell requires charging (next section).

10.3.1 Initial charging

Figure 10.4's cell is made useful by charging it with energy from an external direct current electricity source (Fig. 10.5). A potential of about 1.4 V is applied. The charging reactions are:
At the Ni hydroxide electrode:

$$\underset{\substack{\text{as-made nickel}\\ \text{hydroxide electrode}}}{Ni(OH)_2(s)} + \underset{\text{in electrolyte}}{OH^-(aq)} \rightarrow \underset{\substack{\text{active Ni oxyhydroxide}\\ \text{electrode}}}{NiOOH(s)} + \underset{\text{to electrolyte}}{H_2O(\ell)} + \underset{\substack{\text{electron to as-made alloy electrode}\\ \text{through external circuit,}\\ \text{powered by 1.4 V DC electricity source}}}{e^-} \tag{10.1}$$

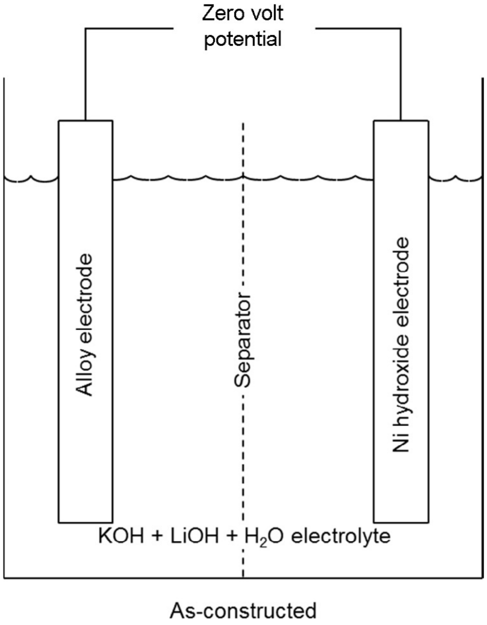

FIG. 10.4

Sketch of as-constructed Ni-MH electrochemical cell (before charging). The alloy electrode contains mainly nickel and rare earth metals. The zero volt cell potential between electrodes is notable. Note that commercial batteries contain many such electrochemical cells (Fig. 10.7).

Drawing by William Davenport.

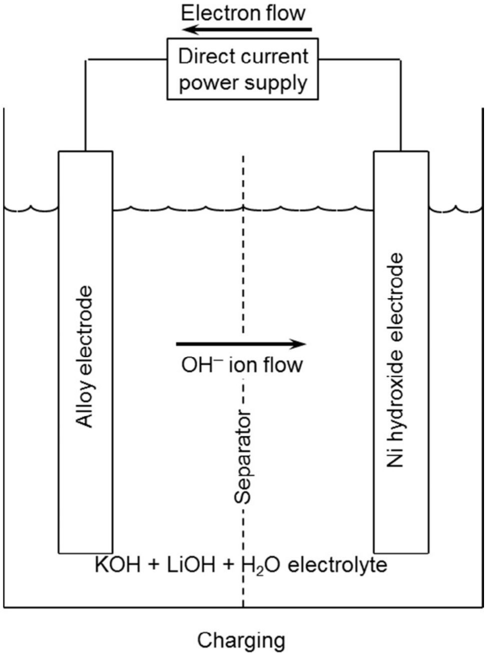

FIG. 10.5

Sketch of Ni-MH cell during its initial charging. Note that: (a) electrons flow externally from the Ni hydroxide electrode to the alloy electrode (b) negative hydroxyl ions convect and diffuse internally from the alloy electrode to the Ni hydroxide electrode.

Drawing by William Davenport.

At the Ni-rare earth metal alloy electrode:

$$\underset{\text{as-made alloy electrode}}{M(s)} + \underset{\text{water in electrolyte}}{H_2O(\ell)} + \underset{\text{electron from external circuit}}{e^-} \rightarrow \underset{\text{active alloy hydride electrode}}{MH(s)} + \underset{\text{into electrolyte}}{OH^-(aq)} \tag{10.2}$$

Commercially, an Ni-MH battery is initially charged with about 0.06 kWh of chemical energy per kg of battery. At this point, the battery's alloy electrode is partially saturated with hydrogen. The electrical potential between the electrodes is 1.2 V. The battery is ready for use. With automobiles, the battery is installed and charged at the automobile manufacturing plant.

10.3.2 Discharging (Use)

The charged battery is used by connecting an electrical load between the charged battery's two electrodes (Fig. 10.6). The reactions are the opposite of the charging reactions and the battery does work.

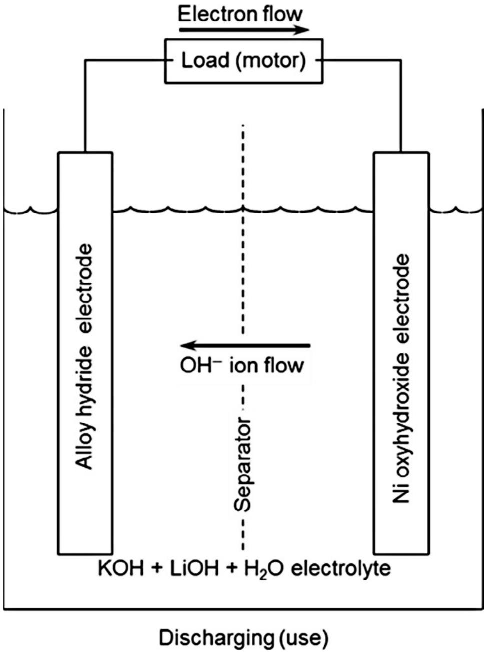

FIG. 10.6

Sketch of charged Ni-metal hydride cell operating in discharge (use) mode. The cell is powering an electric motor. Note the alloy hydride and the nickel oxyhydroxide electrodes. Note also that: (a) electrons flow from the alloy hydride electrode through the motor to the Ni oxyhydroxide electrode; and (b) negative hydroxyl ions convect and diffuse from the Ni oxyhydroxide electrode to the alloy hydride electrode.

Drawing by William Davenport.

The discharge (use) electrochemical reactions are:

(1) at the alloy hydride electrodes:

$$\begin{aligned}&\underset{\text{active alloy hydride electrode}}{MH(s)} + \underset{\text{in electrolyte}}{OH^-(aq)} \rightarrow \underset{\text{partially restored alloy electrode}}{M(s)}\\ &+ \underset{\text{newly-formed water}}{H_2O(\ell)} + \underset{\substack{\text{electron powered through}\\ \text{electrical load by the charged}\\ \text{battery's 1.2 V electrical potential}}}{e^-}\end{aligned} \tag{10.3}$$

i.e., stored interstitial hydrogen (H) reacts exothermically with the electrolyte's hydroxyl ions to form $H_2O(\ell)$.

(2) at the nickel oxyhydroxide electrodes:

$$\begin{aligned}&\underset{\substack{\text{electron from external circuit,}\\ \text{i.e., back from motor}}}{e^-} + \underset{\text{in electrolyte}}{H_2O(\ell)} + \underset{\text{active Ni oxyhydroxide electrode}}{NiOOH(s)}\\ &\rightarrow \underset{\text{partially restored Ni hydroxide electrode}}{Ni(OH)_2(s)} + \underset{\text{hydroxyl ion to electrolyte}}{OH^-(aq)}\end{aligned} \tag{10.4}$$

The overall discharge reaction is given by adding Eqs. (10.4) and (10.5). It is:

$$\begin{aligned}&\underset{\text{active alloy hydride electrode}}{MH(s)} + \underset{\text{active Ni oxyhydroxide electrode}}{NiOOH(s)}\\ &\rightarrow \underset{\text{partially restored alloy electrode}}{M(s)} + \underset{\text{partially restored Ni hydroxide electrode}}{Ni(OH)_2(s)}\end{aligned} \tag{10.5}$$

for which the standard electrode potential is +1.35 V (Fetcenko and Koch, 2011).

Commercially, the actual battery potential is less than calculated, ~1.2 V, due to the battery's internal resistance.

This is the potential that is observed when Fig. 10.6's motor is replaced by a potentiometer.

The total cell potential is positive, which indicates that Reaction (10.5) proceeds spontaneously as written, powering Fig. 10.6's motor.

10.3.3 Recharging

After discharge (use), an Ni-MH battery is recharged—in much the same way as it was initially charged, Section 10.3.1. It is usually charged by a generator attached to a hybrid car's gasoline engine (Fig. 1.5).

10.3.4 Toyota Prius recharging

The Toyota Prius Ni-MH battery normally operates between 40% and 80% of full charge (Toyota, 2013). These conditions maximize battery life and drive-train operating efficiency.

It means that:

(a) the battery is allowed to deplete to 40% of full charge during normal driving whereupon it is:

(b) automatically recharged during gasoline engine driving to about 80% of full charge

and so on.

Another reason that it is not charged to more than 80% full is that it must always be available to accept electrical energy from the Prius' regenerative kinetic energy-to-chemical energy braking system.

10.4 Ni-MH BATTERY COMPONENTS (FETCENKO AND KOCH, 2011; YOUNG AND NEI, 2013)

Figure 10.4 shows the principle components of an as-made (uncharged) Ni-MH battery. They are:

(a) a porous 30 mass% rare earth metal alloy electrode, e.g.,:

$$La_{10.5}Ce_{4.3}Pr_{0.5}Nd_{1.4}Ni_{60.0}Co_{12.7}Mn_{5.9}Al_{4.7}\text{alloy}$$

(where the numbers are atomic% element)

(b) a porous Ni hydroxide electrode, usually also containing Co and Zn, e.g., $Ni_{0.94}Co_{0.03}Zn_{0.03}(OH)_2$

(c) a porous polypropylene-polyethylene composite separator (Figs. 10.4 through 10.7), which prevents electrical contact between adjacent electrodes but allows rapid OH^- ion diffusion

(d) (KOH plus ~1 mass% LiOH) + water electrolyte, mostly contained in the porous electrodes and porous separator (it is highly conductive and not too corrosive)

(e) an external container, usually plastic.

Figure 10.7 shows a model Ni-MH battery. It consists of:

(a) metal hydride electrodes wrapped in polypropylene-polyethylene separator bags

(b) nickel oxyhydroxide electrodes wrapped in polypropylene-polyethylene separator bags

(c) KOH plus ~1 mass% LiOH + water electrolyte.

It shows how much electrode area is packed into a small space, maximizing the amounts of electrical current flow (amperes) and power (watts [joules per second]) that are obtained from a small battery volume.

The following two sections describe how the electrodes are made.

10.5 NICKEL HYDROXIDE ELECTRODE

Nickel hydroxide electrodes are made by:

(a) making $Ni_{0.94}Co_{0.03}Zn_{0.03}(OH)_2$ spheres (~10 μm diameter) by precipitating them from Ni, Co, Zn sulfate aqueous solution with caustic (i.e., NaOH) in the presence of ammonia

FIG. 10.7

Model Ni-MH battery containing many nickel oxyhydroxide and alloy hydride electrodes, all surrounded by polymer separator bags. The electrodes are connected as shown in Fig. 10.6. The inside dimensions of the battery are ∼3 cm across, electrode height ∼5 cm and electrode length (into page) ∼8 cm. All the oxyhydroxide electrodes are connected to one terminal. All the metal hydride electrodes are connected to another terminal.

Photo by William Davenport.

(b) making these spheres into a paste by mixing them with conductive cobalt oxide particles and water
(c) squeezing the paste into a conductive nickel metal foam (electron collector) skeleton.

The nickel hydroxide electrodes are first made in the form of an electrode "belt," then sheared into electrode coupons—ready for battery assembly, initial charging, and use.

10.6 ALLOY (HYDROGEN STORAGE) ELECTRODE

The alloy electrodes are made in much the same way, i.e., by:

(a) preparing the prescribed alloy by melting the specified metal components
(b) casting the alloy and grinding the cast metal into ultra-fine particles ~10 μm diameter
(c) making these particles into a paste by mixing them with graphite particles, Teflon® particles, and water
(d) squeezing the paste into an electron collecting nickel skeleton.

Industrially, they are also made in the form of a continuous electrode "belt," which is subsequently sheared into individual electrode coupons.

The results are porous alloy particle electrodes ready for battery assembly, initial charging, and use.

10.6.1 Charging side effects at the alloy electrode

A side effect of charging the battery is formation of a corrosion-resistant but porous oxide layer around the alloy particles. Additionally, the product oxide contains a great many nickel metal nanoparticles, which greatly increase the current and power capabilities of the battery.

10.6.2 Alloy choice

Alloy electrode composition is chosen to optimize:

(a) hydrogen (hence chemical energy) storage capacity
(b) metal-hydrogen bond strength
(c) discharge-recharge rates
(d) corrosion resistance.
(e) electrode life.

Young and Nei (2013) discuss these in detail.

Most commercial alloys contain rare earth metals but rare earth-free alloys such as:

$$V_{18}Ti_{15}Zr_{18}Ni_{29}Cr_5Co_7Mn_8$$

have been studied extensively and pilot tested (Fetcenko and Koch, 2011). They perform less well than rare earth alloys, but they are ready to go if rare earth prices should once again irrationally increase.

10.7 RECYCLING

Ni-MH batteries typically contain:

25-35 mass% Ni
2-4 mass% Co
6-8 mass% rare earth elements
2-5 mass% Fe
10-30 mass% plastics
balance = O, H, NaOH, and LiOH electrolyte.

They are recycled by:

(a) smelting them unopened in a vertical furnace at 1500 °C under slightly reducing conditions
(b) separating (by gravity) the product molten Ni-Co alloy (specific gravity ~7) from the product molten slag (specific gravity ~3)
(c) hydrometallurgical production of high purity nickel and cobalt chemicals.

Details are given in Chapter 18.

The batteries' rare earth elements end up in the smelting furnace slag. Processes for recovering rare earth elements are now being tested on a pilot plant scale.

10.8 APPRAISAL

Rechargeable rare earth-bearing Ni-MH batteries have the following advantages:

(a) safe operation
(b) long life
(c) Ni and Co recyclability.

An important use is in hybrid motor vehicles. Expectations are that hybrid vehicle use will continue to grow—and along with it, Ni-MH battery and rare earth element use.

It is only fair to say, however, that there is a non-rare earth variation of the Ni-MH battery, one which uses vanadium, titanium, and zirconium in place of rare earth metals in the alloy electrode (Fetcenko and Koch, 2011). It is less efficient than the rare earth alloy version—but is ready to go if rare earth prices skyrocket once again.

10.9 SUMMARY

Nickel-metal hydride batteries contain considerable rare earth metals, particularly La, Ce, Pr, and Nd. About 10% of rare earth production is used in this application.

Charged Ni-MH batteries provide power by oxidizing the hydrogen that is in a charged battery's alloy electrode. The roles of the rare earths in this alloy are to store its hydrogen and rapidly desorb and re-absorb it as needed for high power and quick recharge.

Much of today's Ni-MH battery use is for powering hybrid car electric motors. This market is still growing so the use of Ni-MH batteries (and their contained rare earths) is also growing. Ni-MH batteries also have many consumer uses (Fig. 10.2).

The main competitors for Ni-MH batteries are lithium based batteries. They are lighter and store more chemical energy (per kg) than Ni-MH batteries. They are suitable for fully electric vehicles.

For hybrid vehicles, however, the Ni-MH rare earth battery is king—because of its safe operation and long life.

References

Electric, 2013. Electric Vehicle Battery. Retrieved on August 11, 2013, from http://en.wikipedia.org/wiki/Electric_vehicle_battery.

Fetcenko, M., Koch, J., 2011. Nickel-metal hydride batteries. In: Linden's Handbook of Batteries. McGraw Hill, New York, pp. 22.1–22.51.

Hybrid, 2013. Hybrid Electric Vehicle. Retrieved on August 31, 2013, from http://en.wikipedia.org/wiki/Hybrid_electric_vehicle.

Nickel, 2013. Nickel-Metal Hydride Battery. Retrieved on August 6, 2013, from http://en.wikipedia.org/wiki/Nickel%E2%80%93metal_hydride_battery.

Regenerative, 2013. Regenerative Brake. Retrieved on April 2, 2013, from http://en.wikipedia.org/wiki/Regenerative_brake.

Toyota, 2013. Toyota Prius. Retrieved on September 9, 2013, from http://en.wikipedia.org/wiki/Toyota_Prius.

Young, K., Nei, J., 2013. The current status of hydrogen storage alloy development for electrochemical applications. Materials. 6, 1–44.

Suggested Reading

Wikipedia is an excellent source of battery information. Just Google your desired topic, e.g., Ni-MH battery

Battery, 2013. Battery Statistics. Retrieved on April 2, 2013 from http://batteryuniversity.com/learn/article/battery_statistics.

Kopera, J.J., 2004. Inside the Nickel Metal Hydride Battery, Cobasys. Retrieved on April 2, 2013 from http://www.cobasys.com/pdf/tutorial/inside_nimh_battery_technology.pdf.

Rechargeable, 2013. Rechargeable Battery. Retrieved on April 2, 2013 from http://en.wikipedia.org/wiki/Rechargeable_battery.

Reddy, T.B., Linden, D., 2011. Linden's Handbook of Batteries, fourth ed. McGraw Hill, New York.

Sakai, T., Hazama, T., Miyamura, H., Kuriyama, N., Kato, A., Ishikawa, H., 1991. Rare-earth based alloy electrodes for a nickel-metal hydride battery. J. Less Common Met. 172, 1175–1184.

Standard, 2012. Standard Electrochemical Potential. Retrieved on August 11, 2013 from http://en.wikipedia.org/wiki/Standard_electrode_potential.

CHAPTER

Rare Earths in Alloys and Metals

11

Rare earth metals are used in (i) permanent magnet alloys; (ii) rechargeable battery electrodes; and (iii) mechanical/structural alloys. This chapter is devoted to (iii), mechanical/structural alloys.

About 10% of rare earth production is used in these alloys. In 2014, major applications in this category are in:

(a) cast irons, principally ductile cast irons
(b) magnesium alloys.

11.1 CHAPTER OBJECTIVES

The objectives of this chapter are to describe:

(a) the purpose of rare earths in the above applications
(b) the enhanced properties that they produce (Fig. 11.1).

The biggest use for rare earths in metallurgy is for making ductile cast iron, Sections 11.2–11.6. Cerium and lanthanum are the most used.

11.2 CAST IRON

Cast iron is basically an alloy of iron plus ~3 mass% carbon and ~2 mass% silicon. As the name implies, it is mainly used in the form of castings, for example, pipe and heavy machinery parts. It has a relatively low melting point, ~1200 °C and good fluidity. It is easily cast. It also machines easily and has excellent deformation and wear resistance. It dampens unwanted vibrations in heavy machinery.

However, the iron's carbon tends to precipitate as graphite flakes during casting and solidification—so that the cast iron tends to be brittle. Fortunately, these flakes may be avoided by adding magnesium plus rare earth metals to the molten iron before casting.

These metals cause the graphite to precipitate as small spheroidal nodules, rather than flakes. This, in turn, reduces the brittleness (i.e., increases the ductility) of the product castings (Fig. 11.2).

Rare Earths. http://dx.doi.org/10.1016/B978-0-444-62735-3.00011-5

FIG. 11.1

Sikorsky CHC S-92 helicopter near Christiansund, Norway (Wikipedia creative commons photo). Many of its critical components are made from magnesium-rare earth metal alloys.

FIG. 11.2

Cast iron string support frame in grand piano (underneath the strings) (Wikipedia creative commons deed photo). The iron casting is strong and beautiful. It supports about 230 steel strings (in tension) and a total force of ~3 million newtons.

11.3 DUCTILE CAST IRON

Spheroidal carbon precipitates are encouraged by magnesium, mainly added to molten iron in the form of MgFeSi alloys. The addition alloys also contain small amounts of calcium, aluminum and several percent rare earth metals, principally cerium and lanthanum.

Magnesium is a very strong de-oxidizer. It reacts strongly with oxides and dissolved oxygen in molten iron—to form solid MgO particles (melting point ~2850 °C). These particles then serve as growth sites for exsolving spheroidal (rather than flakey) graphite precipitates (melting point >3000 °C).

However, these MgO particles are considerably less dense (specific gravity ~3.6) than molten iron (specific gravity ~7). This causes them to lose their efficacy by floating out of the molten iron.

This is remedied by including rare earths in the MgFeSi addition agent (Table 11.1).

Rare earth metals are also strong de-oxidizers. Fortunately, their oxides (melting points >2300 °C) are much denser (specific gravity ~7) than MgO. So MgO-rare earth-oxide precipitates remain longer in the molten iron—extending their service as spheroidal graphite growth sites.

11.4 INDUSTRIAL PROCEDURES

Cast iron is mostly made from steel scrap. It is made into ductile cast iron by melting, refining, magnesium + rare earth injection and casting. Molten metal samples are taken and analyzed at all stages to ensure that the iron composition is exactly that prescribed for the designated cast ductile iron product.

Samples of the solid ductile iron product are also taken and examined microscopically for nodularity (Olympus, 2013). Figure 11.3 shows micrographs from ductile cast iron samples with and without rare earth addition.

As expected, the rare earth-inoculated iron has more, smaller graphite nodules—giving minimum flake formation and maximum product ductility.

The product castings are also given tensile and ductility tests and, in the case of ductile iron pipe, leak tests.

Table 11.1 Example Ductile Iron Addition Alloys

Element	Mass% in Addition Alloy
Mg	3.5–25 (usually 3.5–10)
Total rare earths[a]	0–5
Si	42–48
Ca	0–3
Al	0–2
Fe	Balance

[a] *Mainly cerium, but others are present. They are mostly delivered as 0.2 × 1 mm, 2 × 12 mm, and 5 × 20 mm flat pieces. An important advantage of MgFeSi alloys is that they are less explosive than Mg alone when added to molten iron.*

Source: *Data courtesy of Andrew Parker and Don Tittensor, Asmet (www.asmet.com).*

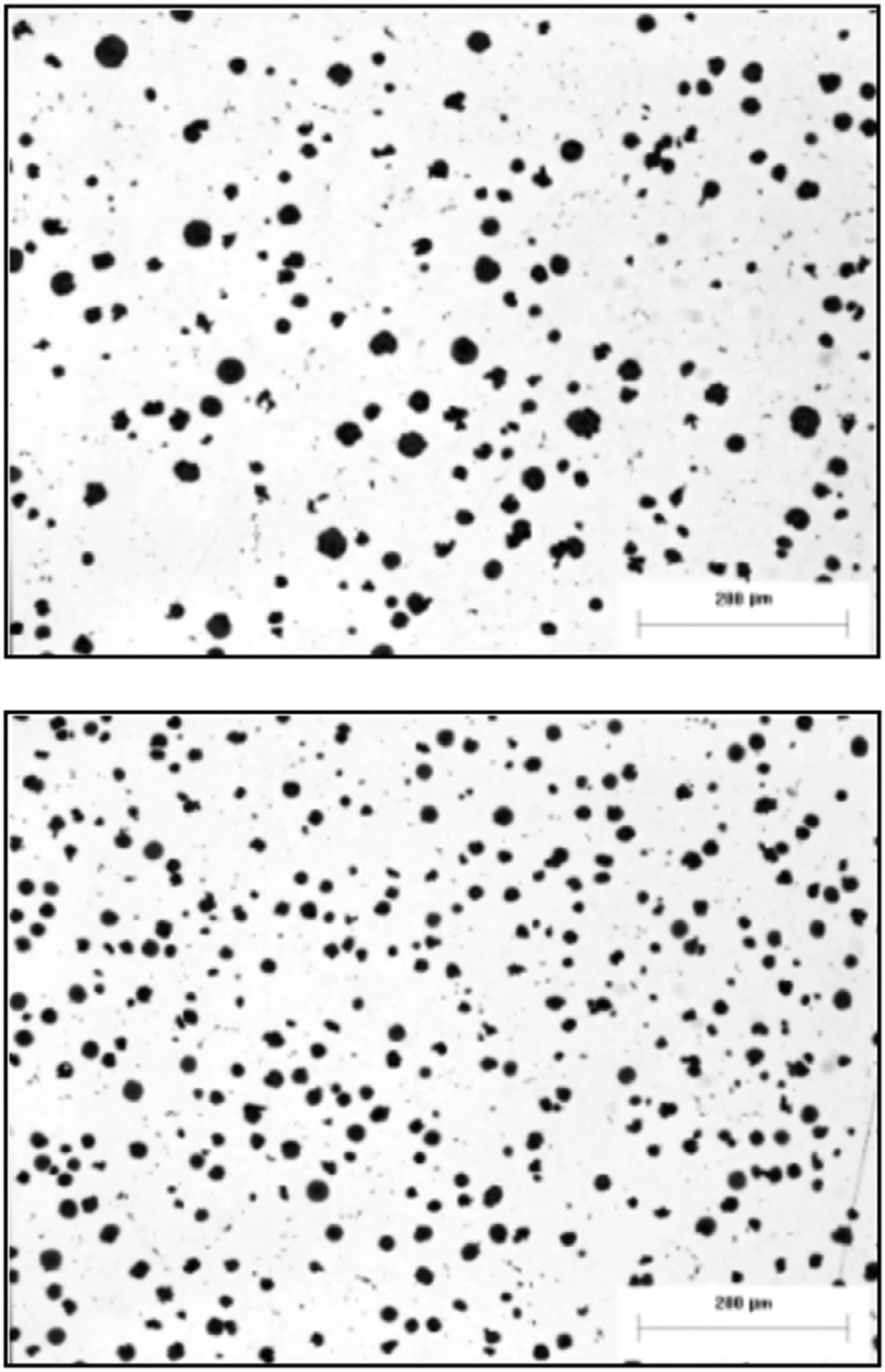

FIG. 11.3

Photomicrographs of ductile cast iron without (top) and with (bottom) rare earth addition (micrographs courtesy of Cathrine Hartung, Elkem ASA). The rare earth cast iron (bottom) has many more graphite nodules and is more ductile. It was inoculated with 1 mass% lanthanum magnesium ferrosilcon alloy. The size indicator represents 200 μm.

11.5 RARE EARTH BENEFITS

The main benefit of rare earths in ductile cast iron is its production of many small, spheroidal nodules—which give good ductility to cast iron products, for example, water and sewage pipes. The rare earths also neutralize the effect of tramp elements that accidentally enter the cast iron from contaminated scrap (Bigge, 2009; White, 2012). This is a second critical rare earth advantage.

The elements most neutralized are Pb, Sb, Bi and As. Untreated, these elements produce vapor voids in the cast ion product. Fortunately, rare earth metals form innocuous compounds with these high vapor pressure elements, eliminating this harmful behavior.

11.6 DUCTILE IRON SUMMARY

Ductile iron is cast iron (∼3 mass% C, ∼2 mass% Si, remainder Fe) in which graphite has precipitated as spheroidal graphite nodules rather than flakes (during cooling and solidification).

Nodular (rather than flakey) graphite particles greatly enhance the ductility of the product cast iron.

Rare earth additions promote nodular graphite formation by providing dense MgO-rare earth oxide graphite growth sites in the molten iron. This is an improvement on MgO, which has a low density hence tends to float out of the molten iron.

11.6.1 Rare earth metal additions to molten steel

Rare earth metals were once added to molten steel to control the number and shape of sulfur inclusions (thereby increasing strength). However, this use has been superseded by the use of calcium and magnesium.

11.7 RARE EARTH-MAGNESIUM ALLOYS

Magnesium is the world's lightest structural metal, specific gravity ∼1.7. For this reason it is used extensively in applications where movement is involved— for example, motor vehicles, aircraft (Fig. 11.4) and personal computers. It is the third most common structural material after Fe and Al.

Rare earths are alloyed with magnesium for many reasons, mainly to improve:

(a) castability
(b) mechanical properties, especially high temperature mechanical strength
(c) resistance to combustion (i.e. flammability resistance)
(d) corrosion resistance
(e) resistance to creep (slow deformation over time, below the yield strength of the material).

FIG. 11.4

Sikorsky S 92 helicopter rotor gear box (Wikipedia creative commons photo). Many helicopter components, for example, gear boxes, tail rotor housings and transmission casings are made from magnesium-rare earth alloys. Their advantages are lightness, high temperature strength and resistance to combustion, corrosion and creep.

These characteristics have caused rare earth-magnesium alloys to be used for such items as:

helicopter gear boxes, tail rotor housings, transmission casings
aircraft engines and other components
high performance automobiles (e.g. engine cradles, gearboxes).

The above improvements are mostly due to solid solution strengthening, precipitation hardening and grain refining (Hort, 2011). Table 11.2 lists some typical rare earth-magnesium alloys. Their enhanced properties and uses are also shown. They provide lightweight parts for many helicopters, airplanes and high performance automobiles.

11.7.1 Rare earth-magnesium microalloying

Considerable research is been done on 0.2-0.4 mass% rare earths in magnesium alloys. The objective is to improve formability and ambient temperature ductility (Hirsch and Al-Samman, 2013). Considerable success has been attained. Research is continuing.

Table 11.2 Magnesium-Rare Earth Metal Alloys, with the kind permission of David Tawil, Elektron Alloys NA

Alloy Designation	Rare Earth Content (Mass%)	Enhanced Properties	Applications
Elektron RZ5	0.8-1.7	High strength	Helicopter gearboxes, aircraft engines
Elektron ZRE1	2.5-4.0	Creep resistant to 250 °C	Applications where tensile strength and creep resistance are important, e.g. high performance automobiles
Elektron 21	Nd, 2.6-3.1; Gd, 1.0-1.7	Excellent mechanical properties up to 200 °C, flammability resistance, ease of casting and corrosion resistance	Helicopter, aircraft and motorsport applications up to 200 °C
Elektron WE43	2.4-4.4	High temperature strength and corrosion resistance	Aeroengines, helicopter transmissions, missiles, racing cars
Elektron WE54	(Yb, Er, Dy & Gd), 1.0-2.0; Nd, 1.5-2.0	High temperature strength Improved corrosion resistance	Transmissions, missiles, high performance cars

The data are mainly from the Magnesium Elektron website (http://www.magnesium-elektron.com/).
Other companies make similar alloys.
Other ingredients, mass% (remainder, Mg)
RZ5: Zn, 3.5-5.0; Zr, 0.4-1.0
ZRE1: Zn, 2.0-3.0; Zr, 0.4-1.0
21: Zn, 0.2 to 0.5%; Zr, saturated
WE43: Y, 3.7-4.3; Zr, 0.4 minimum
WE54: Y, 4.75-5.5; Zr, 0.4 minimum
Table prepared by William Davenport.

11.8 RARE EARTH ALLOYS WITH OTHER METALS

The above sections describe the most common uses of rare earths in structural alloys. Very little is alloyed with aluminum, copper. or lead. Some research has been done on aluminum (Nie et al. 2002) and titanium (Khorev, 2011) but not implemented. Interestingly, cerium and lanthanum oxides have proven to be effective corrosion inhibitors for aerospace aluminum alloys (Fahrenholtz and O'Keefe, 2013).

Also, some magnesium-rare earth alloys (e.g., Elektron WE43, Table 11.2) are being considered for degradable medical implants (Reifenrath et al., 2011). None is yet in service.

11.9 SUMMARY

Rare earth metals are used in:

(a) magnet alloys
(b) nickel-metalhydride rechargeable battery electrode alloys.They are also used in:
(c) ductile cast iron alloys, to precipitate carbon nodules, thereby improving product ductility
(d) magnesium alloys to improve:
  castability
  mechanical properties, especially high temperature strength
  flammability resistance
  corrosion resistance
  creep resistance.

References

Bigge, R., 2009. Tramp elements in grey and ductile iron. In: Ductile Iron MagazineStrongsville, Ohio. Retrieved on August 18, 2013 from, http://www.ductile.org/magazine/2009_2/Tramp%20Elements%20in%20Gray%20and%20Ductile%20Iron.pdf.

Fahrenholtz, W.G., O'Keefe, M.J., 2013. Corrosion Protection Mechanisms of Rare-Earth Based Inhibitors in Aerospace Coatongs. In: Rare Earth Elements 2013. Met Soc of CIM, Montreal, QC, pp. 455–458.

Hirsch, J., Al-Samman, T., 2013. Superior light metals by texture engineering: optimized aluminum and magnesium alloys for automotive applications. Acta Materialia 61, 818–843.

Hort, N., 2011. Applications of rare earth containing magnesium alloys. Paper presented at MagNET research network workshop, Hamilton, Canada, November 7-8, 2011. Retrieved on August 18, 2013 from: http://www.magnet.ubc.ca/wiki/images/3/33/Workshop-8_Hort.pdf.

Khorev, A.I., 2011. Alloying titanium alloys with rare earth metals. Russian Engineering Research 31, 1087–1094.

Nie, Z., Jin, T., Fu, J., Xu, G., Yang, J., Zhou, J., Zuo, T., 2002. Research on rare earth in aluminum. Minerals Science Forum 396–402, 1731–1736.

Olympus, 2013. Cast iron analysis. Olympus Corporation, Tokyo, Retrieved on August 18, 2013 from: http://www.olympus-ims.com/en/applications/cast-iron-analysis/.

Reifenrath, J., Bormann, D., Meyer-Lindenberg, A., 2011. Magnesium alloys as promising degradable implant materials in orthopaedic research. In: Czerwinski, F. (Ed.), Magnesium Alloys – Corrosion and Surface Treatments. 51000 Rijeka, Croatia, pp. 93–108. Retrieved on August 18, 2013 from: http://www.intechopen.com/books/magnesium-alloys-corrosion-and-surface-treatments/magnesium-alloys-as-promising-degradable-implant-materials-in-orthopaedic-research.

White, D.S., 2012. Rare Earths in Ductile Cast Iron. Ashtabula, Ohio. Retrieved on August 18, 2013 from, http://www.ductile.org/magazine/2012_2/Doug%20White.pdf.

Suggested Reading

Apps, P.J., Karimzadeh, H., King, J.F., Lorimer, G.W., 2003. Precipitation reactions in Magnesium-rare earth alloys containing yttrium, gadolinium or dysprosium. Scripta Materialia 48, 1023–1028.

Pekguleryuz, M.O., 2007. Magnesium Materials Development, A Global Overview. McGill University, Montreal. Retrieved on August 18, 2013 from: http://people.mcgill.ca/files/mihriban.pekguleryuz/M_Broad_Horizons.pdf.

Rokhlin, L.L., 2003. Magnesium alloys containing rare earth metals: structure and properties. In: Fridlyander, J.N., Eskin, D.G. editors. Advances in Metallic Alloys. Taylor & Francis, New York.

CHAPTER

12

Polishing with Rare Earth Oxides Mainly Cerium Oxide CeO_2

12.1 INTRODUCTION, CONTENTS OF THE CHAPTER

The demand for polishing powders based on cerium oxide is estimated to be around 16 kilotonnes per year. It represents about 13% of rare earth oxide production. Fluctuation is expected due to variations in the price of cerium oxide.

Ceria is one of the main abrasive materials for glass (or pure silica) fine polishing in the family of classical abrasives (silica SiO_2, alumina Al_2O_3, and zirconia ZrO_2).

Cerium oxide has been used to planarize glass (or pure silica) surfaces as a polishing compound since the 1950s for the polishing of cathode ray tube displays. Nowadays, cerium oxide based powders are used to prepare finished surfaces for (Fig. 12.1):

- Flat glass: beveling and edging for decorative purposes
- Optical glass: ophthalmology, precision lenses for photography, telescopes, and microscopes etc.
- Liquid crystal displays: internal glass layers
- Crystals: decorative and jewels
- Electronic devices: bare silicon wafers, shallow trench isolation (STI) structures, polysilicon capacitor structures, metal plugs and lines, interlayer dielectric layers (ILD), lithographic photomasks, and glass hard disks

The main function of polishing powders is surface material removal in order to obtain planarization and fewer defects to get a finished surface on glass products.

Depending on the application, various grades of powder are used, from micronic to nanometric scale. For advanced optical glasses, micronic to submicronic grades are used. Nanometric particle are mainly used for “electronics” manufacturing processes.

Glass (SiO_2 based) polishing involving ceria as abrasive combines two mechanisms: chemical and mechanical. The process is called chemical mechanical polishing or chemical mechanical planarization (CMP).

This chapter firstly describes the polishing process, the type of applications where polishing is crucial, and some generalities of the manufacturing processes of CeO_2 abrasive. Secondly, some general information is given about cerium chemistry in solution and in the solid state as CeO_2 and Ce_2O_3. Finally, some discussion of CMP of glasses (or SiO_2) by ceria is presented.

Rare Earths. http://dx.doi.org/10.1016/B978-0-444-62735-3.00012-7

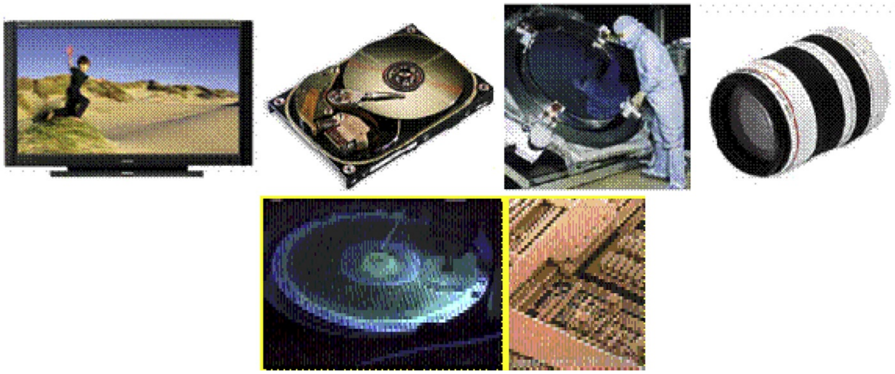

FIG. 12.1

Main applications for CeO_2 polishing powder: flat displays, glass hard disk, precision optics, camera lenses, and silicon wafers.

Photos provided by Thierry Le Mercier, Solvay Rare Earth Systems.

12.2 PRODUCTION OF POLISHING COMPOUNDS

Basic polishing powders are produced from a rare earth mineral concentrates typically derived from bastnasite a rare earth fluorocarbonate $LaFCO_3$ (Chapter 4).

12.2.1 Classical polishing powder (glass applications)

The bastnasite concentrate contains a mix of rare earths: mainly cerium, lanthanum, praseodymium, and neodymium. After precipitation of the insoluble hydroxides, the mixture is treated to produce a powder with particles size varying from 1 to 20 μm, depending on the application requirement. In most of the cases, a fluorination step is also added. Baking temperature and milling are critical operations to ensure good particles size distribution. In the final powder, the total RE oxides ratio is 40-70% (mass). Cerium oxide is dominant: 30-65%. These powders are popular because they are relatively inexpensive compared to pure ceria powder. They are efficient enough to polish a large number of glass pieces in a given time. Indeed they have high stock removal rates (the amount of glass that can be removed through polishing in a given time).

Depending on the required final quality of the finished glass surface, several powder grades are available. As an indication, powders containing 88% total rare earth oxides are used for flat glass TV screens, 90% for optical lenses, and 93% or more for precision lenses and optics.

High grade 99.9% CeO_2 powders with submicronic grain size (0.5-1 μm) are also available for precise glass surface planarization. With these, the risk of contaminating

FIG. 12.2

CeO_2 polishing powders.

Photos provided by Alain Rollat, Solvay Rare Earth Systems.

the product surface with undesirable elements is minimized. These advanced products are represented on Fig. 12.2. They have uniform particle size and shape. However, they are more expensive. Applications include polishing of liquid crystal displays, integrated circuits (ICs), glass memory disks and optical and ophthalmic glasses.

12.2.2 Semiconductor polishing slurries

The colloidal ceria used in IC planarization is generally manufactured from cerium carbonate, with especially high purity. This product is further calcined in air to promote CeO_2 crystallization and then wet milled in order to obtain a final aqueous colloidal suspension, with sizes <200 nm.

A new generation of colloidal ceria has been developed recently, based on fully wet processes. This greatly improves particle size uniformity.

12.3 THE POLISHING PROCESS

When choosing a glass polishing compound the following factors need to be considered.

12.3.1 The type of glass to be polished

The polishing agent should have a hardness similar to the glass surface in order to avoid deep penetration of the grains and formation of large grooves. Table 12.1 gives average hardness values for some glasses and polishing powders. Notice, however, that hardness values are difficult to estimate for nanometer-size abrasive particles.

Table 12.1 Hardness Values in the Mohs Scale for Several Polishing Powders and Target Glasses

Polishing Powder	Hardness (Mohs Scale)	Type of Glass	Hardness (Mohs Scale)
Diamond C	10	Silica SiO_2	7
Alumina Al_2O_3	9	Soda lime: SiO_2, Na_2O, CaO	5.3
Zirconia ZrO_2	8	Borosilicate: SiO_2, B_2O_3 + others oxides	5.8
Ceria CeO_2	6-7	Lead: SiO_2, PbO + other oxides	4.8

Table prepared by Jacques Lucas.

12.3.2 The type of slurry system

Slurry consists of a blend of polishing powder in suspension in a liquid, usually water. A large number of additives are used: to stabilize the suspension, to avoid foaming, to enhance glass removal rate. Slurry compositions are considered proprietary by manufacturers. But they are very important for high polishing quality and efficiency.

Cerium oxide is a very efficient polishing powder because it removes glass both by chemical bonding mechanisms and by soft mechanical abrasion.

Since polishing is sometimes considered to be at the interface of technology and art, considerable knowhow is required. Some additives such as clays, fluorides and other abrasives are used to give to the slurry its appropriate consistency and viscosity.

12.3.3 Type of polishing machine/pad being used and glass surface quality

Many types of polishing machine are used, depending on the shape and the number of pieces to be polished. A polishing pad is attached to the platen of the polishing machine and is used to apply force to the substrate to be polished (Fig 12.3). It is usually a flexible porous disk made of polyurethane and impregnated with slurry. An optimized polishing pad helps to satisfy several conditions such as polishing speed, glass smoothness, flatness, consistency, and defect number. Accordingly, there are several types of pad with different moduli of elasticity and surface textures. Pad choice is made in relationship to the polishing slurry.

In the conventional polishing process, the slurry is continuously supplied to the polishing surface. Pressure (P) is applied to the rotating pad for maintaining good contact with the glass pieces as shown on Fig. 12.3.

The total stress applied to the glass surface is complex. In each case it consists of a vertical force combined with lateral forces due to rotation of the pad.

Optical glass polishing rate R (removal rate) is defined as the thickness of the glass removed per unit time.

R is proportional to the applied pressure P and the linear velocity V at which the pad moves relative to the glass piece.

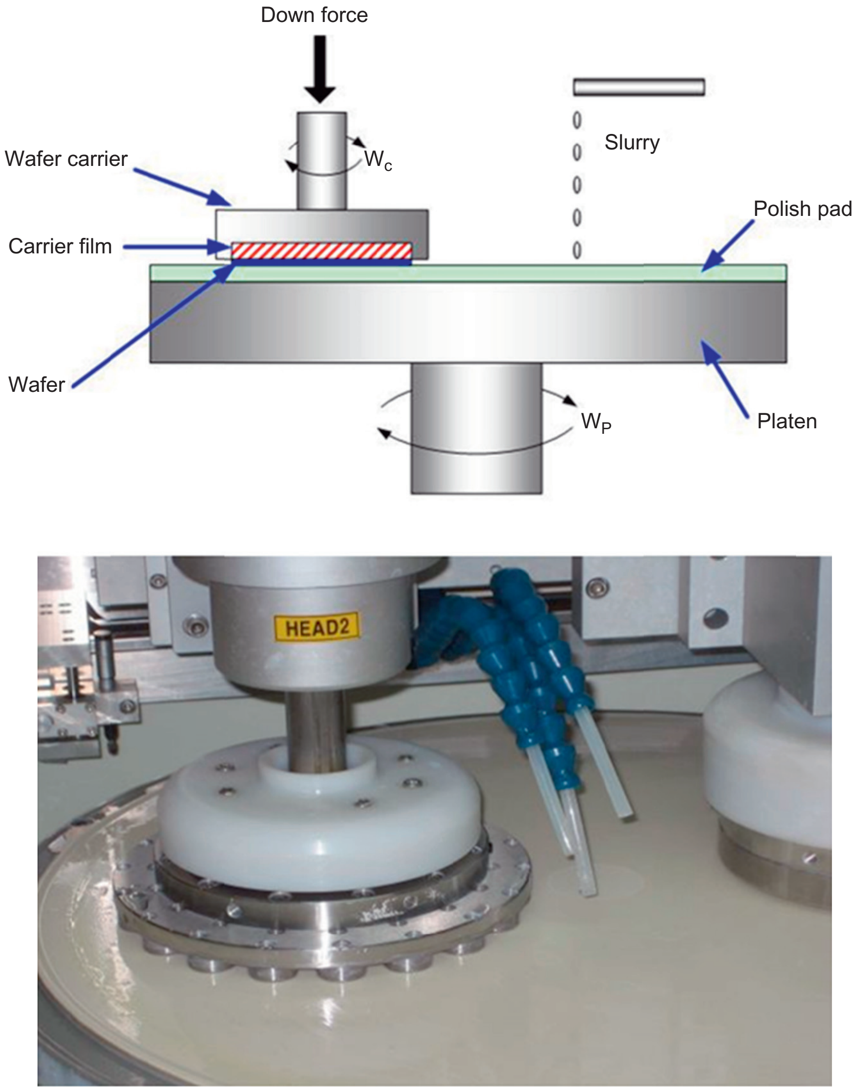

FIG. 12.3

Drawing and photograph of chemical mechanical planarization equipment. The polishing pad is fixed to a metal platen. The polishing target is fixed to a carrier head. Both rotate in the same direction. Fresh polishing slurry is continuously supplied.

Courtesy of David Butler, Nanyang Technological University, Singapore

The relation $R = kPV$ is known as Preston's law where k is an empirical constant for specific experimental conditions.

Specified glass surface quality is the key factor in defining the polishing parameters.

Flat shiny surfaces are the goal. They can be estimated by measuring the planarization of the polished surface as well as surface roughness.

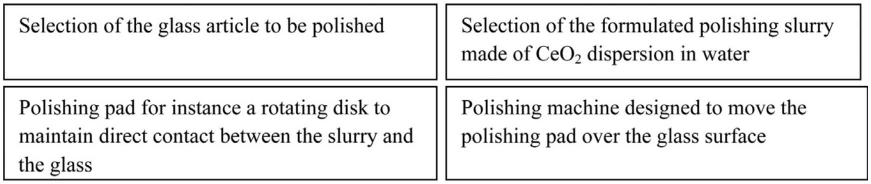

Selection of the glass article to be polished	Selection of the formulated polishing slurry made of CeO_2 dispersion in water
Polishing pad for instance a rotating disk to maintain direct contact between the slurry and the glass	Polishing machine designed to move the polishing pad over the glass surface

FIG. 12.4

Elements involved in glass polishing.

Figure prepared by Jacques Lucas.

During the polishing process, scratches are inadvertently made on the glass surface. Roughness is a measure of height difference between the peaks (asperities) to valleys (grooves) of the glass.

A shiny glass surface is a surface which reflects or transmits visible light without parasitic effects such as scattering or interference. The spectrum of visible light extends from 0.4 μm (blue light) to 0.75 μm (red light). The polishing defects at the surface of a polished glass need to be much smaller than the shortest visible wavelengths namely 0.4 μm. Manufacturers characterize defects according to their size. Depending on the application of the glass, macro-scratches, micro-scratches, or nano-scratches are studied.

The elements of the glass slurry polishing process are summarized on Fig.12.4.

12.4 INDUSTRIAL CERIUM OXIDE POLISHING

12.4.1 Polishing efficiency

CeO_2, because of its medium hardness is known to produce scratches which are less severe than Al_2O_3 and of course diamond—but to the detriment of glass removal rate. Alternatively, silica is often used when low defect rates are targeted, with the drawback of limited removal rates. Overall, ceria is generally a good compromise between removal rate and defect production.

For high quality surfaces, CeO_2 is the best polishing agent but, as discussed later, a chemical mechanism involving hydrated surfaces is the key factor.

High quality cerium oxide powder offers submicronic size grains and chemical polishing that ensures excellent optical quality.

Particle sizes and size distribution of any powder play an important role in polishing performance. Final surface roughness, number of defects left on the surface and polishing rate are the critical factors. Slurry composition needs to exactly fit the type of glass.

Polishing efficiency is related to glass surface hardness. It changes with the type of glass as shown on Fig. 12.5. The expected correlation between efficiency and glass surface hardness (between brackets) is confirmed (soda lime glass (5.5), borosilicate glass (5.8), and silica glass (7)).

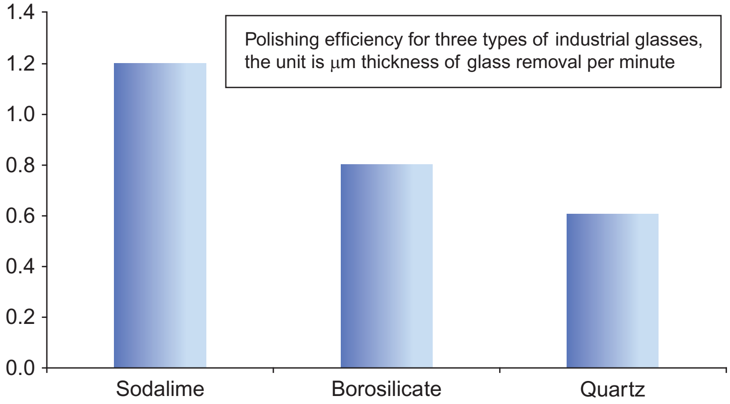

FIG. 12.5

Polishing efficiency for three glasses: pure silica glass (vitrified quartz); sodalime glass made of SiO_2 combined with Ca and Na oxides; and borosilicate glass made of SiO_2 and B_2O_3 combined with other oxides. The polishing powder is Rhodia Cerox 1650.

Graph drawn by Jacques Lucas.

Notice that the hardness Mohs scale is not linear. It is just based on the observed scratching power.

12.4.2 Glass industry—what kind of glasses to polish?

Glass products are typically split into three categories; flat glass, optical glass, and display panels.

Products made from flat glass include windows, mirrors, and decorative pieces for architecture and furniture.

12.4.3 No polishing needed

A majority of flat glass for large applications is made by the float glass process also known as the Pilkington process. No polishing is needed except on the edges.

The float glass process involves spreading molten glass over a liquid metal surface made of tin alloy. The final products are sheets of glass with uniform thickness and very flat surfaces. Most float glasses are made from sodalime glasses. The typical composition for a sodalime glass is 75% SiO_2, 15% Na_2O, and 11% CaO. Small additions of Al_2O_3 and MgO improve resistance to water corrosion.

Another important sector where, in general, glass polishing is not needed is flat display front panels, for example, LCD televisions, computers, and mobile phone screens. This performance is due to a process developed by Corning and called the fusion process. During this overflow drawdown process the glass touches nothing but air. It results in the manufacturing of very thin glass sheets down to 100 μm thickness. The surface is perfectly flat and smooth and the glass sheet is flexible. The glass used is an alkali-free borosilicate glass based on a combination of about 60 mass% SiO_2; 10 mass% B_2O_3 and other oxides such as Al_2O_3, MgO, BaO, and CaO.

12.4.4 Polishing needed

In the flat glass industry, polishing is needed only for edging and beveling glass sheets.

Some flat glass cannot be produced by the float process and still requires polishing. One of the main markets is represented by wired glass. This safety glass contains a wire mesh which helps to prevent shattering on impact or in fires. It is used in environments where safety is important such as schools.

Cerium oxide optical glass polishing is critical in ophthalmology (sight correction) and in precision lenses. The demand comes from photography, telescopes, microscopes, binoculars, and other military, industrial, and scientific equipment.

For some space instruments, a very high standard of polishing is required.

High quality finishing requires a long polishing time and considerable polishing powder. For example, an average of 2 g of polishing powder is consumed for every glass lens produced.

Notice that plastic lenses are molded. They are inexpensive and don't require polishing. They are serious competitors for glass lenses.

In addition to the front glass display panels, liquid crystal displays contain two internal glass substrates. These need to be polished. Their function is to maintain the liquid crystal materials. They need to be polished to high standard in order to reduce the final weight of the product.

Polishing of the glass substrate occurs after the internal cell has been assembled and filled with liquid crystals. Fast glass removal and fast polishing rates are required.

12.4.5 Electronic industry: fine polishing is needed

CMP is applied to planarizing the dielectrics and metal films in silicon integrated circuit (IC) fabrication. The use of CMP in the IC industry started when multilevel interconnected structures and chemical vapor deposition processes were adopted.

The main trend is in the miniaturization of electronic equipment while keeping high quality surfaces. Electronic equipment such as bare silicon wafers, STI structures, polysilicon capacitor structure, metal plugs and lines, ILD, lithographic photomask, and glass hard disk also use surface polishing but on a smaller scale.

Cerium compounds are widely used to polish the silicon wafers in preparation of ICs. CeO_2 nano-powders are needed to polish the SiO_2 layer on silicon active materials. A very flat surface, a low content of scratches and a high quality finish are required. Polishing powder is also chosen on the basis of its selectivity for the desired layer (i.e., SiO_2 vs. silicon nitride) and its avoidance of dishing.

There is an ongoing interest in polishing SiO_2-like surfaces at high rates and with low product roughness using high grade cerium oxide powders.

Cerium oxide polishing is also used for glass magnetic-memory disks. Storage capacity is increased by polishing the glass substrate prior to application of the magnetic layer. This market suffers from competition with solid state flash memory.

The same requirements are needed for lithographic photo-masks in the production of electronic circuits. Photo-masks are made using fused silica. This hard glass requires surface rough polishing, then finer finish polishing and finally edge polishing.

12.5 LEADING PRODUCERS OF RARE EARTH POLISHING POWDERS

Production of polishing powders for glass and electronic applications is a worldwide industrial activity. Only a limited number of companies produce very high quality grades. Demand is expected to grow slowly to a level of 18 kilotonnes of oxide per year in 2015.

12.5.1 China

China is the largest producer and consumer of rare earth polishing powders. China accounts for about 40% of worldwide production.

The major abrasive companies are located in the region of Baotou. Their production capacity is around 10 kilotonnes of oxide per year—more than half of the country's total.

They produce polishing powder with grades varying from 60% cerium oxide to high purity containing 99.999% cerium oxide.

The other Chinese producers are mainly located in Yixing and the province of Hunan. Basic grades as well as submicronic powders for the growing electronic polishing sector are being developed.

12.5.2 Japan

Seimi chemical (a subsidiary of Asahi Glass) is a major player in optical glass polishing.

They have installed polish recycle systems to avoid waste and lower polishing costs.

Other cerium oxide producers are Showa Denko and Mitsui Mining and Smelting.

12.5.3 Europe

Solvay Rare Earth System is the largest producer in Europe. This company imports rare earth raw materials from its Chinese operations and processes them in France. They produce Cerox a cerium oxide powder mainly used for flat glass products and the polishing powder Opaline, which is a high grade material used for fine polishing (see Fig. 12.2).

The other European companies are Treibacher Industry, Silmet, Optical Surface Technologies, Chepetsky mechanical plant, Cerium group and OCI materials.

12.5.4 USA

Ferro Corporation has been involved in ceria particle engineering for a long time. They produce high grade powders for the electronics industry as well as for the glass industry.

Grace Davison produces slurry for CMP. Several grades of cerium oxides powders are available under the brand name Vitrox and Rareox.

12.6 TRIVALENT Ce^{3+} AND TETRAVALENT Ce^{4+} CHEMISTRY

As the synthesis routes for making cerium oxide polishing powders and slurries are based on wet chemistry, it is fundamental to understand the chemical behavior of cerium ions in solution. Cerium is a specific and unique case among lanthanides, since two oxidation degrees can be stabilized, depending on the aqueous environment.

12.6.1 Behavior of Ce^{3+} and Ce^{4+} in aqueous solution

The Pourbaix diagram is basic to our understanding of the redox properties of ions in solution, depending on the potential of the system (in mV). It is established for an ion concentration of 10^{-6} mol/L (Fig. 12.6).

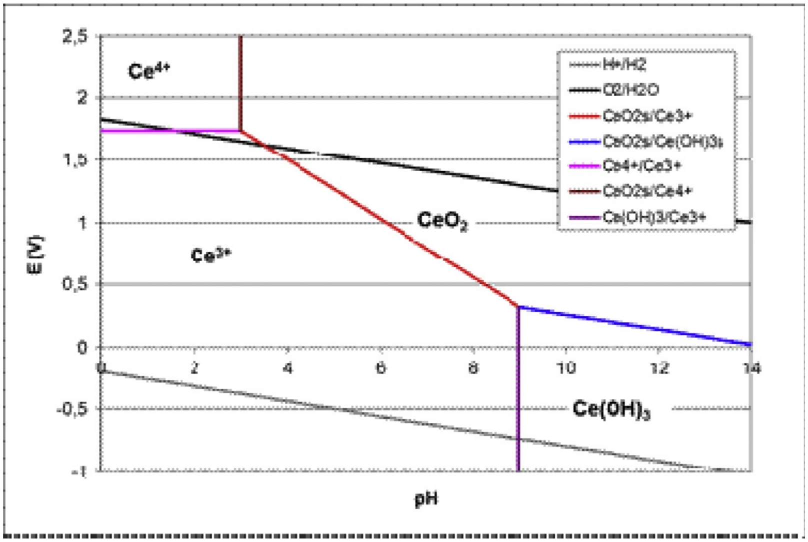

FIG. 12.6

Pourbaix diagram of cerium species at 25 °C.

Graph supplied by Solvay Rare Earth Systems

12.6.2 Ce+III and Ce+IV ions in solution

At very low pH, ionic cerium is observed in solution. The +III cerium (cerous) oxidation state is stable in nitric, sulfuric, and chloride environments, whereas the +IV oxidation state (ceric) is only stable in sulfuric and nitric environments, not in chloride medium.

This is illustrated by the redox potential of the Ce^{4+}/Ce^{3+} couple E (Ce^{3+}/Ce^{4+}) in solution with ligands L around the cerium ions:

$E = 1.71$ volts in water H_2O $E = 1.61$ volts in 1 M HNO_3
$E = 1.44$ volts in 1 M H_2SO_4 $E = 1.28$ volts in 1 M HCl

The Ce^{3+} ion has a charge + III and a large ionic radius. Like the other Ln^{3+} neighbors, it is considered as a Lewis base. In solution, the average coordination number is $CN = 9$ but it can be higher. The complex $Ce^{3+}(L)_9$ contains in its coordination sphere, ligands such as $L = H_2O$, Cl^-, NO^{3-}, OH^-, O^{2-}, etc. Cerium+III solutions are usually not colored. Cerium+III nitrate and Ce+III chloride solutions are the most classical raw materials for ceria material manufacturers.

The Ce^{4+} ion is a medium size ion with rCe^{4+} around 0.95 Å. It is highly charged +IV. Consequently the electric field around Ce^{4+} is strong and the tendency to form complexes is strong. For instance, a strong bond is expected between Ce^{4+} and the lone pairs of H_2O or OH^- plus other ligands, L. It is said that Ce^{4+} is a strong Lewis acid. Molecular orbital overlapping is possible between Ce^{4+} (acceptor) and L (donor) through a mechanism $L \rightarrow Ce^{4+}$. In this molecular orbital system, the bonding electrons are coming from L. They are responsible for light absorption and for the color of Ce^{4+} salts.

12.6.3 Inorganic condensation to CeO_2

Cerium salts in their ionic form are stable in aqueous solutions only at low pH. Under mildly acidic and basic pH, the cerium ions and their OH ligands condense in order to turn to solid cerium hydroxide.

The mechanism can be schematically described as the following $(L)n\text{-}Ce^{3+}\text{-}OH$——$OH\text{-}Ce^{3+}\text{-}(L)n$ condensate with water elimination → $(L)n\text{-}Ce^{3+}\text{-}O\text{-}Ce^{3+}\text{-}(L)n + H_2O$.

The cerium hydroxides are then quickly and usually easily turned to CeO_2 (+IV) in a wide range of potential, pH and temperature conditions, especially in the case of classical conditions under air (oxidizing atmosphere).

Control of the nucleation and growth process of cerium hydroxide/oxide is of major concern in the definition of well controlled oxide nanoparticles. This process has been widely studied, and many particle sizes, morphologies of nano-ceria have been described in the literature over the last 20 years. The most classical route to colloids of nano-ceria consists of conducting hydrothermal treatment of the cerium water solution at high temperature (>100 °C) under pressure, called thermohydrolysis (or thermolysis).

Many additive and alternative raw materials prepared for that purpose (acetates, carbonates, etc.) can be used to fine tune the synthesis conditions.

Despite this active research field, the requirements of nanoceria for polishing are so strict in terms of purity, particle size distribution, and slurry concentration, etc., that only very few colloidal grades are commonly available for the CMP industry.

12.6.4 Crystal chemistry of cerium oxides

CeO_2

CeO_2 belongs to the CaF_2 type. The unit cell represented on Fig. 12.7 is cubic and contains $4CeO_2$ units. The parameter of the cell is a =5.41Å. The inter-atomic distance Ce-O is d=2.34Å.

Four Ce ions are in a face centered cubic geometry: one Ce occupies the corners common to eight cubes 8/8 =1, three other Ce occupy the middle of the six faces

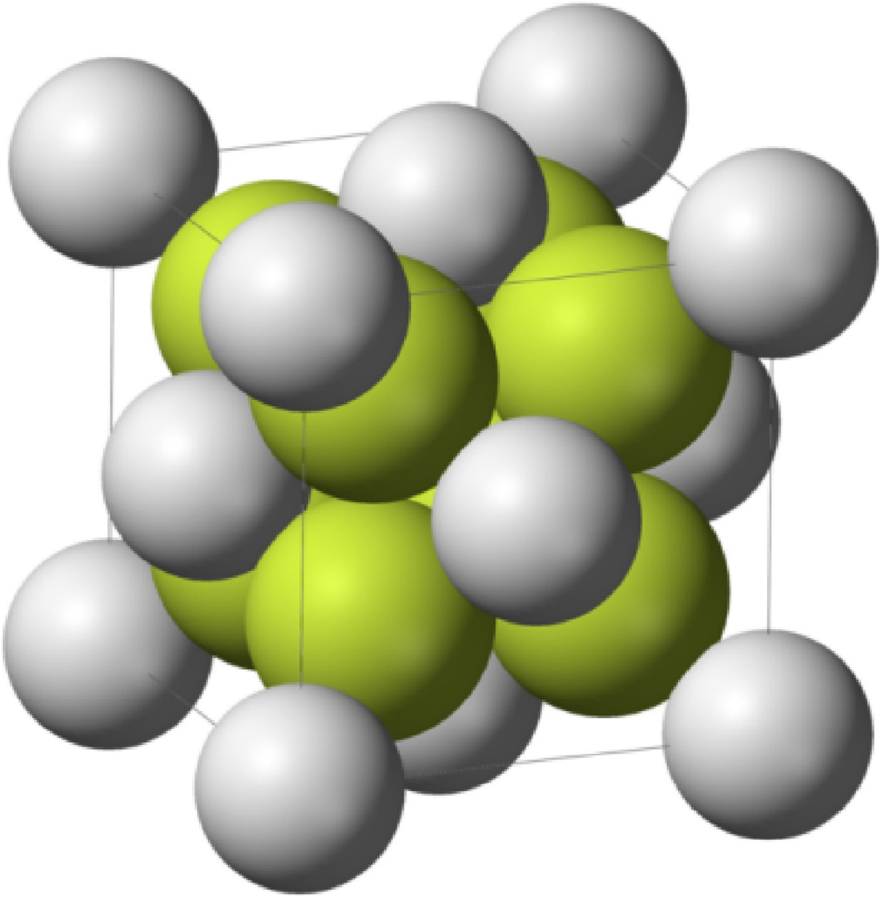

FIG. 12.7

CeO_2 crystal structure.

Drawing by Jacques Lucas research group.

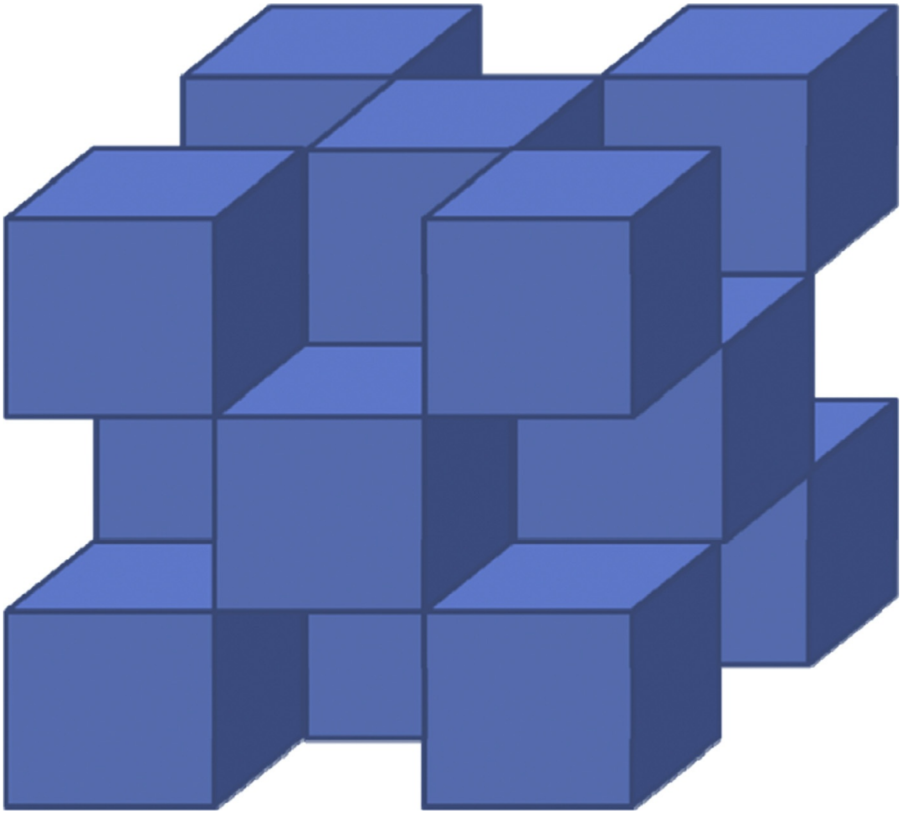

FIG. 12.8

The CeO_2 structure viewed as an association of CeO8 cubes

Drawing by Jacques Lucas research group.

$6/2 = 3$. The eight O are inside the cube. They occupy the eight tetrahedral sites. The coordination number of O is 4, forming OCe_4 tetrahedrons. The coordination of Ce is 8, forming CeO_8 cubes.

The CeO_2 structure can be represented using CeO_8 cubes as building units. The 3D connection of the cubes is depicted on Fig. 12.8.

The cohesion and the stability of the structure is mainly ensured by ionic, coulombic forces expressed by the simplified relation: $F = k\ Q^+Q^-/d$, where:

- Q^+ is the charge of Ce here $4+$ and Q^- is the charge of O here 2^-. Both charges are high compared to CaF_2,
- d is the inter atomic distance Ce-O
- *k* is a constant depending on the spatial geometry of the charge $Q^+$and Q^-

The lattice energy of CeO_2 is mainly due to ionic forces and is very large due to the high values of Q.

Ce_2O_3

The structure of Ce_2O_3 is more complex but is related to CeO_2.

It is well known (see chapter 9) that CeO_2 can lose oxygen at high temperature. The reaction is reversible.

The reaction is $CeO_2 \leftrightarrow CeO_{2-x}\ \square x + 1/2O_2$ where the symbol □ represents an oxygen vacancy. The detailed formula of the solid is $Ce^{4+}{}_{(1-x)}Ce^{3+}{}_{x}O_{(2-x/2)}\square_{x}$.

- For $x = 0$ the formula is CeO_2 the solid contain only Ce^{4+}
- For $x = 1$ the formula is Ce_2O_3 the solid contains only Ce^{3+}

The relation between CeO_2 and Ce_2O_3 is represented on Fig. 12.9. The two structures are strongly related except that cubes CeO_8 are transformed into $CeO_6\square_2$ polyhedras. The vacancies are well ordered and the symmetry of CeO_6 is close to a trigonal prism.

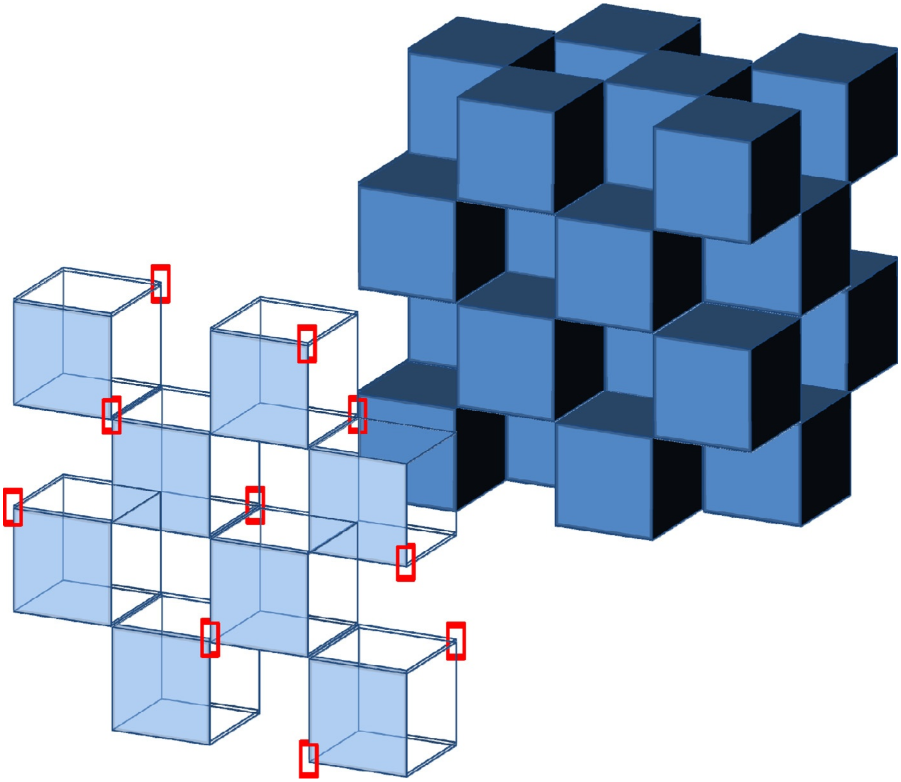

FIG. 12.9

Relation between the cubic CeO_2 network and the O deficient Ce_2O_3 structure. Due to oxygen vacancies the CeO_8 cubes are transformed into $CeO_6\square_2$ polyhedron. Each O is common to 4 Ce. The formula is $CeO_{6/4} \rightarrow Ce_2O_3$. Ordering of the vacancies leads to super cells with hexagonal or cubic symmetry.

Drawing by Jacques Lucas research group.

Depending on the way that the vacancies are ordered two superstructures are possible for Ce_2O_3: either hexagonal or cubic. The structure is the same for La_2O_3 and other RE oxides.

By analogy with CeO_2 the formula of the solid is then $CeO_{6/4} \rightarrow Ce_2O_3$ since each O is common to 4 Ce.

From Fig. 12.9, it is easy to understand why the reaction $Ce_2O_3 + \frac{1}{2}O_2 \leftrightarrow CeO_2$ is reversible. The compound is an oxygen reservoir which is a key factor for catalysis. Native oxygen escaping from CeO_2 at the surface of the grain is very reactive.

Due to vacancies, the lattice energy of Ce_2O_3 is inferior to CeO_2 but this is compensated for by the higher electrochemical stability of Ce^{3+} compared to Ce^{4+}.

12.6.5 Two additional remarks

- Industrial praseodymium oxide is fully black (Fig. 1.1) and has a formula which shows deviation from stoichiometry.

  One of the commercial compositions is $PrO_{1.83}$ which is more stable than Pr_2O_3 and PrO_2. Notice that the oxidation state Pr^{4+} is very unstable and does not exist in aqueous solution.

  The crystal chemistries of Pr and Ce oxides are very similar and are both characterized by nonstoichiometric materials related to the CaF_2 structural type.

  Indeed $PrO_{1.83}$ is equivalent to $Pr_6O_{11}\square_1$. The crystal structure of this black oxide contains 1 vacancy for 11 oxygen instead of 12 oxygen. The complex superstructure is derived from CeO_2 structure because of a precise ordering of the vacancies into the network.

  This semi-conducting oxide has a low band gap and contains 2 Pr^{3+} and 4 $Pr^{4+.}$ Electron exchanges between ions absorb visible light. In these mixed valence materials, charge transfer absorption is responsible for the black color.

- CeO_2 particles are in contact with water during polishing

  At the surface of the particles some substitution $O^{2-} \leftrightarrow OH^-$ is possible with an equivalent formal charge compensation of Ce^{4+} into Ce^{3+}.

  The presence of the OH^- groups on the surface of the particles is probably the key to explaining the CMP process as discussed later.

  In the family of abrasive oxides used for polishing, the situation of CeO_2 is unique. Indeed this material is able to exchange O^{2-} by OH^- on the surface of the grains because of the flexible equilibrium $Ce^{3+} \leftrightarrow Ce^{4+}$.

12.7 A PROCESS TO PREPARE CeO_2 PARTICLES

12.7.1 Synthesis of (sub-) micronic ceria powders

Different access routes to micronic or submicronic ceria-based polishing powders have been industrialized, depending mainly on the accessibility to raw materials.

The starting raw materials are generally a mixture of rare earths (cerium rich), in the form of a lanthanide carbonate, or lanthanide oxyfluoride. A wet process, including basic treatment and in some specific cases, a fluorination step (HF, or NH_4F), is firstly performed to control the particle size range. Then, a firing step is applied to promote the final crystallization state of the abrasive (and its intrinsic hardness). This step usually induces some particle size growth. Thus, one or several milling steps (dry or wet) are applied, which lead to the final ceria-based material, with the suitable mean particle size, and a relatively sharp particle size distribution.

12.7.2 Synthesis of micronic Ceria colloidal nanoparticles

Many procedures have been described to prepare CeO_2 nanosize particles, but industrial routes to colloidal ceria are strictly confidential. The paper by Huey-Ing Chen and Hung-Yi Chang (Chen and Chang (2004)) has been selected as the most informative. It concerns the precipitation of CeO_2 from solutions having different dielectric constants. This is achieved by changing the water/alcohol ratio. The size of the particles can be controlled. The different steps are described below in Fig. 12.10.

The size of the particles depends on the type of alcohol. This includes methanol, ethanol, and others.

At the beginning of ammonia addition, the precipitate is pale yellow. Then it turns to purple during stirring in air. Eventually it forms a yellow suspension.

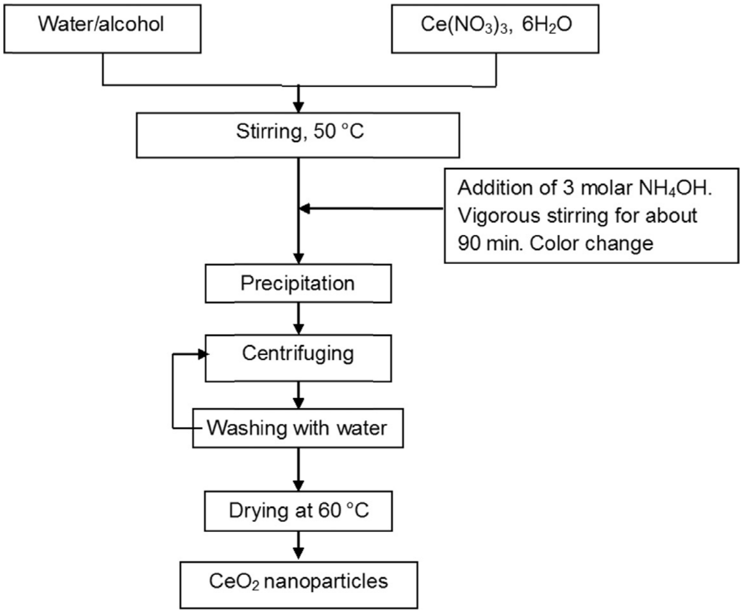

FIG. 12.10

Experimental flow chart for homogeneous precipitation of CeO_2 particles with different nanosizes.

Drawn by Jacques Lucas.

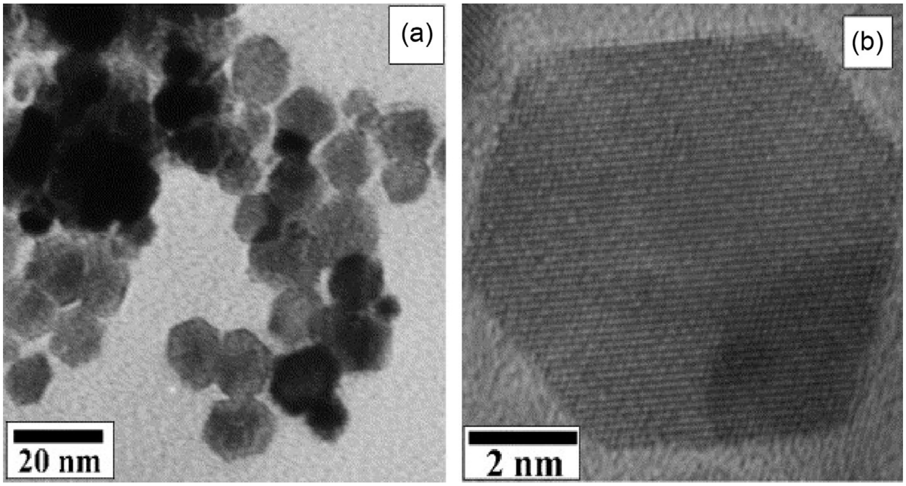

FIG. 12.11

TEM pictures of CeO_2 nanoparticles prepared in water. (a) is by TEM and (b) is by high resolution microscopy.

From Chen and Chang (2004).

The combination of OH addition and vigorous stirring in air contribute to the progressive oxidation of the insoluble $Ce^{3+}(OOH)_nH_2O$ precipitate. This explains the change of color when Ce^{3+} and Ce^{4+} are simultaneously in the mixed valence material.

The final result is the formation of very stable CeO_2 particles. Tetravalent Ce^{4+} is stabilized because of the strong lattice energy of CeO_2.

Fig. 12.11 represents a transmission electron microscope (TEM) image of a dry CeO_2 particle prepared in pure water.

The shape is very regular similar to a single crystal. The size is around 15 nm diameter. In the presence of alcohol, the size of the particles can drop down to 3 nm. The elementary particles tend to aggregate as seen on Fig. 12.11 (a).

The bonding forces between grains to form an aggregate are not known but they could come from the presence of OH at the surface of each grain as discussed before.

12.8 CHEMICAL OR MECHANICAL? THE CMP PROCESS

12.8.1 Introduction

The debate is still open on the precise mechanism that explains the superiority of CeO_2 compared to other oxides (silica, alumina) for silica polishing.

It is clear that excellent roughness and planarization cannot be explained only by mechanical abrasion process. It is also difficult to speculate on real hardness, especially when nanosize CeO_2 particles are used (electronic industry). Nano-indentation measurements are possible but only few labs are equipped to performed them accurately.

Chemical interactions between abrasive and target surface are the other main contributions. The presence of water is critical.

However, the relative importance and impact of each contribution depends on the kind of application. Typically, polishing of glass is very different from polishing of pure silica in semi-conductors, even though ceria abrasive is design to polish "silica" (Si-O-Si bonds) in both cases. Other parameters such as duration of polishing, size of the roughness to eliminate, quantity, and nature of defects are also key factors. Moreover, in semi-conductors, there are strong requirements in term of selectivity of the abrasives towards each layer of the substrate, for example, very fast polishing of the SiO_2 layer and no abrasion of Si_3N_4. Then formulation of slurries plays a key role, but this know-how is not communicated by the formulators. A second large difference is the duration of the polishing: a few seconds in case of semi-conductors and few minutes to few hours for glass polishing. The reactivity of the substrate to water, which is a driver to induce chemical processes, is also very different in the case of glass and the thin silica coating in semi-conductors (porosity, defects, and cation lixiviation processes in glass).

For all those reasons, the remaining of this section is focused on glass polishing.

12.8.2 Choice of ceria: the Cook model

As previously explained, the choice of ceria is not based on purely mechanical properties (hardness) but also on its specific surface chemistry. The most famous model in this domain was suggested by Cook in 1990.

It is based on characterization of the surface chemistry by zeta potential, meaning the determination of the isoelectric point of ceria. Isoelectric point is the pH where the surface of the oxide has equivalent positive and negative charges (resulting overall in zero charge). It is an intrinsic property of the material and does not depend on size or surface chemistry as a first approximation, and when no formulation is used (nanosize range and classical counter-ions). This model is quite empirical and compares the polishing efficiency of oxides of several cations (see Fig. 12.12). The most efficient was found to be CeO_2 which is the optimum in the correlation of this polishing rate versus isoelectric point. However, this approach is not fully understood since no clear explanation was given on the necessity of having an isoelectric point around 7 to polish silica. The role of water and the creation of Si-O-Ce bonds need to be further investigated.

12.8.3 Description of the mechanism

(1) Role of water

H_2O molecules play a key role on both surfaces, i.e., CeO_2 grains and glass silicate surfaces.

In view of Fig. 12.14(b) and Fig. 12.7 it is likely that a surface reaction occurs on the grains in contact with H_2O.

A fraction of the O^{2-} could be substituted by OH^- and accompanied by a Ce^{3+}/Ce^{4+} compensation. The SiO_2 based glass surface is the most vulnerable part of a glass sample.

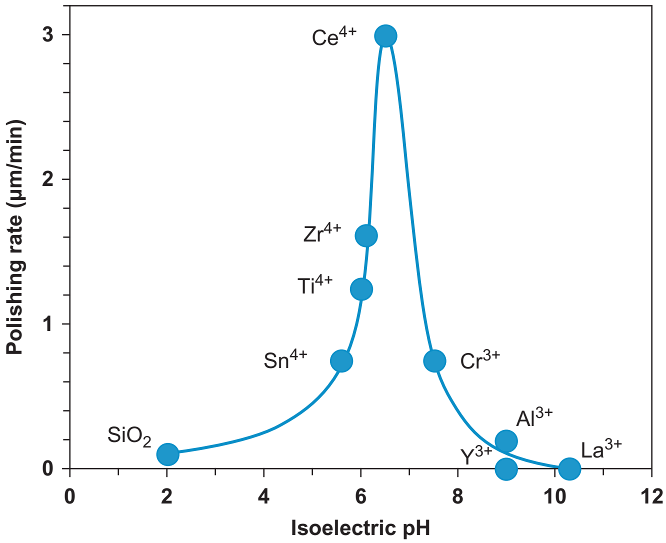

FIG. 12.12

Cook Model.

Elsevier graph, redrawn by Pierre Lucas.

The Si-O-Si-O-Si-O bond is strongly modified by ionic exchange or hydrolysis.

Na^+ ions are exchanged with H_3O^+ with the formation of terminal -Si-OH bonds. Even in pure silica SiO_2 the surface bond -Si-O-Si-O-Si- can react with H_2O. As seen on Fig. 12.13, it results in an opening of the bond with -Si-OH. . .OH-Si-terminal bonds formation.

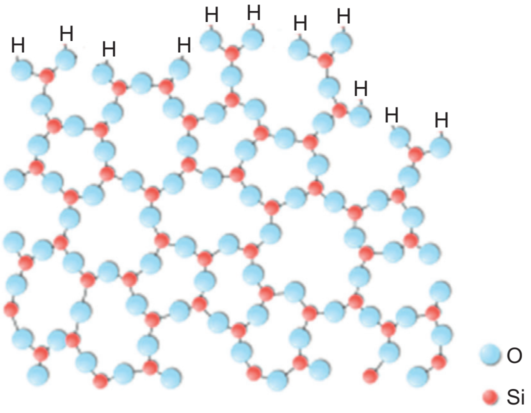

FIG. 12.13

Representation of a sodalime glass.

Drawing by Professor Jacques Lucas research group.

The presence of OH on the surface of a glass is considered as one of the main defects in silicate glass technology. Under strain, this defect is the source of fractures and fracture propagation.

The chemical contribution in the polishing process is essential but the total mechanism involves both mechanical stress and chemical reaction. The following scenario is likely the most general.

(2) Ceria actions on the silica substrate (glass)

Figs. 12.14a and 12.14b are aimed at portraying the two mechanisms which of course occur simultaneously during the polishing operation.

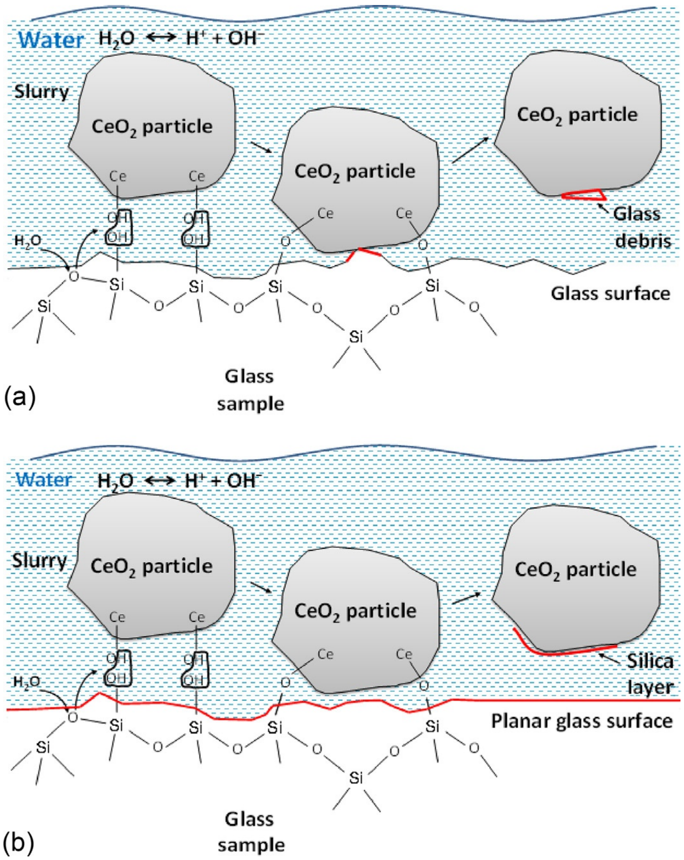

FIG. 12.14

(a) Material removal. Scratching glass asperities and elimination of glass debris by mechanical stress associated with chemical bonding between CeO_2 grains and the surface. (b) Planarization: after abrasion, chemical polishing with strong adhesion between grains and the surface is the dominant factor.

Drawing by Jacques Lucas research group.

(a) The asperities of the glass surface are the first to be sensitive to the mechanical pressure. Micro-fractures are induced and glass debris produced.

At the same time, intimate contact between the abrasive grains and the glass is reinforced by a strong -O-Ce-O-Si-O-Si bond.

As shown on Fig. 12.14a the bonds are formed by condensation between the surface radicals -Ce-OH of the grains and OH-Si- groups of the glass surface.

The role of the CeO_2 grains is to first generate micro-cracks and second to take away the glass surface debris. Fig. 12.14a represents the overall mechanism which is responsible for the so-called "material removal" operation.

(b) The second function of CeO_2 is to produce very flat surfaces with a very low roughness (minimum peak to valley difference).

The mechanism leading to a flat surface is clearly governed by chemistry more than mechanics. The main function of CeO_2 is to create a strong adherence between the particles and the surface layer of the glass. The origin of the chemical bond is also condensation utilizing OH bonds from the Ce side and Si side, see Fig. 12.14b.

Layer by layer the glass surface is chemically eroded and non-planar defects are suppressed. The surface becomes flat. The SiO_2 based materials in thin layers are removed by the CeO_2 grains as depicted on Fig. 12.14b.

12.9 SUMMARY

The technical literature on chemical mechanical planarization (CMP) is very diverse and sometimes confusing.

The objective of this chapter is to attempt to rationalize a very empirical technology where the know-how is more important than knowledge of fundamental mechanisms.

It is clear that in the industry, the two targets are materials removal for decreasing weight as well as achievement of very flat surface and few defects.

As long as the substrate to be polished contains silicon Si for instance silica glass, silicates glasses, silicon wafers for electronics, the CMP model is valid.

It is arbitrary to dissociate the chemical function from the mechanical function—they both coexist.

In most industrial operations, the slurry composition is very complex with several organic additives. It is always confidential.

A complete understanding of polishing mechanisms is a challenge and empirical recipes are usually the rule.

Surface chemistry plays a crucial role in polishing since the modest hardness of the ceria particles cannot explain the final results. This justifies the acronym CMP: a combination of chemistry first and mechanics in second.

References

Chen, H.I., Chang, H.Y., 2004. Homogeneous precipitation of cerium dioxide nanoparticles in alcohol/water mixed solvents. Colloids Surf. A Physicochem. Eng. Asp. 242, 61–69.

Suggested Reading

Roskill report 2011; Rare Earths and Yttrium: market outlook to 2015, chapter on “Polishing,” link at www.roskill.com/rare-earths.

Sabia, Robert, Stevens, Harrie J., 2000. Performance characterization of cerium oxide abrasives for chemical-mechanical polishing of glass. Mach. Sci. Technol.: An International Journal 4 (2), 235–251, link to the article: http://dx.doi.org/10.1080.

Suratwala, T.I., Feit, M.D., Steele, W.A., 2010. Towards deterministic materials removal and surface figure during fused silica polishing. J. Am. Ceram. Soc. 93 (5), 1326–1340.

Tomozawa, M., 1997. Oxide CMP mechanism in solid state technology, link at, http://www.electroiq.com/articles//sst:print:volume-40/issue-7.

Tsai, Ming-Shyong, 2004. Powder synthesis of nano-grade cerium oxide via homogenous precipitation and its polishing performance. Mater. Sci. Eng B 110, 132–134.

Wang, Y.G., Zhang, L.C., Biddut, A., 2011. Chemical effect on the material removal in the CMP of silicon wafers. Wear 270 (1), 312–316.

CHAPTER

13

Permanent Magnets Based on Rare Earths: Fundamentals

13.1 INTRODUCTION

This chapter concerns rare earth (RE) ferromagnetism. It focuses on the materials which dominate the world of industrial strong and permanent magnets.

In this section we will explain why RE alloys have superior magnetic properties. The electronic structure of RE elements contains one to seven unpaired electrons (see Chapter 8) and consequently they are strongly paramagnetic. At the atomic scale each of them is similar to an elementary magnet.

They also can be alloyed with transition metals (TMs) such as iron (Fe) or cobalt (Co), both of them being rich in unpaired electrons.

The two REs neodymium (Nd) and samarium (Sm) are at the origin of the revolution in permanent strong magnets.

High concentration of paramagnetic atoms is not sufficient to describe the exceptional properties of those alloys. Indeed the magnetic anisotropy resulting from an asymmetric charge distribution of the 4f orbitals is also important. It is the key to explain the powerful magnetization and the strong resistance to demagnetization.

The properties of a strong permanent magnet are well represented by the hysteresis loop that defines two key values: the magnetic remanence B_r (power) and the coercitivity H_c (permanence).

In this section the mechanisms of magnetization at the atomic level will be described.

Very high values of B_r and H_c are obtained only in two situations:

- In alloying Sm and Co.
- In alloying Nd and Fe with a small amount of boron (B).

The SmCo magnets are represented by two compositions and two crystal structures: $SmCo_5$ and Sm_2Co_{17}.

The NdFe magnets are represented by only one composition and structure: $Nd_2Fe_{14}B$. They dominate the market due to a lower cost and remarkable performances.

It is usual for commercial purpose to classify the magnets by the product of B_r and H_c called energy product BH_{max}.

Rare Earths. http://dx.doi.org/10.1016/B978-0-444-62735-3.00013-9

An important parameter is also the evolution of the magnetic flux B_r as a function of temperature T. It measures the degradation of the magnet versus T. The critical temperature is the Curie temperature T_c.

Above T_c, the ferromagnetism is destroyed and the power of the magnet vanishes. But below T_c it is also observed that the performances are altered. This is a limiting factor for industrial applications especially for the NdFeB magnets.

As a general comment, it must be mentioned that the modern magnet industry is totally dependent on this new RE-based alloys.

These magnets are vital for many technologies and strategic in many industrial sectors such as automobiles, motors, computers, defenses, new energies, and practical home devices.

In terms of business this sector of the RE industry is expected to be one of the fastest growing and profitable.

Since these RE alloys are worldwide ranked at the top level of the magnets classification, they are in high demand and the need for the year 2015 is estimated to be superior to 60,000 tons expressed in RE oxides.

Finally the RE magnets will be compared to the most traditional ferromagnetic materials such as the alloys AlNiCo and the ferrites.

The fabrication and uses of RE magnets will be discussed in Chapter 14.

13.2 WHAT CAN BE EXPECTED FROM THE PURE RE METALS?

For the preparation of RE metals please refer to Chapter 6.

To produce ferromagnetism and then a magnet the first condition is to select materials having a high concentration of paramagnetic atoms.

Ferromagnetism will be discussed in more detail in the next section.

A paramagnetic atom contains unpaired electrons, each of them being equivalent to a local magnet due to the orientation of the electronic spin.

In order to have a strong magnetic coupling and generate the cooperative phenomena called ferromagnetism two conditions are needed:

- Each atom must be as rich as possible in unpaired electrons.
- They need to be very close to each other, in other words to be close-packed.

The second condition is satisfied in the case of the metallic state except if the atoms are too large. Long interatomic distances are not favorable for magnetic coupling.

- First condition

The first condition is highly favored among RE metals since the gradual filling of the 4f level from 4f1 to 4f13 can generate a large number of unpaired electrons. See Chapter 8.

For example the element gadolinium Gd, in the middle of the group, has the electronic structure 4f7 5d1 6s2 and possesses seven unpaired electrons:

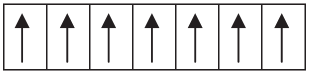

The element samarium Sm 4f5 5d1 6s2 has five unpaired electrons:

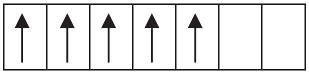

And the neodymium 4f3 5d1 6s2 only three unpaired electrons:

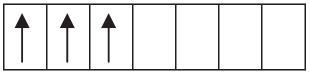

The magnetic moment of individual atoms results from the coupling of two magnetic contributions:

- The electrons rotating on themselves called spin magnetic moment S.
- The circulation of the same electrons along the f ellipsoidal orbital called orbital magnetic moment L.

Since the 4f orbitals are internal, well protected from outside influences, the total magnetic moment is due to the LS coupling called spin-orbit coupling.

The observed magnetic moments M in A m^2 of the RE metals are given in Table 13.1.

All the RE elements listed in Table 13.1 form trivalent RE^{3+} cations in solids except Eu^{2+} and Yb^{2+} which form divalent cations due to the added stability of the resulting half-filled shells 4f^7 and 4f^{14}, respectively.

- Regarding the densities three metals show the lowest values:
  - Yttrium because it is a light element $Z=39$
  - Europium and Ytterbium because of their large metallic radii and unit cell due to Eu^{2+} and Yb^{2+} ionization.
- The metallic radii of Eu and Yb are also out of the monotonic variation for the same reason of divalent ionization. Same remarks are applied for melting points. See Chapter 8
- Concerning the magnetic properties, the table presents the measured values of the paramagnetic moments. Only six RE metals show ferromagnetic properties and these are only observed at low temperature. The highest Curie temperature $T_c=293$ K is observed for gadolinium.
- Notice that four metals La, Yb, Lu, and Y have no unpaired electrons and are diamagnetic. The reasons lie in the electronic structures of the corresponding ion:
  La 4f0: no f unpaired e^- and three delocalized e^-
  Yb 4f14: no unpaired e^- and two delocalized e^-
  Lu 4f14: no unpaired e^- and three delocalized e^-
  Y: no f orbital and three delocalized e^-

Table 13.1 Structural and Magnetic Properties of Rare Earth Metals

Element	Atomic Number (Z)	Atomic Structure	Density	Metallic Radius, r_M (Å)	Melting Point (°C)	Observed Paramagnetic Moment, M	Curie Temperature, T_c (K)
La	57	[Xe] $6s^2\ 5d^1\ 4f^0$	6.146	1.87	918		
Ce	58	[Xe] $6s^2\ 4f^1\ 5d^1$	6.77	1.83	798	2.51	
Pr	59	[Xe] $6s^2\ 4f^3\ 5d^0$	6.773	1.82	931	2.56	
Nd	60	[Xe] $6s^2\ 4f^4\ 5d^0$	7.008	1.82	1021	3.4	
Pm	61	[Xe] $6s^2\ 4f^5\ 5d^0$	7.264	1.81	1042		
Sm	62	[Xe] $6s^2\ 4f^6\ 5d^0$	7.52	1.8	1074	1.74	
Eu	63	[Xe] $6s^2\ 4f^7\ 5d^0$	5.244	2.04	822	8.48	
Gd	64	[Xe] $6s^2\ 4f^7\ 5d^1$	7.901	1.8	1313	7.98	293
Tb	65	[Xe] $6s^2\ 4f^9\ 5d^0$	8.23	1.78	1356	9.77	220
Dy	66	[Xe] $6s^2\ 4f^{10}\ 5d^0$	8.551	1.77	1412	10.83	89
Ho	67	[Xe] $6s^2\ 4f^{11}\ 5d^0$	8.795	1.76	1474	11.2	20
Er	68	[Xe] $6s^2\ 4f^{12}\ 5d^0$	9.066	1.75	1529	9.9	20
Tm	69	[Xe] $6s^2\ 4f^{13}\ 5d^0$	9.321	1.74	1545	7.61	32
Yb	70	[Xe] $6s^2\ 4f^{14}\ 5d^0$	6.966	1.94	819		
Lu	71	[Xe] $6s^2\ 4f^{14}\ 5d^1$	9.841	1.73	1663		
Y	38	[Kr] $4d^1\ 5s^2$	4.472	1.8	1522		

- Second condition

The second condition relates to the maximum of compactness; in other words, short interatomic distances. This aspect is not highly favored in RE metals. Table 13.1 shows the evolution of the atomic radii along the 4f family. This point is also discussed in Chapter 8. The atomic radii of RE metals are larger compared to the classical ferromagnetic metals such as Fe or Co.

For instance, if we compared the most interesting metals for industrial magnets such as Fe, Co, Nd, and Sm the metallic radii are as follows:

$r(\mathrm{Fe}) = 1.26$ Å and $r(\mathrm{Co}) = 1.25$ Å for the 3d TM

While,

$r(\mathrm{Nd}) = 1.82$ Å and $r(\mathrm{Sm}) = 1.80$ Å for the RE 4f metals

As a result of these large metallic radii the magnetic properties of RE metals are limited.

As explained in the next section, ferromagnetism coupling is opposed by thermal agitation which tends to destroy the coupling. This phenomenon occurs above a temperature called Curie temperature T_c.

Examination of Table 13.1 shows that the ferromagnetic properties of RE metals are very limited. Indeed the highest $T_c = 293$ K is observed for Gd metal and all the other RE have their T_c below room temperature (RT).

As a conclusion RE metals, even if very rich in unpaired electrons, have no practical interest and need to be alloyed with TM.

13.3 ABOUT FERROMAGNETISM

Ferromagnetism is a cooperative phenomenon resulting from long range interactions between the spins of unpaired electrons. Each atom produces its own magnetic field which strongly interacts with the neighbors. This results in a spontaneous alignment of spins within magnetic domains below T_c. Above T_c the thermal motion destroys the coupling, the material is paramagnetic as represented in Fig. 13.1a.

Below the Curie temperature and in the absence of any applied magnetic field H the ferromagnetic domains are oriented in all directions as represented in Fig. 13.1b. In these conditions the external magnetic flux is zero.

The domains are separated by domains walls.

The formation of magnetic domains, called Weiss domains, results from a balance between the energetic cost of maintaining a large magnetic field (magnetostatic energy) and the energetic gain from aligning spins within a domain (exchange energy). The creation of domains separated by walls lowers the magnetostatic energy but creates nonaligned spins at the walls surface which raises the exchange energy. The magnetostatic energy decreases with domain volume (cube of domain size) while the exchange energy increases with wall surface (square of domain size) hence a balance is reached at an equilibrium average domain size.

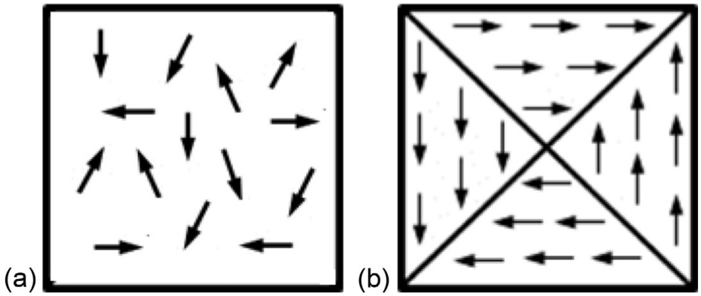

FIG. 13.1

(a) Paramagnetic RE material at T superior to T_c, the Curie temperature. There are no coupling between the individual magnetic atoms; (b) ferromagnetic RE material at T inferior to T_c. No external magnetic field H is applied.

When an external magnetic field H is applied to a ferromagnetic material below T_c, the magnetic spin tends to be aligned in the direction of the field. This external force overcomes all other stabilizing forces so that the domains walls move and tend to orient in the field. The final situation is an almost perfect alignment of the magnetic spin.

13.3.1 Hysteresis loop-first quadrant-magnetization curve-remanence

In Fig. 13.2 the first quadrant shows the first magnetization curve (dotted line).

Inset (a) represents the ferromagnetic domains separated by walls. In the absence of applied magnetic field they are aligned in all direction.

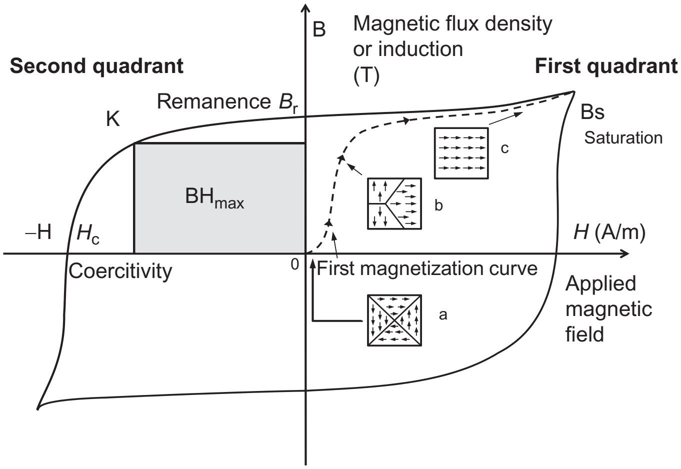

FIG. 13.2

Hysteresis loop of a ferromagnetic material.

Drawing from Jacques Lucas Laboratory.

Inset (b) and (c) represent the evolution of the domains under a horizontal magnetic field *H*. The domains parallel to *H* are growing. Other domains are forced to align. The movements of the domains walls create some constraints on the crystalline network.

Notice that if both the crystalline network and the magnetic dipoles exhibit a compatible anisotropy, the magnetization will be easy. This is the case for the RE magnets as will be discussed in section 13.5.

When the strength of *H* is sufficient, saturation is reached as shown in Fig. 13.2. All the magnetic dipoles are aligned and the magnetic flux density reached the maximum value B_s also called saturation magnetic induction. It means that a strong magnetic flux B_s is created into the magnet.

When the applied *H* is reduced back to zero the dipoles remain parallel. The remaining magnetization is represented by the remanence B_r.

13.3.2 Second quadrant-demagnetization-coercitivity

The second quadrant is critical. It shows how a magnet resists demagnetization and whether it can be defined as a "permanent magnet."

To reverse the dipole alignment an opposite magnetic $-H$ field is applied.

The phenomenon is rather complex but always start by the nucleation of a first small reverse domains.

In order to optimize the magnetic property this nucleation under $-H$ needs to be delayed as much as possible. Usually when these opposite nucleating domains are formed they grow very rapidly and the value of B_r drops down to zero very fast. The letter K (for knee) on the curve represents this region where the performances degrade.

The magnet is totally demagnetized when $-H$ reaches the value H_c called coercitivity.

Coercitivity measures the resistance of a magnet to demagnetization.

RE magnets are characterized by the highest value of coercitivity among all solid state magnets. They retain their magnetization indefinitely in normal conditions.

13.3.3 Hysteresis loop-maximum energy product BH_{max}

Magnetic polarization in the opposite direction can be achieved by applying a magnetic field in the reversed direction. The same process as described above can then be observed in the two lower quadrants of Fig. 13.2.

The whole process describes a curve called "hysteresis loop" represented in Fig. 13.2.

The hysteresis loop corresponds to the fingerprint of a magnet and is a usual control measurement in the magnet industry.

Besides coercitivity and remanence a quality factor for permanent magnet is the quantity BH_{max} which is the maximum product of B_r and H_c called energy product. It corresponds to the maximum density of magnetic energy which is stored into a magnet.

The energy product is represented by the maximum area formed in the second quadrant of the BH hysteresis loop represented in Fig. 13.2. This figure of merit quantifies the stored energy per unit volume of magnet.

The energy product BH_{max} is commonly used to compare the performances of the different magnets, especially when miniaturization is concerned. BH_{max} is a measure of the maximum work that can be performed by a permanent magnet. The units are in megagauss oersteds (MGOe) or kJ/m^3 in SI units. Notice that the values in MGOe need to be multiplied by 7.96 to be converted into kJ/m^3. Values as high as 400 kJ/m^3 are obtained with the NdFeB magnets.

13.3.4 Precision on the units

Some precisions are needed concerning the unit of magnetic field used in the literature and technical documents which can be a source of confusion.

The unit of the magnetic flux density B is the Tesla by reference to SI (Systeme International).

Gauss or oersted was used historically because they are of convenient size. For instance the earth magnetic field is a few gauss. And the field at the read-and-write head in a computer hard drive is around 20-50 gauss.

In a hospital the fields in a MRI machine (magnetic resonance imaging) are much higher from 20,000 to 70,000 gauss.

In summary $1\ T = 10{,}000$ gauss or oersted.

One gauss = 1 oersted in vacuum or in a nonmagnetic substance like air.

The applied field H is also expressed in SI unit: ampere per meter (A/m).

The conversion from SI unit to oersted is as follows: $1\ Oe = 10^3/4\pi$ A/m.

13.3.5 Dependence of magnetization on temperature

As already mentioned the magnetization is very sensitive to thermal agitation which tends to destroy the magnetic coupling. Ferromagnetism disappears totally at temperature superior to T_c, the Curie temperature. High T_c values are therefore desirable. For instance $T_c = 310$ °C for the NdFeB magnets and it is much higher for the SmCo magnets, $T_c = 750$ °C

Nevertheless it is observed that far below T_c there is a degradation of the magnetization versus temperature.

On a practical point of view, a temperature maximum of utilization is defined and is called T_{max}.

T_{max} is the maximum usage temperature for a magnet which ensures a full recovery of its properties when T is lower down.

For instance for pure NdFeB magnets $T_{max} = 80$ °C and for SmCo magnet $T_{max} = 300$ °C.

The quantity T(coef) of B_r represents the dependence of B_r on temperature above T_{max} and is expressed in percent per degree centigrade. It defines how the magnetic flux is changing when the temperature increases.

For example if T(coef) for B_r is -12% the magnetic flux will decrease by 12% for an increase of 100 °C.

Overall the properties of the magnet are significantly deteriorating between T_{max} and T_c and the penalty depends on the shape, the size, and the history of the sample. The system recovers when temperature drops down but with a penalty on the performances.

Fig. 13.3 represents the evolution of the magnets performance with temperature.

13.3.6 Requirements for exceptional magnets

The main requirements can be classified as follows.

High magnetic flux density B_r as well as a steep first magnetization curve.

This indicates that the magnetic dipoles aligned easily along some crystalline directions. The highest values of remanence for the more efficient RE magnets are $B_r = 1.4\text{-}1.6$ T.

A strong resistance to demagnetization with high H_c coercivity values.

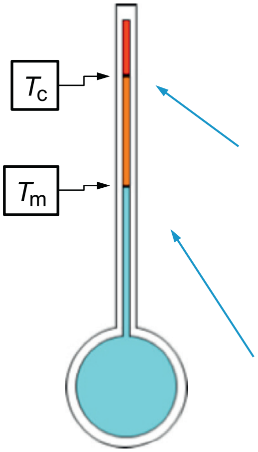

At T superior to T_c the magnetization is destroyed

The magnet will not recover its total performances at room temperature

T_c, Curie temperature

Between T_{max} and T_c the performance of the magnet deteriorates at a rate defined by a coefficient called T_{coef} of B_r

The deterioration is reversible

After cooling down, the magnetization comes back to the initial values

T_{max}: maximum temperature of utilization.

FIG. 13.3

Deterioration of the magnetic properties of a permanent magnet with temperature. Two values are important. T_m called T_{max} is the maximum temperature of utilization. Above T_m the performances decrease. T_c is the Curie temperature. Above T_c the thermal motion destroys the ferromagnetism.

Drawing from Jacques Lucas Laboratory.

The typical values for the best RE magnets coercitivities are around 25 kOe (25 kG or 2.5 T or 2000 kA/m).

A high energy product BH_{max}.

This corresponds to the maximum density of magnetic energy which is stored into a magnet. Values as high as 400 kJ/m^3 are obtained with the NdFeB magnets.

For some applications such as traction engines or permanent magnet generators for electricity production the magnets need to keep high coercitivity even with an elevation of temperature reaching for instance150 °C.
Several other parameters also characterize the quality, durability, and commercial potential of a magnet. Among them are

- The resistance to corrosion especially in humid conditions
- The physical strength such as brittleness, hardness
- Suitable electrical resistivity
- Available size and shape
- The different potentialities for magnetic polarization
- Raw materials cost and availability

13.4 ALLOYING RE METALS AND TM: A BREAKTHROUGH IN THE WORLD OF PERMANENT MAGNETS

The development of RE/TM metals magnet started in 1966 with the discovery at the United States Air Force Material Laboratory of the alloy YCo5 showing a very high magnetic anisotropy and an unusual high coercitivity with H_c around 1 T. This value was higher than the values observed for the traditional magnets such as the alloys aluminum/nickel/cobalt called AlNiCo or the ceramics called ferrites.

This discovery opened the way to the development of new composition based on the combination of samarium and cobalt called the SmCo magnets and latter in 1980 to the discovery of cheaper and more powerful magnets based on the combination of neodymium, iron, and boron called NdFeB magnets.

Table 13.2 presents the performances of several commercial permanent magnets. The numbers correspond to average values and can vary with the grade of the magnets.

The term "sintered" indicates that the magnets are made by powder metallurgy.

The term "modified" means that Co atoms can be partially substituted by Fe, Cu, Zn, and Zr.

The term "bonded" means that the RE magnet powders are mixed with a polymeric resin for easy shaping.

The values of T_{max} change drastically with the RE composition. For instance Pr, Dy, Tb addition raises the T_{max} of the NdFeB magnets. The specifications depend on the magnets producers.

13.4.1 The Sm/Co magnets

Sm/Co magnets are represented by two compositions $SmCo_5$ and Sm_2Co_{17}.

Table 13.2 Comparison of the Properties of Several Permanent Industrial Magnets

Magnets	Remanence, B_r (T)	Coercitivity, H_c (T)	Energy product, BH_{max} (kJ/m^3)	Curie temperature, T_c (°C)
Ferrites	0.36	0.36	25	450
AlNiCo	1.35	0.07	50	750
SmCo5 sintered	1	0.83	160	720
Sm2Co17 modified and sintered	1.15	0.6	180	800
Nd2Fe14B sintered	1.2	1.2	300	310
Nd2Fe14B bonded	0.6	0.6	80	310

The $SmCo_5$ alloy has a hexagonal structure which is formed by alternate layers of Co and mixed Sm/Co. The result is a strong anisotropy leading to an easy magnetization along the c axis of the unit cell. The phenomena is enhanced due to the strong magnetic anisotropy of Sm atoms.

By reference to Fig. 13.2b this means that during the magnetic polarization the resistance of the material to the dipole alignment is minimized. As a consequence the applied field H is moderate.

In addition, the demagnetization is difficult leading to a high value of coercitivity $H_c = 5\text{-}10$ kOe or 0.5-1 T. This indicates that once the grains forming the final material have been magnetically aligned to saturation the reverse operation is difficult.

This is the sign of a strong barrier to the nucleation of reverse magnetic domains.

$SmCo_5$ magnets were the first to attain an energy product of 20 MGOe or 160 kJ/m^3.

The Sm_2Co_{17} magnets correspond to more complex compositions in which Co can be partially substituted by Fe, Cu, Zn, and Zr. The objectives are to decrease the cost of the magnet in lowering the percentage of expensive Co as well as to increase some performances such as the resistance to demagnetization with temperature.

The material is more complex and the performances are related to microstructures control which requires a critical heat treatment. Here, high field is necessary for the initial magnetization. The crystal structures are related to two types: the rhombohedral Th_2Zn_{17} or the hexagonal Th_2Ni_{17}. Both of them exhibit high anisotropy due to their layer structure. Compare to $SmCo_5$ which belong to the $CaCu_5$ crystal type the unit cell is much larger.

The superiority of this magnet, as shown in Table 13.2, is due to a high $T_c = 800$ °C as well as a high energy product. Even if those magnets are rather expensive because of the high cost of Co and rarity of Sm they are desirable for selected applications; for instance, when resistance to temperature is needed and when cost is not a limiting factor such as in defense applications.

The industrial preparation of the SmCo magnets is a delicate operation due to the sensitivity of both metals Sm and Co to oxygen. All the operations need to be conducted under controlled atmosphere usually argon in order to avoid oxidation. More information on the preparation of Sm metal is given in Chapter 6.

Powder metallurgy is used and the different steps to produce the magnets are the following: (1) melting of the metals into an induction furnace in a highly controlled atmosphere, (2) casting of the alloy by fast quenching techniques followed by crushing, grinding, or milling under neutral argon to obtain particles with an homogeneous size of about 5 μm. (3) Compaction of the powder via mechanical or isostatic pressing. The powder is magnetically aligned during or prior to compaction. (4) After compaction the compressed powder is sintered.

The density of the ingots prior to compaction is about 50% but is 100% after the sintering operation. High density and good magnetic properties are obtained by adding a small amount of powder containing excess of Sm metal before compaction. This process which aids in attaining high density is called liquid phase sintering.

More complete information on the fabrication of RE magnets will be given in Chapter 14. It must be noticed that the SmCo magnets are known to be brittle and that the sensitivity to air corrosion increases with temperature. They need to be protected by an inert metallic coating such as Ni.

13.4.2 Nd/Fe/B magnets

Many efforts to produce cheaper permanent magnets led to two simultaneous discoveries of the composition $Nd_2Fe_{14}B$ corresponding to a tetragonal structure having a strong uniaxial anisotropy and a high $T_c = 300$ °C located significantly above RT.

Discovery was announced by Sumitomo special metals Co in Japan in 1984 using a process similar to the method used for the fabrication of $SmCo_5$. Almost, at the same time, an equivalent composition was published by General Motor Co using a slightly different procedure based on rapid solidification technique. Taking into account the importance of the technological breakthrough this situation has led to patents disputes.

Magnets prepared through both routes can be obtained in large scale for commercial production and have largely replaced the Sm/Co alloys because of their lower prices. Fe is far cheaper than Co, while Nd is cheaper and about four times more abundant than Sm.

In addition, the $Nd_2Fe_{14}B$ composition contains relatively little RE elements with only ~12 atomic %.

It is interesting to notice that all the REs, except La, are able to form this remarkable uniaxial tetragonal structure. They can form solid solutions without phase separation. As a consequence Nd can be partially substituted by heavy RE such as Dy or Tb.

Both metals are important because they increase coercivity as well as the resistance to demagnetization with temperature. This observation is critical for practical applications at high temperature and raises the question of Dy availability. A similar situation is met when partially replacing Fe by Co which raises the Curie temperature and improves remanence but on the contrary decreases coercivity.

Examination of the $Nd_2Fe_{14}B$ structure indicates that the solid can be described as a layer structure with alternate stacking sequence of a Nd-rich layer and a sheet formed only by Fe atoms. The boron atoms which are in minority and as light atoms difficult to detect by X-ray diffraction are probably located in the vicinity of the RE. The small boron atoms which are diamagnetic and nonmetallic do not participate in the magnetism but like C atoms in steel contribute to reinforce the cohesion of the material by strong covalent bonding. Examination of the Fe/Nd/B phase diagram in the vicinity of the strategic composition $Nd_2Fe_{14}B$ indicates that the role of boron is to bring the alloy close to the liquid phase of a eutectic composition which helps improve homogeneity.

The powder metallurgy for NdFeB magnet is the same as for the SmCo magnets with only minor differences. The grains size of the powder before compaction is about 3 μm. More details on the powder metallurgy will be given in the next chapter.

13.5 MAGNETO-CRYSTALLINE ANISOTROPY, THE KEY TO THE EXCEPTIONAL PROPERTIES

The main reason for the superiority of RE permanent magnets lies in their high magnetocrystalline anisotropy which is defined as the stability of the magnetization direction with respect to the crystal axes. Strong uniaxial magnetic anisotropy is a prerequisite to outstanding magnets and is the explanation for high coercitivity and remanence which distinguished “hard” permanent magnets from “soft” materials.

The anisotropy is a combined effect of spin-orbit coupling and electrostatic crystal-field interactions.

As described in Chapter 8, 4f electrons are shielded from the crystalline field generated by the local ionic environment. As a result the spin-orbit coupling is not perturbed by the crystalline field, that is, the magnetic moment generated by an electron spin interacts strongly with the magnetic field created by the electron’s own orbital motion. This in turn ensures that the 4f electronic cloud is rigidly coupled to the spin as depicted in Fig. 13.4.

This property is key to understanding the magnetocrystalline anisotropy which results from preferential orientation of the orbitals along specific crystalline axis due to the electrostatic interaction between the 4f charge cloud and the ionic crystalline field. This interaction depends on the shape of the 4f shells and the symmetry of the crystalline field (Fig. 13.5).

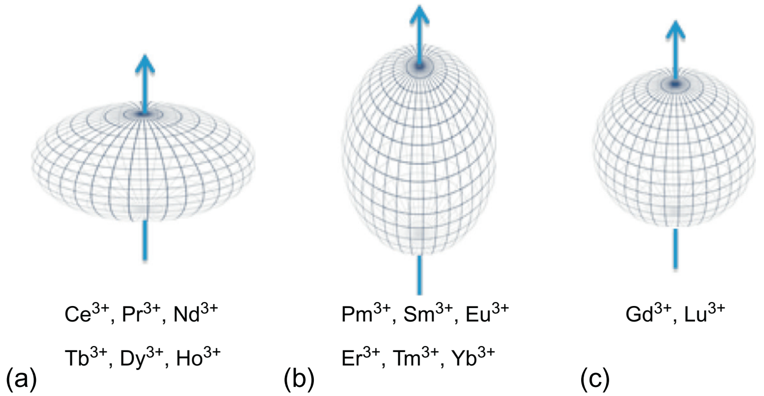

FIG. 13.4

Rare earth single ion anisotropy showing the oblate and prolate shape of the 4f electron cloud for various lanthanide ions.

Drawing by Prof. Lucas.

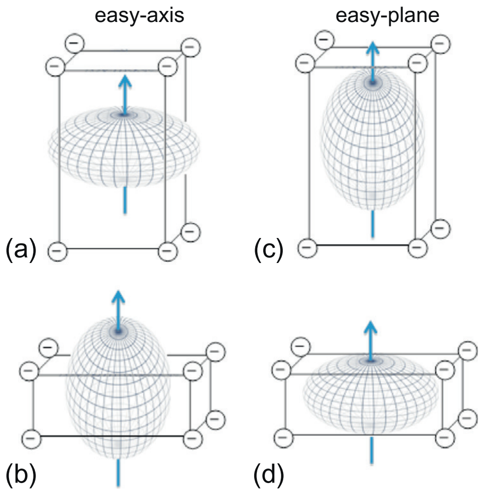

FIG. 13.5

Crystal-field interaction of prolate and oblate ions in a tetragonal environment. The arrow represents the magnetization direction. Easy-axis configurations lead to strong permanent magnet while easy-plane configurations lead to soft magnets.

Drawing by Prof. Lucas.

The 4f charge clouds exhibit asymmetric shapes as a result of Hund's second rule. The 7f orbitals have different shapes and are filled in a specific order according to Hund's rule. Orbitals with positive angular momentum have prolate character elongated along the *z*-axis while orbitals with negative angular momentum have oblate character flattened along the *x*-*y* basal plane. Hund's rule states that when electrons are orbiting in the same direction (positive orbital angular momentum) they meet less often and consequently experience less repulsion.

As a result, filling of 4f shells in RE ions starts with oblate orbital and leads to the overall shape depicted in Fig. 13.4a which is adopted by Ce^{3+} ($4f^1$), Pr^{3+} ($4f^2$), and Nd^{3+} ($4f^3$).

The filling continues with prolate orbitals leading to the 4f charge cloud shape depicted in Fig. 13.4b which is adopted by Pm^{3+} ($4f^4$), Sm^{3+} ($4f^5$), and Eu^{3+} ($4f^6$).

A full shell then results in a spherical shape (Fig. 13.4c) adopted by Gd^{3+} ($4f^7$).

The pattern repeats itself for the heavy RE with:

Tb^{3+} ($4f^8$), Dy^{3+} ($4f^9$), Ho^{3+} ($4f^{10}$): prolate shape
Er^{3+} ($4f^{11}$), Tm^{3+} ($4f^{12}$), Yb^{3+} ($4f^{13}$): oblate shape
For Lu^{3+}($4f^{14}$) the full shell again results in a spherical shape.

The magnetocrystalline anisotropy originates from the preferential alignment of the 4f electronic cloud along the crystal-field axis in a way that minimizes repulsion from the crystal-field charges as depicted in Fig. 13.5.

For example the tips of the prolate charge cloud in Fig. 13.5c would be repelled by the tetragonal crystalline field while the oblate charge cloud in Fig. 13.5d would be repelled by the quasi-planar distribution of negative crystal-field charges. As a consequence, the magnetization would be forced from the *z*-axis into the *x*-*y* plane and this configuration is therefore termed "easy-plane."

In contrast, the configuration depicted in Fig. 13.5a and b involves an electronic cloud pointing away from the crystal-field charges which leads to strong magneto-crystalline anisotropy and results in superior permanent magnet properties.

A striking illustration of this effect is observed in $Ln_2Fe_{14}B$ compounds where the crystal field is of the type depicted in Fig. 13.5c. As shown in Fig. 13.4 Sm^{3+} is a prolate ion and consequently $Sm_2Fe_{14}B$ exhibits easy-plane anisotropy and has soft magnetic properties. In contrast Nd^{3+} has an oblate shape which adopts the easy-axis configuration shown in Fig. 13.5a. As a result, $Nd_2Fe_{14}B$ is the strongest permanent magnet ever developed.

It should be clearly emphasized that the high anisotropy of these magnets is largely due to the RE sublattice despite the fact that REs usually represent a small fraction of the atomic composition.

By contrast the 3d elements such as Fe which are in majority ensure the strong magnetization and Curie temperature in bringing a maximum of unpaired electrons to the magnets.

For example $SmCo_5$ and $Nd_2Fe_{14}B$ magnets contain a large amount of the TM Fe ($3d^64s^2$) and Co ($3d^74s^2$). Both are very rich in unpaired electrons.

13.6 QUALIFICATION, CODIFICATION OF THE RE MAGNETS

As already mentioned the NdFeB magnets are dominating the market and the SmCo materials are used only when the performances of the NdFeB magnets are affected namely with an elevation of the temperature.

For instance at RT the average energy product BH_{max} for SmCo is 25 MGOe or 200 kJ/m^3.

In the same condition BH_{max} for the NdFeB magnets is 40 MGOe or 320 kJ/m^3 and values as high as 400 kJ/m^3 have been reached. This means clearly that the Nd-based magnets are almost twice as powerful as the Co-based magnets.

13.6.1 What are the changes of the performances with temperature?

First remember that the Curie temperature T_c is 300 °C for NdFeB and 750 °C for SmCo. This is an indication that the Nd magnets will be more affected than the Sm magnets by temperature.

If one refers to the average values of the industrial literature it is well accepted that the limit of utilization T_{max} for NdFeB is 80 °C and for SmCo is 300 °C.

The two magnets have almost the same BH_{max} at $T = 150$ °C but above this temperature the SmCo magnets have superior performance.

Table 13.3 allows a comparison of the technical characteristics of the different industrial magnets.

13.6.2 How to improve the temperature dependence of the Nd-based magnet?

Nd-based magnets, also called *NIB* for Nd/iron/boron or *Neo* for neodymium, are common commercial products but depending on the producer, they can vary slightly in composition as well as in synthesis method.

Substitution of the light RE Nd ($4f^3$) by the neighbor Pr ($4f^2$) has been used as a way of reducing production cost by using Nd metal which has not been purified from Pr. In addition to reducing cost it can help tuning the performances.

To improve T_{max} it has been demonstrated that the partial substitution of Nd^{3+} by the heavy RE Dy^{3+} ($4f^9$) with five unpaired electrons was very beneficial. The composition of such magnets produced industrially by Shin-Etsu is depicted in Fig. 13.6.

Table 13.3 Comparison of Technical Characteristics for Industrial Magnets

Family	B_r (T)	H_c (T)	BH_{max} (kJ/m^3)	T_{coef} of B_r (%)	T_{max} (°C)	T_c (°C)
Ferrites	0.39	0.36	25	−0.20	280	280
AlNiCo	1.25	0.07	50	−0.02	540	540
SmCo	1.15	0.8	200	−0.04	300	300
NdFeB	1.3	1.2	320	−0.12	80	80

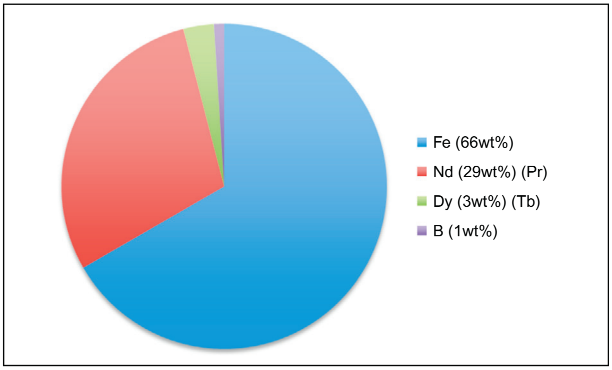

FIG. 13.6

Composition of Dy-substituted NdFeB magnet.

Courtesy of Shin-Etsu RE magnets.

This situation improves the anisotropy and consequently the resistance to demagnetization, in the present case due to thermal motion. Dy^{3+} can be mixed with neighboring Tb^{3+} ($4f^8$) without affecting the properties.

The microstructure plays a crucial role on the magnetic properties. Magnetization as well as demagnetization can be altered or improved by controlling the size, shape, and orientation of the grains. This will be discussed in the next chapter.

There are currently many industrial magnet producers. Among them are for instance Arnold, Magcraft in the USA, Shinetsu-rare earth magnets in Japan, Tasman Metals in Europe, and China Rare Earth Magnet LtD in China.

13.6.3 Codification of the magnets

In order to normalize the magnet specifications the producers have assigned a code to each magnet which represents the material grade.

The codification of a Nd magnet is for instance N30, M40, H35, SH40, EH35, and UH35.

The numerical value corresponds to the maximum energy product and is expressed in MGOe.

The letters codify the maximum utilization temperature:

N = 80 °C, M = 100 °C, H = 120 °C, SH = 150 °C, UH = 180 °C, EH = 200 °C.

The characteristics of several NdFeB magnets according to their codification are presented in Table 13.4.

13.7 SUMMARY

This chapter reviewed the fundamental properties of RE magnets.

Two main family of RE magnet are currently produced industrially: NdFeB and SmCo.

Table 13.4 Codification of NdFeB Magnets According to Their Performances

Codification	Remanence, B_r (T)	Coercitive Force, H_c	BH_{max} (kJ/m^3)	T_{max} (°C)
N40	1.26-1.29	1.05-1.20	300-320	80
M50	1.40-1.46	1.08-1.25	370-400	100
H44	1.32-1.36	1.08-1.3	330-350	120
SH40	1.26-1.22	1.08-1.20	300-320	150
UH33	1.14-1.17	1.03-1.15	250-280	180
EH35	1.17-1.21	1.08-1.15	260-280	200

NdFeB are stronger magnets but have a low Curie temperature (the temperature at which the thermal motion leads to loss of magnetization).

SmCo have much higher Curie temperature and are consequently selected for applications requiring high temperatures.

The REs represent only a small fraction of the atomic composition but are the main source of the superior magnetic properties due to their strong anisotropy.

The RE anisotropy, also called magnetocrystalline anisotropy, is the result of strong spin-orbit coupling of the 4f electrons which aligns the magnetic moment with the axis of the electronic cloud.

Strong coupling of the electronic cloud with the crystalline field called "easy-axis" configuration leads to strong magnetocrystalline anisotropy and results in hard magnet properties.

The next chapter will be devoted to the manufacturing and the uses of the magnets.

Suggested Reading

Anderson, J.J., 2010. Structural and magnetic properties of neodymium-iron-boron clusters. Thesis 2010. University of Nebraska, Lincoln.

Constantinides, Steve, Arnold Magnetic Technologies Corporation, 2012. The demand for rare earth materials in permanent. In: 51st Annual Conference of Metallurgist COM 2012, Niagara Falls September 30 to October 3, 2012.

Cullity, B.D., Graham, C.D., 2008. Introduction to Magnetic Materials, second ed. Wiley.

Kramer, M.J., et al., 2010. Prospects for non-rare earth permanent magnets for traction motors and generators. JOM. 64 (7), 752.

Coercivity and remanence in permanent magnets. hyperphysics.phy-astr.gsu.edu/.../magperm.html.

Sagawa, Masato, Fujimura, Setsuo, Yamamoto, Hitoshi, Matsuura, Yutaka, Hiraga, Kenji, 1984. Permanent magnet materials based on rare earth-iron-boron tetragonal structure. IEEE Trans. Magn. 20 (5), 1584–1589.

Skomski, R., Sellmeyer, D.J., 2009. Anisotropy of rare earth magnets. J. Rare Earths. 27 (4), 675.

CHAPTER

14

Rare Earth-Based Permanent Magnets Preparation and Uses

14.1 INTRODUCTION

Chapter 13 described the fundamental role of rare earth (RE) in high performance magnets.

This second chapter focuses on the synthesis and practical use of RE magnets.

RE magnets have a figure of merit BH_{max} up to 10 times higher than conventional ferrous magnets.

The low temperature resistance T_{max} of NdFeB magnets can be considerably improved by substitution with Dy or Tb. The content of these expensive heavy RE elements can be minimized by localizing them at grain boundaries while retaining optimal magnetic properties.

The production of magnet is achieved by powder metallurgy following a process involving purification of components followed by induction melting in the final appropriate composition, casting, grinding, compaction and magnetic alignment of grains, sintering, and pulse magnetization.

NdFeB alloys are by far the most widely used magnets due to their high energy product BH_{max}. However, they are sensitive to oxidation and must be coated with a metallic (Ni) or polymeric (epoxy) layer.

These magnets are used in a very diverse range of applications including power generation (e.g., windmills), electrical motors, loudspeakers, magnetic separation, medical instrumentation, and household products such as latches or kids toys.

14.2 THE SUPERIORITY OF THE RE MAGNETS

As discussed in Chapter 13 it is well established that RE magnets dominate the world of commercial magnets.

Fig. 14.1 illustrates the historical trend in the improvement of the maximum energy product BH_{max} for commercial magnets. BH_{max} is a figure of merit which combines the two critical properties of a magnet: the magnetic strength characterized by the remanence (B_r) and the resistance to demagnetization characterized by the coercivity (H_c) (see Chapter 13).

Fig. 14.1 clearly illustrate why RE magnets are now dominating the market.

Rare Earths. http://dx.doi.org/10.1016/B978-0-444-62735-3.00019-X

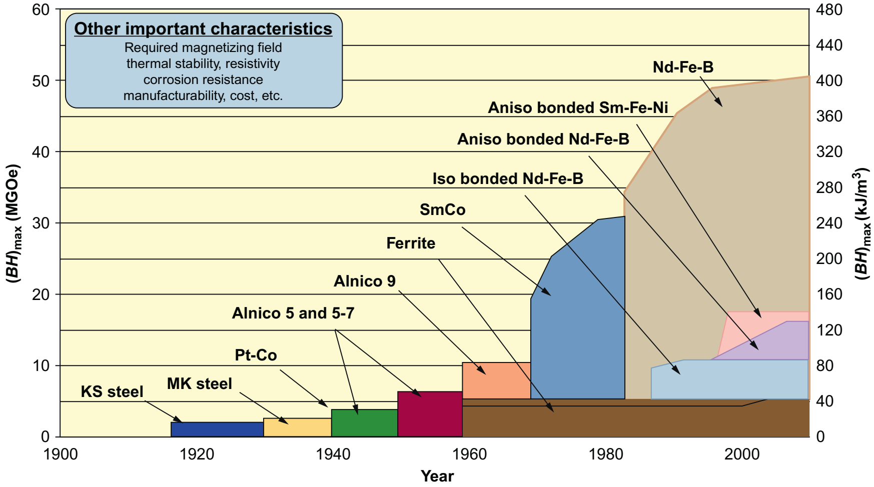

FIG. 14.1

Evolution of the energy product BH_{max} at room temperature during the last decades for commercial permanent magnets.

Courtesy of Arnold Magnetic Technologies.

NdFeB and SmCo magnets have a figure of merit, respectively, 10 times and 6 times superior to standard ferrite magnets. Even AlNiCo magnets made from aluminum, nickel, and cobalt exhibit far lower performances.

It should also be mentioned that “bonded” magnets are made of grains of magnetic RE materials dispersed into a polymeric matrix such as an epoxy resin. The easy shaping allowed by these composite materials comes at the cost of significantly lower performances.

Nd and Sm are relatively inexpensive relative to other REs (see Chapter 2); hence, the production of these RE magnets is economically viable. Nevertheless, the rapidly increasing demand for these strategic materials stemming from the rapid growth of new technologies such as hybrid cars or wind turbines raises the question of their industrial and geopolitical availability.

14.3 SOME LIMITATIONS OF RE MAGNETS AND CURRENT REMEDIAL STRATEGIES

The decay in magnet strength with increasing temperature is a critical factor as explained in Chapter 13. For many important applications, such as traction motors and power generators, stable performances are required above 150 °C.

Yet, the most effective RE magnets, NdFeB, have a maximum working temperature $T_{max} = 80$ °C. Since mass production of NdFeB magnets is the most economical solution, it is desirable to increase its maximum working temperature T_{max} to much greater values.

This operation is realized by partially substituting Nd with Dy or Tb. The different approaches used to optimize this process are described in the following sections.

14.3.1 Direct substitution of Dy in Nd-Fe-B alloys

The direct substitution of Nd by Dy in NdFeB alloys permits to raise T_{max} up to 220 °C for a substitution level of 12% in weight as illustrated in Fig. 14.2.

Dy substitution also simultaneously yields a linear increase in coercivity (H_c) and a linear decrease in remanence (B_r) as shown in Fig. 14.2, so that the overall figure of merit BH_{max} is not significantly altered.

This increase in coercivity, that is, the resistance to demagnetization by a magnetic field is consistent with the observation that the magnetization is also more resistant to thermal motion.

The Dy^{3+} ion with the atomic structure $4f^9$ has the same oblate configuration as Nd^{3+} and therefore also induces a strong magnetic anisotropy into the material (see Chapter 13). This factor is clearly beneficial for stabilizing the magnet against demagnetization.

The gain in temperature stability (T_{max}) is critical because for major applications such as power generators stability in time and temperature is more important than

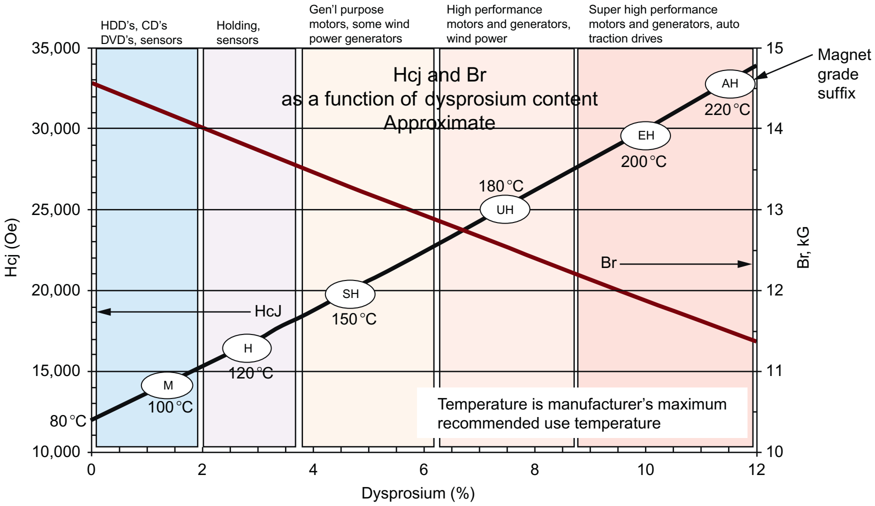

FIG. 14.2

Evolution of magnetic properties as a function of Dy substitution in Nd/DyFeB magnets. The letter symbols represent the magnet grade and are described in Table 13.4.

Courtesy of Arnold Magnetic Technologies.

power. The lifetime of a magnet for a generator is estimated to be 25 years and for traction drive motor 10 years or more.

The general use of magnets according to their grade is described at the top of Fig. 14.2. It is clear that Dy-containing magnets are needed for traction motors such as in the hybrid cars as well as in some wind power generators where temperature elevation cannot be excluded. Both sectors correspond to a growing market.

The major penalty of this substitution is in a more expensive alloy due to the significantly higher price of Dy. Hence novel approaches have been thought out to minimize its fraction while retaining its beneficial properties.

14.3.2 Substitution of Dy and Tb by grain boundaries diffusion method

Novel generations of RE magnets require high remanence, high coercivity, and high resistance to temperature. For economic reasons they must have the lowest content of heavy rare earths (HRE) such as Dy or Tb.

It has been demonstrated that optimum performances are observed when the HRE are concentrated at the grain boundaries of the ferromagnetic domains.

Indeed high accumulations of Dy or Tb at the grain boundaries prevent the nucleation of reverse magnetic domains which is the initial source of magnet degradation.

Two alloying processes have therefore been devised to localize the HRE at the grain boundary thereby reducing their overall fraction while retaining superior magnetic properties.

(1) In the first method called "two alloys process," two powders are prepared separately, one corresponding to the pure Nd alloy and the second to the alloy containing Dy or Tb.

The two powders are mixed and then sintered at high temperature. During sintering the HRE diffuse through the interface of the grains which results in a selective distribution of HRE near the grain boundary as depicted in Fig. 14.3.

This morphology leads to heat resistance and improvement in coercivity.

(2) The second method is called "grain boundary diffusion." In this method the NdFeB powder is coated with a thin layer of oxides such as Dy_2O_3 or fluoride TbF_3

Coating is made by dipping the samples into a slurry consisting of the Dy or Tb compounds in suspension into an aqueous or organic solvent.

Drying and heat treatment result in diffusion of HRE which concentrates at the grain boundaries. This process is even more effective at improving coercivity and enhancing the heat resistance as depicted in Fig. 14.4.

This method is suitable for mass production and is consuming a considerably smaller amount of HRE.

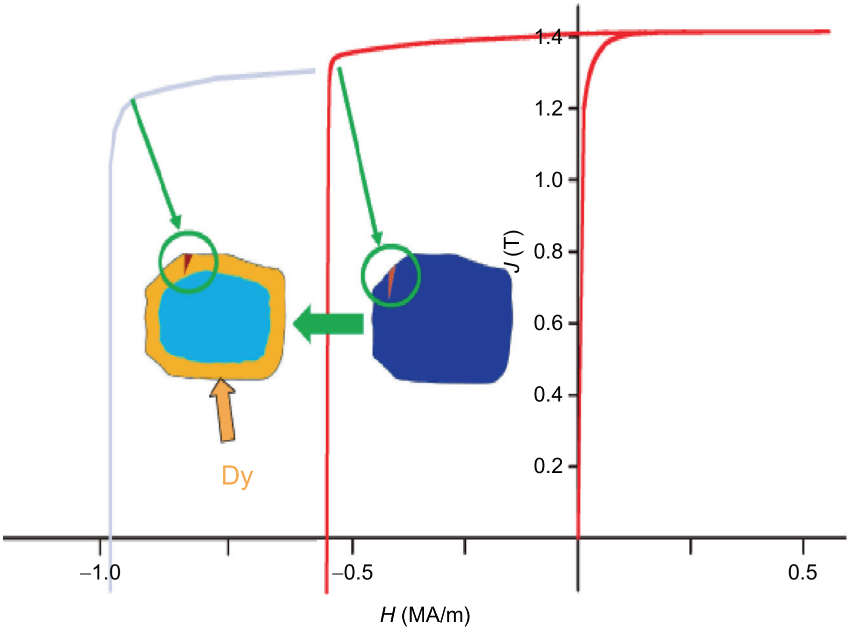

FIG. 14.3

Resistance to demagnetization of a NdFeB magnet treated by diffusion of Dy at the grain boundary. The nucleation of reversed magnetic domain shown by the arrow is hampered by the diffusive layer of Dy.

Courtesy of Shin-Etsu.

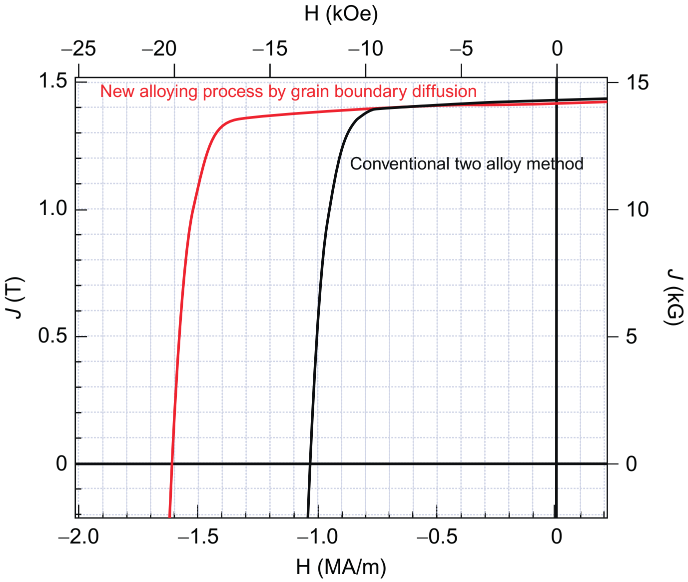

FIG. 14.4

Gain in coercivity for a RE magnet prepared by the two alloys method and the grain boundary diffusion process.

Courtesy of Shin-Etsu.

14.4 PREPARATION OF RE MAGNETS BY POWDER METALLURGY

The fabrication of RE magnets is a complex process which involves several steps including:

- Production of the component metals
- Induction melting in appropriate composition ratio
- Milling into fine powder
- Compacting and magnetic alignment of grains
- Sintering into a dense solid and pulsed magnetization

Each of these steps is described in the following section.

14.4.1 Production of neodymium-iron and dysprosium-iron alloys

For the fabrication of the NdFeB magnets Nd and Dy are not prepared as pure metals. Indeed they are directly alloyed to Fe during a unique electrolysis process called "oxides feed-fluoride molten salt electrowinning" described in Chapter 6.

In this method Nd^{3+} is reduced to Nd^0 metal by electrolysis in a molten salt composed of a mixture of CaF_2, LiF, BaF_2, and NdF_3 in which Nd_2O_3 is dissolved to produce Nd^{3+} ions.

The originality of the method resides in the fact that the cathode is in pure iron (Fe) which combines with Nd^0 to form an alloy containing about 55 at.% of Nd.

The process is continuous since the Fe electrode is replaced when needed and the molten salt is permanently fed with pure Nd_2O_3.

Dysprosium-iron alloys are produced in a similar way.

This method yields Nd/Fe and Dy/Fe alloys of purity around 99.9 wt.% which can be directly used for magnet production.

14.4.2 Production of samarium metal

In contrast, Sm metal is not made by electrodeposition because the electrical potential required to decompose the oxides and halides is higher than the decomposition potential of suitable fused salts.

Samarium metal is prepared by metallo-thermic reduction using lanthanum as a reductant according to the following reaction:

$$Sm_2O_3\ \text{solid} + \text{La metal liquid} \rightarrow \text{Sm metal vapor} + La_2O_3\ \text{solid}$$

The reaction is conducted under vacuum in a tantalum container at a temperature of 1200-1300 °C and the vapors of Sm^0 are collected in the cold part of the system.

This process is discontinuous.

14.4.3 Heating and casting the RE alloys

Once the pure metallic components are obtained, the alloys are melted in appropriate ratio to produce the magnets.

As a general comment, all the operations leading to the production of a metallic complex melt followed by casting need to be conducted under oxygen-free atmosphere, usually under argon.

The melt is obtained by heating the appropriate quantity of Nd (Dy), Fe, and B into an induction furnace as shown in Fig. 14.5.

14.4.4 Preparation of fine particles

After casting the melt, the alloy is first transformed into medium size particles by coarse grinding (Fig. 14.6a).

The NdFeB cast alloy is then conveniently turned into fine powder at low energy cost using the hydrogen decrepitation method. In this method the lattice expansion generated by absorption of hydrogen generates stresses, leading to the decrepitation of the alloy by intergranular fracture. This process is conducted very simply by exposing the alloy to pure hydrogen environment.

Fine and homogeneous powder is then obtained by jet milling as shown in Fig. 14.6b.

SmCo alloys are sufficiently brittle that hydrogen decryption is not necessary.

At the end of milling or pulverization, the grains sizes are around 3 µm for the NdFeB alloy and 4-5 µm for SmCo alloy.

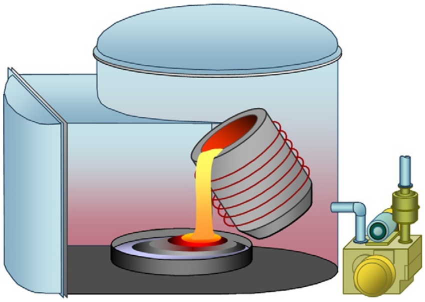

FIG. 14.5

Production of RE magnet by vacuum induction melt. The starting materials Nd/Fe alloy + additional Fe + B are melted under controlled atmosphere in a vacuum induction furnace and cast.

Courtesy of Shin-Etsu.

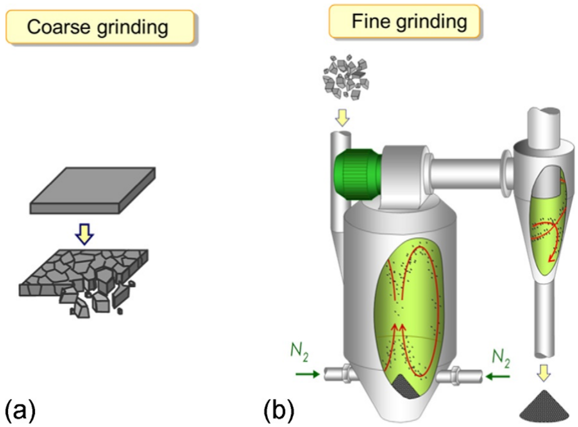

FIG. 14.6

(a) Coarse grinding of a casted metal plate. (b) Schematic representation of the pulverization process.

Courtesy of Shin-Etsu.

14.4.5 Compaction of the fine particles and magnetic alignment

The compaction of the powders is made by mechanical, hydraulic, or isostatic pressing. The mold used for compaction must be designed to match the final shape of the desired object.

Magnetic grain alignment is conducted *in situ* during compaction by magnetic alignment under a strong magnetic field as depicted in Fig. 14.7a.

The powder is compacted and magnetically polarized at the same time under a magnetic field $H \approx 3$ T.

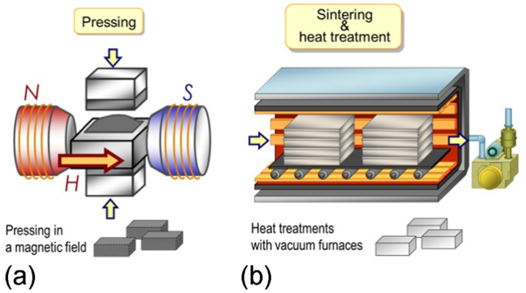

FIG. 14.7

(a) Schematic view of compaction and magnetic grain alignment conducted simultaneously; (b) schematic view of the sintering and annealing process.

Courtesy of Shin-Etsu.

14.4.6 Sintering at high temperature and pulse magnetization

The next operation is sintering at 1000 °C and then annealing to the final density.

The density of the samples prior to sintering is about 50% of the true density but reaches 100% after sintering. Through the process the ingots dimensions shrink by about 70-80% and their volume is reduced by about 50%. A schematic representation of the sintering process is shown in Fig. 14.7b

At that point the magnet has reached its final morphology and only needs to be magnetically activated. This is performed by pulsed magnetization due to the extremely high field (6 T or 60 kOe) required for RE magnet in comparison to conventional magnets (1 T, 10 kOe).

The magnetic field is produced in a magnetizing coil using high pulsed currents (30 kA) as depicted in Fig. 14.8. The magnetization process is very rapid and pulse durations of less than a millisecond are sufficient.

The last step of the procedure is to control the samples magnetic properties by submitting it to cyclic magnetic polarization as represented in Fig. 14.9.

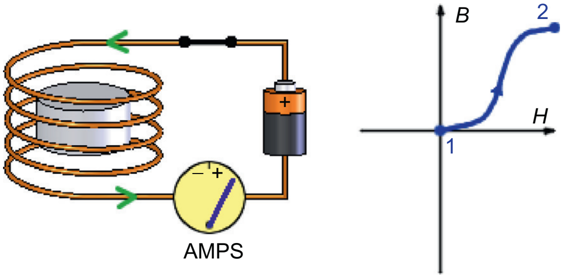

FIG. 14.8

Magnetization of a rare earth (RE) alloy by delivery of pulsed of high current in a magnetization coil.

From K&J Magnetics.

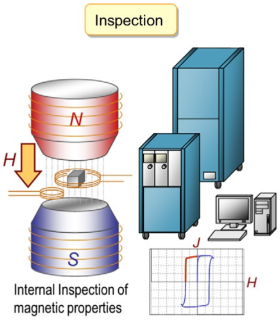

FIG. 14.9

Inspection of the magnetic properties of the samples.

Courtesy of Shin-Etsu.

The control consists in measuring B_r, H_c and performing a hysteresis loop experiment.

14.5 SOME PRACTICAL INFORMATION CONCERNING NdFeB MAGNETS

14.5.1 Shaping and surface protection by coating

The final complex shape of NdFeB magnets is obtained by grinding, slicing, holes drilling, and/or machining.

This is not an easy process since sintered Nd-Fe-B magnets behave like a ceramic and have tendency to crack and chip when drilled.

Additionally, the powder produced when machining these magnets is flammable.

The NdFeB magnets are produced under huge varieties of shapes and designs as represented in Fig. 14.10.

NdFeB alloys are very easily oxidized; hence, commercial magnets must be protected from corrosion by surface coating.

Epoxy coating can be used for low temperature applications while metal coating by electrodeposition is most common for higher temperature applications.

High-grade NdFeB magnets are most commonly plated with nickel. Ni provides a hard and shiny coating that is corrosion resistant. In addition to nickel, other metals such as copper, zinc, tin, silver, and gold can be used. Multimetal deposition such as Ni/Cu/Ni provides a very efficient barrier against corrosion.

Metal deposition is performed by electroplating as depicted in Fig. 14.11.

Notice that the SmCo magnets are very resistant to corrosion. They do not need to be coated.

14.5.2 Magnetic orientation

A magnet can be magnetized in a variety of directions. Fig. 14.12 describes some examples of magnetization pattern from simple axial to complex multipolar orientations.

In some production methods magnets need to be incorporated into assemblies in a nonmagnetized state. They will be magnetized latter when the assemblies are completed.

Magnetization of a multipole magnet such as that described in Fig. 14.12 is a complex process requiring electric coils with complex geometry.

Fig. 14.13 illustrates different strategies for polarizing such magnet using an anisotropic applied local magnetic field.

14.5.3 Bonded magnets, packaging, and safety issues

Bonded magnets are polymer-based magnets. They are obtained by mixing the powder of the magnetic materials with various polymers.

FIG. 14.10

Samples of NdFeB magnets.

Courtesy of Shin-Etsu RE magnets.

The main motivation is to gain in materials flexibility for complex shaping. Another benefit is a good protection of the magnetic grains against corrosion.

Once the magnetic powder has been mixed with polymer it can be injection molded or cast into flexible magnetic sheets.

As expected, the drawback of bonded magnets is in their low energy product. In average $BH_{\max}$ is divided by four compared to a sintered magnet.

Packaging of strong permanent magnets poses a unique challenge due to their intense magnetic flux which can damage electronic instruments such as cell phones,

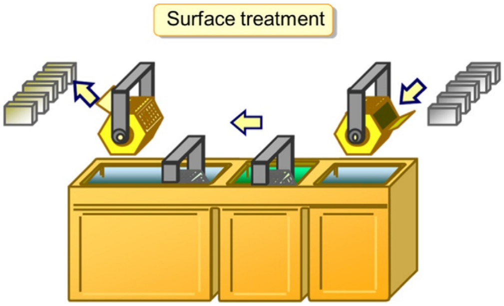

FIG. 14.11

Schematic representations of magnets coating.

Courtesy of Shin-Etsu.

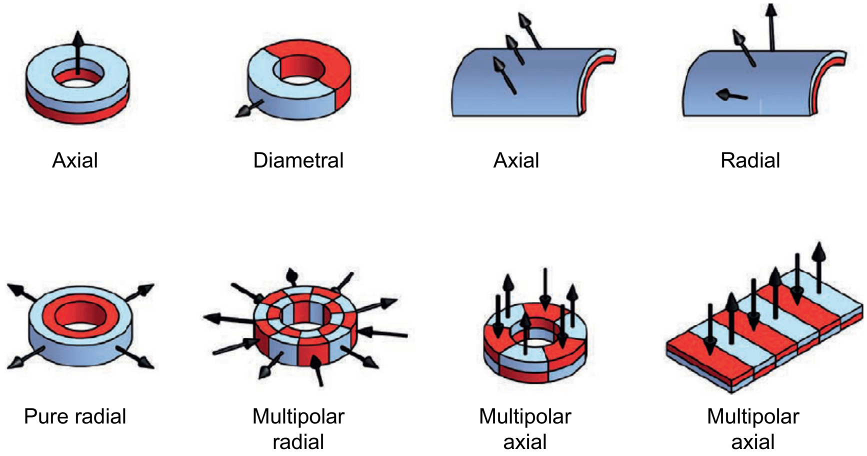

FIG. 14.12

Different magnetic polarizations depending on the shape of the magnet.

Courtesy of Brian R. Palakow, Le USA Walker Scientific Inc.

TV, computers, or information storing devices such as credit card, floppy disk, magnetic ID, and video tapes.

Magnetic flux can be only redirected by using for instance steel which provides a path for the flux to move.

14.6 APPLICATIONS OF RE MAGNETS

As described in Fig. 14.1, NdFeB alloys constitute the most recent generation of RE permanent magnet materials and have largely surpassed the two Sm/Co alloys due to their combination of high performance and low price.

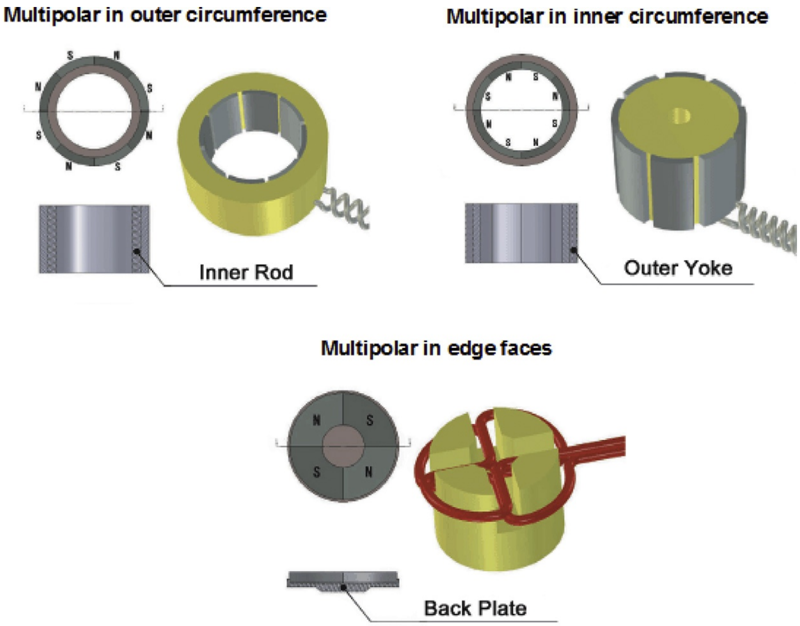

FIG. 14.13

Multipolar magnetizations of RE magnets using anisotropic field application.

Courtesy of Shin-Etsu Rare Earth Magnets.

They are widely adopted in many fields such as energy, transportation, machinery, medical treatment, home appliances, and others. Table 14.1 presents a breakdown of percentages of RE magnets used in each application.

The application domains of permanent magnet cover several broad categories of applications. The main domains of application are discussed in the following section.

14.6.1 Applications related to attractive magnetic forces

The category of applications most familiar to general consumers relates to the unique attractive force produced by magnets. This includes numerous household applications for magnetic holding devices such as latches or simple fridge magnets.

This function is illustrated in Fig. 14.14 which portrays the strong holding capability of the magnet. A high-quality NdFeB magnet can easily lift thousand times its own weight.

The same principle of attractive force is used industrially in magnetic separators. These devices are used to remove metal particle contamination from agricultural product, coal, chemicals, pharmaceuticals, plastic and rubber recycling, etc.

Table 14.1 Projected 2015 Industrial Uses of Neodymium-Iron-Boron Permanent Magnets

Application	Estimated 2015 % of Use
Permanent magnet motors: industrial, automobile, etc.	25
Hard disk drives: compact disk, digital video disk	14
Wind power generators	10
Electric bicycles and scooters	8
Transducers, loudspeakers	7
Hybrid and electric traction drives	7
Magnetic separation	4
Torque-coupled drives	3
Energy storage systems	3
Air conditioning compressors and fans	3
Magnetic resonance imaging scanners	2
Sensors	2
Hysteresis clutches	2
Generators	1
Miscellaneous gauges, brakes, relays and switches, pipe inspection, levitated transportation reprographics, refrigeration, and all others	9

Permanent magnet electric motors are the largest application.
Prepared by William Davenport from data kindly provided by Steve Constantinides.

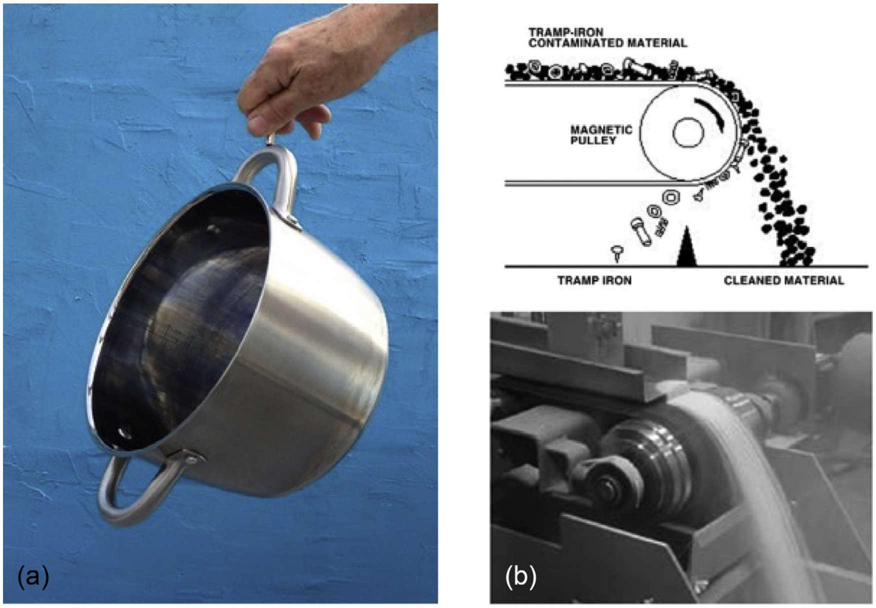

FIG. 14.14

(a) Example of strong attraction between a NdFeB magnet and a soft magnetic component such as a piece of iron or steel. The size of the magnet in the picture is 4 mm in diameter and 30 mm in length. The holding power is 2.7 kg. Photo Jacques Lucas Tone Andresen; (b) Schematics and image of a magnetic roll separators made from RE magnets used for dry stream separation.

Courtesy of Eriez Manufacturing Co.

Many configurations of magnetic separators can be used depending on the application, including plates, grates, rolls, or tubes. An example of RE roll magnetic separator is illustrated in Fig. 14.14.

Other applications include magnetic torque limiters or magnetic bearings which rely on magnetic levitation to support moving parts without physical contact.

14.6.2 Applications related to power generation

This category of applications involves the uses of strong magnetic fields to convert mechanical energy into electricity.

Fundamental laws of electromagnetism show that when a magnet moves in the neighborhood of an electrical conductor such as copper it induces the displacement of electrons.

Among the most important applications are the magnetos, the alternators, and the power generators. The need for alternative source of energy has recently driven a considerable regain interest for wind turbines. The production of windmills is indeed one of the fastest growing markets for NdFeB permanent magnet. An example of offshore windmills is represented in Fig.14.15a. Each power generator uses several tons of NdFeB permanent magnet in the hub at the top of the windmill.

One of the key mechanical parts in a classical wind mill is the gearbox which converts the propeller speed from around 10 to 20 RPM in normal wind conditions into a much faster speed. Due to mechanical stresses the gearbox is the weak point in a windmill.

The use of NdFeB magnets enables novel low speed generator designs without the need for gearboxes (Fig. 14.5b). This improves windmill reliability and lifetime by lowering vibrations and reducing the number of moving parts by 50%. The resulting reduction in maintenance is particularly important for offshore installations.

14.6.3 Applications related to electrical motors

The third category of application and by far the most important in terms of market involves the use of magnets to convert electrical energy into mechanical energy.

The principle is opposite to that of power generation and in this case the magnets are put into motion by a magnetic field produced by an electrical current. The source of electrical energy can be that of the regular power grid but it is increasingly coming from batteries, in particular for electrical vehicles such as golf carts, electrical scooters, and hybrid cars.

Magnets for motors must be designed into specific shapes and polarization orientations as shown in Fig. 14.16a. The RE magnet is normally contained in the rotating assembly (rotor) while the stationary armature (stator) is composed of a conductor that induces a rotating magnetic field when connected to an electrical load as depicted in Fig. 14.16b.

NdFeB magnets are used in industrial motors, car motors, electric bicycle motors as well as in the small sophisticated motors driving the hard disks of our computers.

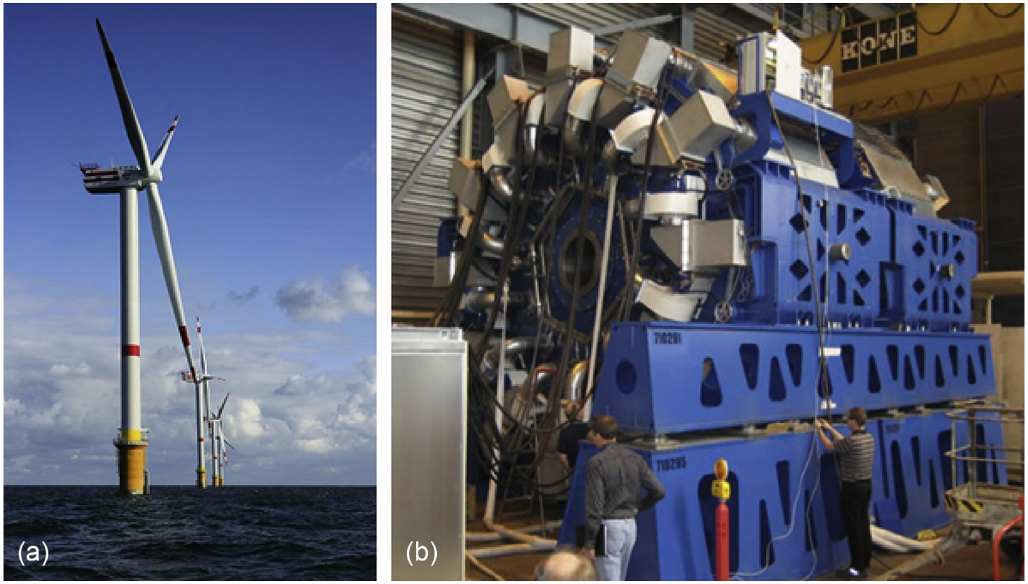

FIG. 14.15

(a) Photography of offshore wind turbines equipped with permanent magnet generator (PMG). These turbines produce 3.5 MW of power using about 2 t of magnets, which correspond to 0.6 kg of NdFeB alloys for the production of 1 kW. Rotor blades are up to 80 m long (Wikipedia commons photo). (b) PMG of a wind turbine using NdFeB magnets. Strong magnets enable gearbox-free generators to improve reliability and lower maintenance. Technicians give the size of the generator.

Courtesy of The Switch.

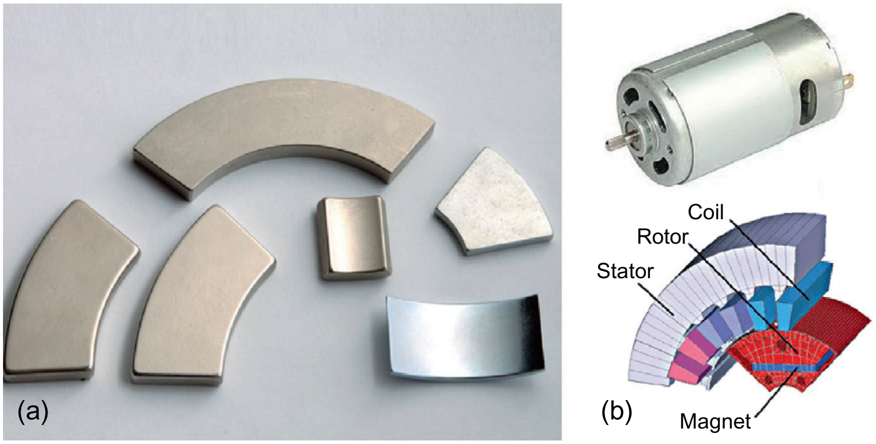

FIG. 14.16

(a) NdFeB magnets shaped in several forms and magnetized in different directions for designing motors for many types of applications. (b) Electrical motors. In the majority of designs the rotor contains the RE magnet and the stator is electrically connected to a load.

Courtesy of Shin-Etsu.

Electric traction motors used in hybrid vehicles such as the Toyota Prius represent an important growing market for the Nd magnets. About 1-1.5 kg of neodymium is used in each car.

14.6.4 Application related to transducers and sound production

Transducers are devices that convert an electrical signal into a mechanical signal and in the case of loudspeakers into an acoustic signal.

The principle of operation is based on the dynamic interaction between a static magnet and an oscillating metal coil attached to a diaphragm (see Fig. 14.17). When

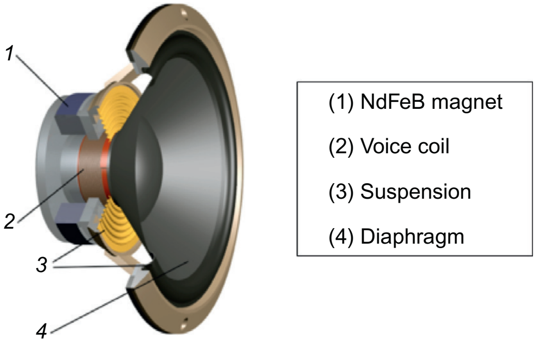

FIG. 14.17

Magnets for the growing market of loudspeakers.

From Wikipedia public domain.

an electrical signal is applied through the coil, the induced magnetic field repels the coil and the diaphragm. The resulting oscillatory motion produces sound waves which propagate in air.

Audio products are still an important market for magnets but they are increasingly being replaced by piezoelectric transducers especially for miniaturized devices. This market is therefore not expected to grow significantly in the future.

14.6.5 Application related to medical applications and imaging

This last category involves the use of RE magnets in medical and scientific instrumentation such as magnetic resonance imaging (MRI) or ion beam lithography.

Magnets are used for two general purposes:

- Aligning magnetic spins for resonance imaging and spectroscopy
- Manipulating beams of charge particles such as ions and electrons

In the first type of application, strong magnetic fields are used to align the nuclear spin of atoms in molecules or biomolecules. Flipping the spin in opposite direction to the field requires a small amount of energy corresponding to a radio wave with a frequency specific to the identity of the nuclei.

This method is widely used by chemists to identify molecules by placing them in a magnetic field and exposing them to radio waves. This spectroscopic method is called nuclear magnetic resonance.

The same principle is now widely used for imaging biological molecules such as tissues and blood vessels. This method is called MRI. In this case a patient is introduced in a magnetic field (Fig. 14.18a) and a three-dimensional image of the body or organs is recomposed layer by layer (Fig. 14.18b).

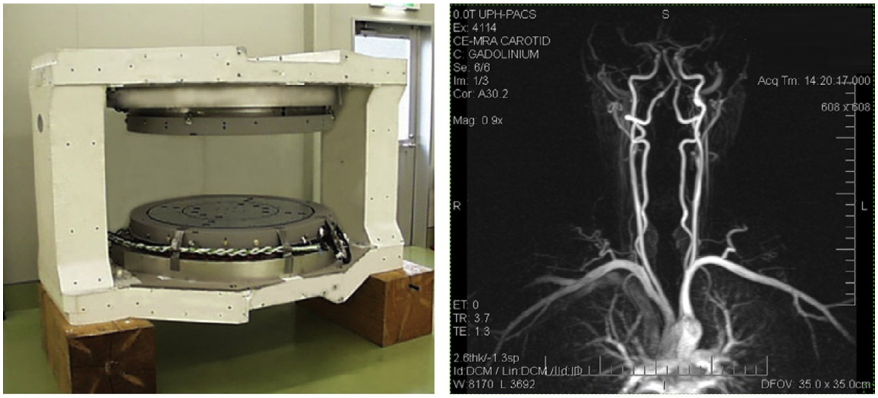

(a) (b)

FIG. 14.18

(a) Magnetic circuit of a medical magnetic resonance imaging (MRI) instrument (Courtesy of Shin-Etsu.); (b) MRI of the vascular system of one of the author (P. Lucas) acquired with gadolinium as a contrast agent.

This constitutes an invaluable diagnostic technique for critical organs such as the brain or heart.

The second type of application involves using RE magnets to direct, shape, and control beams of electrons or ions. Since ions and electrons are charged particles, exposing them to a magnetic field induces Lorentz forces which affect their trajectory.

This property is used to focus and orient ion beams for applications in medicine such as irradiating a tumor, or for materials processing such as lithography of semiconductor circuits.

The same principle applied to electron beams is used for imaging samples in electron microscope with resolution far below that allowed by visible light.

14.7 SUMMARY

RE magnets based on NdFeB alloys have an energy product almost twice as large as their SmCo counterparts and are also much cheaper to produce due to the lower cost of Nd. Consequently they constitute 95% of the RE magnet market.

Their high temperature resistance is low but it can be drastically improved by partial substitution of Nd by Dy.

RE magnets are produced by induction melting of purified metals followed by hydrogen decrepitation and jet milling into fine powder. These fine magnetic particles are then simultaneously compacted and magnetically aligned, followed by sintering into a dense solid. The resulting solid is then permanently magnetized using high pulse current in a magnetization coil.

RE magnets find application in a very wide variety of field ranging from simple household products to strategic and high-tech applications such as energy production, computer hard drives design, and medical imaging.

The largest markets are for electrical motors, computer hard drives, and windmills. Electrical vehicles such as scooters and hybrid cars are also fast-growing markets for RE magnets.

Suggested Reading

Constantinides, S., 2012. The demand for rare earth materials in permanent magnets. In: Rare Earths 2012. Metsoc of CIM, Montreal, QC, pp. 293–307.

Hajime, N., 2010. Improvement of magnetic properties of NdFeB sintered magnets produced by the grain boundary diffusion process. In: Proceedings of the 4th International Conference on Magnetism and Metallurgy, Freiburg. Magnetic Research Center, Shin-Etsu, Japan, p. 283.

Kramer, M.J., McCallum, R.W., Anderson, I.A., Constantinides, S., 2012. Prospects for non-rare earth permanent magnets for traction motors and generators. JOM. 64 (7), 752.

CHAPTER

Introduction to Rare Earth Luminescent Materials

15

Production of light has always been a major fascination and development issue for mankind, whose only original sources of light were the sun, fire, and flashes of lightning. These natural phenomena are linked to two different physical mechanisms that human beings have tried to understand and master: incandescence and luminescence.

Luminescent materials are widely used in everyday life, for example, for lighting (energy saving lamps), displays (laptop, cathode ray tube (CRT) TV, liquid crystal display (LCD) TV, Plasma TV (PDP)), DVD player (laser), diagnosis (X-rays, tomography), or manufacture of devices and materials (by laser).

The common point for all these technologies is mastering of the photon source, or generally speaking, of light.

In most of the above examples, rare earths have faced a major development in the past 50 years. They have greatly contributed to improving the performance of luminescent materials and finally the devices using them, due to their unique intrinsic properties, which derive from unpaired 4f electrons:

- Lanthanum, yttrium, cerium, europium, and terbium are widely used for lighting devices and displays.
- Ytterbium and neodymium for lasers.
- Erbium optical fibers as amplifiers.
- Gadolinium, cerium, lutetium, and terbium in medical devices.

A deep understanding of the luminescence of rare earths needs a large knowledge in quantum physics, solid-state physics, and chemistry. Here, we will focus on description of phosphors (materials with luminescent properties) and luminescent mechanisms without mathematical development. References of relevant books are given at the end of this chapter.

15.1 BASICS OF LUMINESCENCE PHENOMENA

15.1.1 Introduction to the luminescence

Luminescence is an emission of photons which is not due to heat. It is the opposite of incandescence. Due to their electronic structure, some materials are able to absorb energy after external excitation, even at low temperature. If the energy is high enough, an electron can be "excited" from its fundamental state in an upper electronic layer (Fig. 15.1, left). The de-excitation to its fundamental level is made either

Rare Earths. http://dx.doi.org/10.1016/B978-0-444-62735-3.00014-0

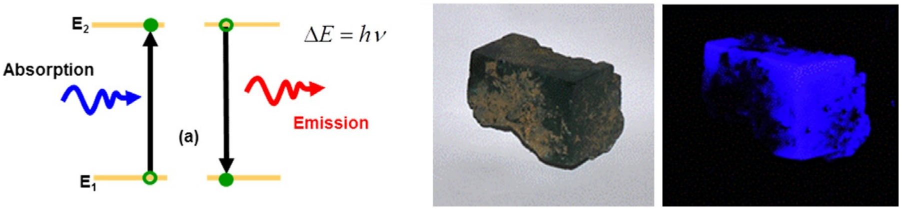

FIG. 15.1

(Left) Schematic energy levels involved in luminescence process. (Right) Fluorite natural fluorite (CaF_2:Eu^{2+}) before and after UV excitation.

Right picture : Courtesy of Tangui Le-Bahers.

by nonradiative de-excitation (emission of heat through vibrational energy levels) or by radiative emission corresponding to the emission of a photon (Fig. 15.1, right, for the natural mineral, fluorite CaF_2:Eu^{2+}). This phenomenon is called "Luminescence" (from Latin *lumen,* meaning light). The energy (and the color) of emitted photons are given by the equation:

$$\Delta E(\text{eV}) = h\nu = \frac{hc}{\lambda(nm)} \sim \frac{1240}{\lambda(nm)}.$$

The nature of excitation can be very diverse, leading to subcategories of luminescence types (Table 15.1). As an example, if the excitation source is photonic, the science is called photoluminescence.

Table 15.1 Classification of Luminescence Types Depending on Excitation Source

Excitation Source	Luminescence	Applications
Photons	Photoluminescence	Fluorescent lighting Ligth Emitting Diode (LED), lighting Displays (LCD, PDP) Anticounterfeiting tags Lasers (CD, manufacturing, and medical) Radioluminescence (medical) Fluorescent inks
Electrons	Cathodoluminescence	Cathode ray tube (old TV)
Electric field	Electroluminescence	LED and OLED
Chemical reaction	Chemiluminescence	Emergency lighting, glow sticks, blood detection, etc.
Biochemical reaction	Bioluminescence	Some animals (firefly, fish etc.)
Mechanical force	Triboluminescence	Damage, pressure probe
Heat (no incandescence)	Thermoluminescence	Dating

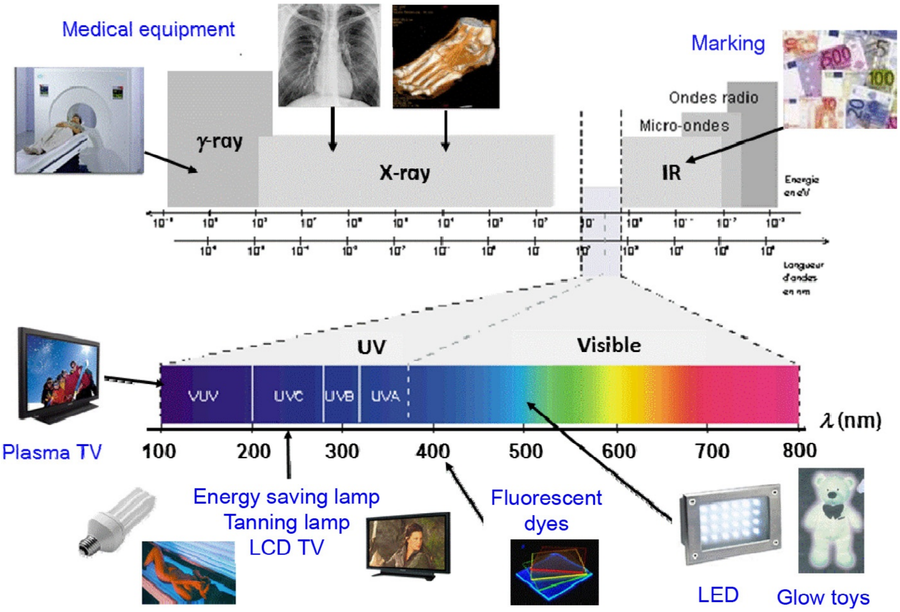

FIG. 15.2

Applications of photoluminescence depending on excitation range.

Courtesy of Thierry Le Mercier, Solvay.

The materials involved in these phenomena can have different names, depending on their composition and their physical properties: phosphors, fluorophores, fluorochromic materials, scintillators, and afterglow pigments (persistent luminescence).

Photoluminescence is the most important domain in terms of application scope. Figure 15.2 gives some detailed examples, depending on the wavelength of the excitation. In all these applications, rare earths play a key role.

- Scintillators for tomography and positron emission tomography scan are excited by γ particles.
- Radiographic images are using phosphors which are excited by X-rays.
- The UV-C excitation is widely used as an excitation source in lighting (fluorescent lamps), displays (plasma display panel (PDP) and LCD backlighting), tanning lamps, and phototherapy lamps.
- The UV-A excitation (near UV, for example, from the sun) is used as excitation source for optical brighteners and fluorescent inks.
- The visible light is used in LED devices to excite red phosphors and classically in afterglow pigments widely used in toys and exit signals.
- Infrared excitation is mainly used for counterfeiting applications.

15.1.2 Luminescence characteristics (emission and absorption spectra, efficiency, and decay time)

Rare earth-doped phosphors are characterized by the following points:

- Emission spectrum (Fig. 15.3 right), which gives, for a particular excitation energy, the intensity of photon emission as a function of wavelength. It consists of either fine peaks (in the case of 4f-4f transitions) or large bands (in the case of 4f-5d transitions).
- Absorption spectrum, which describes the intensity of absorption, as a function of wavelength. Efficient phosphors have strong absorption resulting from specific transitions (4f-5d, charge transfer (CT) or band gap transitions) and low energy losses (minimizing the stokes shift, multiphonon processes, or photoionization).
- Excitation spectrum, which is observed for a particular selected energy emission. This spectrum gives all the energies responsible for the emission as a function of wavelength.
- The performance of phosphors in terms of photon generation is described in two different ways: quantum efficiency and light output (or external luminescence yield).

$$\text{Quantum efficiency}: \eta_{\text{int}}(\lambda) = \frac{\text{Number of emitted photons}}{\text{Number of absorbed photons}}$$

$$\text{External quantum efficiency}: \eta_{\text{ext}}(\lambda) = \frac{\text{Number of emitted photons}}{\text{Number of incident photons}}$$

  The ratio $\eta_{\text{ext}}(\lambda)/\eta_{\text{int}}(\lambda)$ is the absorption $A(\lambda)$ of the material at the λ wavelength. From an industrial perspective, the external quantum efficiency is the most important value, since it gives some indication of all optical phenomena, including incident photon absorption efficiency. The internal yield only explains the optical processes after absorption of the excitation source. The former value is generally given as a percentage of a calibrated reference phosphor.
- The lifetime of luminescence (decay time) is defined as the time required for the luminescence intensity to decay from some initial value to e^{-1} of that value.

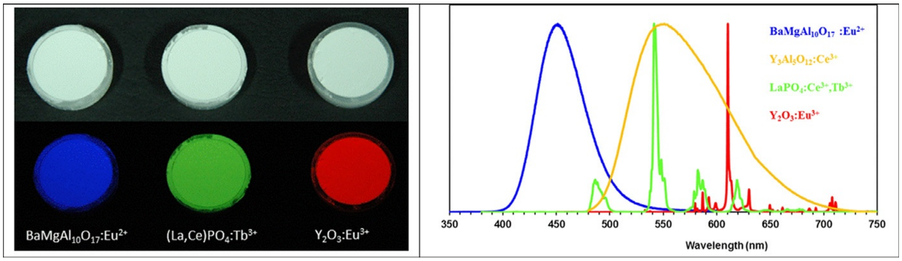

FIG. 15.3

(Left) Phosphor powders before (top) and after excitation under 254 nm (bottom) light. (Right) Emission spectra of classical rare earth phosphor materials.

Courtesy of Solvay Rare Earth.

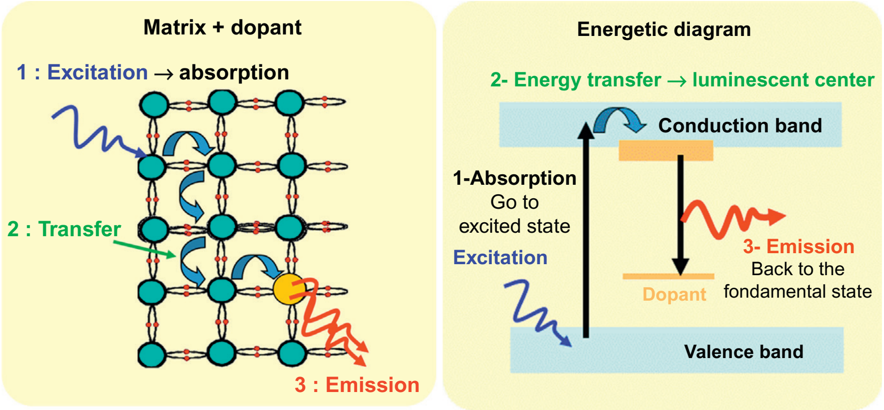

FIG. 15.4

Simplistic representation of phosphor materials. (Left) Atomic dimension (matrix + dopant). (Right) Energy levels dimension.

Drawing by Thierry Le Mercier, Solvay.

15.1.3 Rare earth luminescent materials definition

Most rare earth-based phosphors are inorganic compounds, a few are organic. These materials are composed of a matrix, where rare earth ions substitute some cations (Fig. 15.4, left). Notice that the substitution ratio is generally low, below 10%.

Most rare earth ions accept a large range of coordination number (CN) from 6 (octahedral) to 12 (dodecahedral) according to their ionic radii. The largest is La^{3+} (1.36 Å for CN = 12) and the smallest is Lu^{3+} (0.86 Å for CN = 6). Thus, the nature of the matrixes is very wide: oxides, phosphates, borates, silicates, nitrides, and sulfides. In order to manage rare earth substitution, matrixes are composed of cations with similar ionic radii as lanthanides.

For trivalent rare earths, the matrix host could have La^{3+} and Y^{3+} (sometimes Gd^{3+}) as inactive host cations; this is the case of $Y_{2-x}Eu_xO_3$ (Eu^{3+} in sixfold coordination) or $La_{1-x-y}Ce_xTb_yPO_4$ (Ce^{3+} and Tb^{3+} in ninefold coordination).

For divalent rare earths, alkaline earths are mainly used; e.g., Ba^{2+}, Sr^{2+}, and Ca^{2+} are used in phosphors. The most famous case is $Ba_{1-x}Eu_xMgAl_{10}O_{17}$ (Eu^{2+} in ninefold coordination).

Luminescent mechanisms can be easily visualized in Fig. 15.4 as well as the correspondence between the real dimension (atoms) and the energetic dimension (energy levels). First, exciting energy is absorbed by the matrix (or the dopant directly). Then energy is transferred through the network to the dopant where the emission occurs.

15.2 LUMINESCENCE OF RARE EARTHS

15.2.1 Electronic configuration of rare earths

The rare earth elements have the electronic configuration $[Xe]6s^25d^14f^n$. In the ionized state, the electrons from the layers 6s and 5d are lost, leading to the configuration [Xe]4f^n for the trivalent ones. Depending on the atomic number, the 4f orbitals are more or less filled, the electron number varying from 0 (La^{3+} or Ce^{4+}) to 14 (Lu^{3+}).

For the rare earths, two different orbitals are usually involved in electronic transitions:

- The 4f orbitals (example of Eu^{3+} or Tb^{3+}): The nonpaired electrons of the 4f orbitals are at the origin of the very special electronic and magnetic properties of the rare earths. The 4f orbitals are said to be "internal" to the ion, since they are shielded from the neighborhood by the 5s and 5d orbitals, which have wider radial expansion. The optical properties associated with 4f-4f transitions are almost independent of the host matrix.
- The 5d orbitals (example: Ce^{3+} or Eu^{2+}): In terms of energy, 5d levels are above the 4f fundamental level. The energy position corresponding to the five 5d orbitals are external and strongly impacted by the crystal field and the symmetry of the host matrix. In the case of Ce^{3+} and Eu^{2+} ions, they are positioned at low energy leading to possible luminescence processes in the visible range (4f-5d absorption and 5d-4f emission). Due to their sensitivity to the chemical nature of the host matrix, a huge variety of color emission is accessible. As an example, Eu^{2+} can have emission color in the blue—in some aluminates—and in the red—in the case of sulfide SrS (see Fig. 15.7 for more information).

The free ion case corresponds to the situation where the RE^{3+} ions are considered as isolated and only subject to internal interactions.

The physics of electron-electron interactions and spin-orbit coupling leads to the determination of the spectroscopic levels $^{2S+1}\Gamma_J$ (more details are given in Appendix 15.1) were S is the angular moment of spin and J the total orbital moment. In the case of 4f levels of rare earths, this description is often sufficient and is rationalized in the Dieke diagram (Fig. 15.5).

This diagram is a common and standard reference in the rare earth luminescence community.

For each trivalent ion, the energy levels are positioned considering the electron-electron interaction of each unique configuration in a first step. In a second step, the spin-orbit coupling partially splits the degeneration of the electron-electron interaction into spectroscopic levels. The Dieke diagram has been built for lanthanides in the LaF_3 matrix, but it can be applied to other matrixes since the 4f levels are only slightly dependent on the host matrix.

Then, depending on symmetry considerations, the most probable transitions between these levels can be identified. They are represented here by arrows (see next paragraph on intraconfigurational transitions).

In a "real" dielectric material, the crystal field can affect the emitting center environment and can largely modify the free ion scheme. This is the case when external orbitals are implied (5d for rare earths). *The crystal field theory* enables the calculation of energy levels (see more details in Appendix 15.2).

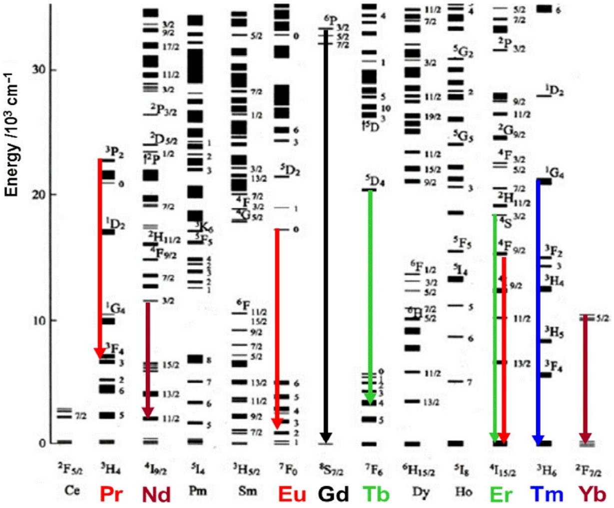

FIG. 15.5

Energy levels of trivalent rare earths in LaF_3 (adapated from Carnall et al.).

The host matrix is then characterized by the nature of the neighboring atoms (Ligand L) and the crystallographic structure (symmetry of different sites, coordination, covalence, etc.). All of them modify the position of the energy levels.

15.2.2 Electronic transitions in rare earth-based phosphor materials (4f-4f, 4f-5d, and CT)

Following the previous description about energy levels, the main optical transitions among rare earth-based materials can be classified as:

- Intraconfigurational electronic transition between 4f levels: $4f^n \rightarrow 4f^n$
- Interconfigurational electronic transition between 4f and 5d (4f5d): $4f^n \rightarrow 4f^{n-1}$-$5d^1$
- CT electronic transition between 4f and the ligand (L): transition $4f^n$-$L \rightarrow 4f^{n+1}$-L^{n-1}

The nature and the intensity of electronic transition between energy levels are explained by the interaction between an electromagnetic field and matter. This leads to various transitions more or less allowed: electric dipolar (ED), magnetic dipolar (MD), electric quadrupolar (EQ), etc. (See more details in Appendix 15.3).

According the Laporte's rules, ED transition occurs when involved orbitals have a different symmetry: 4f-5d and CT transitions. On the contrary, DE is forbidden for 4f-4f transitions. In this case, MD transitions can be observed. The selection rules are strictly true in the free ion. In a real material, all these restrictions can be partially transgressed through the effect of the lattice. As an example, if the rare earth is placed in a non-centrosymmetric site, then the mixing of the 4f and 5d orbitals induced by the crystal field allows ED transitions. Such transitions are said to be "forced" or "induced." This is the well-known case of all Eu^{3+}-based classical red phosphors.

In any case, the dipolar electric interactions are largely more intense ($ED \ggg MD$ in the relative ratio $\sim 1\text{-}10^{-5}$). In practical materials, the allowed transitions (4f-5d and CT) are in most cases preferred to 4f-4f transitions for the absorption mechanism.

15.2.3 Focus on 4f-4f transitions (intraconfigurational transitions)

The main properties of 4f-4f transitions are described here.

- They always consist of *sharp peaks* because the crystal field of the matrix has no dynamic effect (see *configurational coordinate diagram theory*). In other terms, the coupling with phonons (vibrations of the matrix) is very low.
- The energy (or wavelength) of a particular 4f-4f transition of a given rare earth is equivalent, whatever the host matrix (at some nm). Only their intensities change. This fact is due to the small effect of the crystal field of the matrix on the 4f energy level positioning.
- Their *intensities are very low* because of the selection rules (according to Laporte's rules, DE transitions are forbidden). Nevertheless, "forced" DE is enough to give intense (and useful) emissions (Eu^{3+} or Tb^{3+}). The intensity of the transition can be calculated through *Judd-Ofelt theory*. They are strongly linked to the symmetry of the site where the rare earth is located (*group theory*).
- Due to the huge number of energy levels (see Dieke diagram, Fig. 15.5), most of rare earths show numerous electronic transitions between 4f levels. This can be unfavorable for emission properties, since it implies a poor chromatic quality and often reduced quantum yield. As a consequence, only few and selected 4f-4f transitions are used in practical cases to give color emission: Eu^{3+} ($^5D_0 \rightarrow {}^7F_J$) as a red emitter, Tb^{3+} ($^5D_4 \rightarrow {}^7F_J$) as a green emitter, Gd^{3+} ($^6P_j \rightarrow {}^8S_{7/2}$) as a UV emitter.

Figure 15.6 shows emission spectra in the case of red Eu^{3+} emitters or Tb^{3+} green emitters for various host matrixes. In all cases, the former emit spectra in the range of 550-750 nm whether it is in borate, oxide, vanadate, or oxysulfide. The latter emit spectra in the range of 450-650 nm whether it is in phosphate, aluminate, or borate. Eu^{3+} shows more complex behavior because the site symmetry impacts strongly the intensity of $^5D_0 \rightarrow {}^7F_J$ peaks. It is referred to as a "hypersensitive" ion. This leads to orange emission (YBO_3) to deeper red emission (Y_2O_2S). On the contrary, Tb^{3+} emission spectrum is always composed of four peak families ($^5D_4 \rightarrow {}^7F_J$) with the same intensities. Only their relative intensities are impacted by symmetry and the crystal field.

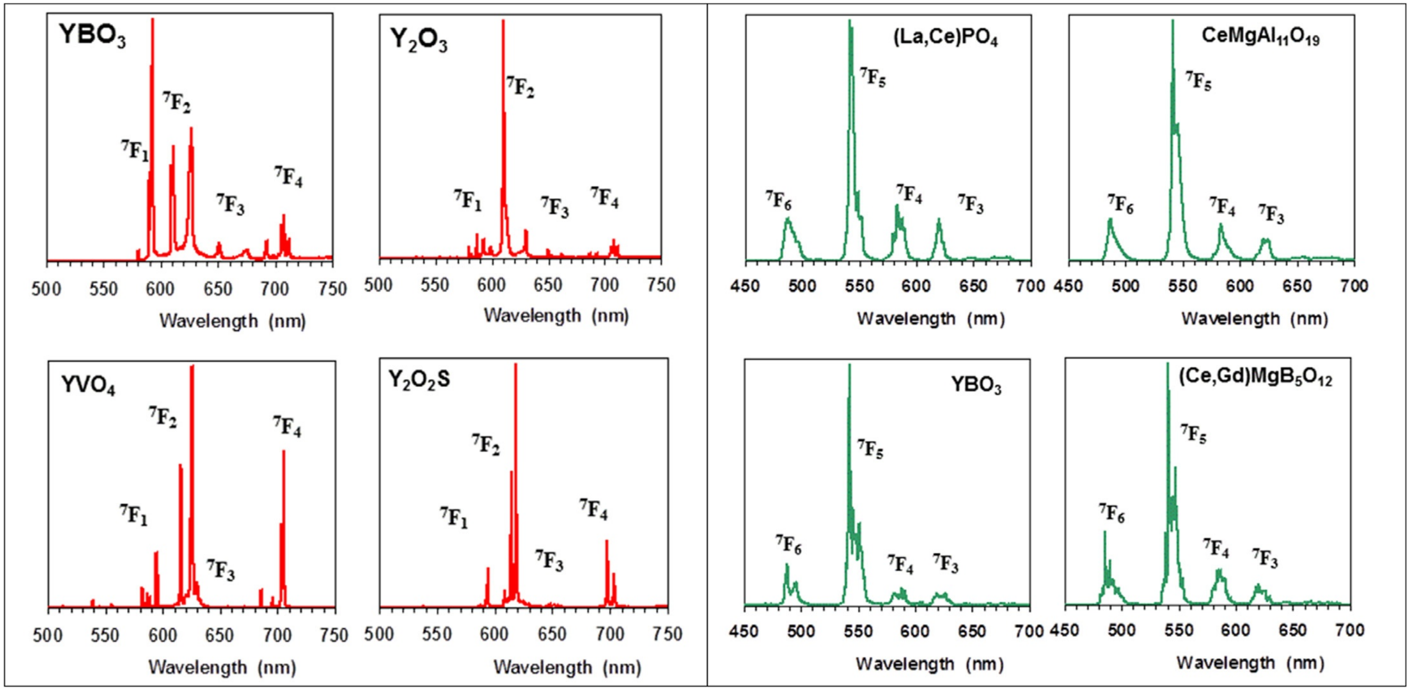

FIG. 15.6

Emission spectra under UV excitation of Eu^{3+} (left four graphs) and Tb^{3+} (right four graphs) based phosphors.

Courtesy of Solvay Rare Earth.

The concentration of rare earth dopant can also have impact on the emission spectra. For Eu^{3+} and Tb^{3+} emitters, at low concentration, new small peaks appear ($^5D_1 \rightarrow {}^7F_J$ and $^5D_3 \rightarrow {}^7F_J$, respectively) leading to a bluish emission color.

15.2.4 Focus on 4f-5d transitions (interconfigurational transitions)

The main properties of 4f-5d transitions are described succinctly here.

- The absorption-emission spectra of 4f-5d/5d-4f transitions always consist of a *broad band*. The effect of the crystal field (5d orbitals) is strong. The coupling with phonons is high.
- For a rare earth, energies (wavelengths) of the 4f-5d transition are strongly dependent on the chemical nature of the host matrix. As an example, Eu^{2+} 4f-5d transitions occur from the UV to IR range.
- Their intensities are very *high* (ED transitions allowed). There are five 5d orbitals giving a maximum of five 4f-5d transitions according to the group symmetry of the site where the rare earth is located.
- For most of the rare earths, the 4f-5d transitions are *too energetic* to be used in classical applications. For trivalent lanthanides, only Ce^{3+}, Pr^{3+}, and Tb^{3+} are practically having 4f-5d absorption transitions not too far from the visible range (above 200 nm in wavelength). On the contrary, the energies of the 5d bands are quite low for the divalent lanthanides. The lowest ones are found with Eu^{2+} and Yb^{2+}. As a consequence, Ce^{3+} and Eu^{2+} ions have been mostly studied due to their absorption in the UV-Vis range and their emissions in the visible wavelengths in many compounds.

The particularities of the 4f-5d transitions are illustrated in Fig. 15.7, where schematic splittings of the Eu^{2+} 5d levels are given for several compounds. The increase in the strength of the crystal fields around Eu^{2+} ions (from SrB_4O_7 to SrS) leads to a decrease

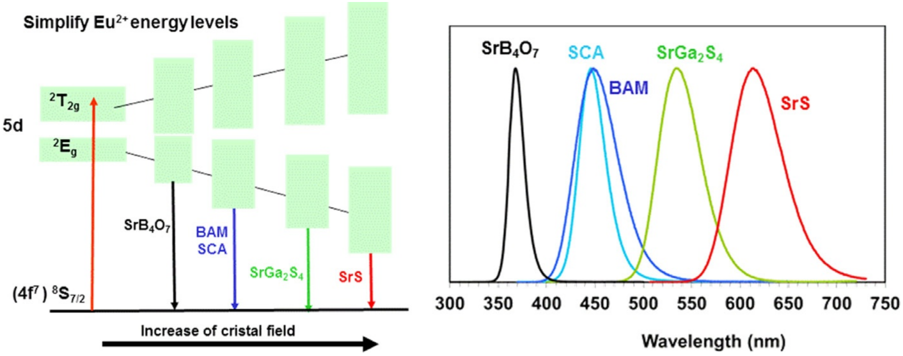

FIG. 15.7

Schematic splitting of the Eu^{2+} 5d levels in several host matrixes and the associated emission spectra (obtained under UV excitation).

Courtesy of Solvay Rare Earth.

of the lower 5d energy level. The consequence is a red shift of the emission spectra (Fig. 15.7, right). Thus, it is possible, with Eu^{2+} doping to design phosphors emitting in the UV (SrB_4O_7:Eu), in the blue ("BAM" $BaMgAl_{10}O_{17}$:Eu), in the green (Ba_2SiO_4: Eu), and in the red (SrS:Eu). Note that the same behavior is observed with Ce^{3+} ions.

15.2.5 Focus on the charge transfer transitions (interconfigurational transition)

The charge transfer transition plays a crucial role in the absorption mechanism of many phosphors, particularly for Eu^{3+} red phosphors. Here, the exciting light is not absorbed through a modification of the electronic distribution between the rare earth and the ligand, e.g., oxygen. The energy is then transferred to the rare earth.

- The CT bands are linked to electronic energy transfers between the highest filled energy level of the ligand (e.g., 2p electrons of oxygen) toward the partially filled or empty levels of the rare earths. It is generally believed that the electron comes from the top of the valence band of the material.
- The half-filled and fully filled configurations have the most ability to be oxidized, and thus have the CT band at the lowest energy. In the case of trivalent lanthanides, the energy of the CT band increases following the series: Eu^{3+} ($4f^6$) < Yb^{3+} ($4f^{13}$) < Sm^{3+} ($4f^5$) < Tm^{3+} ($4f^{12}$).
- The CT band positioning also depends on the ligand type (O, F, etc.).
- Finally, the lanthanide-ligand charge transfer transitions are generally used for absorption. However, CT emission bands are only observed for Yb^{3+}.

The CT mechanism is also possible through absorption by an M-O bond of a transition metal (M) complex such as $(VO_4)_3^{3-}$ in the vanadate $YVO_4:Eu^{3+}$. In both cases, the electron remains localized in the excited state. In some case, the electron can reach the conduction band from the valence band and become delocalized.) This kind of CT band is used in some applications where the incident energy is high (plasma display panels, for example)

Figure 15.8 shows the relative intensities of 4f-4f and 4f-5d or charge transfer transitions. It is clear that 4f-4f transitions are not sufficiently intense to give useful absorption in real applications.

15.2.6 Summary

- *Absorption* is done through intense transitions (allowed according the Laporte's rules) such as 4f-5d or charge transfer (including VB → CB transitions or metal transitions, Table 15.2). Absorption-excitation spectra are made of wide bands.
- *Emission* is done via 4f-4f or 5d-4f transitions. The former gives emission spectra with sharp peaks and the latter gives wide bands.

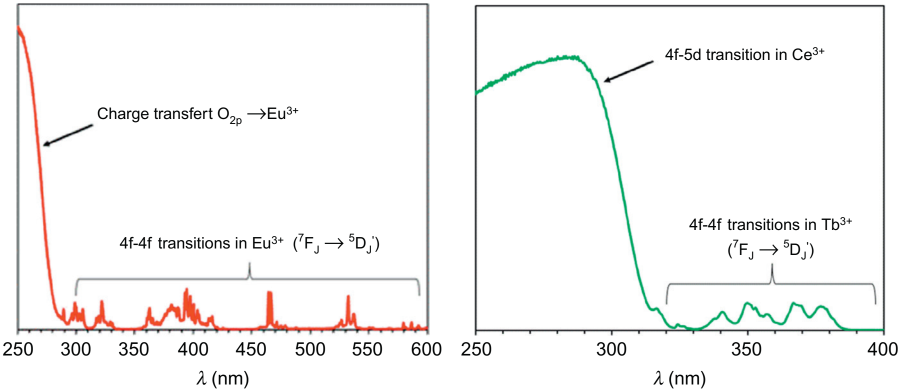

FIG. 15.8

Excitation spectra of $Y_2O_3:Eu^{3+}$ (left graph) and $(La,Ce)PO_4:Tb^{3+}$ (right graph) phosphors.

Courtesy of Solvay Rare Earth.

Table 15.2 Interconfigurational Transitions Used in Rare Earth Luminescent Materials

Transition Type		Transition	Example
Charge transfer	Host lattice	VB → CB	$BaMgAl_{10}O_{17}:Eu^{2+}$ for PDP displays
	Ligand-rare earths	$4f^nL^m \rightarrow 4f^{n+1}L^{m-1}$	$O^{2-}(2p) \rightarrow Eu^{3+}$ (4f) in $Y_2O_3:Eu^{3+}$ Energy-saving fluorescent lamp: excitation 254 nm
	Ligand-transition metals (nd^0)	$3d^0L^m \rightarrow 3d^1L^{m-1}$	$O^{2-}(2p) \rightarrow V^{5+}$ (3d) in YVO_4: Eu^{3+} High color rendering index lamp: Excitation 365 nm
Rare earths	Ce^{3+}, Eu^{2+}	$4f^n \rightarrow 4f^{n-1}5d^1$	$(La,Ce)PO_4:Tb^{3+}$ or $BaMgAl_{10}O_{17}$: Eu^{2+}

15.3 THE MOST CLASSICAL RARE EARTH-DOPED LUMINESCENT MATERIALS

15.3.1 Eu^{3+}, the most common red emitter

15.3.1.1 Emission properties

The Eu^{3+} ion is the main red emitting dopant for displays and lighting devices. The principal emission lines (forbidden 4f-4f transitions), located between 550 and 750 nm, are mainly due to the $^5D_0 \rightarrow {}^7F_J$ transitions (Fig. 15.6). Due to its hypersensitivity to the symmetry of the host matrix, the emission color varies from orange (YBO_3, main emission at 585 nm) to deep red Y_2O_2S (main emission at 627 nm). Many academic scientists are using this property of Eu^{3+} ions as a local probe to determine the symmetry of a given structure.

In the 1960s, Eu^{3+}-based phosphors were universally adopted by the TV world for CRTs first with $(Y,Eu)VO_4$ and then with $(Y,Eu)_2O_2S$.

Nowadays, $(Y,Eu)_2O_3$ is the most common, since the red $^5D_0 \rightarrow {}^7F_2$ (610 nm) transition completely dominates the emission spectrum giving to this phosphor exceptional red color purity. This red line fits perfectly with the NTSC standard TV color.

15.3.1.2 Absorption mechanism

In displays and lighting devices, the exciting flux in the UV range cannot be efficiently absorbed by the 4f-4f transitions of Eu^{3+}, which are forbidden by the selection rules. In order to obtain an efficient phosphor, it is necessary to absorb the radiation through an allowed transition. As the Eu^{3+} ion is easily reduced, a charge transfer band appears at low energy.

The energy absorbed through the charge transfer (CT) band will be transferred to ^5D_J levels, and finally to ^7F_J emitting ones. The position of the CT band depends on the ligand nature, the size and the nature of the host cation, and the coordinence of the site. The more covalent the host matrix is, the higher the energy of the CT band ($YBO_3 > Y_2O_3 > Y_2O_2S$). Thus, a Y_2O_3:Eu phosphor can only be efficiently excited under 254 nm (classical Hg emission in linear fluorescent lamps), while YBO_3:Eu can only be excited at higher energies (172 nm, classical Xe-Ne excitation line in PDP application). It cannot be used in classical lighting.

The most commercialized Eu^{3+}-based phosphors are (or were):

- $Y_2O_3:Eu^{3+}$: fluorescent lamps (tube and compact) for lighting, LCD backlight, plasma display, projector TV (ray tube technology)
- $(Y,Gd)BO_3:Eu^{3+}$: plasma display
- $Y_2O_2S:Eu^{3+}$: CRT
- $Y(V,P)O_4$ Eu^{3+}: high mercury pressure fluorescent lamp (to improve the rendering index)

Today, due to the technology evolution, the "YOX" phosphor, namely, $(Y, Eu)_2O_3$ is used in almost all applications. Some fine tuning of particle size, Eu content, and minor codoping have also been developed to improve its properties. Another very important advantage is its high chemical stability.

15.3.2 Tb^{3+}, the most common green emitter

15.3.2.1 Emission properties

Most of the industrial green phosphors use Tb^{3+} as a dopant, which is able to emit a yellowish-green light due to the $^5D_4 \rightarrow {}^7F_J$ transition. Four groups of fine peaks (forbidden 4f-4f transitions) are observed between 550 and 750 nm, with a main peak around 542 nm. These transitions are nearly insensitive to the site or its symmetry, as illustrated in the Fig. 15.6. The relative intensities of the four groups of lines are almost the same. Only small differences due to crystal field effects can be observed in peaks.

15.3.2.2 Absorption mechanism

There are two main ways to obtain green emission from trivalent terbium. At high excitation energies, it is possible to reach directly the 5d orbitals of the Tb^{3+} which are positioned usually at an intermediate energy level ($\lambda < 230$ nm). This depends on the matrix type (as example in YBO_3).

At lower excitation energies, the 4f-5d transition is not accessible. The excitation is then made through the use of a sensitizer ion such as Ce^{3+} (Fig. 15.9). The absorption occurs in the 4f-5d transition of Ce^{3+} and is further transferred to 4f orbitals of Tb. This mechanism is used in the phosphors for trichromatic lamps (254 nm excitation). This energy transfer is very efficient.

The most commercialized Tb^{3+}-based phosphors are (were):

- In lighting devices (tube or compact fluorescent lamps), both phosphors use $CeMgAl_{11}O_{19}:Tb^{3+}$ (CAT) and $(La,Ce)PO_4:Tb^{3+}$ (LAP). Note that $(Ce,Gd)MgB_5O_{12}:Tb^{3+}$ can also be used, but to a lesser degree.
- For displays, despite the poor chromatic purity of the color emission, Tb^{3+}-based phosphors are used due to their good chemical stability (compared to those of $Zn_2SiO_4:Mn^{2+}$, for example): LAP for LCD backlight, and $(Y, Gd)BO_3:Tb^{3+}$ for plasma displays. For high energy intensity excitation, $Y_3Al_5O_{12}:Tb^{3+}$ or $Y_2SiO_5:Tb^{3+}$ were also used due to their exceptional chemical stability.
- $Gd_2O_2S:Tb^{3+}$ is used as an X-ray green phosphor in some medical equipment.

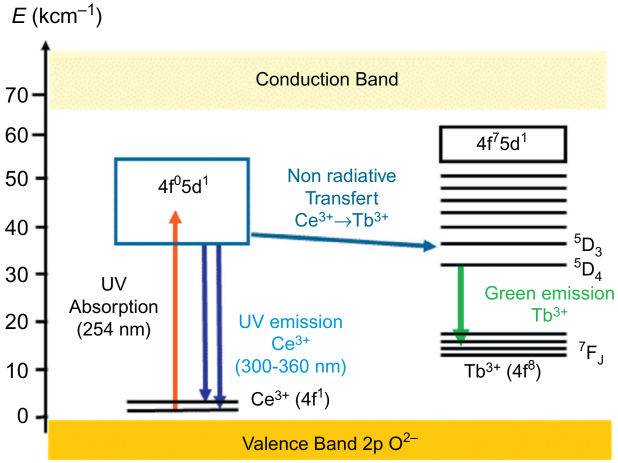

FIG. 15.9

Sensitization of Tb^{3+} by Ce^{3+} (e.g., in $LaPO_4$).

Drawing by Thierry Le Mercier, Solvay.

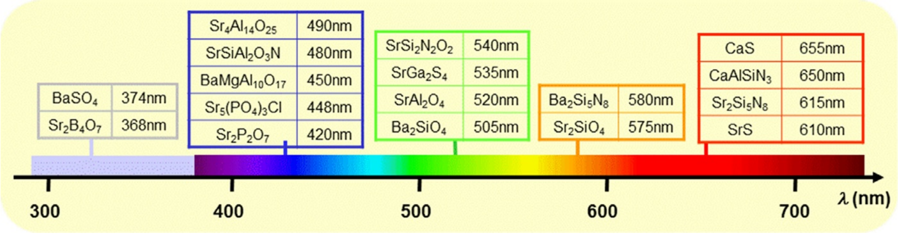

FIG. 15.10

Position of 4f-5d emission band of Eu^{2+} in various materials.

15.3.3 Eu^{2+}, the most common blue emitter

15.3.3.1 Emission properties

Due to their strong dependence on the crystal field, Eu^{2+} ions give color emission from the UV to red spectral range (see Fig. 15.7). This aspect is illustrated in Fig. 15.10, given the position and color of the emission band in several compounds. In all cases, a band is observed due to the strong phonon coupling with the host matrix. The intensity is high due to the strong permitted transition from the lowest 5d levels to fundamental 4f level (singlet $^8S_{7/2}$). The "BAM" composition is the classical blue phosphor used in fluorescent lighting and plasma displays.

Active research on white LED devices, based on the use of phosphors excited by the GaN blue chip, have boosted the research of new nitride materials over the past two decades. The electronegativity of the N-Eu bond is stronger than the Eu-O bond. The nephelauxetic effect is thus more pronounced, which shifts down the barycenter of the 5d orbitals. Moreover, the formal charge on the ligand is higher (N^{3-} compared to O^{2-}), which increases the crystal field around the dopant, and leads to higher splitting of the 5d levels. Thus, the nitride compounds have an emission shifted to a higher wavelength compared to oxides (red shifting). This led to the discovery of efficient red phosphors that can be excited by blue wavelengths, and thus to the development of LEDs with a high rendering index for lighting and LCD backlighting purposes.

15.3.3.2 Absorption properties

Eu^{2+} ions generally strongly absorb light through the 4f-5d permitted transitions. As well as emission, excitation bands also strongly depend on crystal field. Absorption from VUV to yellow can be observed with Eu^{2+}-based phosphors.

The energy difference between the absorption and the emission is called "stokes shift." A high stokes shift means a low phosphor efficiency.

The most commercialized Eu^{2+}-based phosphors are (were):

- The hexaaluminate $BaMgAl_{10}O_{17}$:Eu^{2+} (called BAM) is the main blue emitting component in lighting devices and displays (Plasma or LCD). In this case, 5d orbitals are perfectly positioned between 400 and 200 nm which are useful for fluorescent lamps (254 nm Hg excitation). For plasma TV, the VUV (172 nm mainly) excitation of the Xe-Ne plasma is absorbed by the matrix itself (promotion of electrons in the conduction band) and then transferred toward the 5d energy levels.

- Besides direct Eu absorption-emission, efficient transfer is observed between Eu^{2+} and Mn^{2+}. Emission occurs from Eu^{2+} and Mn^{2+} ions. Depending on the Eu-Mn content, high performing blue-green (low Mn-Eu ratio) or green phosphors (high Mn-Eu) can be obtained. Absorption is performed through the europium (under 254 nm excitation). During relaxation, blue emission is done from Eu^{2+} and green emission from Mn^{2+}. Blue emission vanishes with high manganese content. The mechanism is similar to those of Ce-Tb transfer. The Mn, Eu codoped hexaaluminate (BAM-Mn or BAM-green) is used in compact and linear fluorescent lighting bulbs, as a secondary blue-green phosphor to increase the color rendering of the light.
- Another blue phosphor used for lighting, to a lesser extent, is SCA, $Sr_5(PO_4)_3Cl:Eu^{2+}$
- The most popular inorganic phosphorescent compound also called persistent luminescence or afterglow pigment is $SrAl_2O_4:Eu^{2+},Dy^{3+}$. During the daylight, this compound absorbs and stores the solar light. This energy is then emitted back during darkness. Absorption (UV to 450 nm) and emission (green, around 520 nm) come from the Eu^{2+} ions. During absorption, a part of energy is trapped in the matrix by deep structural defects, typically electrons and holes. The energy relaxation is thermally activated at room temperature, giving a green emission. The Dy^{3+} is added to increase the phosphorescence time, which can reach more than 16 h. This product is now widely used in safety signs, phosphorescent toys, safety lamps, and advertisements. Notice that blue phosphorescence is also possible using $CaAl_2O_4:Eu^{2+},Nd^{3+}$. The emission occurs around 450 nm.
- The UV-emitting phosphor: $SrB_4O_7:Eu^{2+}$ has been developed for photocopying, backlighting, and sun tanning.
- Red and green phosphors for electroluminescent diodes (LED), excited under blue light, are still under development and improvements are in progress. A majority of red and green phosphors are based on Eu^{2+}. Besides $(Ca,Sr)S:Eu^{2+}$ and $SrGa_2S_4:Eu^{2+}$, which were developed early, the most classical ones today are $Sr_2Si_5N_8:Eu^{2+}$ and $CaAlSiN_3:Eu^{2+}$ as red phosphors, the α-SiAlON:Eu^{2+} and $Ba_2SiO_4:Eu^{2+}$ families for orange emission, and $Sr_2Si_2O_2N_2:Eu^{2+}$ for green emission.
- Finally, the compound $BaFBr:Eu^{2+}$ is used as X-ray phosphor detection systems in some medical equipment.

15.3.4 Ce^{3+}, a versatile candidate for phosphor materials

15.3.4.1 Emission properties

Ce^{3+} ions with the configuration $4f^1$ do not have any 4f-4f transitions. The transition observed is purely an interconfigurational 4f-5d type. The lifetime is in the range of 20 ns, much shorter than divalent europium (up to μs). The 4f level splits into two levels due to spin-orbit coupling, and the 4f-5d band shape is different from the one

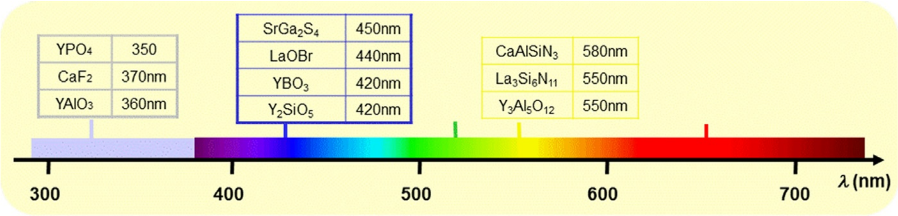

FIG. 15.11

4f-5d band position of Ce^{3+} in various phosphor matrixes.

of Eu^{2+}, as shown in Fig. 15.3: two large bands appear in the case of Ce^{3+}, instead of only one for BAM.

As in the case of Eu^{2+}, the sulfides and nitride matrixes have an emission at a longer wavelength than oxide ones (Fig. 15.11), but the type of color range accessible is more restricted with Cerium: it can be adjusted from UV to blue and greenish yellow emissions.

15.3.4.2 Absorption properties

They are similar to those of Eu^{2+}.

The most commercialized Ce^{3+}-based phosphors are (were):

- The green phosphors CAT and LAP content cerium ions playing the role of sensitizer (absorption of UV light) for the green emission of terbium (see Section 15.3.2).
- The $Y_3Al_5O_{12}$:Ce^{3+} (YAG) phosphor, which is one of the most famous phosphors, is able to emit yellow light under blue emission, and is widely used in white LED devices. The 5d emitting level of the lowest energy is $^2D_{5/2}$. The two emission transitions $^2D_{5/2} \rightarrow {}^2F_{5/2}$ et $^2D_{5/2} \rightarrow {}^2F_{3/2}$ occur in the visible light range, and their combination gives the yellow color, with a global band shape maximum around 550 nm (Fig. 15.3).
- The UV phosphor for tanning lamps, mainly YPO_4:Ce^{3+} (335 and 355 nm) and to a lesser extent, $LaPO_4$:Ce^{3+} (316 and 335 nm).
- Lu_2SiO_5:Ce^{3+} monocrystals are used for detection in positron emission tomography medical equipment.
- Y_2SiO_5:Tb^{3+} were used for TV projection (CRT technology).

15.3.5 Yb^{3+} and Er^{3+}, a perfect couple for up-conversion

Up-conversion corresponds to a photon addition mechanism which allows, e.g., transformation of invisible IR light into visible light.

The photon addition is assisted by a transfer of energy between two ions. In this case, the excitation occurs at lower energy than the emission, for example, from infra-red to green and red emission. This property is widely used in counterfeiting

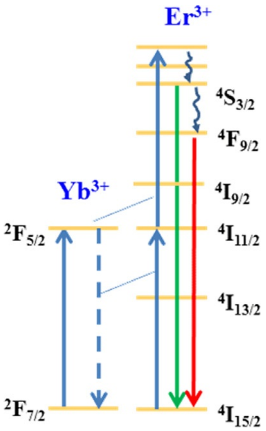

FIG. 15.12

Yb-Er up-conversion mechanism.

applications, mostly with Yb and Er codoping. The classical host materials are fluorides: YF_3 or $NaYF_4$.

In this application, a strong IR excitation source is used (solid-state laser diode). The IR light is absorbed by the Yb^{3+} ions (4f-4f transition). If the dopant concentration is high enough, the energy will be transferred to Er^{3+} ions by a cross-relaxation process directly in the excited state.

As the lifetime of the excited state in Er^{3+} ion is long enough, IR photons are also absorbed by the excited level and promote the ion to a higher energy emitting level. Finally, the system relaxes by emitting green and red light as shown in Fig. 15.12. All these processes have a low efficiency. They need to use a highly energetic excitation source (a solid-state laser for example). To improve the efficiency, matrixes with low energy phonons are preferred, such as fluoride materials.

15.3.6 Other cases

- Nd^{3+}, Yb^{3+}, and Er^{3+} are mainly used in laser and optical amplifier devices (Chapter 15). The host matrix is either a glass or an oxide such as the garnet $Y_3Al_5O_{12}$:Nd^{3+}, which emits at 1.06 μm and Yb^{3+}, which emits at 1.03 μm.
- Er^{3+} emitting at 1.55 μm is the main candidate for telecommunication optical amplifier devices. The emission in the low loss region of silica fiber is used to amplify the telecom signal.
- Pr^{3+} shows the shortest decay time observed for 4f-4f transitions ($^3P_0 \rightarrow {}^3H_J$ or ^3F_J, around 10 ms which is classically in the order of milliseconds for Tb^{3+} or Eu^{3+} ions. This property is used for fast information processing.
  For example, Gd_2O_2S:Pr^{3+},Ce^{3+} ceramic has been developed for an X-ray

detector in X-ray-computed tomography. Recent developments are proposed to use Pr^{3+}-based phosphors for UV lamps (low-pressure Hg lamp technologies). Indeed, in some host matrixes, 5d-4f emissions are very intense (YBO_3, YPO_4).

- $Sm^{3+}$and Dy^{3+} are rarely used, except as additives in red CRT phosphors (Sm^{3+}) and in afterglow pigments (Dy^{3+}). Note also that Dy^{3+}-doped crystals ($CaSO_4$ or CaF_2) are also used in some dosimeters, for monitoring exposure to ionizing radiation, such as γ-rays or neutrons.
- No application is reported for Ho^{3+} or Tm^{3+} ions despite researches in the field of up-conversion for the former and blue emitter in electroluminescent devices for the latter.
- Y^{3+}, La^{3+}, Gd^{3+}, and Lu^{3+} are optically inactive, but still very important for phosphor materials.
- Y^{3+}, La^{3+}, and Lu^{3+} are totally inactive ions due to their empty or complete electronic configuration ($4f^0$ or $4f^{14}$). Their role is essentially to host other active rare earths. Yttrium is smaller than lanthanum leading to smaller crystallographic size and coordinence. The main application of lutetium is for the scintillator crystal Lu_2SiO_5:Ce.
- Gd^{3+} ions have a $4f^7$ electronic configuration (half-full) with a lowest excited 4f level ($^6P_{7/2}$) located in the UV range. This can lead to UV emission (around 315 nm) toward the fundamental state used in certain phosphors (UV medical application). This excited level can also sensitize the luminescence of other rare earth ions. Nevertheless, the main application of this ion is to be part of the host matrix, particularly in X-ray phosphors. Indeed, the Gd^{3+} ion has a high absorption cross section due to its large atomic number.

15.4 RARE EARTH LUMINESCENT MATERIALS: SYNTHESIS ROUTES

15.4.1 Requirements for a good phosphor material

The intrinsic luminescent properties (absorption and emission wavelength, lifetime, internal and external theoretical quantum yield) are defined by the choice of matrix and dopant, as described in the previous section, where the physics of luminescence is described for "perfect" materials, without defects, i.e., without interfaces or synthesis defects.

However, the practical usage of phosphor materials requires managing and controlling many parameters. For example, size is critical from centimeter single crystals to micrometric powders or nanometric colloidal suspensions. Other challenges are minimization of defects, a reasonable production route in compliance with good safety conditions, reasonable costs, and equipment. Overcoming these additional constraints is essential for optimizing routes for manufacturing efficient real materials.

In most of the cases, the luminescent material is a micronic powder. The typical size of the phosphor particles for fluorescent lighting and PDP displays ranges from 2 to 10 μm diameter, and as much as possible, with a uniform size. Size control down to few micrometers introduces many difficulties that have been overcome in the past 20 years through constant improvement of the synthesis routes. In general, the smaller the size, the lower the efficacy of the phosphor, due to two phenomena:

- The highest quantity of defects localized at the surface,
- The smallest sizes are often obtained through gentler synthesis routes or with energetic grinding. It results in poor crystallinity with many crystalline defects in the bulk and at the surface.

Besides crystalline defects, impurities are at the source of light yield decreases. As a consequence, luminescent materials must be very "pure" to be efficient, which leads to major industrial challenges. First of all, the discovery of highly efficient phosphors was made during the sixties, and is the result of developing industrial methods for separating rare earths (especially a pure source of europium). Second, many metallic elements such as iron are dramatic luminescence quenchers. Thus, special dedicated industrial equipment is required to produce phosphors with extremely low levels of Fe (typically less than 50 parts per million).

Some new applications requiring nanoparticles (medical, tagging) are very sensitive to defects, due to these particles' extremely high surface to volume ratio.

The next paragraphs are devoted to describing the synthesis routes to micronic powder materials, which are used in a wide range of applications. The routes can be arranged in two classes: the "solid-state" route from separated elements (generally from oxides or carbonates), and the "precursor" route, which consists of an improvement over the solid-state route, starting from precipitated mixed compounds (called "precursors").

Whatever the route, phosphors need to have a high crystallinity. Usually, this implies a high temperature calcination step with the assistance of a few mass% of melting agent (flux). The flux helps with the fusion-recrystallization mechanism and reduces the firing temperature. For each phosphor, optimization of firing temperature and flux (nature and amount) are required. The flux is usually fluoride (NaF, LiF, NH_4F), chloride ($BaCl_2$), or borate ($Li_2B_4O_7$, H_3BO_3). Figure 15.13 shows the dramatic effect of flux during synthesis of the blue phosphor BAM.

Let it be said that the science of fluxes and management of firing conditions are quite empirical. They are managed case by case by phosphor makers, depending on their own process and industrial equipment.

15.4.2 The traditional solid-state route

The solid-state route entails mixing the powders of all the input components. The mixture is then fired at high temperature in order to access to the desired crystal

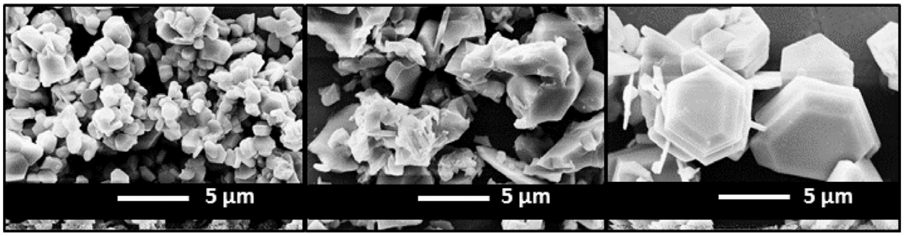

FIG. 15.13

Morphology of BAM obtained with different fluxes.

Courtesy of Solvay Rare Earth Systems.

structure. The final cake is further ground after calcination in order to obtain the desired particle size. This ceramic route is simple and cheap, but it generally leads to coarse and inhomogeneous particle sizes and requires high-temperature firing routes.

As a consequence, many optimizations have been performed in order to fine-tune this synthesis route (see Fig. 15.14):

- Control particle size, surface area, and purity of the preliminary oxides-carbonates
- Mix the raw materials well in an adequate blender
- Control perfectly the stoichiometry of the incoming materials
- Add a “flux” in small quantity (less than few percent) to the mixture, which helps to melt the blend at lower temperature, and enables a better control of particle shape.
- The firing step is generally performed in a tunnel furnace, in small crucibles (few kilograms maximum). The temperature profile in each region of the furnace needs also to be very carefully adjusted, as well as the crucible type, shape, and filling rate.

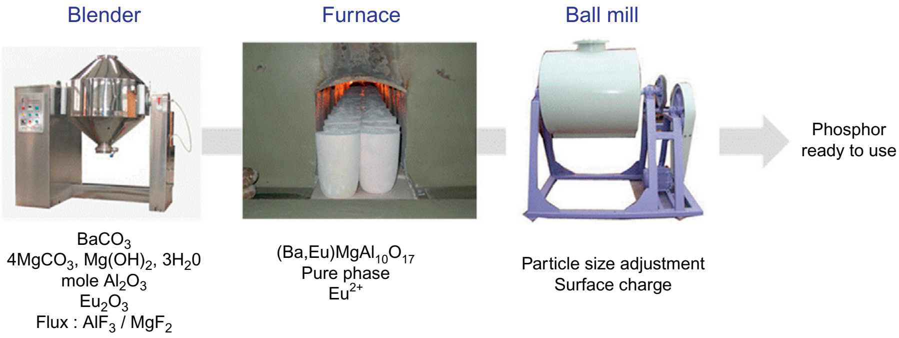

FIG. 15.14

Classical steps and equipment used in the solid-state route of phosphor manufacture.

- The firing step can be performed under air (to eliminate excess of oxygen-carbonate). Some additional firing under reducing atmosphere is often necessary to control the oxidation state of the rare earth (Eu^{2+}, Ce^{3+}, Tb^{3+}).
- A crusher helps to manage the cake grinding into smaller parts (ten to several hundred μm).
- Some postwashing is used to help cake softening, as well as to remove some noncrystalline residues, or impurities.
- The equipment for grinding is adjusted depending on cake hardness and targeted grain sizes (jet-milling, wet and dry ball milling).

This synthesis route was used in the past for all lighting phosphors, but is used today mainly for BAM ($Ba_{0,9}Eu_{0,1}MgAl_{10}O_{17}$), CAT ($Ce_{0,66}$ $Tb_{0,33}MgAl_{11}O_{19}$), and YAG ($Y_3Al_5O_{12}$:Ce) phosphors.

The chemical reactions and the starting materials are described here for some specific cases. For simplicity, off-gases have been omitted.

BAM:
$0.9\ BaCO_3 + 0.2\ [4MgCO_3, Mg(OH)_2, 3H_2O] + 5\ Al_2O_3 + 0.05\ Eu_2O_3 \rightarrow Ba_{0.9}Eu_{0.1}MgAl_{10}O_{17}$
Flux: MgF_2 or AlF_3
Firing under N_2/H_2, at temperatures of 1500-1600 °C

CAT:
$2/3\ CeO_2 + 1/12\ Tb_4O_7 + 0.2\ [4MgCO_3, Mg(OH)_2, 3H_2O] + 5.5\ Al_2O_3 \rightarrow Ce_{0,66}Tb_{0,33}MgAl_{11}O_{19}$
Flux: MgF_2 or AlF_3
First firing under air, at 1600 °C, followed by grinding
Second firing under N_2/H_2 at about 1200 °C.

The improved solid-state route is able to produce high-quality phosphors such as BAM and CAT, with mean particle sizes in the range of 5-15 μm.

Some major improvements in terms of particle size reduction (down to 2.5 μm) and in terms of brightness have been made for YOX and LAP phosphors, by the use of the precursor route (next section).

15.4.3 The Precursor route

The objective of the precursor route is to replace the blend of oxide and carbonate raw materials by an advanced material called a "precursor." This is a fine mixture of all the elements with suitable stoichiometry, a strict homogeneity of the dopant concentration, and a fine particle size (close to the target phosphor size). It often already has the appropriate crystal structure. This advanced precursor is obtained by wet chemistry.

This allows lowering the firing temperature and duration, thus giving much better control of the sintering step. Gentle posttreatments are thus used, which lead to many fewer defects in the final product, and hence to better luminescence properties.

The main steps and equipment for the finishing steps are similar to those used in the solid-state route.

This innovation relies in good management of the precursor precipitation step.

15.4.3.1 Example of YOX Phosphor (*Fig. 15.15*)

The wet chemistry route for manufacturing the oxide YOX entails:

- Preparation of a co-nitrate (or co-chloride) of Y/Eu solution
- Precipitation of the precursor with oxalic acid, under controlled acidity conditions
- Filtering and washing to eliminate residual salts
- Firing at medium temperature (700-900 °C) to decompose the oxalate and obtain the final YOX oxide precursor.

Many variations of the precipitation conditions permit control of the particle size and morphology of the precursor. At this step, the crystalline structure is suitable but the crystallinity is too low. Brightness is then limited.

In a second step, the precursor is usually carefully blended with a flux (based on barium carbonate and boron) and further refired at between 1400 and 1500 °C in air, to enhance crystallinity. The postcrushing, grinding, and washing steps are much gentler than for the classical solid-state route.

The success of the precursor relies in perfect distribution of Eu in the Y lattice.

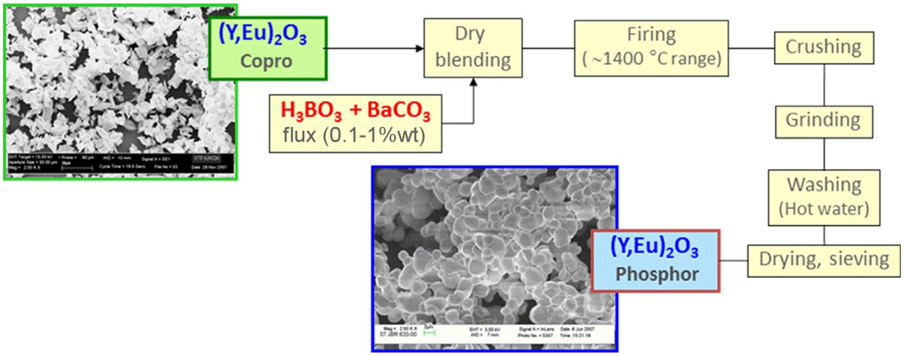

FIG. 15.15

Wet YOX phosphor route.

Courtesy of Solvay Rare Earth Systems.

Also, the gentle phosphor-firing step is only necessary to fine-tune the crystallinity and the morphology of the primary particles, not to crystallize the phase.

This precursor route was established in the 1990s. It has made it possible to develop much brighter phosphors, with smaller particle sizes and uniform size distributions.

15.4.3.2 Example of LAP Phosphor (Fig. 15.16)

When the LAP formula is made through a purely solid-state route, it is quite impossible to manage the oxidation state of all the Ce at the +III level. It is also difficult to manage particle size and avoid phasic impurities. Thus, the precursor route was developed in the 1990s, which greatly improved the product and made it possible to use LAP widely in lighting applications.

The precursor is synthesized through precipitation from rare earth salts and a phosphate source in water, then washing and firing in air, in order to obtain monazite $(La,Ce,Tb)PO_4$, with controlled particle size, and an oxidation state of Ce and Tb oxidation state which is mostly at +III.

Second, a blend with small quantity of borate flux is added before the firing at medium temperature (around 1100 °C) under a gentle reducing atmosphere (N_2/H_2) in order to consolidate the crystallinity of the phase and perform full reduction of the rare earths. Gentle grinding and washing are used to obtain a final high-performance phosphor.

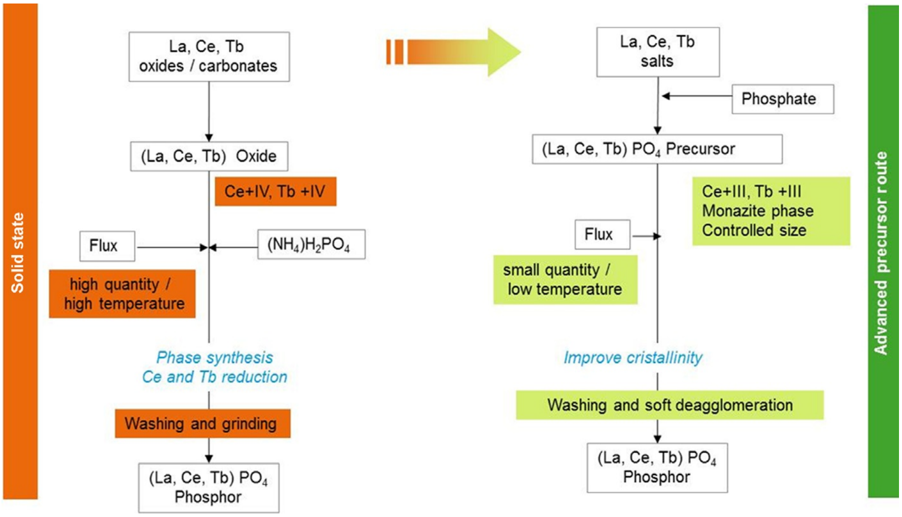

FIG. 15.16

Wet LAP phosphor route.

Courtesy of Solvay Rare Earth Systems.

APPENDIX 15.1 4f ENERGY LEVELS OF RARE EARTHS

Electrons in atoms are ranked in shells and subshells defined by two quantum numbers: n, the principal quantum number and l, the angular quantum number. Each subshell has $2l$-1 orbitals, with a maximum of $4l+2$ electrons. As a consequence, the 4f subshells of rare earths ($n=4$ and $l=3$) have seven orbitals with room for 14 electrons ($m_s=\pm 1/2$). Considering that each electron can have ½ or −½ spin, there are $\frac{(4l+2)!}{n!(4l+2-n)!}$ ways to arrange the electrons in the orbitals, and thus, as many energy levels. Then, there are 20 for the p electrons, 252 for the d electrons, and 3432 energy levels for the f electrons!! This huge number explains the complexity of classifying the 4f energy levels.

The interactions between electrons of a unique configuration lead to *spectroscopic terms* noted $^{2S+1}\Gamma$ where S is the angular moment of spin $\left(\vec{S}=\sum_{i=1}^{n}\vec{s_i}\right)$ and Γ represents the L value, which is the orbital angular moment $\left(\vec{L}=\sum_{i=1}^{n}\vec{l_i}\right)$. The Γ letter is written as S, P, D, F, G…, when the L value is 0, 1, 2, 3, 4…

The only term which can be easily determined with the Hund rules is the fundamental term: the highest S value and the highest L value.

Let us take Eu^{3+} as an example. The spectroscopic terms of the two configurations ^7F ($L=3, S=3$) and ^5D ($L=2, S=2$) are represented below. The ^7F term is the fundamental term.

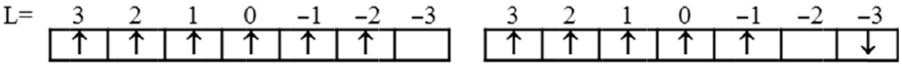

Each term has $(2S+1)(2L+1)$ energy levels, which are degenerated, since they have same S and L values. The energy gap between two terms is variable, in the range of $20{,}000\ \mathrm{cm}^{-1}$.

The splitting of spectroscopic terms is made through the action of spin-orbit coupling. This leads to the spectroscopic levels $^{2S+1}\Gamma_J$ with $\vec{J}\rightarrow\vec{L}+\vec{S}$, where J is the total orbital moment. It represents the interaction of L and S magnetic moments. The values of J can vary from $(L+S)$ to $(L–S)$. The configuration where each level is characterized by a triplet (L, S, J) is termed Russell-Saunders coupling or LS coupling. The intensity of spin-orbit coupling is characterized by a constant (λ). λ is positive if 4f is less than half filled, and negative elsewhere. In the case where 4f is half filled ($n=7$), there is no coupling since $S=0$.

The third Hund rule is able to give the fundamental level. If $n<(2l+1)$, the fundamental level is the one having the minimum J. On the contrary, if $n>(2l+1)$, the fundament level is the one with the highest J. Then, the levels are arranged with equal energy gap, the gap between two adjacent levels J and $J'=J+1$ has a value of $\lambda J'$. Each of these levels has a multiplicity of $2J+1$.

Coming back to the example of Eu^{3+}, the ^7F fundamental term is divided into seven levels: $^7F_0$, $^7F_1$, $^7F_2$, $^7F_3$, $^7F_4$, $^7F_5$, and $^7F_6$, and the fundamental one is $^7F_0$. The Fig. 15.17 gives the energy levels of Eu^{3+} free ion.

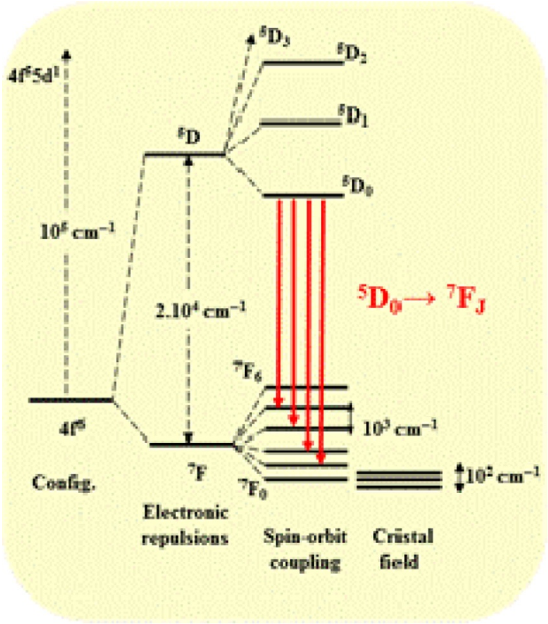

FIG. 15.17

Energy levels of Eu^{3+} free ion.

APPENDIX 15.2 5d ENERGY LEVELS OF RARE EARTHS (THE CRYSTAL FIELD THEORY)

The five 5d orbitals play a big role in phosphors. They are empty in the normal state but could get an electron from 4f levels during excitation.

In the free ion, the five 5d have the same energy. Contrary to 4f orbitals, the energy of the 5d levels will decrease when an ion lanthanide Ln^{Q+} is placed in a host (A). This phenomenon is called "red shift," and is illustrated by D(Q,A) in Fig. 15.18.

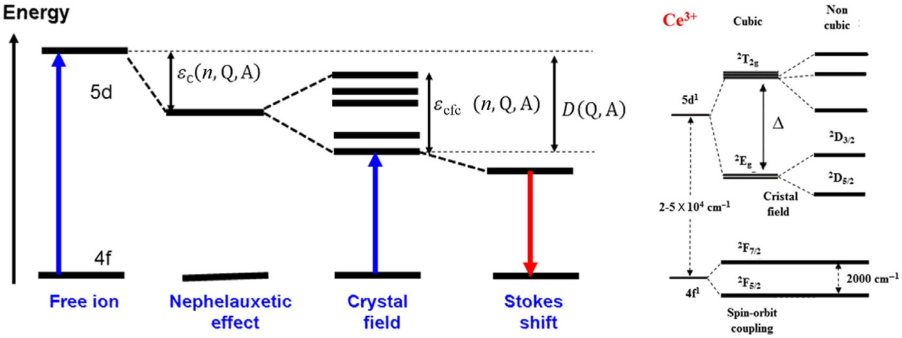

FIG. 15.18

Red shift diagram.

Adaptated from P. Dorembos in "Phosphor Handbook", see suggested reading.

The corresponding energy levels are always noted ^2D (only one electron can be excited). For cubic symmetry, we find two groups: ^2E_g and $^2T_{2g}$.
The red shift is due to two phenomena:

- the nephelauxetic effect, which shifts the barycenter of the 5d in a range of $\varepsilon_c(n,Q,A)$
- the crystal filed (CF) splitting of the 5d orbitals in a range of $\varepsilon_{cfc}(n,Q,A)$

The emission of 4f-5d transition is also affected by Stokes shift (ΔS) which results from the electron-phonon due to host matrix vibrations.

The nephelauxetic effect (from Greek "spread of the cloud") induces a shift of the barycenter of the d orbitals with a value of $\varepsilon_c(n,Q,A)$ compared to free ion. When the electronic cloud of the rare earth is surrounded by a ligand field, part of it is delocalized toward the ligands. This induces a global reduction of the electrostatic interaction. This value is 6.35 eV for the Ce^{3+}. This effect increases with the polarizability of the ligand ($Se^{2-} > S^{2-} > N^{3-} > O^{2-} > F^-$) and with the charge density of the anionic ligand ($O^{2-} > AlO_4{}^{5-} > SiO_4{}^{4-} > BO_3{}^{3-} > PO_4{}^{3-} > CO_3{}^{2-} > SO_4{}^{2-} > H_2O$).

This CF splits the 5d orbitals without modifying the barycenter position. $\varepsilon_{cfc}(n,Q,A)$ is defined as the energy difference between the lowest and the highest 5d levels. ε_{cfc} depends upon the size of the site, the covalence of the bonds, and the coordination of the site. It increases with the charge of the ligands and decreases with their size: $O > S > F > Cl > Br > I$.

For a given ligand, the nephelauxetic effect and crystal field depend on:

- The ionic radius, r, from the cation (M) which is substituted by the rare earth: the biggest r, the lowest overlap between cation and anion orbitals. This will reduce the nephelauxetic and crystal field effect.
- The coordination of the rare earths. It varies from 6 to 12 in inorganic compounds. The nephelauxetic and CF effect will decrease with the increase of coordination.
- The inductive effect of the neighbors (M′) in the matrix. The covalence of the rare earth-ligand bond is strongly influenced by the M′-ligand bond. The more the covalence, the more the decrease in nephelauxetic and CF effects. This will be more obvious when the number of M-Ligand bonds will increase.

Energy levels of 4f and 5d orbitals do not show the same evolution versus the number of 4f electrons:

- For $4f^n$ configurations: the variation with n is always under a zig-zag shape with maxima observed in the lanthanide series for $n = 7$ and $n = 14$. The $n + 7$ is always the more stable configuration, with the highest energy of the 4f-4f5d transition compared to the n configuration. This evolution is true whatever the environment: in free ion, in materials... Only the value of binding energy is shifted compared to the free ion. Between Ce and Lu, the binding energy varies in the 6 eV range. This evolution is explained by the refined spin-pairing theory (Jorgensen).
- For 5d configurations: the 5d energy level has more or less the same bond energy across the lanthanide series: only 0.5 eV of variation is observed between Ce and Lu.

APPENDIX 15.3 TRANSITION SELECTION RULES

The emission of a photon by a luminescence mechanism is the consequence of excitation of an emitting center (a rare earth, for example) under an external energetic solicitation.

The radiative probability between two levels Ψ_a and Ψ_b ($\Delta E_{b\to a} = h\omega = hc/\lambda$) is proportional to the matrix $\langle \psi_a | H_{int} | \psi_b \rangle^2$. Without going through the details of the calculation, the Hamiltonian of interaction, H_{int} between electromagnetic wave and matter is given by:

$$H_{interaction} \cong \sum_i \left[\boxed{\begin{array}{c} e r_i . E_k^0 \\ \text{ED} \end{array}} + \boxed{\begin{array}{c} \frac{e}{2m} (l_i + 2s_i).\ B_k^0 \\ \text{MD} \end{array}} + \boxed{\begin{array}{c} \frac{1}{2} e r_i . r_i . k E_k^0 \\ \text{EQ} \end{array}} \right]$$

E and B are the electric and magnetic parts of the electromagnetic field, k is the polarization mode, r_i is the coordinate of the ith electron, l_i and s_i are its angular and spin orbital moments.

This Hamiltonian reveals three terms, which explains the main electronic transitions in solids: dielectric dipolar, MD, and EQ.

The relative intensities of transitions linked to this interaction can be classified as ED ⋙ MD > EQ in the relative ratio $\sim 1{:}10^{-5}{:}10^{-6}$. The dipolar electric interactions are largely more intense.

In the case of rare earths:

- The selection rules define the existence of the transition. They are linked to the symmetry of the site where the rare earth is substituted and are explained by the group theory.
- The intensity of the transition can be calculated through Judd-Ofelt theory.
- The principal transitions occurring are of the ED and MD type.

The dipolar electric transitions, when allowed, are the more intense ones. Their probability is in the range of $10^8\ s^{-1}$.

The allowed ED transition exists when the Laporte's rule is fulfilled, meaning $\Delta l = \pm 1$. This implies that the allowed transitions are linked to a change in parity of the orbitals, which is an interconfigurational electronic transition.

In other words, if the electron changes its orbital during the transition, the mean distance between electron and core will vary a lot, as well as the dipolar moment. In that case, the transition is allowed and is intense. For the rare earths, it is the case of 4f → 4f5d (for Eu^{2+} and Ce^{3+}) and charge transfer (Eu^{3+} and Yb^{3+}) transitions.

In practical materials, these types of allowed transitions are in most of the cases preferred to 4f-4f transitions for the absorption mechanism.

On the contrary, in the case of intraconfigurational transitions, the orbitals are of the same parity. The dipolar moment varies little. The transition is thus forbidden and of weak intensity. It is the case of 4f-4f transitions in rare earths.

The selection rules can be transgressed in many cases of materials. For example, if the rare earth is placed in a non-centrosymmetric site, the mixing of the 4f and 5d orbitals induced by the crystal field is able to enable the DE transitions. The ED transitions are called “forced” or “induced,” and their intensity is still lower than a pure DE transition. They are often the most intense ones in the case of rare earth emission spectra.

By using the Judd-Ofelt model, which describes the intensity of these transitions in details, and considering the spin-orbit coupling and the crystal field terms, we can define the selection rules for forced ED transitions:

$\Delta l = \pm 1$ (parity change)	$\Delta L \leq 6$	$\Delta S = 0$	$\Delta J = \lvert \leq 6 \rvert$

Moreover:

- If $J = 0$ for one of the levels, the transition is allowed only if the variation of J is a multiple of 2, with $\Delta J \leq 6$.
- The $J = 0$ to $J' = 0$ transitions are allowed only in the case of C_n, C_s, C_{nv} symmetries.
- The $\Delta J = \pm 2$ transitions are termed “hypersensitive” to the symmetry of the rare earth site. A small deviation to the centrosymmetry induces a very high intensity of the transitions. This unique effect is used in everyday life, in the most common phosphor $Y_2O_3:Eu^{3+}$: the $^5D_0 \rightarrow {}^7F_2$ transition is very intense; this phosphor has a bright red emission.

The dipolar electronic transitions are far less intense than the ED ones. The selection rules are the same for the free ion and for the ion in a matrix. They are defined by:

$\Delta l = 0$ (no parity change)	$\Delta L = 0, \pm 1$	$\Delta S = 0$	$\Delta J = 0, \pm 1$

References

More Specific Paper

Carnall, W.T., Goodman, G.L., Rajnak, K., Rana, R.S., 1989. A systematic analysis of the spectra of the lanthanides doped into single crystal LaF_3. J. Chem. Phys. 90, 3443. http://dx.doi.org/10.1063/1.455853.

Suggested Reading

History of Luminescence

Harvey, E.N., 1957. A History of Luminescence. American Philosophical Society, Philadelphia.

Generalities About Phosphors

Blasse, G., Grabmaier, B.C., 1995. Luminescent Materials. Springer-Verlag, New York.

Yen, W., Shionoya, S., Yamamoto, H., 2007. Phosphor Handbook, second ed. CRC-Press, Boca Raton, FL.

Physics

Di Bartolo, B., 2010. Optical Interactions in Solid, second ed. World Scientific Books, Singapore.

Henderson, B., Imbusch, G.F., 1989. Optical Spectroscopy of Inorganic Solids. Clarendon Press, Oxford.

Jorgensen, C.K., 1971. Modern Aspects of Ligand Field Theory. Elsevier, North Holland, Amsterdam.

Applications of Rare Earth Luminescent Materials

16

Phosphors represent about 9% of the rare earth global market but consist of high-value materials (Fig. 16.1). Ninety-seven percent of phosphors are devoted to lighting and display applications (Fig. 16.1).

The rare earth elements are widely used in applications where light emission is a criterion of performance. It is the case of lighting devices and displays, such as:

- Trichromatic lamps (or energy-saving lamps), where lanthanum, yttrium, cerium, terbium, and europium are mainly used to control the color
- Light-emitting diodes (LEDs), using mainly yttrium, cerium, and europium
- Plasma displays, old cathode ray tubes (CRTs), and liquid crystal displays (LCDs) with fluorescent backlighting, consuming lanthanum, yttrium, cerium, terbium, and europium.

Other important applications using rare earth phosphors are

- Special lamps for tanning or phototherapy
- Medical equipment: lutetium, gadolinium, cerium, etc.
- Afterglow pigments, containing europium, and dysprosium
- Marking for fighting counterfeiting.

Rare earths are key elements because of the following points:

- Control of color emission for display and lightning: mainly Eu^{2+} for blue emission, Eu^{3+} for red emission, and Tb^{3+} for green emission. High-emission efficiency is achieved.
- They exhibit a strong absorption through 4f-5d or charge transfer transitions.
- They are able to capture high-energy photons (X-rays or γ-rays) due to their high atomic number (Z) value and high-density.

Due to their ability to accept various chemical environments and coordination, a large range of host material is available.

Inorganic host matrixes provide high chemical and thermal stability.

Rare Earths. http://dx.doi.org/10.1016/B978-0-444-62735-3.00015-2

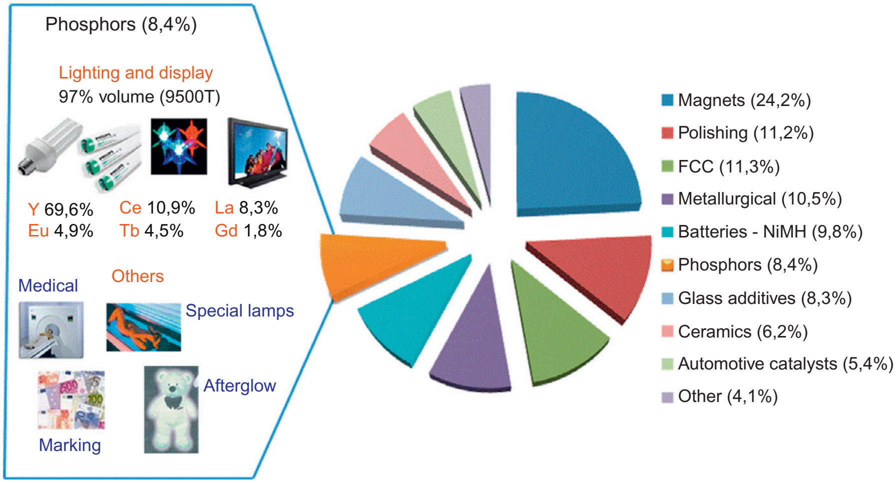

FIG. 16.1

Main applications of phosphor materials.

Courtesy of Thierry Le Mercier, Solvay.

16.1 RARE EARTH FOR LIGHTING APPLICATION

A light source is defined by several characteristics:

- Luminous efficiency (lm/W): lumen output per watt of electricity provided
- Color temperature T_c (in Kelvin): T_c is used to define the sensation of color of the emission. If $T_c = 2700$ K, the color emission is yellow, thus human beings have a feeling of comfort, this color is called "warm." When $T_c = 6500$ K, the color emission is white (with blue shade), despite of high T_c value, this color is called "cold" (or "industry") because human beings have no feeling no heat/comfort. . .
- Color rendering index, noted CRI (unitless): used to define the ability of a light to reproduce the color of an object lighted by the sun. A CRI equals to 100 is given for the sun. A good CRI is superior to 80.
- Trichromatic coordinate (or color point), often given in the (x,y) reference system. A perfect white emission corresponds to $x = 0.33$ and $y = 0.33$.

Note: The notion of trichromatic coordinate (or color point), color temperature T_c, CRI, and gamut are very important for lighting and display applications. The interested reader can find the basic theory of colorimetry in Appendix 16.1.

16.1.1 Lighting devices, an overview

The discovery of electricity dramatically modified lighting, with the development of many lamp types. Among them are the incandescent lamps, energy-saving

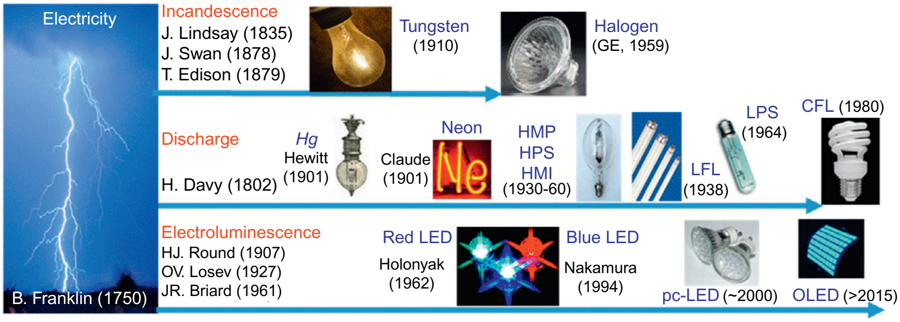

FIG. 16.2

Evolution of modern lighting technologies.

Courtesy of Thierry Le Mercier, Solvay Rare Earth Systems.

fluorescent lamps, and LEDs. Figure 16.2 shows a simplistic scheme of the evolution of lighting devices (combustion technology—candle, oil, gas, or petrol lamps—is not included).

16.1.1.1 Incandescent lamps

Incandescent lamps were developed at the end of the nineteenth century, consisting of a metallic filament placed in a glass bulb containing a rare gas. When electricity is passed through the filament, it warms up by the Joule effect up to incandescence and thus light emission. The tungsten filament was adopted in 1910. Main components of Incandescent lamp are given in the following picture.

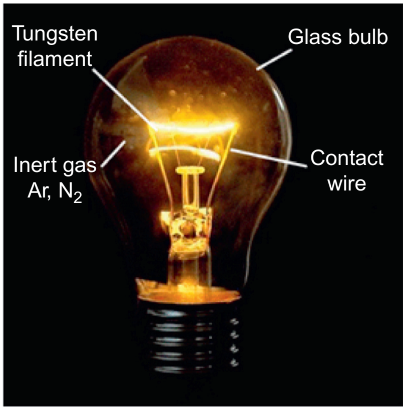

The light emission from these lamps follows the Planck black-body law: a continuous emission in the visible and infra-red, providing a CRI of 100, and a low-color temperature (2700 K, yellowish). The energetic efficiency of these lamps is low (<10%), mainly due to losses in the infra-red which lead to heating of the lamp.

The technology was improved in 1960, with the use of halogen (iodine or bromine derivatives) in the gas, commonly named *halogen lamps*. This increases the resistance of the filament, and thus the ability to use the lamps at higher temperature, giving a brighter and whiter light, but with a higher power consumption.

Today, a new generation of energy-saving halogen lamps has been developed based on IR photon management.

Most low efficiency incandescent lamps are now banned in many countries.

16.1.1.2 Discharge lamps

Discharge lamps operate with another type of physical phenomenon. They are made of a glass tube, filled with gas and/or metallic vapor, through which power is applied via two electrodes leading to plasma creation and finally to light emission. Energetic photons occur from electronic transitions of various excited atoms from the plasma. The emission spectrum is discrete and depends on the nature and the pressure of the gas. The first artificial arc discharge lamp was reported in 1705 and was studied up to the nineteenth century. The technology is based on discharge lamps using mercury vapor (UV and bluish emission), rare gas (red with neon, white with xenon,. . .), or sodium vapor (yellow). The first reported inventors of Hg-discharge lamps are J.T. Way in 1860, L. Arons in 1892, and P.C. Hewitt in 1901. The paternity of the neon lamp is classically attributed to G. Claude (1902), and the Na-discharge lamp to A. Compton (1920).

Today, several technologies of lamps have arisen from this early discharge technology.

16.1.1.2.1 High-pressure discharge lamps

High-pressure discharge lamps (HDL) are used for outdoor lighting (street lighting, sports grounds, etc.). The discharge tube is inserted in a glass bulb with argon gas, enabling the use of these devices under high power, leading to very high brightness. There are three types (main components of HDL are given in the following picture):

- Mercury lamps (HMP, High Mercury Pressure lamp), developed in the 1930s, at very low cost, used in the past for street lighting, with bluish light
- Sodium (HPS, High-Pressure Sodium lamp). The yellowish emission is due to high sodium vapor pressure. CRI can be corrected by addition of rare earth based phosphors.
- Mercury lamps with metallic halogen (MHL, Metal Halide lamp), developed in the 1960s, are based on the use of metallic halogens (Na, Sc, Li, Th, In, or Dy iodides) vaporized in the plasma. These are the best performing HDL lamps in terms of lumens per watt and color rendering index.

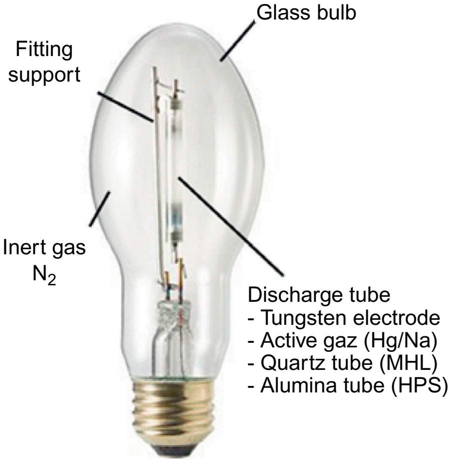

16.1.1.2.2 Neon lamps

Neon lamps, commercialized since 1910, are based on the use of specific gas discharge (Ne, CO_2, He, Hg) to produce monochromatic light. These lamps are widely used in advertising signs.

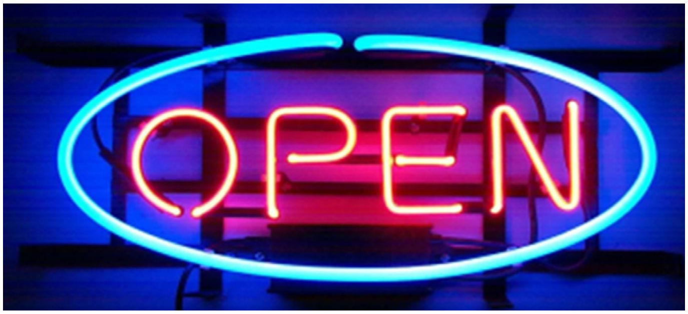

16.1.1.2.3 Sodium low-pressure discharge lamps

Sodium Low-Pressure discharge lamps (LPS), developed in 1930, have a very high lumen efficiency (up to 200 lm/w), long life time, but a poor CRI, with a monochromatic yellow emission. These are still widely used in street lighting (tunnel).

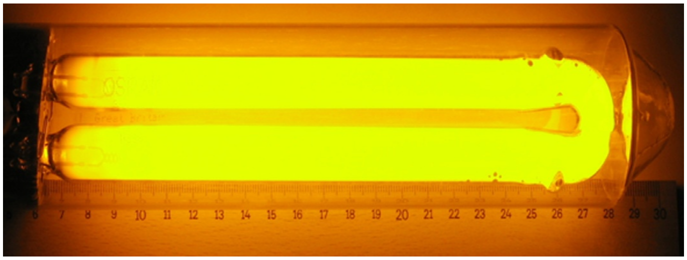

16.1.1.2.4 Mercury low-pressure discharge lamps

Mercury Low-Pressure discharge lamps (LPM) are based on the use of the UV emission of mercury plasma at 254 nm. A coating of fluorescent powder is applied on the interior of the glass tube, in order to convert the UV light from the plasma into visible white light. These lamps were commercialized in the 1940s, with a linear (linear fluorescent lamp, LFL) or circular shape. The rendering index and color temperature can be tuned depending on the type of fluorescent coating, which can consist of one to four types of phosphors. Since the 1980s, the wide use of rare earth-based efficient phosphors has led to high-efficiency lamps, up to 110 lm/W, with good CRI (80 or 90) and adjustable color emission (from 2700 to 6500 K). These lamps operate at low power. They are used in professional and domestic lighting. The LFL became popular for domestic applications in the 1970s. In the 1980s, right after first oil crisis, compact fluorescent lamps (CFLs) were promoted to replace incandescent lamps, consisting of small fluorescent tube curved in spiral or U shapes. The technology is very close to LFL lamps, they can also provide much higher efficiency (70 lm/W) than incandescent bulbs, despite lower CRI. These lamps were widely promoted in the 1990s for household lighting, under the name "energy-saving lamps." These lamps rely completely on the use of rare earth-based phosphors. They are also utilized as UV lamps for sun tanning, phototherapy, black light, photo curing, copy machine lamps, and agriculture lamps.

16.1.1.3 Electroluminescent lamps

LED lamps are based on the emission of light from a semiconductor (SC) under an applied voltage. The physical phenomenon, known since 1907, is the following. Under enough voltage, valence electrons from the SC are excited into the conduction band. Relaxation processes lead to photon emission, with a wavelength close to the gap of the SC (2.7 eV for the blue, to 2 eV for the red).

The first red LED was invented by Holonyak in 1962, based on AsGa. Since then, many improvements have been made, up to the discovery of efficient blue LEDs by Nakamura in 1994, based on InGaN. These LEDs found early applications in gadget devices up to the early twenty-first century.

But the discovery of a blue chip enables the use of LEDs in lighting, either by combination of red, green, and blue chips or by combination of the blue chip with a yellow phosphor, and in some cases, a red phosphor. These are called pc-LEDs (phosphor-converted LEDs). The phosphors are based on rare earth compounds. The previous pictures show three blue, red and green monochromatic LED (first one)and pc-LED (second one). Both are able to give white emission.

The main advantage is very low electricity consumption. Today, this technology is commercialized for household lighting, still at high prices, and it is entering professional lighting, in the shape of LED tubes. The main challenges today are the management of light directionality, management of heat, and cost reduction of these devices. Progress is being made continuously. This technology is expected to be dominant by the year 2020.

The next generation will probably encounter the emergence of OLED technology (organic LED), where the inorganic SC is replaced by organic layers. It should offer lightweight, conformable, and semi-transparent devices.

16.1.1.4 Short comparison of commercial lamps

As a conclusion, Table 16.1 gives the typical characteristics of the main lamps used for general lighting. The underlined lamps use phosphor materials. Performances are representative. Within type, they depend on lamp manufacturer and lamp grade.

The following sections give more detailed descriptions of rare earth lighting technologies, that is, low-pressure mercury lamps (fluorescent tubes and compact lamps) and LEDs.

Table 16.1 Typical Characteristics of Main Lamps Used for General Lighting

Type		Lm/W	Color *T* (K)	CRI	Lifetime (h)	Phosphor
Candle		<0.5	1800	/	/	/
Incandescent		5-15	2700-2800	98-100	~1000	No
Halogen		10-30	2700-3400	98-100	1700-2500	No
HDL	*Hg*	40-60	6800	20	>20,000	No
	HPS	40-140	2300	20-30	24,000	Yes
	MHL	70-115	3700	70		No
LPS		100-190	1800	<0	18,000	No
LFL		55-110	2700-6500	60-95	10,000-16,000	Yes
CFL		40-70	2700-6500	50-70	6000-12,000	Yes
LED		30-120	2540-10,000	70	>25,000	Yes

Table courtesy of Thierry Le Mercier, Solvay Rare Earth Systems.

16.1.2 Focus on trichromatic fluorescent lamps (fluorescent tubes, and CFL)

16.1.2.1 Basics of trichromatic fluorescent lamps

Trichromatic fluorescent lamps are LPM. The glass tube is filled with argon gas as at low pressure (0.2-0.7 kPa) and a few milligrams of mercury. The lamp is then plugged into an electrical circuit via two pins, both metallic electrodes. The tube is covered inside with a complex coating, mainly composed of phosphors. A schematic drawing and a SEM image of the phosphor layer are given in the following picture. The quality and composition of the coating are the key parameters in lamp efficiency and color rendering. All advanced lamps use rare earth materials, especially high atomic number (heavy) rare earths (Eu, Tb).

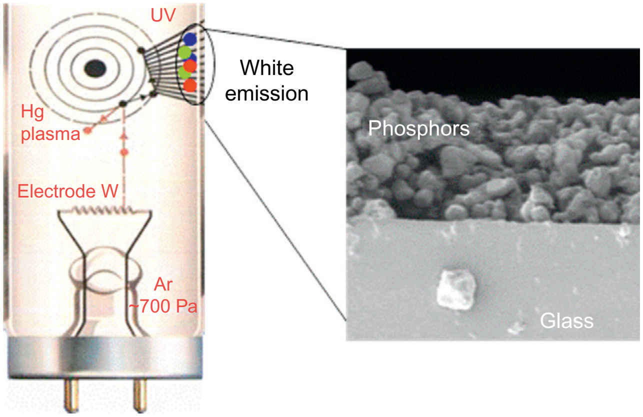

Courtesy of Thierry Le Mercier, Solvay.

During start-up of the lamp, an electric discharge is generated by the high voltage applied between the electrodes. It leads the overheating of the tungsten filament, and an electronic thermoemission from the oxide paste covering the electrode. The generated electrons are accelerated by the electric field between the two electrodes, leading to high number of collisions inside the gas, ionization of the gas, and finally vaporization of the mercury (plasma formation). This plasma emits high-energy photons in the UV range. After start-up, a smaller voltage is enough to maintain electronic mobility from anode to cathode and to maintain the plasma. Note that the argon gas pressure helps to control the free path of the electrons and prevents dissipation of energy on the glass tube.

The temperature inside the tube and the quantity of mercury control the saturation vapor pressure of the mercury. In classical lamps, the optimal Hg pressure is around 1 pascal, which corresponds to the use of few milligrams of Hg per tube.

Emission of the ionized Hg consists of fine lines. In the case of low-pressure lamps, the most intense emission occurs in the UV range (254 and 185 nm), as well as a few weak lines in the visible (405, 436, and 546 nm) light range. About 65% of the power is converted to UV photons, 6% to visible photons while 29% is lost, mainly by heat.

The UV light emitted by the plasma is then converted to visible light by the phosphor coating. The energetic conversion from UV light to visible light by the phosphor is efficient, with a yield of about 40%. This leads to an overall lamp efficiency of 25%, which is much better than incandescent lamps (efficiency of 10%), hence the name “energy-saving lamps.”

16.1.2.2 Process manufacturing of fluorescent lamp

The fluorescent lamp manufacturing process may be summarized as:

http://www.siemens.com

- The phosphor slurry is prepared by a mixing of red, green, and blue phosphor powders, dispersed in water-based formulation. It is coated by gravity or pumping inside the tube, in a form of a micronic coating. The tube with the wet coating is dried and fired briefly in air, at moderate temperatures (400- 600 °C) to burn off all the organic additives. The mechanical consistency of the coating is made through electrostatic bonds
- The two electrodes are sealed to the glass
- The tube is drained and filled with Ar via a blowhole in one of the electrodes. A drop of Hg is inserted in a similar way
- The pin is positioned
- All the lamps are electrically tested.

The coating of the phosphor blend is crucial. The blended suspension requires excellent homogeneity to ensure uniform coating. This is important for the esthetics of the lamp and for its performance. The use of organic additives in the formulation avoids cracks or defects in the coating, and enables the good dispersion of the three colors all along the tube. The densities of the three phosphors are not the same (the blue is much lighter), so there is a risk of segregation of colors along the tube (one end reddish, the other bluish).

The thickness of the phosphor coating is also an important parameter for the performance of the lamp. Too thin a coating gives a low lumen output while too thick a coating leads to light losses and a high lamp operating cost. The optimum thickness in linear fluorescent lamps is 15-30 μm.

The optimal thickness of the coating can be achieved only by a strict management of the particle size distribution of each of the three phosphors. A quick calculation indicates that 3-5 layers of particles are necessary to provide a homogeneous coating. The optimum phosphor particle size is 3-8 μm diameter.

Additionally, some precoating, such as alumina, is usually used to improve the lifetime of the lamp and its performance, by increasing the total UV flux in the phosphor coating.

The color temperature (T_c) and the color rendering index are controlled by the relative proportion of red, green, and blue phosphors in the blend. Commercial fluorescent lamps are defined by a three digits code XAB. X defines the range of CRI ($6 \rightarrow \mathrm{CRI} > 60$, $8 \rightarrow \mathrm{CRI} > 80$...) and AB the T_c ($27 \rightarrow 2700$ K, $65 \rightarrow 6500$ K...).

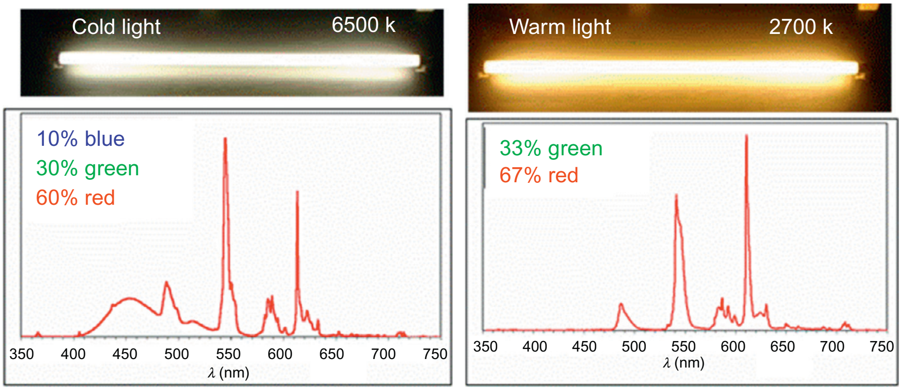

FIG. 16.3

Example of two different RGB blend phosphors leading to different T_c and color rendering index.

Courtesy of Thierry Le Mercier, Solvay.

For warm white light (2700 K), only red and green are used (about 66% of red, and 33% of green by weight), whereas for cold white (6500 K), a blend of red (55-60%), green (30-35%), and blue (10%) is used. An illustration is given Fig. 16.3.

Note that improving phosphor stability and gas discharge management has reduced the tube diameter requirement from T12 size (12/12 of inch) to T8 (8/12 of inch) and T5 (5/12 of inch).

16.1.2.3 Phosphor requirements for fluorescent lamps for general lighting

The phosphors used in trichromatic fluorescent lamps are chosen by the following strict requirements:

(1) In terms of optical properties
- Absorbs efficiently at 254 nm (high absorption cross-section at 254 nm), and no absorption in the visible range (380-700 nm)
- Converts efficiently the UV photons into blue, red, and green photons (the internal quantum yield is high, and the emission wavelength is centered on maximum eye detection)

(2) In terms of compatibility with lamp manufacturing
- Being manufactured as a fine micronic powder, to be coated as a homogeneous layer, with controlled thickness. As such, the particle size of the phosphor is strictly monitored in the range of 3-10 µm, with monodisperse distribution

- Stable after firing under air at relatively high temperature (500-600 °C, for 15-30 min)
- Stable against UV exposure and Hg plasma exposure during lamp use

In practical applications, the choice of the phosphors results from the compromise between the best intrinsic properties of luminescence, the matrix stability in application, the ability to make the material with desired morphology, crystallinity, and particle size at reasonable cost.

16.1.2.4 Evolution of phosphor materials in trichromatic fluorescent lamps for general lighting

The Table 16.2 summarizes the types of phosphors used in the past, and used today, in the main types of linear and compact fluorescent lamps.

Before the 1950s, the luminous efficiency (~40 lm/W) and the lifetime (<2000 h) of the lamps based on the early phosphors such as $MgWO_4$ (bluish, 482 nm) and $(Zn,Be)_2SiO_4:Mn$ (green-red) were very poor.

The discovery of beryllium toxicity speeded up the development of halophosphates which made a great improvement in lamp efficiency up to 50-60 lm/W. These phosphors have the general formula $Ca_5(PO_4)_3(Cl,F):Sb,Mn$, having a broad white emission—the color temperature being tuned by the Sb/Mn ratio. In the 1980s, the halophosphate technology represented 85% of lighting phosphors. Even after years of improvement, high performances (80 lm/W) were limited to low CRI (60), or high CRI to low efficiencies. Today, this phosphor is still used in about 50% of fluorescent lamps, especially for low-cost applications, where the CRI is not at stake.

The availability of pure separated lanthanides on an industrial scale (Rhône-Poulenc, 1960-1970) led to their use in lamp applications. In 1971, calculations showed that the blend of three red (610 nm), green (540 nm), and blue (450 nm) phosphors would lead to high luminous efficiency (100 lm/W) with CRI>90. One year later, the experimental proof was achieved with a blend of $Sr_5(PO_4)_3Cl:Eu^{2+}$ (SPCE) for blue, $Zn_2SiO_4:Mn^{2+}$ (ZSM) for green, and $Y_2O_3:Eu^{3+}$ (YOX) for red.

Table 16.2 Characteristics of Main Phosphors Used in Trichromatic Fluorescent Lamps

General Lighting	Main Phosphors		
Early technology (1938)	$MgWO_4$ (bluish, 482 nm), $(Zn,Be)_2SiO_4:Mn^{2+}$ (green-red)		
Low cost technology (low CRI, low lm/W)	$Ca_5(PO_4)_3(Cl,F):Sb^{3+},Mn^{2+}$ (White)		
Standard technology (good CRI, high lm/W)	$BaMgAl_{10}O_{17}:Eu^{2+}$	$CeMgAl_{11}O_{19}:Tb^{3+}$ $(La,Ce)PO_4:Tb^{3+}$	$Y_2O_3:Eu^{3+}$

lm/W = lumens per watt.

These lamps were commercialized promptly, having a high CRI, but (unfortunately) a short lifetime due to the poor stability of ZSM.

The second major improvement came from the discovery of a better green emitter based on terbium, the aluminate (Ce,Tb)$MgAl_{11}O_{19}$ (CAT), with much better stability than the silicate. Then, in the late 1980s, the introduction of a new blue phosphor $BaMgAl_{10}O_{17}:Eu^{2+}$ (BAM) and a brighter green phosphor (La,Ce)$PO_4:Tb^{3+}$ (LAP) improved again the performances of the fluorescent lamps, with a better lumen efficiency, color rendering, lifetime, and cost.

Today, the YOX (red), CAT or LAP (green), and BAM (blue) are used in all triband fluorescent lamps, which represent about half the fluorescent lamps worldwide (about 10,000 tons of phosphors). The emission spectra of these phosphors are given in Figure 3 of Chapter 15. Table 16.3 summarizes the main characteristics of classical fluorescent lamp rare earth phosphors.

In some specific cases, when high CRI are required, an additional fourth phosphor is added, such as BAM:Eu^{2+}, Mn^{2+} (blue-green). In rare cases, a deep red is also added, such as $Mg_4GeO_{5.5}F:Mn^{4+}$.

The performances of the lamp phosphors have been closely related to the availability of pure raw materials (from rare earth separations, e.g., at La Rochelle). Indeed, even small amounts of impurities, such as metallic ions (Fe, Ni) or other rare earths, are very harmful to quantum efficiency. Secondly, the cost and performances of the lamps have been linked to improvements in the synthesis routes, which are able to produce high-brightness phosphors with small and monodisperse particle size. These two aspects are generally achieved with opposite synthesis parameters.

Table 16.3 Main Characteristics of Classical Fluorescent Lamp Rare Earth Phosphors

	BAM (Blue)	***CAT (Green)***	***LAP (Green)***	***YOX (Red)***
Composition	$Ba_{1-x}Eu_xMgAl_{10}O_{17}$	$Ce_{1-x}Tb_xMgAl_{11}O_{19}$	$La_{1-x-y}Ce_xTb_yPO_4$	$Y_{2-x}Eu_xO_3$:Eu
Structure	Alumine β	Magnetoplumbite	Monazite	Bixbyite
%mol dopant	$x \sim 0.1$	$x \sim 0.33$	$x \sim 0.2$-0.4, $y \sim 0.1$-0.2	$x \sim 0.03$-0.08
Densité	3.84	3.4	5.2	5
Emission	Eu^{2+} (5d→4f band)	Tb^{3+} (4f-4f peaks)	Tb^{3+} (4f-4f peaks)	Eu^{3+} (4f-4f peaks)
	$\lambda = 450$ nm	$\lambda = 543$ nm	$\lambda = 543$ nm	$\lambda = 611$ nm
Excitation	Eu^{2+} (4f→5d band)	Ce^{3+} (4f→5d band)	Ce^{3+} (4f→5d band)	Eu^{3+}-O^{2-} CT
Baking stability	Poor	Middle	Middle	Very high

Courtesy of Thierry Le Mercier, Solvay.

Table 16.4 Phosphors Used in Trichromatic Fluorescent Lamps for Nonlighting Applications

Application	Phosphors
UV tanning	$SrB_4O_7:Eu^{2+}$ (371 nm) or $BaSi_2O_5:Pb^{2+}$ (351 nm) are moved progressively by $YPO_4:Ce^{3+}$ (335/355 nm) and $LaPO_4:Ce^{3+}$ (316/335 nm)
Photo-therapy	Tanning and pigmentation: $(Ce^{3+},Mg)SrAl_{11}O_{18}:Ce^{3+}$ (338 nm) Erythema: $SrAl_{12}O_{19}:Ce^{3+},Mg^{2+}$ (300 nm) Psoriasis: $GdBO_3:Pr^{3+}$ and $(La,Gd)B_3O_6:Pr^{3+}$ (312 nm), $(Y,Gd)MgB_5O_{10}:Ce^{3+},Pr^{3+}$ Blood treatment: $Sr_2P_2O_7:Eu^{2+}$ (420 nm)
Copy machine	$Ba_2SiO_5:Pb^{2+}/SrB_4O_7:Eu^{2+}/Sr_2P_2O_7:Eu^{2+}$ (420 nm)
Black light	$Ba_2SiO_5:Pb^{2+}/SrB_4O_7:Eu^{2+}$
High pressure	$Y_3Al_5O_{12}:Ce^{3+}$ (565 nm)/$Mg_4GeO_{5.5}$ F:Mn^{4+} (660 nm)/$Y(P,V,B)O_4:Eu^{3+}$ (619 nm) $(Sr,Mg)_3(PO_4)_2:Sn^{2+}$ (627 nm)
Advertisement (High voltage)	Blue: $CaWO_4:Pb^{2+}$ $MgWO_4$ $Sr_5(PO_4)_3Cl:Eu^{2+}$ Cyan: $Ba_2P_2O_7:Ti^{4+}$ $BaMgAl_{10}O_{17}:Eu^{2+},Mn^{2+}$ Green: $Zn_2SiO_4:Mn^{2+}$ $CeMgAl_{11}O_{19}:Tb^{3+}$ Red: $Y_2O_3:Eu^{3+}$ $Mg_4GeO_{5.5}$ F:Mn^{4+} Pink: $CaWO_4:Sm^{3+}$ $CaSiO_3:Eu^{2+},Pb^{2+}$

Courtesy of Thierry Le Mercier, Solvay (Adaptated from Phosphor Handbook, see suggested reading).

16.1.2.5 Phosphors for other lamp applications

Today, many applications are derived from fluorescent lamp technology: UV lamps for tanning or phototherapy, germicide lamps, black light lamps, copy machine lamps, infrared lamps, and lamps for agriculture, etc.

For each of these applications, the requirements are adapted in terms of luminous efficiency, emission wavelength, color point, and color rendering index. The Table 16.4 gives an nonexhaustive overview of the phosphors used in these technologies, many of them based on lanthanides.

16.1.3 Focus on LED and the phosphors

16.1.3.1 Basics of phosphors converted LED

The emergence of white LEDs for lighting has been possible since the development of high-efficiency blue chips in the 1990s. The chips are based on the n-GaN/InGaN/p-GaN n-p junction, grown on substrates such as sapphire or silicon carbide (Fig. 16.4). The photon emission corresponds to the gap of the $In_{1-x}Ga_xN$ semiconductor (420 nm for $x=0.8$ to 440 nm for $x=0.7$).

The chip is positioned in a reflective cavity and recovered by an encapsulant (e.g., silicone) which protects the device. A polycarbonate lens covers the whole device.

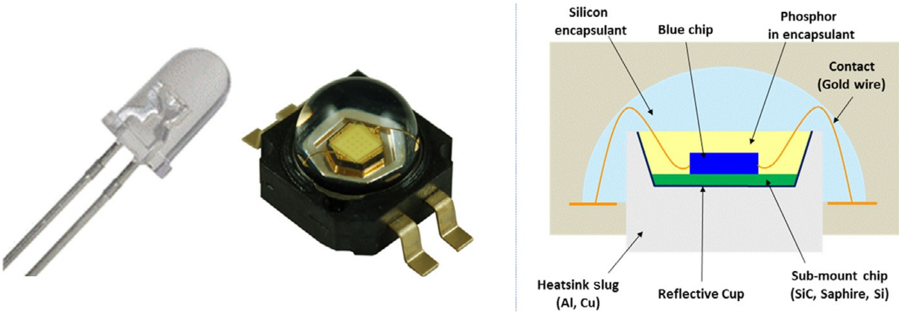

FIG. 16.4

Two kinds of light-emitting diodes (LED) and their schematic representation.

Courtesy of Thierry Le Mercier, Solvay.

Below the chip, a metallic radiator is placed with the essential role to remove the heat from the device.

The white light is generally obtained by combining this blue light with a yellow-emitting phosphor that absorbs partially the emitted blue light. The combination of blue and yellow leads to cold white emission with poor CRI.

Some improvement in CRI and color temperature is achieved by adding some red phosphor, and in some cases substituting the yellow phosphor by a green phosphor.

Today, the large majority of pc-LEDs use blue chip LEDs. UV-LEDs also exist, based on a UV-emitting chip and red, green, and blue phosphor combinations.

The LED devices are *a priori* very efficient: 50% of electric power is transformed into light (vs. 25% for the LFL or CFL) and 50% lost is in thermal radiations (mainly in heating of the silicon chip itself). The thermal losses induce a high device use temperature up to 150 °C, which leads to thermal quenching of the device's phosphors and yellowing of the device's polymers.

Phosphors can be positioned several ways in LED devices (Fig. 16.5):

- Diluted dispersions in the encapsulant (classical design)
- Concentrated in the encapsulant close to the chip (conformal coating technology)
- Sintered as a transparent ceramic, covering the chip
- Dispersed in a plastic layer far from the chip (remote phosphor technologies).

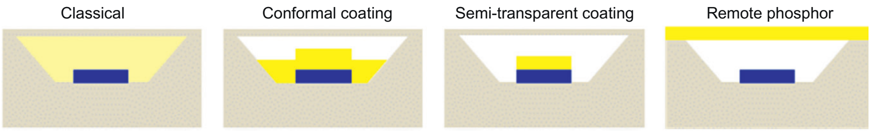

FIG. 16.5

Schematic architecture of various modern light-emitting diodes.

Courtesy of Thierry Le Mercier, Solvay.

16.1.3.2 Phosphor materials used in LED for general lighting

The requirements of general lighting phosphors are similar to those of fluorescent lamps—in terms of the wavelength of excitation (440-480 nm) and the temperature and moisture stability requirements. The particle size is adjusted to optimize the scattering of the light in the device and to reduce the directionality of the chip emission. Usually, micronic phosphors are used, in the range of 10 μm diameter.

Efficient blue-excited phosphors were very rare up to the 1990s, only $Y_3Al_5O_{12}$:Ce^{3+} “YAG” (yellow emission), and a few sulfides such as $SrGa_2S_4$:Eu^{2+} (green, the beautiful one) and SrS:Eu^{2+} (red) were identified at that time.

Figure 16.6 shows that the absorption spectrum of YAG fits perfectly to the emission one of the blue chips. The combined blue (from the chip) and yellow (from the YAG) gives an overall white emission.

Today, the YAG yellow phosphor is widely used in almost all white LED devices, due to its exceptional properties in terms of quantum efficiency and unique stability. Many improvements and fine tunings have been made in terms of synthesis routes (elimination of all crystal defects), doping (mostly Gd, Lu, Ga) to improve efficiency, and also to be able to adapt the absorption band of Ce^{3+} exactly to the blue emission of the chip.

Contrary to YAG, the definition of new red and green phosphors is still the subject of active research in the 2010s. In these cases, the main issues are (i) to reach high efficiency under blue light excitation and (ii) to obtain enough stability in application (temperature, moisture). The objectives are to achieve colder T_c (<3000 K) and higher CRI (>85).

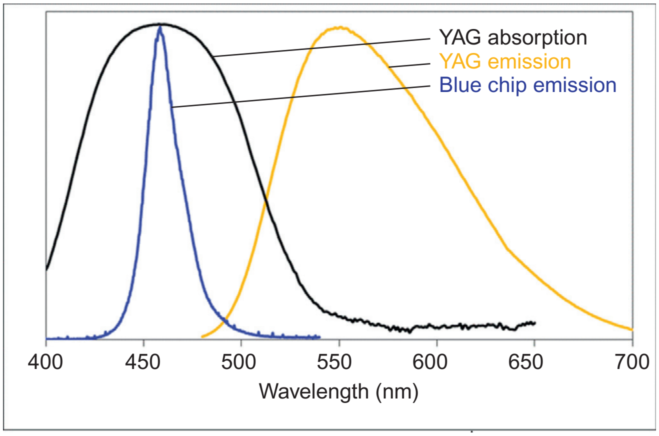

FIG. 16.6

Absorption (black) and emission (yellow) of YAG compared to blue chip emission (blue).

Courtesy of Thierry Le Mercier, Solvay.

Table 16.5 Classical Phosphors Used in Light-Emitting Devices (2014)

	Yellow	**Red**
β-SiAlON:Eu^{2+}	$(Y,Gd)_3(Al,Ga)_5O_{12}$:Ce^{3+}	$Sr_2Si_5N_8$:Eu^{2+}
$(Ba,Sr)_2SiO_4$:Eu^{2+}	$La_3Si_6N_{11}$:Ce^{3+}	$CaAlSiN_3$:Eu^{2+}
$Ba_3Si_6O_{12}N_2$:Eu^{2+}	$(Sr,Ba)_2SiO_4$:Eu^{2+}	
$Lu_3Al_5O_{12}$:Ce^{3+}		

Courtesy of Thierry Le Mercier, Solvay.

Today, composition variations around YAG have shown that a very good green phosphor is achieved by complete substitution of the Y matrix by a lutetium matrix (LuAG). However, Lu being very expensive, this green phosphor is only used when a very stable green phosphor is necessary.

The sulfide (Ca,Sr)S:Eu^{2+}, the original red phosphor, has now been replaced by nitrides, which have a better chemical stability, but very complex synthesis routes.

Some tremendous improvements came from the discovery of europium (and cerium)-based nitrides and oxynitrides. The first nitride-based red phosphor was $Sr_2Si_5N_8$:Eu^{2+} in association with YAG, in the year 2005. Its emission occurs around 640 nm. This phosphor has a high quantum efficiency and quite good thermal and chemical stability. An alternative nitride is $CaAlSiN_3$:Eu^{2+}, with similar performance. All these phosphors are still being improved in composition and synthesis route.

Some interesting green oxynitrides have been developed in the same way. The most classical one is β-SiAlON:Eu^{2+}.

All of these nitride and oxynitride compounds require very specific industrial equipment. They are locked by several patents and do not fulfill perfectly all performance requirements. As a consequence, an alternative family has been developed, based on silicates $(Ba,Sr)_2SiO_4$:Eu^{2+}. A broad family with variations around this composition has been proposed, with emissions from green to orange. Some stability issues are still to be overcome.

To summarize, Table 16.5 gives the most classical phosphors used today for blue pc-LED.

16.1.4 Last evolution of the lighting market

Two factors have completely changed the lighting market in the past decade: the banishment of incandescent bulbs in developed countries, by the use of energy-saving lamps (fluorescent lighting), and the technological improvement of LED lighting (Fig. 16.7).

The banishment of incandescent bulbs has consolidated the market share of fluorescent lighting: compact fluorescent lamps for household lighting and linear fluorescent tubes for professional lighting. The linear fluorescent tube is a mature technology, which does not require scientific improvement, but a cost decrease. It

FIG. 16.7

Commercial LED technology in lighting: (left to right) tube, bulbs, and remote phosphors (Creative common photos).

will be partially replaced by LED tubes, when extremely low consumption and long lifetime are at stake, and when LED tubes and devices decrease in price.

On the contrary, CFLs are not yet fully accepted by consumers, since their cost is still rather high and when fast start-up and warm color light are required. In many cases, halogen lamps are preferred, and a new generation of energy-saving halogen lamps has found some market in the past decade, especially in western countries.

Some significant benefits are thus expected from LED bulbs, which are today not fully mature in terms of design and cost. Improvements are necessary in terms of integration into existing lighting systems and in defining new ways of lighting, management of the directionality of the light emission, lifetime of warm light LEDs, and cost reduction. Their very low-energy consumption is an advantage in emerging countries, which are expected to jump directly from incandescent to LED lighting.

In the long term, organic light emitting diode lighting will enable the design of wide and conformable luminescent surfaces, additionally semitransparent. A new era for designers and architects will emerge, if the technology keeps its promises.

Finally, the lamp market is expected to be split between fluorescent T5 and T8 tubes and LED devices (tubes and bulbs). In 2020, LED should represent 50% of the market. Fluorescent tube lighting is expected to be 30% of the total market of commercial lighting.

16.2 RARE EARTHS FOR DISPLAY APPLICATION

Rare earth phosphors played an important role in the development of almost all kinds of displays. Today, many technologies are commercialized, adapted to each application segment (smart portable devices, T, projection, etc.).

The main criteria in selecting a type of display are contrast (quality of black and white), luminosity, angle view, range of accessible color (gamut), lifetime, definition (number of pixels), weight and size, electricity consumption and finally cost.

The technologies of displays can be classified in two categories (Fig. 16.8): direct visualization or visualization by projection. Direct visualization can be emissive or nonemissive.

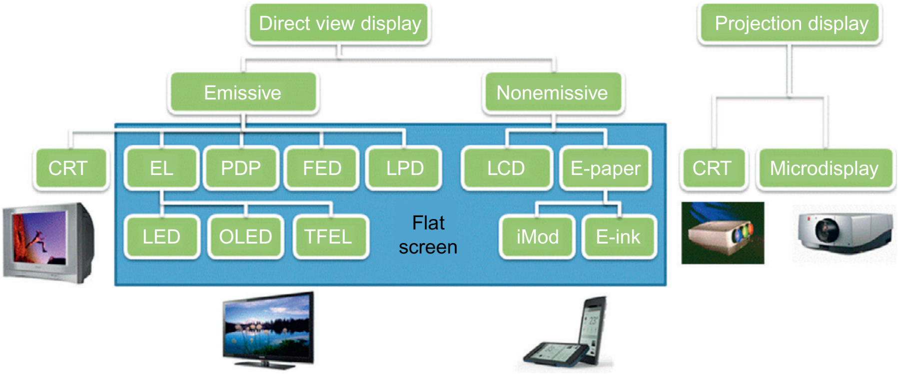

FIG. 16.8

Various kinds of commercialized displays. CRT: cathode ray tube, EL: electroluminescent, PDP: plasma display panel, FED: field emission display, LPD: laser phosphor display, TFEL: thin film electroluminescent, LCD: liquid crystal display.

Courtesy of Thierry Le Mercier, Solvay.

- In the case of emissive devices, three primary colors (red, green, and blue) are combined to obtain white, and the modulation of the relative intensities defines all the colors of the gamut triangle. The main emissive displays are
  - Cathode ray tubes, where the excitation source is electrons
  - Plasma display panels (PDPs), where the excitation source is vacuum ultra violet photons
  - Organic light-emitting diode displays, where the excitation source is an electric field.
- In the case of nonemissive panels, a white light source is filtered with three color filters (blue, red, and green), by which transmission is modulated, generally with liquid crystal displays, or by reflection with micromirrors (microdisplays). The white light source is called the back light, which can be created by a fluorescent tube, a white LED (both for LCD), a Xenon lamp (microdisplays), or a day light (e-paper)

All the emissive displays are based on inorganic or organic luminescent compounds to generate the three primary colors. The backlighting technologies (fluorescent or LED) also use some phosphors to generate the white light, which are similar to the ones defined in the lighting sections.

Concerning phosphors for emissive displays, some specific characteristics are required:

- Short lifetime, <10 ms to avoid afterglow of the image.
- Stability under excitation source $>10{,}000$ h.
- High external quantum yield to achieve high luminescence of the display.
- Chromatic purity of each of the three colors. This part is much more drastic than for lighting, since the challenge is to be able to generate the maximum of color from the color triangle, and not only white light. Standards are: red ($x>0.65$ and $y<0.35$), green ($x<0.21$ and $y>0.71$), and blue ($x<0.15$ and $y<0.06$).

Of course, the size and morphology of the phosphors need to be adapted to the production process, and especially to pixel size. High-definition devices will generally require finer-sized phosphors.

16.2.1 Cathode Ray Tube (CRT), the use of electron beam for early color TV

CRT technology derives from studies on cathodic rays and oscilloscopes at the end of nineteenth century. The first monochromic television displays were commercialized in 1922, and the first color TV in 1954.

The operating principle is the following (main components of CRT are given in the figure below):

- electrons are emitted from a cathode, by thermionic emission
- the electrons are then accelerated to the anode with a high voltage (~10-40 kV) in a tube under vacuum. Magnetic coils direct the beam in two dimensions
- electrons hit a network of phosphors coated on the panel glass, which further emit light through cathodoluminescence.

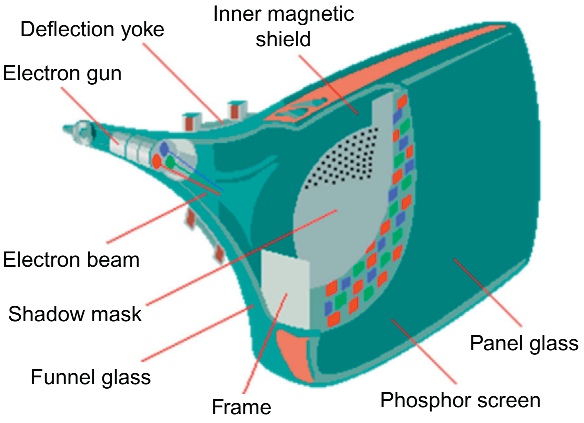

Adapted by Thierry Le Mercier, Solvay.

For color TV, three distinct beams scan the screen, in order to generate the three primary colors (red, green, and blue) with the desired intensity. The phosphors were optimized during 3 decades, in composition and with coatings. Today, the optimum ones are ZnS:Ag (blue), (Zn,Cd)S:Cu,Al (yellow), and $Y_2O_2S:Eu^{3+}$ (red, YOS).

The definition of the red phosphors in the early 1960s, in early stage YVO_4:Eu, then Y_2O_3:Eu, and finally Y_2O_2S:Eu, has boosted research and use of rare earths for all luminescent applications. The YOX is preferred for its very high efficiency under electronic excitation. Lately, in order to improve the contrast of the displays, a thin coating of red pigment α-Fe_2O_3 has been used on the red YOS phosphor. This coating is able to filter the orange emission of Eu^{3+}, to keep only red lines. Additionally, small dopings of Tb^{3+} and Sm^{3+} helped to further improve the performance of YOS.

For decades, cathode ray technology has been used for very large screen projectors. In these devices, the excitation energy is very high, and the phosphors have been adapted to avoid saturation of the light emission. $Y_3Al_5O_{12}:Tb^{3+}$ is used for green, and YOX for red.

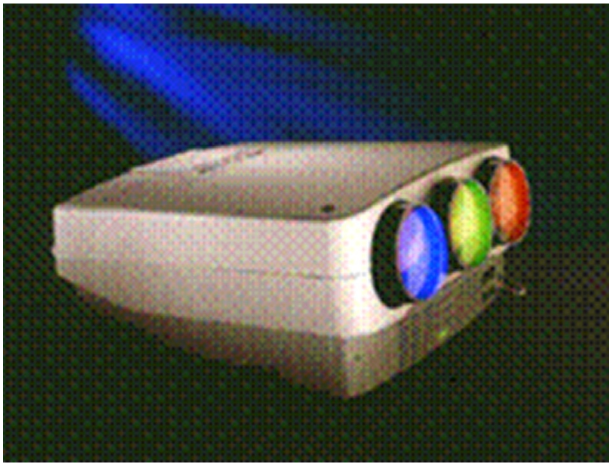

CRT technologies dominated the market from the 1960-90s. Today, they have been replaced by flat displays liquid crystal displays and plasma display panels. A flat CRT technology was developed in the 2000s, with minor market share (field emission display).

16.2.2 PDP (plasma display panels), high photonic excitation

The PDP operating principle is similar to fluorescent lighting (see the figure below). High-energy UV photons, mainly at 147 and 172 nm, are generated by a plasma (Xe-Ne gas). These photons then excite three phosphors. Each PDP pixel is composed of cells coated with a phosphor and filled with the gas. An electric discharge is set to vaporize or not vaporize the gas, and thus to light up or not light up the cell. The intensity depends on the applied voltage. Its main advantage is that it can be used with flat panels.

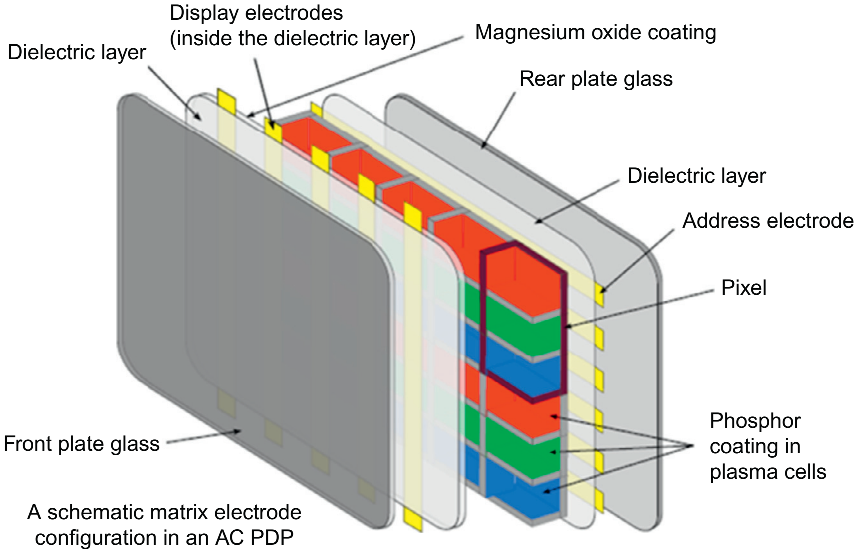

A schematic matrix electrode configuration in an AC PDP

Table 16.6 Classical Phosphors Used in PDP Devices with Associated Color Points

Red (0.67/0.33)	**Green (0.21/0.71)**	**Blue (0.14/0.08)**
$(Y,Gd)_2O_3$:Eu 0.64/0.35 $(Y,Gd)BO_3$:Eu 0.64/0.36 $Y(P,V)O_4$:Eu 0.66/0.35	Zn_2SiO_4:Mn 0.23/0.70 $(Y,Gd)BO_3$:Tb 0.15/0.75	$BaMgAl_{10}O_{17}:Eu^{2+}$ 0.14/0.06 $CaMgSi_2O_6:Eu^{2+}$ 0.19/0.21

Table courtesy of Thierry Le Mercier, Solvay.

This technology was invented in early twentieth century, but color PDP TV appeared at the beginning of 1990s. After many improvements, the current phosphors are as shown in Table 16.6.

These phosphors have been chosen because of their short decay time (<10 μs), stability, and non-saturation even with high-excitation fluxes and high energies, due to the use of a vacuum ultra violet excitation source. Moreover, they have excellent color coordination and the purest primary colors. Stability under radiation is a challenge for the phosphors.

The red phosphor is classically $(Y,Gd)BO_3$:Eu, which has the best stability and luminescence efficiency, but orange color emission and toxicity problems due to boron. It is being replaced by YOX. Deeper red can be achieved when necessary for a wide color gamut, by $Y(P,V)O_4$:Eu.

For green emission, a blend of $(Y,Gd)BO_3$:Tb and Zn_2SiO_4:Mn is usually used. Indeed, the silicate provides the best green color but has a lack of stability, whereas the borate provides high stability with poor green emission.

For blue, BAM is now used widely, due to its perfect color emission and high efficiency. Also, special synthesis routes are used, providing high-quality phosphors, sometimes with inorganic coatings, in order to secure stability under commercial operating conditions.

16.2.3 The LCD display and their backlighting (CCFL and LED backlights)

Today, the most popular display technology is LCD technology. In this case, a homogeneous white light source is used to light up pixels composed of liquid crystals, which will be more or less polarized in order to modulate the intensity of the white light. For each pixel, three filters (red, green, and blue) recreate the desired color. The image is finally composed by addition of the three color beams (Fig. 16.9—right and middle).

The color quality of the display (gamut) comes essentially from both the quality of the color filters and the type of white light, i.e., the initial spectrum of the white light. Improvement of the color filter is still an active domain of research.

The white backlight (Fig. 16.9—left) is generated from a very thin fluorescent tube (CCFL, cold cathode fluorescent tube), or by LEDs. The latter has the biggest market share today, due to its thinner devices and lower electricity consumption.

If the principle is the same as for lighting, the choice of phosphors in CCFL, or for pc-LED, has been tuned in order to provide the widest possible color triangle.

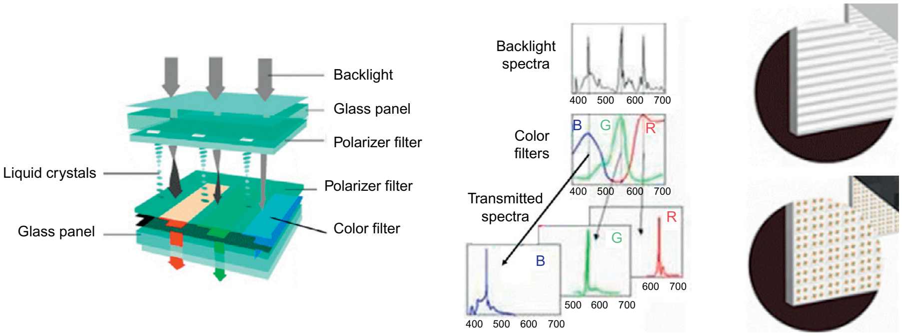

FIG. 16.9

Liquid crystal display technology. Left: global scheme—Middle: evolution of light spectra during LCD operation—Right: cold cathode fluorescent tube (top) or light-emitting display backlight (bottom).

In case of CCFL backlight, the fluorescent tube diameter is lower than classical T5, which increases the ultraviolet flux and the temperature seen by the phosphor. Thus, there is a need to choose the highest stability phosphors from among all the available UV-excited phosphors. Moreover, the color gamut (range) can be improved by using a blend of 4 or 5 phosphors. Blue-green and deep-red emitters may be added in the mix.

In case of LED backlight, classical white LED (with YAG:Ce phosphor) may not be enough to get a large color gamut. Once again, new phosphors are needed, to enlarge the gamut. Color emission of these new materials should fit with green (mainly silicate doped Eu^{2+}) and red emissions (mainly nitride doped with Eu^{2+}).

LCD technology is now the dominant one for display devices: televisions, computers, projectors, etc.

16.2.4 Last evolution of the display market

As previously said, the CRT has almost disappeared of consumer flat displays, which are today dominated by LCD devices, with light-emitting display backlights.

A small part of the market is still devoted to PDP displays for very large screens, which have the reputation of having a slightly better image quality (deeper black color, image fluidity), but more weight and a higher electricity consumption. Both technologies are still improving.

On the side of small devices, organic light-emitting diode displays are penetrating the market, especially on smart phones. The prospect of using them on large screens is exciting.

16.3 RARE EARTH FOR MEDICAL EQUIPMENTS

Medical diagnoses have improved significantly over recent decades, with the massive use of 2D and 3D imaging technologies (Fig. 16.10), in parallel to digitalization of classical X-ray and gamma radiography.

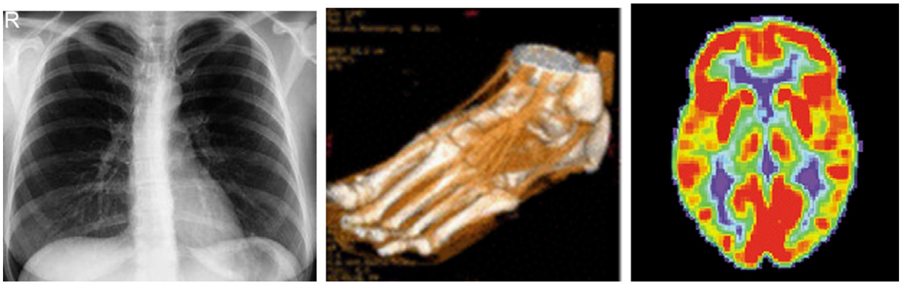

FIG. 16.10

Examples of radiography: 2D X-ray (lungs), 3D X-ray (foot), and γ-rays PET (brain).

Rare earth-based phosphors have strongly contributed to the development of these new medical imaging technologies, being able to absorb high-energy rays, transforming them into visible light.

Such materials are called scintillators, i.e., they exhibit *scintillation*, which is luminescence that is excited by ionizing radiation, such as X-rays or γ-rays. Scintillators are used in a wide range of applications, including medical imaging, high-energy physics, well logging, space exploration, and homeland security.

Note that some authors use the term scintillator only when the luminescent material is a scintillation monocrystal and keep the term phosphor for scintillation powder.

The main applications of scintillators are the following (see examples in Fig. 16.11):

- X-ray radiography: used when the contrast is enough (bone/flesh/muscle)
  - Planar X-ray photography: Rare earths are used to decrease radiation dosage to the patient. Technologies are mainly intensifying screens and photo-stimulation storage phosphor screen.

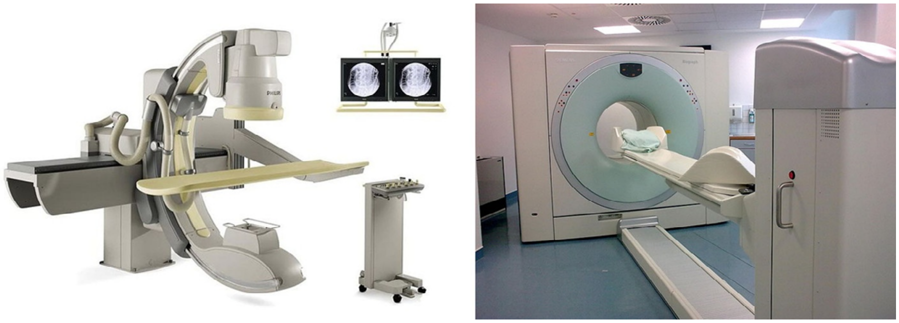

FIG. 16.11

Example of commercial medical equipments, from left to right: X-ray (planar) and γ-rays (positron emission tomography-computed tomography).

  - X-ray computed tomography (CT, 3D): 3D images are obtained by scanning an X-ray source and detector (scintillator) ring around the patient.
- Gamma ray radiography: γ-rays are emitted by a radioactive isotope that is injected into the patient and which accumulates in an organ (e.g., for detection of tumors) or the blood stream (to image blood flow through the heart or brain). The main technique is positron emission tomography (PET). The tracer emits positrons which interact with electrons resulting in the emission of two γ photons in opposite directions. A PET scanner detects these emissions "coincident" in time. A 3D image is reconstructed (tomography) from the pattern of the detected γ-rays.

The scintillation process occurs in several main steps: (see the drawing below).

1. After high-energy absorption, the ionization event creates an inner shell hole and an energetic primary electron, followed by radiative decay (secondary X-rays), nonradiative decay, and inelastic electron-electron scattering in the time domain of 10^{-15}-10^{-13} s.
2. When the electron energy becomes less than the ionization threshold, hot electrons and holes thermalize by intraband transitions and electron-phonon relaxation. During this stage, luminescent centers are excited by impact with hot electrons over a time scale ranging from 10^{-12} to 10^{-8} s.
3. The excited luminescent species returns to the ground state by nonradiative quenching processes or by emitting a photon.

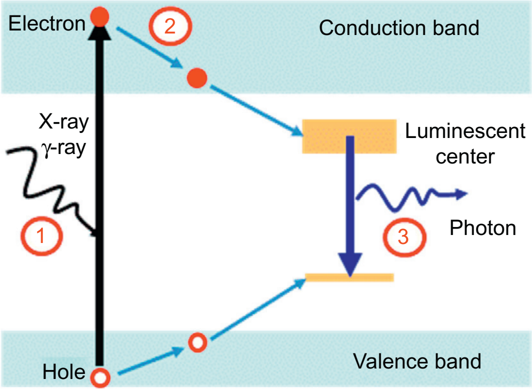

Drawing by Thierry Le Mercier, Solvay.

16.3.1 Focus on x-ray intensifying screens

Intensifying screens have been used since the discovery of X-rays by W. Röntgen in 1895. X-rays are not strong enough to sensitize argentic (Ag) photographic paper. To reduce patient exposure time, a layer of X-ray phosphor is added before the paper (the irradiation time is reduced by a factor of 1000).

Figure 16.12 shows a classical cartridge where photographic paper is positioned between two layers of X-ray intensifiers. They are composed of X-ray phosphor powder in a plastic binder. The emitted visible photons are absorbed by the

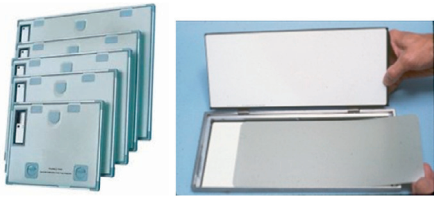

FIG. 16.12

Classical commercial x-ray intensifying screens.

photographic film to form the radiographic image. Note that the emitted photons are more diffuse than direct X-ray excitation leading to a loss of resolution. The size of phosphor grain is typically 3-10 μm diameter.

Requirements for phosphors in this application are:

- High X-ray absorption (achieved by high-density materials and high atomic number (Z) value)
- Efficient blue-green emission, which fits well with photographic paper sensitivity
- Chemically stable
- Low price.

The earliest phosphor was $CaWO_4$. This imperfect phosphor shows a broad blue emission band, an afterglow and relatively low X-ray capture in the 30-80 keV energy range. Since 1970, new X-ray phosphors with higher luminescence efficiency and stronger absorption properties have been developed, for example, $Gd_2O_2S{:}Tb^{3+}$ (green), $LaOBr{:}Tm^{3+}$ (blue), and $YTaO_4{:}Nb$ (UV).

16.3.2 Focus on photostimulated storage phosphor screen

Superior images can be obtained using radiography based on photostimulated luminescence. Under X-ray irradiation, electrons are trapped in some structural defects. The radiography is revealed by a laser which releases the trapped energy, further transferred to a luminescent ion. An efficient photostimulable material is $BaFBr{:}Eu^{2+}$ whose stimulation can be performed with a helium–neon laser ($\lambda = 633$ nm). Emission occurs at 390 nm. Requirements of photostimulable X-ray phosphors are

- X-ray absorption (achieved by high-density materials, barium based is suitable)
- The amount of energy storage in the phosphor by a unit X-ray dose must be large
- Short decay time (<10 μs, which is why Eu^{2+} 5d-4f transition is suitable)
- Fading of information stored in the phosphor must be slow
- Stimulation must be possible in the IR or near-IR. Emission must be detectable by a charge coupled device detector.

Rare earth materials are particularly interesting for this application. Besides $BaFBr{:}Eu^{2+}$, several compounds have been proposed such as $Ba_5SiO_4Br_6{:}Eu^{2+}$, $Ba_3(PO_4)_2{:}Eu^{2+}$, or $Y_2SiO_5{:}Ce^{3+}$.

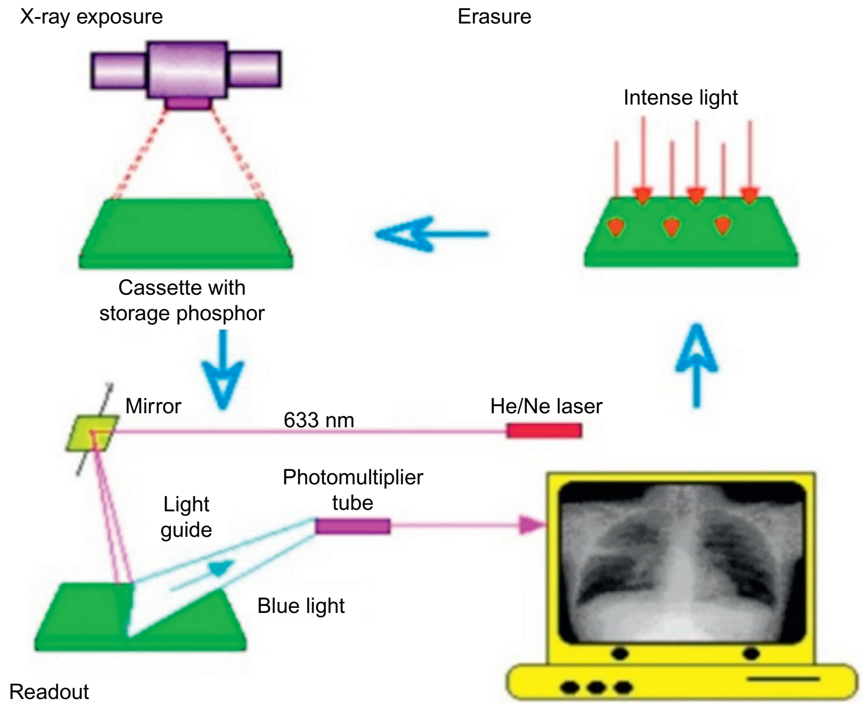

(Public domain drawing)
http://en.wikibooks.org/wiki/Basic_Physics_of_Digital_Radiography/The_Image_Receptor

16.3.3 Focus on tomography medical equipment: X-ray CT and PET

X-ray CT and PET techniques use multi-channel detectors. Each channel is composed of a transparent scintillator coupled with a photodiode. The X-ray or γ-ray is absorbed by the front face of the scintillator, where the luminescence occurs. After that, the emission is guided toward a photodiode where the signal is recorded.

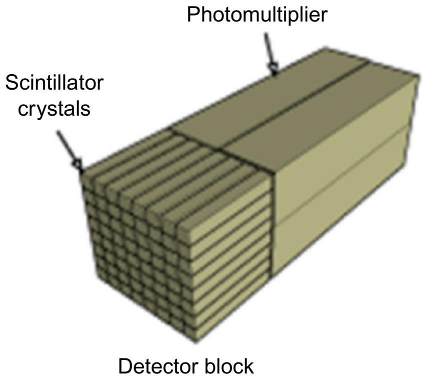

Thus, the scintillator should be transparent, which has led to the use of monocrystals or transparent ceramics.

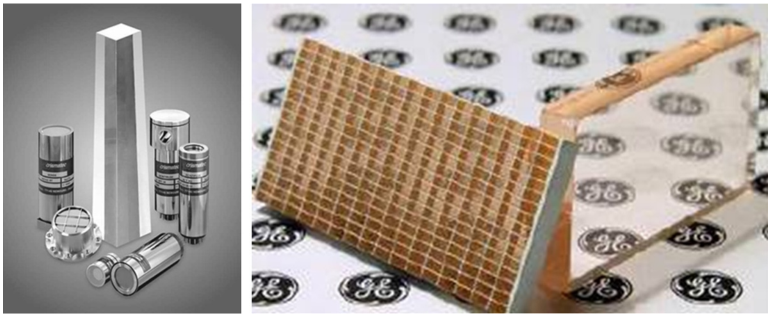

FIG. 16.13

Right: scintillation crystal surrounded by various scintillation detector assemblies (Source: Saint-Gobain Crystals). Right: Transparent ceramic $(Y,Gd)_2O_3$:Eu (Source: GE).

For crystal growth, a Czochralski method is generally used. Materials with incongruent melting are prohibited in order to avoid decomposition during fusion. Homogeneity (defects, dopants, etc.) is mandatory to get well-performing scintillators. After growing, single crystals are cut and polished to be used in this application (Fig. 16.13).

Ceramic scintillators are polycrystalline objects composed of grains, typically a few microns or less in size, and bonded together by high-temperature processes, usually greater than 1500 °C. Transparency is obtained by hot-pressure treatment of purified raw materials. Generally, cubic structures are preferred in order to avoid light scattering. Impressive examples are shown in the Fig. 16.13 with $(Y,Gd)_2O_3$ transparent ceramics (Source General Electric).

The physical characteristics of a good scintillator material are the following:

- A high-density and a high X- or γ-ray stopping power: basically proportional to ρZ_{eff}^4 (ρ is the density in g/cm^3 and Z_{eff} the effective atomic number). A scintillator must contain a maximum of high atomic number (heavy) elements (rare earths are good candidates) to quickly stop the energy. The volume is reduced when the density increases
- Light yield output (LY): must be the highest to reduce the patient's exposure time. Increased LY is important for improving accuracy and spatial resolution. The light output is typically given as the number of photons emitted per million electron volts (MeV) of incoming radiation energy (photons/MeV). Materials showing a small band gap give the best LY by increasing the number of electron-hole pairs. The LY must be proportional to the incident energy to get good energy resolution
- Emission range: must be well-matched to the detector sensitivity
- Decay time: Fast signal rise and decay times are important for good timing resolution and high counting rates, especially in PET scanners since coincident detection of γ-rays is crucial. The absence of afterglow is important in medical imaging. Lifetimes and rise times below 100 ns are required. For CT scanners and planar X-ray photography, response times in the μs and even ms time regime are acceptable. Rare earths have many advantages.

Table 16.7 Characteristics of Classical Scintillators Used for CT and PET Technology

	Density (g/cm^3)	Crystal System	Emission (nm)	LY (photon/MeV)	Decay Time (ns)
NaI:Tl	3.67	Cubic	415	62,000	230
CsI:Tl	4.51	Cubic	550	66,000	600, 3400
$CdWO_4$	7.90	Monoclinic	470, 540	28,000	10, 5000
$Bi_4Ge_3O_{12}$	7.13	Cubic	480	9000	300
$YAlO_3$:Ce	5.55	Orthorhombic	350	17,000	27
Gd_2SiO_5:Ce	6.71	Monoclinic	440	8000	60
Lu_2SiO_5:Ce	7.40	Monoclinic	420	30,000	40
$LaCl_3$:Ce	3.86	Hexagonal	330	49,000	26
$Lu_2Si_2O_7$:Ce	6.20	Monoclinic	380	30,000	30
$LaBr_3$:Ce	5.29	Hexagonal	358	61,000	35
LaI_3:Ce	5.6	Hexagonal	472, 535	95,000	24
Gd_2O_2S: Pr,Ce,F	7.34	Trigonal	510	40,000	3000
Gd_2O_2S:Tb	7.34	Trigonal	510	40,000	10^6
$(Y,Gd)_2O_3$:Eu	5.90	Cubic	610	19,000	10^6

Adapted from C. Ronda & A. Srivastava in Luminescence : From Theory to Applications, Wiley-VCH, 2008.

- Radiation hardness: Radiation damage, which may be irrelevant for detectors in many imaging applications, is extremely important for detectors in high-energy physics experiments.

The Table 16.7 gives the most current commercial scintillator materials for CT and PET applications.

16.3.3.1 X-ray computed tomography

In this system, the X-ray tube and the detector are opposite side of the patient. Their rotation around the patient is coupled during the scan (1-2 s).

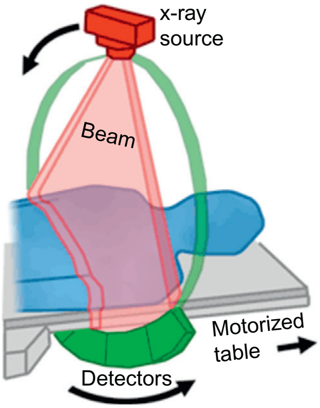

(Public Domain Drawing)

Several kinds of single crystal have been proposed for CT applications. All of them have drawbacks: NaI:Tl (afterglow and hygroscopic), CsI:Tl (afterglow and light output maintenance), $CdWO_4$ (toxicity), $ZnWO_4$ (low light output), and $Bi_4Ge_3O_{12}$ (BGO) (low light output).

A new generation of materials has recently been developed: transparent ceramics. The most promising materials are rare earth-based

- $(Y,Gd)_2O_3:Eu^{3+},Pr^{3+}$ (Eu^{3+} red emission)
- $Gd_2O_2S:Pr^{3+},Ce^{3+}$ (Pr^{3+} red emission)
- $Gd_3Ga_5O_{12}:Cr^{3+},Ce^{3+}$ (Cr^{3+} IR-red emission).

Red emissions are suitable for Si photodiode detection. The afterglow of phosphors is reduced by adding a small amount of codopant (Pr^{3+}, Ce^{3+}).

16.3.3.2 PET

A PET scan requires that the patient has absorbed a radioactive substance that emits positrons. Positrons react with the tissue and are annihilated by electrons generated by producing two 511 keV gamma rays in opposite directions. The detector is located around the human body as a cylinder in the PET equipment for detecting these γ-rays and for image reconstruction.

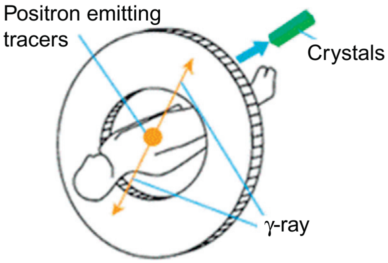

Modern PET machines are composed by several thousand single crystals (typical volume 1-4 cm^3). Their decay time is very fast to accuratly reconstruct the image. Thus, emitters with allowed electronic transitions are required (see Chapter 15).

Three kinds of materials are currently used in PET:

- NaI:Tl (known since 1948): A blue emitter (410 nm) with high efficiency (40,000 photons/MeV), but its response time is too long (230 ns). Nevertheless, the crystals are easy and cheap to make. Another drawback is its hygroscopy, which requires sealing.
- BGO (discovered in 1973). This material is stable in air. Large monocrystals are easy to manufacture (low melting point). BGO has high-density and high Z value. The LY is relatively low (9000 photons/MeV at room temperature), and its decay time (300 ns) could be shorter. Peak emission occurs at 480 nm. BGO are used in current (2014) PET.

- $Gd_2SiO_5:Ce^{3+}$ (GSO), $Lu_2SiO_5:Ce^{3+}$ (LSO), and $(Lu,Y)_2SiO_5:Ce^{3+}$ (LYSO) are promising materials for PET application. Rare earths provide high Z values and high densities. 5d-4f blue emissions occur with very fast decay times (40 ns for LSO). The LY of LSO is 25,000 photons/MeV. The main drawback of this family is afterglow. Monocrystals are very expensive due to the presence of lutetium. Many small quantities of rare earth dopants have been used and optimized to reduce the decay time of cerium. Note that the close compound $Lu_2Si_2O_7:Ce$, discovered recently, gives similar properties but without afterglow.

To finish, a new family of materials has recently been recently proposed for PET applications (2002): $LaX_3:Ce^{3+}$ (X = Cl, Be, I). Their performances are remarkable but their chemical stability needs to be improved (hygroscopic).

16.4 OTHER RARE EARTH APPLICATIONS

16.4.1 Gadolinium as contrast agent for NMR (not luminescent properties)

Gadolinium is used as contrast agent in magnetic resonance imaging (MRI), in order to increase the visibility of internal body structures, i.e., to enhance the relative differences of signal intensity between two adjoining tissues. It was commercialized in the 1980s (two examples are given below).

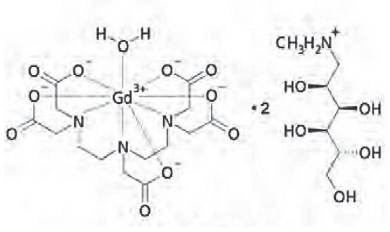

(a) Gd-DTPA
Gadopentetat-Dimeglumin, Magnevist®

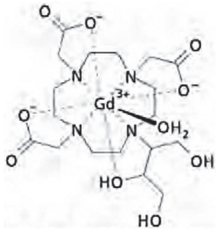

(b) Gd-BT-DO3A/Gd-DO3A-butriol
Gadobutrol, Gadovist®

A contrast agent has several requirements for MRI diagnosis purposes: ability to modify some tissue properties involved in image contrast, tissue specificity, reasonable clearing period, low toxicity, and long shelf life. There are three types of MRI contrast agent today: paramagnetic (Gd), superparamagnetic (iron oxide nanoparticles), and diamagnetic.

The Gd (+III) is a paramagnetic agent, with unpaired outer electrons, which decreases T_1 relaxation time of neighborhood protons. It is called a positive contrast agent; which if different from superparamagnetic agents that play on T_2 (negative contrast agent). It is usually used as an organic complex of Gd and is administrated during the examination. Ligand chelation by polyaminocarboxylates helps to reduce the toxicity of the free Gd ion, which has the same ionic radius as Ca^{2+}.

16.4.2 Afterglow pigment

Phosphorescent materials, also named afterglow pigments, are used in various applications, like safety signs, lamp switches, or markers, the great advantage being that no electrical power is necessary to emit light for several hours.

Wikipedia creative commons photo.

Phosphorescence was discovered in the seventeenth century, by a Bologna shoemaker, also alchemist following the heating of $BaSO_4$ (barite) stone in presence of coal. After firing, the stone still emitted light in the night. This was the first observation of mineral phosphorescence ("phosp" means light in Greek, and "phorein" means wear). They finally named this product "Bologna phosphors" which is BaS-based materials.

Today, the best materials are based on $SrAl_2O_4$:Eu,Dy aluminate, with a phosphorescence time of about ~10 h. It was discovered in 1996. This greatly improves the former generation of ZnS:Cu-based materials, which emitted only up to a maximum of 1 h with poor chemical stability (discovered in 1866). Progress in phosphorescent materials is very difficult. It seems always due to luck. On the market, only few materials exist:

- ZnS:Cu^{+},Co^{2+}: green emission (530 nm), few hours (1953)
- $SrAl_2O_4$:Eu^{2+},Dy^{3+}: green emission (520 nm), 10 h (1995)
- $CaAl_2O_4$: Eu^{2+},Nd^{3+}: blue emission (440 nm), few hours (1998)
- $Sr_4Al_{14}O_{25}$: Eu^{2+},Dy^{3+}: blue-green (485 nm), few hours (2001)
- Y_2O_2S: Eu^{3+},Mg^{2+}, Ti^{4+}: red emission (615 nm), few hours (1996).

The very basic mechanism for $SrAl_2O_4$:Eu,Dy phosphorescence is the following (see the drawing below):

1. Excitation by daylight (or UV) through 4f-5d transitions of Eu^{2+}
2. Some electrons are trapped by defects (vacancy, Dy^{3+} depending on the authors) in the matrix by photoionization through the conduction band leading to oxidation of Eu^{2+} to Eu^{3+}.
3. Thermal energy releases (detrapping of electron) at room temperature (kT energy is enough)
4. Glowing through Eu^{2+} permitted 5d→4f emission

Defects or additives (as Dy^{3+}, B^{3+}...) affect only phosphorescence duration. Color emission is not affected.

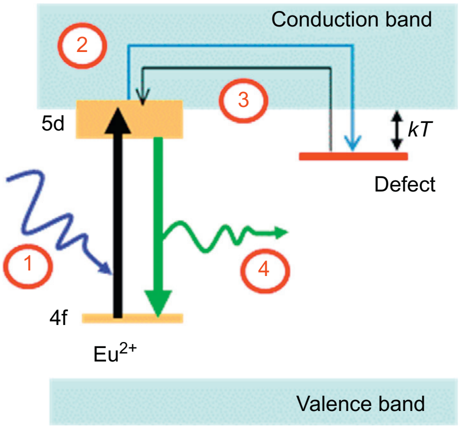

Drawing by Thierry Le Mercier, Solvay.

The mechanism is the same as those which use for BaFBr:Eu^{2+} in X-ray photostimulated storage phosphor applications. But in this case, the energy release is done by lasers because the defects are deeply trapped.

16.4.3 Rare earth for anti counteracting marking & tagging

The fight against counterfeiting is an important application for rare earth materials. Their multiple color emissions enable printing of elaborate complex optical codes. Classical examples are their use in all modern banknotes, credit cards, and official documents (driver license, passports, etc.). Of course, the chemical compositions are always secret.

(Public domain photograph).

Phosphors for counterfeiting applications can be organic or inorganic, as ink or as powder. They can emit visible designs under black light lamps or under infrared light. The second type is called an upconversion phosphor.

16.4.3.1 Upconversion phosphor

Upconversion with rare earths was discovered in the early 1960s by F. Auzel. The best performing system is found with the Yb^{3+}-Er^{3+} couple. The upconversion mechanism is as follows:

1. IR excitation (1000 nm) is absorbed by Yb^{3+} ions.
2. Energy is transferred from Yb^{3+} ions to Er^{3+} ions ($^4I_{11/2}$ level) by a cross-relaxation process. Energy is transferred to upper levels of Er^{3+} by another absorption from Yb^{3+}. This second step is possible because the lifetime of this excited state is very long.
3. After nonradiative relaxation, red or green photons are emitted.

The technology become commercial in the 1980-90s with the development of cheap and high-powered InGaAs diode lasers emitting at around 980 nm.

The upconversion process has intrinsically a low efficiency due to a nonlinear emission process.

To improve the efficiency, matrixes with low-energy phonons are preferred, such as fluoride materials (YF_3 or $NaYF_4$), with a high concentration of Yb and Er dopants.

Upconversion phosphors can be used as an anti-counterfeiting agent and for biolabeling tagging.

Suggested Reading

Generalities about phosphors for various applications

Blasse, G., Grabmaier, B.C., 1995. Luminescent Materials. Springer-Verlag, New York.

Yen, W., Shionoya, S., Yamamoto, H., 2007. Phosphor Handbook, second ed. CRC Press, Boca Raton, FL.

Generalities about fluorescent lamps

Butler, K.H., 1980. Fluorescent Lamp Phosphors: Technology and Theory. Pennsylvania State University Press, Pennsylvania.

Very interesting Edison techcenter website: www.edisontechcenter.org.

Generalities about LED

Fred Schubert, E., 2006. Light-Emitting Diodes, second ed. U.K Cambridge University Press, Cambridge.

Generalities about colorimetry

Malacara, D., 2011. Color Vision and colorimetry: Theory and applications, second ed. SPIE Press, Bellingham, Washington.

ANNEX 16.1 BASICS OF COLORIMETRY

Color emission is based on the addition of photons. A white light source is provided then blue, red, and green photons are added. It is the reverse phenomenon of pigments in paints or the printing industry, where there is subtraction of photons from the primary colors magenta, yellow, and cyan. Their combination gives a black color.

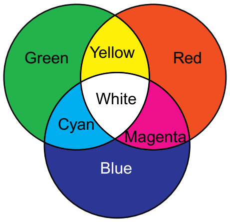

Light source
photon addition

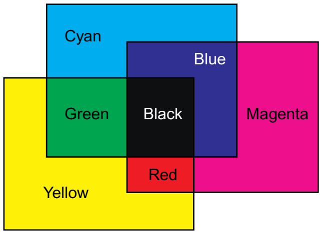

Painting
photon substraction

The human eye

The colorimetry of a light is intrinsically linked to the receptor for which it is intended. In the case of lighting and displays, it is of course the human eye. As a spectrometer, the eye does not perceive all the wavelengths with the same sensitivity. The retina is covered by light receptors of two types: cones and rods. The cones are

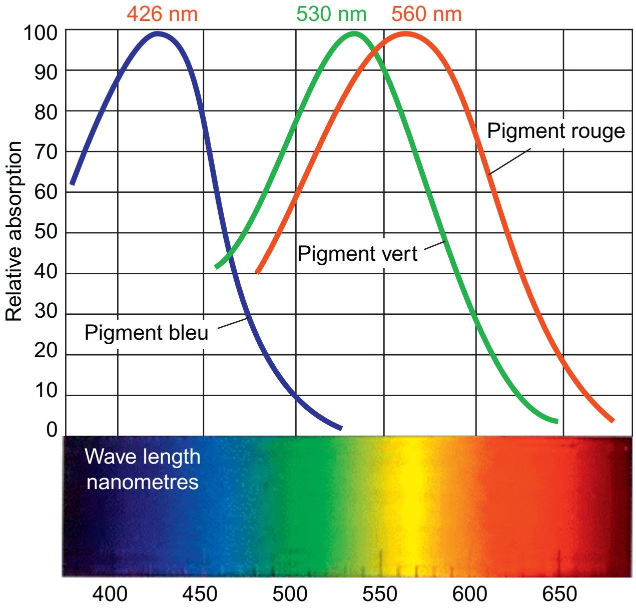

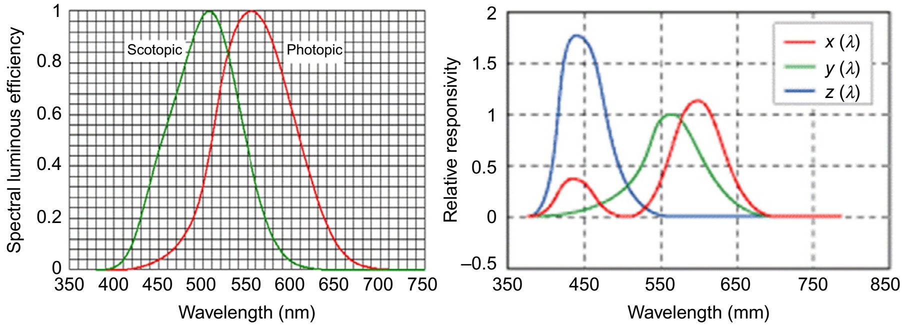

FIG. A16.1

(a) Global efficiency of diurnal and nocturne human vision. (b) XYZ function defined by Comité International de l'Eclairage.

in charge of day vision. Their spectral sensitivity is located in the blue (426 nm), green (530 nm), and red (560 nm). The split of eye response in three spectral areas is the reason for the use of trichromatic systems, both for paintings and light sources.

The number and efficiency of the cones in the three regions give a resulting optimal perception around 555 nm, described by the photopic distribution curve V(λ). For night vision, the rods are the more active ones, with an optimal sensitivity around 505 nm described by the scotopic distribution curve.

The reference curves are determined by the CIE (Comité International de l'Eclairage), measured by a representative number of observers, in 1931, updated in 1964 and 1976 (Fig. A16.1).

The trichromatic color diagram

In order to quantify color and its quality, the Comité International de l'Eclairage has determined three functions $X(\lambda)$, $Y(\lambda)$, and $Z(\lambda)$, named tristimulus curves. All the color perceived by the eye can be defined by a linear combination of these three functions. The calculation of the color point is then easy. From the record of the emission spectrum of the light source, the three function X', Y', and Z' are calculated by:

$$X' = \sum\nolimits_{\lambda} EM(\lambda)\cdot X(\lambda) \quad Y' = \sum\nolimits_{\lambda} EM(\lambda)\cdot Y(\lambda) \quad Z' = \sum\nolimits_{\lambda} EM(\lambda)\cdot Z(\lambda)$$

Then, the trichromatic coordinate x and y are given by $x = \dfrac{X'}{X'+Y'+Z'}$ and $y = \dfrac{Y'}{X'+Y'+Z'}$.

These values are generally placed in a trichromatic coordinate diagram, in the form of horseshoe, which is convenient to use.

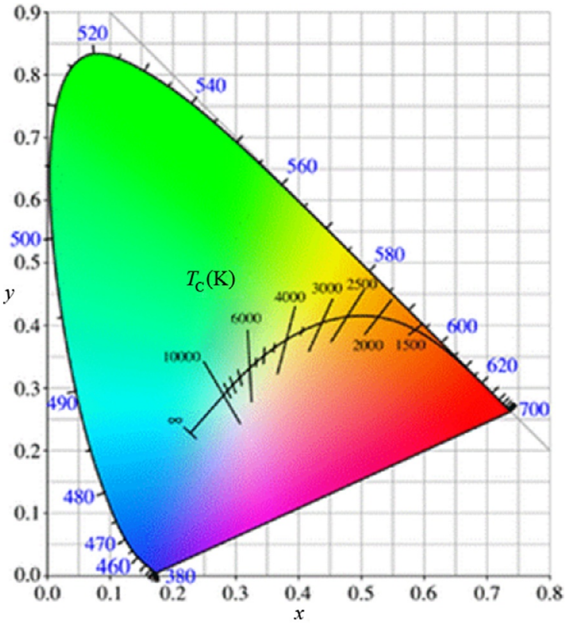

The borders of the diagram represent monochromatic emission in the range of 380-770 nm, except for the line connecting the endpoints of the horseshoe, which has no spectral equivalent, and is called the line of purples. Each zone inside defines a color. They are all the result of a polychromatic emission.

The middle line is the black-body locus, the curve of the Planckian emission. These coordinates are calculated from the spectrum of a black body at a given temperature. These temperatures correspond to those of the sun at different periods of the day.

The color point of a blend of two phosphors is placed on the line drawn between the color point of each of the phosphors, with a weight depending on the phosphor efficiency and its relative amount in the blend. In the same way, the color point of a blend of three phosphors is located in a triangle linking their (x,y).

The small color differences that are not noticeable by the human eyes can be calculated and are represented by an ellipsis. The ellipses are wider in the green and red than in the blue. The nuances in the type of blue light are easily differentiated by the eye, where several phosphors emitting in green can have easily the same color perception.

In other terms, two different spectra can have exactly the same color of light in the trichrimatic diagram. It is then possible to mimic sunlight or incandescence light by a discontinuous spectrum made of red, green, and blue phosphors.

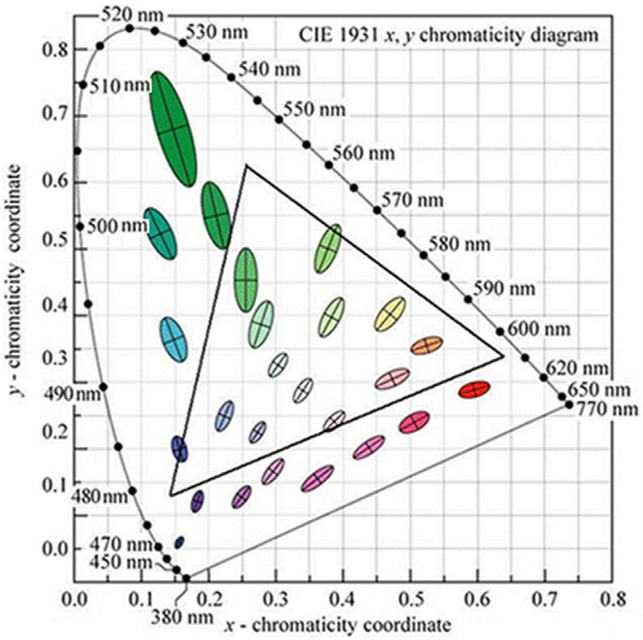

Note that each zone inside the diagram represents a color and the results of a polychromatic light. The representation of this Comité International de l'Eclairage diagram gives an undue portion to the green area. A new set of color coordinates (derived from *x*, *y*) has recently been proposed to correct this point (u', v' basis as example).

For displays, the color gamut is the space of color than can be achieved by the screen phosphors. The wider the triangle, the better the ability of the display to reproduce natural colors on the screen. The choice of phosphor is thus critical, and the need of a "deep blue," "deep red," and real green is necessary.

CHAPTER

Rare Earth Doped Lasers and Optical Amplifiers

17

Chapter 15 describes the luminescent properties of transparent materials that contain rare earth ions. Luminescent materials that contain rare earths are used in several industrial applications including:

(a) fluorescent lamps
(b) lasers
(c) optical amplifiers
(d) medical sensors such as scintillators for X-ray imaging.

This chapter describes the use of rare earth ions in the design and fabrication of optical gain media. Rare earth optical gain media are used in several technological applications, including:

(a) optical amplifiers for telecommunication networks (using mostly Er^{3+})
(b) solid state lasers including:
  (i) crystal lasers (using mostly Nd^{3+})
  (ii) fiber lasers (using Nd^{3+}, Yb^{3+}, Er^{3+}, Tm^{3+}, $Ho^{3+}$and Pr^{3+}).

The materials used as optical gain media for these applications include crystals, glass and glass ceramics.

17.1 GAIN MEDIA

Gain media are used for light amplification. Rare earth ions RE^{3+}, when distributed inside a solid matrix such as a single crystal, a transparent glass ceramic, or a glass can play the role of optical gain media. A gain medium is optically pumped into an excited electronic state by an external energy source through the process of absorption (Fig. 17.1). The excited electron can then relax radiatively through emission of a photon of identical energy—or non-radiatively through thermal vibrations. However, the radiative relaxation process can also be triggered by another incident photon. This process is called *stimulated emission*.

17.1.1 Stimulated emission

When a photon triggers the emission of an excited rare earth ion, a second photon is produced, thereby resulting in a net amplification as depicted on Fig. 17.1. A gain medium can therefore amplify a beam by the process of stimulated emission.

Rare Earths. http://dx.doi.org/10.1016/B978-0-444-62735-3.00016-4

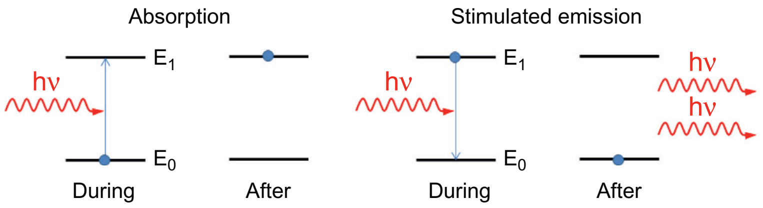

FIG. 17.1

Optical excitation of a gain medium through absorption of a pump source—and beam amplification through the process of stimulated emission.

Drawing by Pierre Lucas.

A typical gain medium contains a very large population of rare earth ions. For a photon incident on a gain medium, the probability of absorption versus stimulated emission is proportional to the population of rare earths in the ground and excited state, respectively. Hence, a net amplification process can only occur if more rare earth ions are in the excited electronic state than in the ground state. This is called *population inversion*. It is required for light amplification.

17.1.2 Population inversion

If only two electronic levels are present, a population inversion can never be achieved because the probability of excitation is equal to the probability of stimulated emission. At best a 50% population of excited ions can be reached, which does not permit amplification. At least three levels are required to obtain population inversion via fast non-radiative transition as depicted in Fig. 17.2 for an Nd^{3+} ion embedded in a yttrium aluminum garnet (YAG) crystal.

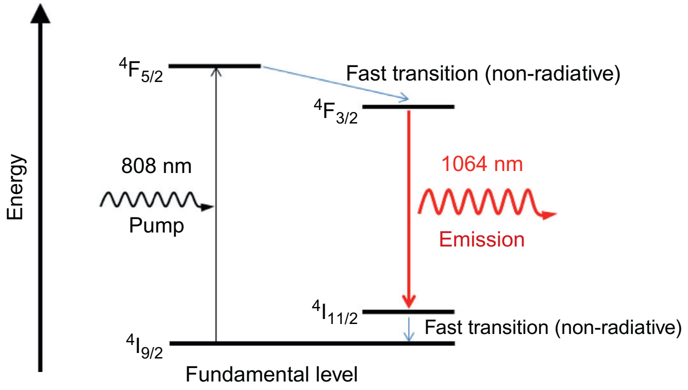

FIG. 17.2

Simplified energy level scheme of Nd^{3+} in a yttrium aluminum garnet laser.

Drawing by Pierre Lucas.

The pump light excites the electrons of an Nd^{3+} ion into an excited state ($^4F_{5/2}$) which rapidly decays into an adjacent level ($^4F_{3/2}$) through non-radiative relaxation. Through this process, population inversion can be rapidly achieved between the $^4F_{3/2}$ and $^4I_{11/2}$ levels thus permitting amplification of light at 1064 nm.

The many electronic levels associated with 4f levels in rare earth ions are conducive to the process of population inversion and consequently to light amplification.

In the case of the Nd^{3+} yttrium aluminum garnet crystal (Fig. 17.2) the lower level $^4I_{11/2}$ is quickly depleted through fast non-radiative relaxation to the fundamental level. This is important because the lower level ($^4I_{11/2}$) population will be effectively zero, thereby leading to population inversion for any appreciable excitation into the upper level ($^4F_{3/2}$). Since only a few rare earth ions are needed to produce population inversion, such four-level systems are highly effective gain media.

Several rare earth ions including Nd^{3+}, Er^{3+}, Yb^{3+}, Tm^{3+}, Ho^{3+}, Pr^{3+} generate four-level systems and are consequently broadly used to produce efficient lasers and amplifiers.

A gain media containing rare earth ions (Fig. 17.2) constitutes an *optical amplifier*. This permits amplification such as that required in optical telecommunication networks.

When an optical amplifier is placed in a resonant optical cavity, one then obtains a *laser*. A laser permits achievement of an extremely high light intensity.

17.2 OPTICAL AMPLIFIERS

An optical amplifier is a device that permits regeneration and amplification of a low intensity light signal. The low intensity light signal, such as a pulse, is passed through an excited gain media and is amplified through stimulated emission. The principal application of optical amplifiers is in optical fiber telecommunication networks. All commercial telecom amplifiers use Er^{3+} ions as the optically active species.

17.2.1 Erbium doped fiber amplifier (EDFA)

Billions of kilometers of silica SiO_2 fibers are networking the planet to transmit information across the world. The information is carried in the form of light pulses that propagate inside a silica glass fiber. This is possible only when using the high optical transparency region of silica where optical loss is very low.

This region is located in the middle of the optical window between:

(a) the ultraviolet region where bonding electrons absorb light

and

(b) the mid infrared region where vibration attenuates the light.

The lowest loss region is located in a narrow region around 1.55 μm. This wavelength has therefore been selected for optical communication. An ultrapure silica optical fiber has an attenuation of 0.2 decibels per kilometer. It means that the optical signal travelling inside the fiber needs to be regenerated, i.e., re-amplified, about every 80 km.

Optical amplification is also required in urban areas where dense optical networks involve multiple coupling and splitting, both of which cause large light losses.

Er^{3+} ions offer the most efficient and elegant way to achieve optical amplification due to their strong light emission in the telecom wavelength region at 1.55 μm.

An erbium doped fiber amplifier (EDFA) is made of a silica fiber that is rendered optically active by doping the core with a small amount of Er^{3+}, <0.1 atomic%. The final device is a single mode fiber having an Er^{3+} doped core (Fig. 17.3).

The pumping light can be 980 or 1480 nm using appropriate laser diodes (Fig. 17.4). Pumping with 980 nm light results in excitation into the $^4I_{11/2}$ which rapidly produces population inversion in the $^4I_{13/2}$ through fast non-radiative decay.

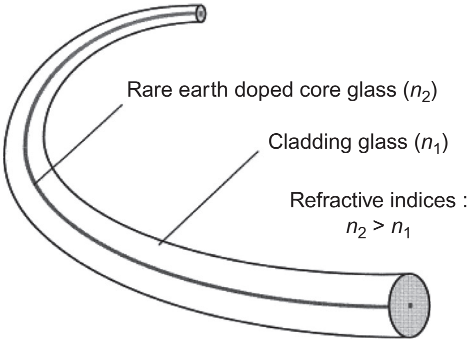

FIG. 17.3

Single mode rare earth ion doped glass fiber.

Drawing by Jacques Lucas.

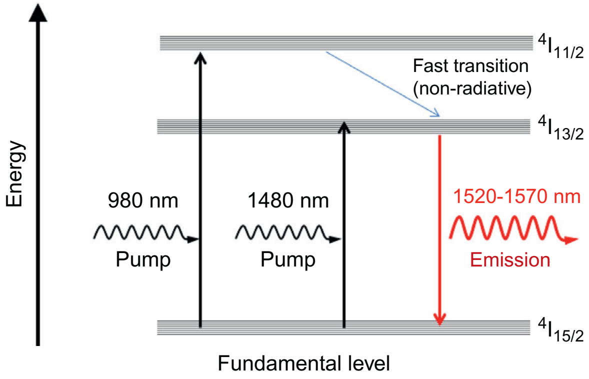

FIG. 17.4

Energy diagram of the Er^{3+} ion in a SiO_2 glass matrix. Note the broad energy levels resulting from the disordered nature of the amorphous matrix.

Drawing by Pierre Lucas

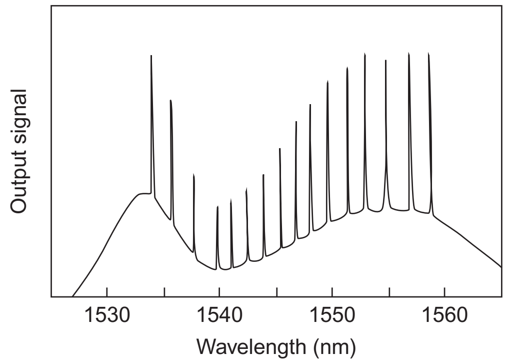

FIG. 17.5

Output telecom signal divided in several channels after amplification via an Er^{3+} doped silica fiber amplifier.

Drawing by Jacques Lucas research group, University of Rennes.

Due to the disordered structure of the glassy SiO_2 matrix, the Er^{3+} ions are distributed over a wide range of local environments which result in broad energy levels (Fig. 17.4). As a result, the probability for absorption is highest at 1480 nm while the probability for stimulated emission is highest over 1520-1570 nm. Effective population inversion and amplification can therefore take place between the two levels $^4I_{13/2}$ and $^4I_{15/2}$.

The resulting output of a telecom signal is depicted in Fig. 17.5. The amplified optical signal is rather broad, typically between 1520 and 1570 nm because the Er^{3+} is in a glassy host.

It is fortunate that this broad amplification signal is right in the middle of the low loss region of silica. This wavelength region is called the C-band.

Instead of launching only one wavelength into the silica fiber, it has been demonstrated that several signals with different wavelengths can be launched into the fibers. As shown in Fig. 17.5 many distinct wavelengths can be simultaneously amplified as shown by the sharp amplified peaks. These channels are sufficiently separated to carry information without interferences or overlap.

This telecom signal division technology is called wavelength division multiplexing (WDM).

The power of the Er^{3+} doped fiber amplifier is in its ability to amplify multiple channels (e.g., telephone calls) in the same fiber. Nowadays, dense WDM technology enables simultaneous transmission of up to 160 channels.

17.2.2 How an optical amplifier works

Optical amplifiers are positioned along the telecom optical fiber line to regenerate a telecom signal which has been attenuated after travelling tens of kilometers inside a silica fiber.

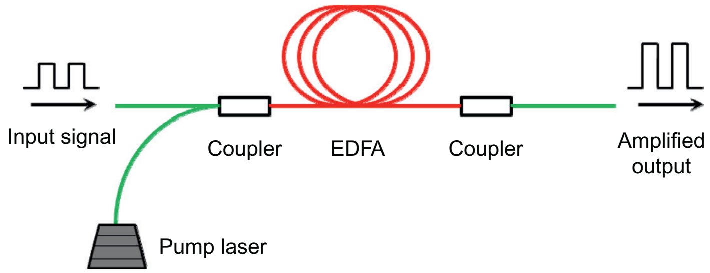

FIG. 17.6

The Er $^{3+}$-doped fiber amplifier (EDFA) is coupled to the transmission line. The role of the EDFA is to regenerate (amplify) the telecom signal. The optical amplifier is a Er^{3+} doped silica fiber. The pump laser powers the amplification. Its operation requires ~1 watt of electric power (into the pump laser).

Drawing by Jacques Lucas research group, University of Rennes.

To achieve this goal, strict specifications are required. The optical amplifier needs to be a fiber made from silica for easy splicing and coupling with the telecom fiber. Use of the same glass for the amplifier and the transmission fiber ensures refractive index matching and minimal coupling loss.

After propagating tens of kilometers in the silica fiber, an EDFA is coupled to the main line to regenerate the signal (Fig. 17.6). In order to activate the Er^{3+} gain medium for stimulated emission, a pump laser with 980 or 1480 nm wavelength is jointly coupled into the EDFA. Hence, when a low intensity pulse travels through the EDFA, it undergoes a net gain in intensity.

Usually the EDFA is made of a few meters of Er^{3+} doped SiO_2 fiber coiled in a plastic box.

This invention had been identified as a critical discovery in the world of telecommunications.

17.3 LIGHT AMPLIFICATION BY STIMULATED EMISSION OF RADIATION

When a gain medium is placed in an optical cavity, the emitted light is trapped in a resonant cavity. This permits to achievement of extremely high light intensities. Such a device is called a *laser*.

17.3.1 Definition of laser

Laser is an acronym for Light Amplification by Stimulated Emission of Radiation.

The term *laser* was originally a principle of operation. It now denotes a device.

The first laser device was developed by Theodore Maiman in 1960 (Theodore, 2014). It was based on a ruby crystal. The optical matrix was a single crystal made of aluminum oxide (Al_2O_3) doped with active Cr^{3+} ions.

Laser technology has been growing very fast, essentially because laser light has a number of very special properties.

Laser beams have a very small divergence and can propagate over long distances while remaining highly collimated.

Laser light is monochromatic and is composed of a single color or wavelength. This is very different from traditional lamps which emit a very broad optical spectrum.

The laser light can be produced continuously or in the form of short or ultra-short pulses. The duration of the pulses can vary from a microsecond down to few femtoseconds (1 femtosecond $= 10^{-15}$ s)

These remarkable properties are, to a large extent, the consequence of the very high degree of coherence of laser radiation.

It means that all the photons are produced at the same time with a high degree of spatial coherence. A consequence of this is that the laser beam has a low tendency to extend in transversal directions. So it can be focused on very small spots, e.g., for drilling micrometer size holes.

17.3.2 How a laser works

A laser is comprised of an optical resonator (also called a laser resonator or a laser cavity) in which light can recirculate, for instance, between two mirrors (Fig. 17.7).

The rare earth ion gain medium is positioned inside the resonator. The gain medium can be a rare earth doped single crystal, glass or glass-ceramic. It is pumped by an external source in order to activate the rare earth ions and produce light emission.

Photons emitted by spontaneous emission along the cavity axis are trapped between the two mirrors and reflect back and forth, each time passing through the gain medium and inducing further stimulated emission. This is called the gain.

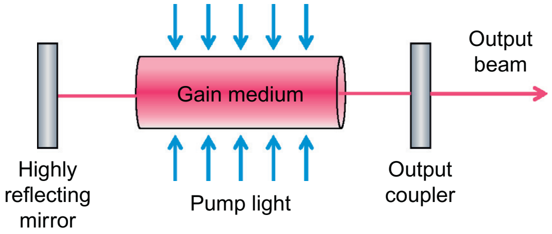

FIG. 17.7

Schematic view of a simple optically pumped laser. The gain medium is for instance a rare earth doped single crystal, a rare earth doped transparent ceramic or a rod of rare earth doped glass. The laser resonator is made of a highly reflecting mirror and a partially transmitting mirror called an output coupler. The role of the output coupler is to extract some of the circulating laser light as useful output. The side pumping is realized using a flash lamp or by light emitting diodes.

Drawing by Pierre Lucas.

Without the gain medium, the circulating light in the resonator would become weaker and weaker because of the reflection losses on each mirror.

A laser cannot operate if the gain is smaller than the resonator loss. Under these conditions, the device is below the so-called laser threshold and just emits some luminescence.

If the gain is larger than the power, loss the light inside the resonator quickly rises.

Some fraction of the light power circulating in the resonator is usually transmitted by a partially transparent mirror, the so-called output coupler mirror. Dielectric mirrors (Bragg reflectors) coated on a glass substrate, are used to control the reflectivity of the cavity mirrors with high accuracy.

The resulting output beam is the useful output of the laser.

Some rare earth lasers emit light continuously. They are called continuous-wave lasers. Others can generate pulses which are very brief and which can be very intense.

The duration of the pulses can vary from microsecond (10^{-6} s) to nanoseconds (10^{-9} s) or picoseconds (10^{-12} s) or even to ultra-short pulses in the order of few femtoseconds (10^{-15} s).

The optical bandwidth of a rare earth laser beam can be very small. The higher the quality of the resonator, the narrower the bandwith. The optical bandwidth also depends on the distribution of rare earth ions inside the host matrix.

In a single crystal such as an yttrium aluminum garnet, the active ions Nd^{3+} are distributed on the Y^{3+} sites and are therefore situated in a highly regular and homogeneous configuration. All Nd^{3+} ions therefore have identical energy levels and emit photons of an identical wavelength.

On the other hand, when rare earth ions are doped into a glass host, which is a disordered material, the local field generated by the matrix is highly inhomogeneous. The population of rare earth ions therefore adopts a broader distribution of energy levels (Fig. 17.4). This results in a broader range of wavelength emission.

A broad emission offers the advantage of tuning the wavelength of the laser light by adjusting the resonance conditions of the cavity. Tunable lasers are of interest as a source of laser beams with different adjustable wavelengths.

The presence of OH groups in the laser matrix is known to induce phonon coupling with the rare earth ions, resulting in non-radiative relaxation instead of radiative relaxation. This is called fluorescence quenching. It is detrimental to laser medium efficiency.

17.4 THE RARE EARTH CANDIDATES FOR LASER EMISSION

Rare earth doped lasers are among the most popular solid state lasers. The host matrix is either a single crystal, a glass or a transparent ceramic. In any case the rare earth is a trivalent rare earth ion (RE^{3+}) that can substitute for ions having almost the same

Table 17.1 Rare Earths Used in Lasers

Rare Earth Ions RE^{3+}	Host Media	Important Lasing Wavelengths (μm)
Neodymium Nd^{3+} (4f3)	YAG, YLF, silicate, and phosphate glasses	1.03-1.1, 0.9-0.95, 1.32-1.35
Ytterbium Yb^{3+} (4f13)	YAG, silica glass	1.0-1.1
Erbium Er^{3+} (4f11)	YAG, silica glass	1.5-1.6, 2.7
Thulium Tm^{3+} (4f12)	YAG, silica, and fluoride glass	1.7-2.1, 1.45-1.53, 0.8, 0.48
Holmium Ho^{3+} (4f10)	YAG, YLF, and silica glass	2.1, 2.8-2.9
Praseodymium Pr^{3+} (4f2)	Silica, fluoride glass	1.3, 0.6, 0.49
Cerium Ce^{3+} (4f1)	Fluoride crystals	0.28-0.33

The hosts are single crystals, transparent ceramics, or glasses. Several laser oscillations can be observed for each rare earth. YAG, yttrium aluminum garnet; YLF, yttrium lithium fluoride.
Table prepared by Jacques Lucas.

size. The doping concentration is small (<0.1 atomic%) to avoid concentration quenching which results in non-radiative relaxation between adjacent rare earth ions.

Table 17.1 shows the most common laser-active rare earth ions, the different kinds of host and the lasing wavelengths.

For bulk lasers, the most important rare earths are neodymium, erbium, and ytterbium. Most rare earth doped fiber lasers are based on ytterbium.

17.4.1 Rare earth doped crystals

A wide range of single crystal materials can serve as host media for laser active rare earth ions.

The single crystals need to be grown with a high optical quality. The chemical composition must be suitable for substituting host ions with RE^{3+}. Size and charges must be the same. The maximum doping concentration is important as well as the uniformity of doping.

Since production of heat is always present, high thermal conductivity is desirable to avoid crystal expansion and thermal shock.

Frequently used materials are oxides, which can be grown in normal atmospheric conditions.

Reaction between $5Al_2O_3$ and $3Y_2O_3$ leads to yttrium aluminate $Y_3Al_5O_{12}$.

This cubic material is isostructural to the mineral garnet. The acronym YAG is for yttrium-aluminum-garnet. The Y^{3+} sites can be substituted easily by a small amount of RE^{3+}, typically 1 atomic%.

An example of a Nd-YAG rod is shown in Fig. 17.8. The crystal has a pink color which originates from the higher absorbing levels of the Nd^{3+} ions especially in the green/yellow region around the 500-600 nm wavelength.

FIG. 17.8

0.5 cm diameter Nd-doped yttrium alumina garnet rod used as a laser gain medium.

Wikipedia creative commons photo

The crystal size varies from a few millimeters to several centimeters in diameter and tens of centimeters in length, depending on the power required.

Yttrium aluminum garnet crystals have a high optical quality and thermal conductivity and dominate the market.

Some other oxides such as YVO_4 (the yttrium vanadates) or yttrium/potassium tungstates $KY(WO_4)_2$ are also used. They offer some advantages such as a strong absorption of pumping light.

The second family of laser hosts is represented by fluoride single crystals such as yttrium lithium fluoride $YLiF_4$ or YLF.

The fluorides are not hard or mechanically strong, but they have an excellent transparency for pumping in the ultraviolet region.

17.4.2 Rare earth doped glasses

Rare earth doped laser crystals often exhibit sharply defined lasing and pumping transitions because the rare earth ions RE^{3+} occupy only one type of site.

In contrast, glasses have much broader transitions. In silicates or phosphate glasses, the rare earth ions substitute for Na^+ or Ca^{2+} ions of the same size.

Their environment is not well defined. The local coordination changes from site to site. This multi-site distribution results in the broadening of the absorption spectra as well as in the laser emission.

The advantage of a glassy matrix is in the fabrication of large pieces of RE^{3+} doped laser.

The disadvantage is in the poor thermal conductivity of the glassy state due to short range disorder that leads to phonon scattering. This makes the glass laser sensitive to thermal shocks.

Fluoride glasses based on the glass-forming ability of ZrF_4 are called fluorozirconate glasses. Their acronym ZBLAN refers to the atomic composition, Zr, Ba, La, Al, and Na.

Active RE^{3+} can substitute for La^{3+}. Here the RE^{3+} ions are glass formers and their environment is well defined. Absorption and emission spectra are similar to fluoride crystals, with just a small broadening.

Fluoride glasses transmit light up to 7 μm and are, therefore, low phonon materials. Their advantage is weak phonon coupling with RE^{3+} and laser emissions in the near and mid infrared.

17.4.3 Rare earth doped transparent ceramics

Ceramics are superior to glasses and crystals because of better thermo-mechanical properties. To be used as laser host, they need to be fully transparent in the pumping and emitting region.

Transparency is obtained by controlling the size and the distribution of the grains, which need to be as small as possible to avoid light scattering.

Vacuum sintering processes are used to produce nanometer size grains. The porosity is very low, leading to scattering losses that are not significantly larger than those from single crystals.

Neodymium laser ceramics made from yttrium aluminum garnet ultrafine particles have achieved the same performance as Nd-YAG single crystals. Also, higher concentrations of Nd are possible without the concentration quenching effects that degrade laser efficiency.

Oxides such as Y_2O_3 are difficult to grow as single crystals because of their high melting point. They can be prepared as transparent ceramics more easily because the sintering temperature is much lower than the melting temperature.

The remarkable high thermal conductivity of Y_2O_3 may make this material preferable to YAG.

These new generations of laser materials are cheaper to fabricate, especially for high volume production.

Large pieces can be manufactured for powerful lasers. In this field, ceramics compete successfully with laser glasses because of their better thermo-mechanical properties.

17.5 LASER APPLICATIONS

The light generated by a laser is very different from light from other sources.

The laser beam has a high degree of spatial coherence. It means that it can propagate over long distances with moderate divergence. It can be focused on very small spots.

Laser light generally has a narrow spectral bandwidth. The light is almost completely monochromatic. When the laser is made of glass the emission is broad but it can be tuned by adjusting the resonant cavity.

The light produced inside a fiber laser has an excellent quality. Only one mode is extracted and it can be easily guided towards a target and focused with a great precision. Drilling micro-holes, precise marking, and delicate laser surgery require this kind of high quality light.

Rare earth lasers offer a large variety of wavelengths from UV to the mid-infrared.

In many cases, the laser light frequency can be doubled by using special non-linear crystals. For instance the invisible 1064 nm light from an Nd-YAG laser can be converted into a 532 nm green light. This is one way to make the Nd laser light visible.

The laser light emitted by Nd or Yb lasers is in the one micrometer region. This region is out of the perception of the retina and the light is invisible. They are dangerous because in this spectral region the bio-tissues are not very absorbing especially the bio-molecules inside the eye. The laser beam can reach the retina and destroy this very sensitive photo-detector. All the wavelengths around 1000 nm are not eye-safe and safety goggles must be worn. On the other hand, wavelengths around 1.5-2.9 μm are strongly absorbed by the OH group of tissues. They lose their energy before reaching the retina and are called eye-safe laser light.

17.5.1 Material processing, manufacturing

Laser light is widely used in manufacturing and offers many advantages as compared to mechanical approaches. Laser material processing is a non-contact operation. It is irreplaceable in operations such as: *cutting, drilling, welding, cladding, soldering, engraving, marking, surface treatment, micromachining, pulsed laser deposition for coating, and ablation.*

The key factors are the pulsed beam light with high intensity and the ability to precisely focus. There is no mechanical stress and very accurate drilling and engraving are possible. The selection of the wavelength is also critical and adjustable depending on the target. Plastic is different from metal or bone.

The recent development of powerful and flexible lasers such as the Yb fiber laser can precisely guide light to a target. This device, along with robots, is extensively used in the car industry for assembly line welding.

17.5.2 Medical applications

The light produced by rare earth lasers is mainly in the near infrared region. Neodymium and ytterbium emit around 1 μm, erbium around 1.5 and 2.9 μm, thulium and holmium in the 2 μm region.

Rare earth lasers are in competition with many other lasers. They are not candidates for commercial applications in the visible and ultraviolet range.

The ~1.06 μm light emitted by a Nd-YAG laser is not strongly absorbed by biotissues. Its disadvantage or danger is that an uncontrolled light beam can reach and damage the retina. Its advantage is that the laser beam can cross some tissues and then can be focused on the retina. Short and controlled pulses can then be used to repair detached retinas. With them, a physician can weld the retina back into place without the delicate operation of cutting open the eye.

Rare earth yttrium aluminum garnet lasers are also used for cataract removal when opacification occurs in the interior of the eye. Laser surgery is also very useful for removing extraneous blood vessels.

The light around 1.5 and 2-2.9 μm is strongly absorbed by tissues. So laser beams can be used by dermatologists for removing suspicious tissues from the skin.

However, the main application is in laser surgery.

Enough power can be produced by Tm laser fibers and Er YAG lasers to cut tissues. These non-contact laser scalpels operate with great precision and with a minimum risk of contamination.

Rare earth lasers are also used on prostate tissues because of their precise incisions, rapid vaporization, and adequate blood coagulation.

17.6 SUMMARY

Rare earth ions are used widely in optical gain media. The most important applications are in:

(a) optical amplifiers for telecommunication networks, especially erbium doped fiber amplifiers
(b) solid state lasers including:
  (i) crystal lasers (using mostly Nd^{3+})
  (ii) fiber lasers (using Nd^{3+}, Yb^{3+}, Er^{3+}, Tm^{3+}, Ho^{3+}, and Pr^{3+}).

Erbium-doped fiber amplifiers are by far the most common amplifiers in the world's fiber communications system. They are used to amplify weakened signals about every 80 km along a fiber transmission line. They are compact, rugged, and reliable. They are able to handle up to 160 channels, e.g., 160 simultaneous telephone conversations, per fiber.

Rare earth ions are also used in lasers, specifically in the near infrared region. Neodymium lasers emit at around 1 μm, erbium 1.5-2.9 μm, thulium and holmium ~2 μm.

These lasers are mainly used in medical applications, especially for cataract removal (Nd^{3+}) and laser surgery (Tm^{3+} and Er^{3+}).

However, they must be handled with extreme care to avoid damaging other tissues, especially the retina.

References

Theodore, 2014 Retrieved from http://en.wikipedia.org/wiki/Theodore_Maiman on January 26, 2014.

RP photonic Encyclopedia GMBH by Rudiger Paschotta. http://www.rp-photonics.com/rare_earth_doped_g.

Digonnet, M.J.F., 2001. Rare-Earth-Doped Fiber Lasers and Amplifiers, Revised and expanded. CRC Press.

IPG's High Power Fiber Laser Brochure - IPG Photonics. www.ipgphotonics.com.

CHAPTER

Rare Earth Recycle

18

This chapter discusses rare earth recycle. Its objectives are to describe and discuss:

(a) the extent of rare earth recycling in 2014
(b) reasons for this limited recycle extent
(c) current rare earth recycling technologywith emphasis on recycle of:
(d) nickel-metalhydride rechargeable batteries
(e) fluorescent lamp rare earth phosphors
(f) rare earth-transition metal permanent magnets
(g) others, including rare earth oxide polishing media, rare earth automobile emission abatement catalysts and rare earth petroleum refining catalyst.

Recycling is advantageous in every respect. It:

(a) slows depletion of our natural resources
(b) uses less energy than primary rare earth production
(c) avoids additional mining wastes
(d) minimizes land fill expansion.

And, for rare earth production, it also avoids additional byproduct radioactive material storage, Chapter 4.

18.1 EXTENT OF RARE EARTH RECYCLE

In 2014, only 1 or 2% of the rare earths in end-of-use objects are being recycled (Binnemans et al., 2013)—this compared to:

- 90% for iron and steel
- 80% platinum group metals
- 70% for aluminum
- 60% for copper.

18.1.1 Reasons for this miniscule rare earth recycle extent

Binnemans et al. (2013) indicate that the main reasons for rare earths' minuscule recycle extent are:

(a) technological difficulties
(b) lack of incentives, financial, and otherwise
(c) inefficient end-of-use objects collection.

Rare Earths. http://dx.doi.org/10.1016/B978-0-444-62735-3.00017-6

To this we add that:

(a) end-of-use rare earths are often present in difficult-to-decompose compounds, for example, cerium zirconate in automobile emission reduction catalysts
(b) rare earths are often present at very low concentrations in end-of-use products, for example, ~2 mass% lanthanum in fluid petroleum cracking catalysts
(c) end-of-use rare earths are often present in objects that are located deep within consumer products, for example, rare earth magnets in electric motors that are themselves located deep within cars and trucks.

All of these make end-of-use rare earth recovery difficult and expensive.

18.2 TWENTY-FIRST CENTURY RARE EARTH RECYCLE INCREASE

This decade has seen significant improvements in rare earth recycle, particularly in Ni-MH rechargeable battery recycle (Tytgat, 2011) and fluorescent lamp phosphors recycle (Solvay, 2012).

Improvements are also being made in magnet recycle (Ferron and Henry, 2013).

18.3 NICKEL-METALHYDRIDE RECHARGEABLE BATTERY RECYCLE

Ni-MH rechargeable battery recycle (Fig. 18.1) entails:

(a) 1500 °C smelting of end-of-use batteries (from scrap collectors) to produce molten rare earth oxide slag and molten Ni-Co alloy (Co is always present in Ni-MH battery electrodes)
(b) gravity separation of the molten rare earth oxide slag (specific gravity ~3) from the molten Ni-Co alloy (specific gravity ~8) in the smelting furnace
(c) tapping the molten slag from a high taphole
(d) tapping the molten Ni-Co alloy from a low taphole
(e) granulating the slag in a huge torrent of water and treating the granules hydrometallurgically to produce individual high purity rare earth chemicals
(f) granulating the alloy in a huge torrent of water and treating the granules hydrometallurgically to produce high purity Ni and Co battery chemicals.

A furnace in Hoboken, Belgium (Fig. 18.5) smelts up to 7000 tonnes of batteries (including 500 tonnes of rare earth metals) per year (Fig. 18.2).

Ni-MH batteries typically contain:

- 25-35 mass% Ni
- 2-4 mass% Co
- 6-8 mass% rare earth elements
- 2-5 mass% Fe
- 10-30 mass% plastics
- balance = O, H, NaOH and LiOH electrolyte.

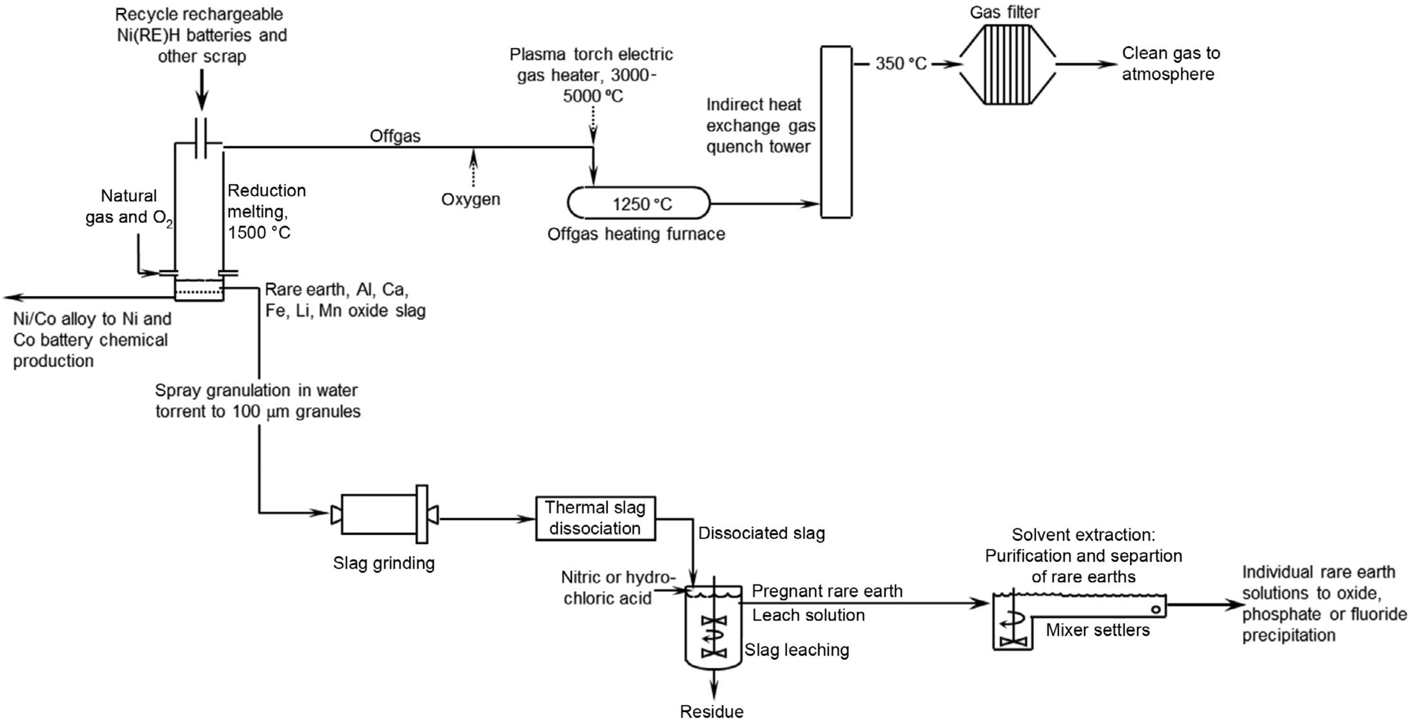

FIG. 18.1

Schematic flowsheet for producing (i) pure individual rare earth chemicals and (ii) pure Ni and Co battery chemicals from recycle Ni-MH rechargeable batteries. The process is continuous. Its main processing unit is a natural gas/oxygen fueled vertical shaft furnace. It is operated slightly reducing at 1500 °C. The gas purification system (top) is notable (Gomez and Van Damme, 2009). It heats the furnace offgas to 1250 °C to decompose hydrocarbons then quenches the gas to 350 °C to prevent formation of dioxins, furans and other volatile organic compounds.

Flowsheet drawn by William Davenport.

FIG. 18.2

End-of-use computer batteries ready for feeding into Fig. 18.5's battery recycle furnace.

Photo courtesy Maarten Quix, Umicore.

They are used in hybrid cars and a myriad of consumer products. The batteries are removed from their battery-packs or charged directly to the smelting furnace (Fig. 18.3 and 18.4).

Lithium ion batteries can also be included in the smelting furnace feed—for recovery of their Ni and Co (and potentially their lithium).

18.4 INDUSTRIAL RECYCLE SMELTING

The battery recycle furnace at Hoboken, Belgium (Fig. 18.5) is a vertical shaft furnace, about 2 m diameter and 10 m tall. It blows air and natural gas through several tuyeres near the bottom of the furnace—causing hot gas to rise up through the furnace. This hot gas heats input batteries, which melt and form separate molten rare earth slag and Ni-Co alloy layers in the furnace hearth.

The furnace is operated at about 1500 °C to ensure that the product Ni-Co alloy (melting point ~1480 °C [Kaufman and Nesor, 1978]) and slag are fully molten and ready for tapping from the furnace.

FIG. 18.3

End-of-use portable power tool batteries ready for feeding to Fig. 18.5's battery recycle furnace.

Photo courtesy Maarten Quix, Umicore.

FIG. 18.4

End-of-use hybrid car batteries being prepared for feeding to Fig. 18.5's battery recycle furnace. The battery packs are dissembled before the batteries are charged into the furnace.

Photo courtesy Maarten Quix, Umicore.

FIG. 18.5

Recycle battery smelting furnace. Its position in a battery recycle flowsheet is described in Fig. 18.1.

Photo courtesy Maarten Quix, Umicore.

The furnace is also operated under slightly reducing conditions so that any cobalt oxide that accidentally forms in the furnace is reduced back to metal, i.e.,:

$$\underset{\text{in descending slag}}{\mathrm{CoO}(\ell)} + \underset{\text{in ascending gas}}{\mathrm{CO(g)}} \xrightarrow{1500^\circ\mathrm{C}} \underset{\text{in descending alloy}}{\mathrm{Co}(\ell)} + \underset{\text{in ascending gas}}{\mathrm{CO_2(g)}} \tag{18.1}$$

$$\underset{\text{in descending slag}}{\mathrm{CoO}(\ell)} + \underset{\text{in ascending gas}}{\mathrm{H_2(g)}} \xrightarrow{1500^\circ\mathrm{C}} \underset{\text{in descending alloy}}{\mathrm{Co}(\ell)} + \underset{\text{in ascending gas}}{\mathrm{H_2O(g)}} \tag{18.2}$$

$NiO(\ell)$ reduces more easily than $CoO(\ell)$, so the CO(g) and $H_2O(g)$ levels required to prevent $Co(\ell)$ oxidation are also sufficient to prevent $Ni(\ell)$ oxidation.

Rare earths, on the other hand, bond very strongly to oxygen. They leave the furnace in its oxide slag.

CO(g) and $H_2(g)$ levels are controlled by adjusting the air/fuel ratio in the input tuyere feed gas. Some oxygen may also be injected (in place of air) to adjust temperature and gas flowrate.

18.5 RECYCLE FURNACE SLAG REQUIREMENTS

The first requirement of recycle furnace slag is that it must be completely molten at the operating temperature of the furnace, ~1500 °C. This means that its melting point must be below 1500 °C. This is achieved by adding small amounts of alumina (Al_2O_3) and lime (CaO) with the furnace charge. Soda ash (Na_2CO_3) may also be added in an emergency.

Slag melting point and viscosity are also lowered by smelting recycle lithium batteries along with the Ni-MH batteries. The Li chemicals are oxidized during smelting, providing Li_2O to the slag—further lowering slag melting point and viscosity. This lithium may soon be recovered.

18.5.1 Avoiding glassiness after granulation

The water-granulated slag from the recycle furnace is (i) ground then (ii) leached in preparation for hydrometallurgical rare earth recovery/refining. Both of these steps require rough, friable (not glassy) granules. Rough, friable granules are promoted by excluding glass-forming oxides (especially silica, SiO_2) from the furnace charge. This is always done.

18.6 RECOVERY OF RARE EARTHS FROM SLAG

The molten oxide slags from 1500 °C Ni-MH battery recycle smelting contain about 10 mass% rare earth cations, remainder being oxygen ions plus Al, Ca, Fe, Li, and

Mn cations. The rare earth concentration is lower if lithium batteries are included in the smelting furnace feed because:

(a) lithium ion batteries don't contain rare earths
(b) the batteries' lithium chemicals are oxidized in the recycle furnace so that lithium leaves the furnace as lithium oxide in slag, lowering the slag's rare earth concentration.

This slag is (i) water-granulated to ~100 μm diameter particles; (ii) ground very fine; (iii) leached with nitric or hydrochloric acid; and (iv) purified and separated into individual rare earth solutions by solvent extraction. The leaching and pure rare earth recovery are done at Solvay's rare earth plant in La Rochelle, France.

18.7 RECOVERY OF NI AND CO FROM THE RECYCLE FURNACE PRODUCT ALLOY

The furnace's product alloy (80 mass% Ni, 15% Co plus Cu, Fe, and Mn) is tapped from the furnace into a torrent of water, which granulates it to ~100 μm diameter granules. These granules are then treated for Ni and Co recovery/separation by:

Recycle plant feed-to-product nickel and cobalt recoveries are 90+%. The remainder is lost in smelting slag and leach residues.

18.8 OFFGAS TREATMENT

The offgases from the battery recycle furnace contain mainly N_2(g), CO_2(g), and H_2O(g). However, they may contain volatile organic compounds that tend to form from plastics-in-feed near the battery feed point. These volatile organic compounds are continuously destroyed (Fig. 18.1) by:

(a) oxidizing them at a very high temperature using a 3000-5000 °C plasma torch
(b) immediately quenching the gas so that hydrocarbon compounds (e.g., dioxins, furans) can't re-form.

Dusts are also captured in several filters and fluorine may be captured by scrubbing the offgas with cold water or by reacting it with sodium silicate solutions (Hasselwander, 2009).

18.9 SUMMARY OF RARE EARTH BATTERY RECYCLE

In 2014, rare earth rechargeable battery recycle is in industrial production. A smelter in Hoboken, Belgium can process up to 7000 tonnes of recycle batteries (containing about 500 tonnes of rare earths) per year. These rare earths are recovered as pure individual rare earth compounds by Solvay Rare Earth Systems in their La Rochelle rare earth plant.

18.10 RECOVERING RARE EARTHS FROM END-OF-USE FLUORESCENT LAMPS

Fluorescent lamps contain a layer of phosphorescent material on the interior surface of their glass "bulbs." This phosphorescent material always contains rare earth phosphors. This section describes recycle of end-of-use fluorescent lamps and recovery of rare earths from their phosphors. Figs. 18.8 and 18.9 are flowsheets for the process.

The feed to the process consists mainly of end-of-use fluorescent lamp bulbs, mostly the folded or curly types, Figs. 18.6 and 18.7. The products of the process are individual high purity rare earth oxide and phosphate powders. Production is estimated to be several hundred tonnes of contained rare earth elements per year.

The end-of-use lamp bulbs are collected by specialist companies that crush the bulbs and sort the crusher product into:

- glass
- metal
- plastic

and:

- impure rare earth phosphor powder.

These companies also remove and capture mercury during crushing.

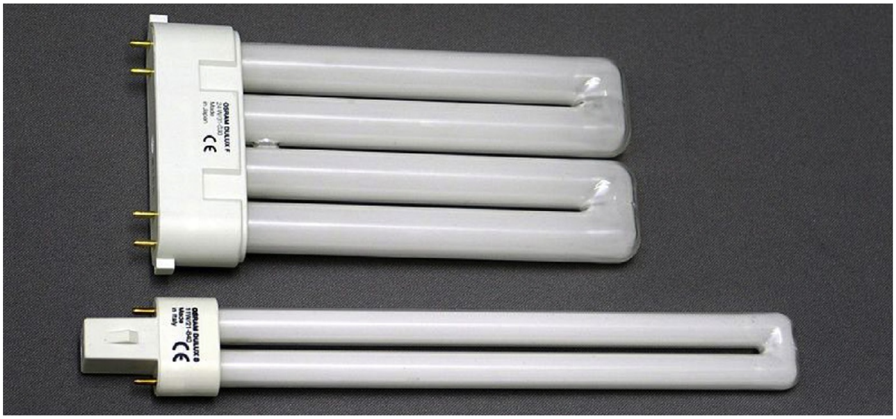

FIG. 18.6

Folded tube style fluorescent lamps. End-of-use lamps of this style are crushed by specialized recycling companies. The principal crushing product is impure rare earth phosphor powder. Pure rare earth oxides and phosphates are made from this phosphor powder by heating, leaching, solution purification, solvent extraction, rare earth separation and precipitation.

Wikipedia creative commons photo.

FIG. 18.7

Spiral type fluorescent lamp. These lamps are recycled much like Fig. 18.6's folded type.

Wikipedia creative commons photo.

The rare earth phosphor powder (about 3 mass% of lamp mass, Binnemans et al., 2013) is sent to rare earth recycling companies for rare earth recovery. The other products are sent to glass, metal, and plastics recyclers.

18.11 PHOSPHORS AND THEIR COMPOSITIONS

Fluorescent lamp phosphors are compounds that produce various colors of visible light when bombarded by a fluorescent lamp's interior ultraviolet light. They are coated on the inside of the lamp's glass bulb.

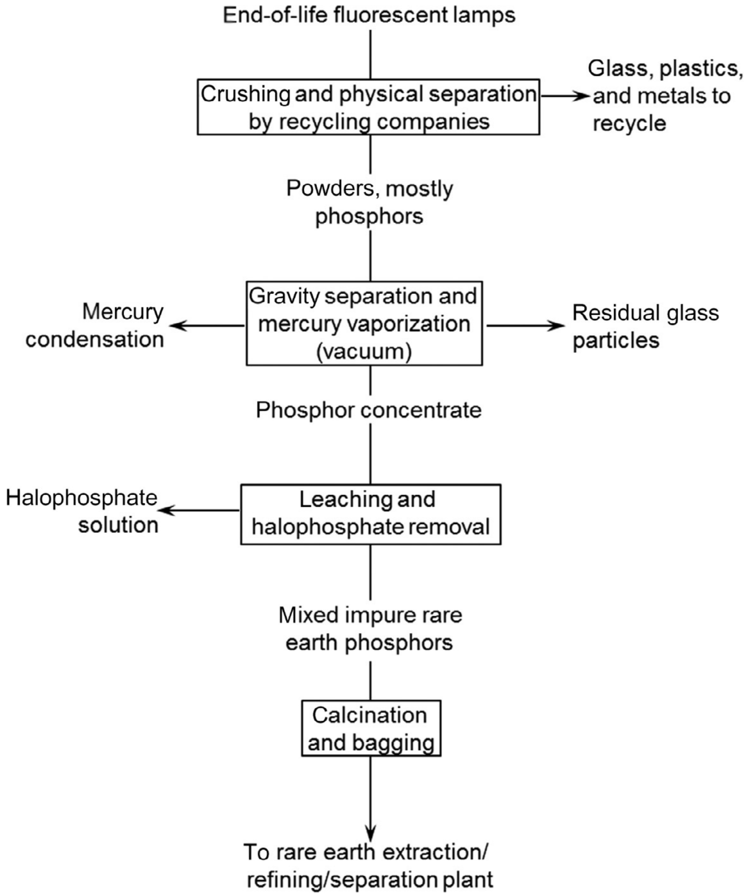

FIG. 18.8

Schematic flowsheet for producing mixed rare earth phosphor powder. The process is continuous. The product is sent to a rare earth extraction/purification/separation plant.

Flowsheet drawn by William Davenport.

They most often contain:

$(La,Ce,Tb)PO_4$,	LAP a green phosphor
$GdCeTbMgB_4O_{10}$	a green phosphor
$(Ce,Tb)MgAl_{11}O_{19}$	CAT, a green phosphor
$BaMgAl_{10}O_{17}:Eu^{2+}$	BAM, a blue phosphor
$Y_2O_3:Eu^{3+}$	YOX, a red phosphor.

Together, these phosphors emit a warm white light, much liked by the public.

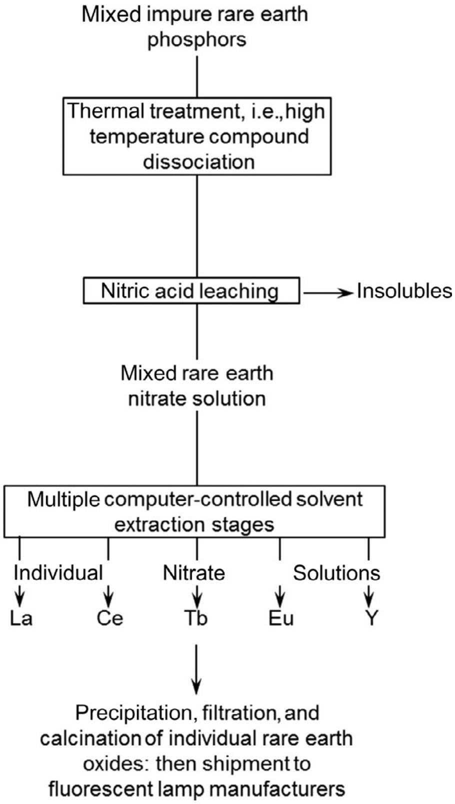

FIG. 18.9

Flowsheet for producing high purity individual rare earth oxides and phosphates from mixed impure rare earth phosphor powder. The process is continuous. The product rare earth compounds are usually sent back to fluorescent lamp manufacturing plants.

Flowsheet drawn by William Davenport.

18.11.1 Recycle objective

The objective of recycling these phosphors is to recover the phosphor's rare earth elements as individual oxides and phosphates, suitable for making new phosphors and other products. Figs. 18.8 and 18.9 outline the recycle process.

18.12 THE RECYCLE PROCESS

Phosphor recycle (as practiced by Solvay Rare Earth Systems) consists of two main steps:

(a) recovery of phosphor powder from end-of-use fluorescent lamps
(b) production of pure individual rare earth oxide and phosphate powders from the recovered powder.

Step (b) requires a computer controlled solvent extraction-rare earth separation plant.

18.12.1 **Recovery of phosphor powder from end-of-use fluorescent lamps** (Fig. 18.8)

Recovery of mixed phosphor powder from used fluorescent lamps entails:

(a) lamp collection and crushing
(b) phosphor powder isolation
(c) glass and mercury removal
(d) leaching and halogen-phosphate removal
(e) calcination and shipping to a rare earth extraction/purification/separation plant.

The intermediate product of this sequence is a bone dry phosphor powder mixture, made up of the Section 18.11 phosphors.

18.12.2 **Rare earth oxide production** (Fig. 18.9)

Preparation of individual rare earth oxide powders from Section 18.12.1's intermediate product (as practiced in La Rochelle) entails:

(a) thermally dissociating the phosphors in preparation for:
(b) nitric acid leaching and liquid/solid separation
(c) discard of the solid leach residues
(d) solvent extraction purification of the pregnant leach solution
(e) separation of leaching's La, Ce, Tb, Gd, Eu, Y purified pregnant nitrate solution into individual rare earth nitrate solutions, for example, La nitrate, by computer-controlled solvent extraction
(f) precipitation of oxalates and bicarbonates
(g) oxidizing these precipitates to oxides by heating in air.

18.12.3 **Rare earth phosphate production**

Rare earth phosphates are also precipitated from the above individual nitrate solution. They are precipitated by reaction with phosphoric acid and ammonium hydroxide, i.e.:

$$\underset{\text{individual rare earth solution}}{\left(RE^{3+}, 3X^{-}\right)(aq)} + \underset{\text{phosphoric acid}}{H_3PO_4(aq)} + \underset{\text{ammonium hydroxide}}{3\left(NH_4^{+}, OH^{-}\right)(aq)} \rightarrow$$

$$\underset{\text{rare earth phosphate}}{REPO_4(s)} + 3\left(NH_4^{+}, X^{-}\right)(aq) + \underset{\text{byproduct solution}}{3H_2O} \qquad (5.13)$$

They may also be precipitated as mixed rare earth phosphates from mixed nitrate solutions, for example:

$$(La, Ce, Tb)PO_4$$

which is LAP, a green phosphor.

The product precipitates are filtered off and heated to improve structure and morphology. These products are made from nitrate solutions by Solvay Rare Earth Systems in their La Rochelle (France) and Liyang (China) refineries.

18.13 RARE EARTH MAGNET RECYCLE

Recycle of rare earth magnet alloys has begun with the recycle of Nd-Fe-B magnet manufacturing wastes (Liu and Chinnasamy, 2012). The easiest material to recycle is metalworking waste (swarf). It is collected, cleaned and re-melted with virgin magnet alloy (Fig. 18.10).

However, the product of swarf+virgin metal smelting is slightly less pure than virgin smelting alloy. It makes lower grade, inferior magnets. Also, magnet weakness increases with increasing swarf/virgin ratio—thereby limiting the amount of swarf that can be recycled this way.

This type of recycle is very seldom done for Sm-Co magnet swarf because Sm vapor loss is excessive.

Sm-Co magnet wastes are sometimes smelted for cobalt recovery, in which case the samarium is lost.

FIG. 18.10

Metalworking swarf (including compressed swarf block, top) much like that produced during magnet-making.

Wikipedia creative commons photo by Glenn McKechnie.

18.13.1 End-of-use magnet recycle

End-of-use magnet recycling has begun in China, Japan, and France (Solvay Rare Earth Systems).

Japanese companies have, for example, developed automated systems for extracting rare earth magnets from recycled end-of-use products, for example, air conditioners and disk drives (Ferron and Henry, 2013). These magnets are then re-used in new model air conditioners, etc. which are specifically designed to re-use these recycle magnets. This is possible in Japan because Japanese companies co-operate in win-win projects like these.

18.14 SUGGESTED END-OF-USE RARE EARTH MAGNET RECYCLE METHOD

A possible way forward to recycling end-of-use rare earth magnets is to begin adding a small quantity of Nd-Fe-B end-of-use scrap to Fig. 18.5's battery recycle furnace. The magnets' Fe could be reduced into the Ni-Co alloy phase by providing stronger reducing conditions in the furnace (by slightly increasing the furnace's fuel/air ratio). The Fe could then be removed hydrometallurgically in the Co,Ni recovery circuit.

Alternatively, the Fe might be allowed to enter the slag phase by leaving the reducing conditions much the same as for all-battery recycle furnace operation (Fe oxidizes more easily than Co and Ni). However, the Fe-in-slag might interfere with Fig. 18.1's subsequent rare earth-from-slag recovery processing.

This suggested process would not be suitable for Sm-Co magnets because Sm would vaporize during smelting.

18.14.1 In between

Of course, there are many other possible intermediate processes between:

(a) the Japanese re-use process in Section 18.13.1

and:

(b) the end-of-use scrap-as-ore process in Section 18.14.

The choice will be decided on subsequent magnet performance (Ott et al., 2013) and cost.

18.15 CERIA POLISHING POWDER RECYCLE

About 15 kilotonnes of rare earth oxides (equivalent to about 12 kilotonnes of rare earth elements) are used for glass polishing each year. After use, the polishing powder is contaminated with:

(a) silica particles from the polished glass
(b) alumina particles from hydrolysis of poly-aluminum chloride, which is used as a flocculent in polishing powder slurries.

Both of these contaminants cause uneven polishing.

There is very little end-of-use polishing powder recycle in North America and Europe. However, there is a significant amount in Japan and probably in China. The process entails:

(a) drying the waste polishing powder slurry
(b) separating the silica and alumina particles from the ceria particles by gravity, size and electrostatic differentiation methods.

The recent fall in rare earth prices has mostly eliminated commercial polishing powder recycle.

18.16 FLUID CATALYTIC [PETROLEUM] CRACKING CATALYST RECYCLE

Some end-of-use fluid [petroleum] cracking catalyst is used in cement manufacture. Most, however, is discarded in landfills.

This lack of recycle is due to:

(a) the small concentration of rare earths in the catalyst, ~2 mass%
(b) the fact that the dominant rare earths in the catalyst are low price La (with some Ce).

Some petroleum refining uses platinum-rhenium alloy catalyst. It is used to convert petroleum refinery naphthas with low octane ratings into high-octane liquid products. It is recycled for platinum and rhenium recovery but not for oxide substrate recovery.

18.17 AUTOMOBILE EMISSION REDUCTION CATALYST RECYCLE

Most end-of-use automobile emission reduction catalyst is recycled—for palladium, platinum, and rhodium recovery but not for rare earth element recovery.

The lack of rare earth recovery is due to:

(a) the small concentration of rare earth elements in emission abatement catalytic converters, ~5 mass%.
(b) the fact that the dominant rare earth element in the catalysts is low priced cerium.

18.18 CURRENT RECYCLE ACTIVITY

Ferron and Henry (2013) list recent rare earth recycling activities—including the following:

(a) Honda is recycling its own Ni-MH batteries
(b) Mitsubishi has developed equipment to extract rare earth permanent magnets from air conditioners and washing machines, with the magnets being re-used as-is

(c) Hitachi has developed equipment to recover rare earth metal-transition metal magnets from air conditioners and disk drives, with the magnets being re-used as-is

(d) Ganzhou Recycle Hi-Tech Co. Ltd. is operating a plant that recycles rare earth magnet 'swarf' and scrap

(e) Showa Denko KK has built a rare earth magnet scrap recycling plant in Viet Nam.

These are in addition to the already well-advanced rare earth recycling by Umicore and Solvay Rare Earth Systems.

18.19 SUMMARY

In 2013, only 1 or 2% of rare earths in end-of-use products are recovered by recycling—this compared to 90% for iron and steel.

The reasons for this low recovery are:

(a) the low concentrations of rare earths in many end-of-use products, for example, catalysts

(b) the presence of rare earths in difficult-to-decompose compounds, for example, cerium zirconate in automobile emission reduction catalysts

(c) the presence of rare earths in objects (e.g., magnets) that are located deep within devices (e.g., electric motors) that are themselves located deep within consumer products (e.g., cars and trucks).

However, progress is being made in the recycling of (i) Ni-MH rechargeable batteries and (ii) rare earth fluorescent lamp phosphors.

No rare earths are yet recovered from automobile or petroleum catalysts, both of which are large rare earth users. This is because of the small concentration of rare earths in the catalysts and the relatively low prices of their main constituents, La and Ce.

References

Binnemans, K., Jones, P.T., Blanpain, B., Van Gerven, T., Yang, Y., Walton, A., Buchert, M., 2013. Recycle of rare earths. J. Clean. Prod. 51, 1–22.

Ferron, C.J., Henry, P., 2013. A review of the recycling of rare earth metals. In: Rare Earth Elements 2013. Met Soc of CIM, Montreal, QC, pp. 517–531.

Gomez, I., Van Damme, G., 2009. The unique Umicore closed loop solution. Umicore S.A, Hoboken, Belgium.

Hasselwander, K., 2009. Gas cleaning designs for smooth operations. Sulphur 321, 36–43.

Kaufman, L., Nesor, H., 1978. Coupled phase diagrams and thermochemical data for transition metal binary systems-II. Calphad 2, 98.

Liu, J. and Chinnasamy, C. (2012). Rare Earth Magnet Recycling. Landsville, PA. Retrieved on August 17, 2013 from http://www.clu-in.org/download/issues/mining/liu-presentation.pdf.

Ott, R.T., Jones, L.L., Dennis, K.W., McCallum, R.W., 2013. Recycling of rare earth elements for the synthesis of permanent magnet alloys. In: Rare Earth Elements 2013. Met Soc of CIM, Montreal, QC, pp. 553–554.

Solvay, 2012. Solvay's Rare Earth Recycling Technology Receives ICIS Award for Best Innovation for Sustainability. Solvay S.A, Brussels, Belgium, Retrieved on September 25, 2013 from http://www.solvay.com/EN/NewsPress/20121022_UrbanMineICIS.aspx.

Tytgat, J., 2011. Umicore Battery Recycling. Umicore S.A, Brussels, Belgium Retrieved on June 28, 2013 from http://www.green-cars-initiative.eu/workshops/joint-ec-eposs-ertrac-expert-workshop-2011-on-battery-manufacturing/presentations/2_4%20Jan%20Tytgatcore.pdf.

Suggested Reading

Dent, P., 2012. Rare earth permanent magnet supply chain and technology advances overview. In: Rare Earths 2012. Met Soc of CIM, Montreal, QC, pp. 309–316.

Goode, J.R., Moloveanu, G., Rayat, M.S., 2012. Rare Earths 2012. Metsoc of CIM, Montreal, QC.

Hitachi, 2010. Hitachi develops recycling technologies for rare earth metals. Hitachi press release, Japan, Retrieved on August 17, 2013 from http://www.hitachi.com/New/cnews/101206.html.

London, I.M., Goode, J.R., Moldoveanu, G., Rayat, M.S., 2013. Rare Earth Elements 2013. Metsoc of CIM, Montreal, QC.

Meekers, C.E.M., Hageluken, C., Van Damme, G., 2009. Green recycling of EEE: special and precious metal recovery from EEE. In: EPD Congress 2009. TMS, Warrendale, PA, pp. 1131–1136.

Ortegon, K., Nies, L.F., Sutherland, J.W., 2013. Preparing for end of service life of wind turbines. J. Clean. Prod. 39, 191–199.

Rollat, A., 2012. How to Satisfy the Rare Earths Demand Rhodia Rare Earth Systems Initiatives. Le Studium, La Rochelle, France, Retrieved on August 17, 2013 from http://lestudium.cnrsorleans.fr/anglais/rubriques/actu/conferences/conf_klaver/presentations/rollat.pdf.

Tanaka, M., Oki, T., Koyama, K., Narita, H., Oishi, T., 2013. Recycling of rare earths from scrap. In: Handbook on the Physics and Chemistry of Rare Earths, vol. 43. Elsevier B.V, Amsterdam, Holland, pp. 159–211.

Verhaeghe, F., Boubin, F., Yazicioglue, B., Schurmans, M., Thijsw, B., Haesebroek, G., Tytgat, J., Van Camp, M., 2011. Valorisation of battery recycling slags. In: Second International Slag Valorisation Symposium, Leuven, Belgium, Retrieved on June 28, 2013 from http://www.slag-valorisation symposium.eu/2011/images/presentations/s4_12_pres_verhaeghe.pdf.

CHAPTER

Epilogue

19

We started writing this book in April 2012, just after rare earth prices had (i) peaked and (ii) begun to fall, Chapter 2. As today, China dominated rare earth mining/extraction (90+%). The objective of this chapter is to describe rare earth events during our writing and just before.

19.1 WORLD EVENTS

A few years before starting our writing (~2006), the Government of China began curtailing rare earth exports to the rest of the world—reducing rest-of-world supply (Fig. 19.1) and thereby increasing rare earth prices, Chapter 2. The official reason for curtailing exports was to reduce the environmental damage being caused by rare earth mining/extraction operations.

The most easily observed consequences of this export curtailment were rare earth price increases up to 30-fold from 2009 through 2011 (Fig. 2.5) and a slowing of apparent rare earth production (Fig. 2.1).

19.2 CONSEQUENCES

The export curtailment destabilized rare earth markets around the world. It also resulted in many other changes.

19.2.1 Recycling

Rest-of world rare earth shortages prompted:

(a) immediate studies into rare earth recycle by governments, universities, and manufacturing companies
(b) implementation of end-of-use rare earth recycling with government encouragement (particularly in Europe and Japan)
(c) implementation of rare earth recycle by manufacturing companies, especially in Japan.

Rare Earths. http://dx.doi.org/10.1016/B978-0-444-62735-3.00018-8

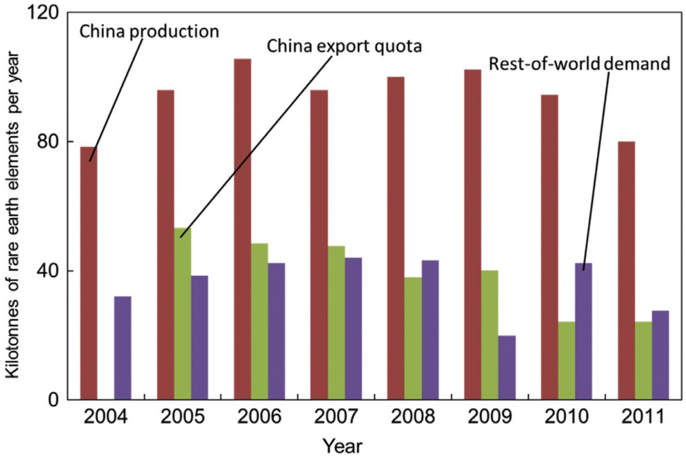

FIG. 19.1

Rough estimates of Chinese rare earth production; Chinese rare earth export quotas; and rest-of-world rare earth demand, 2004-2011. The rest-of-world rare earth shortages in 2010 and 2011 are notable.

Graph drawn by William Davenport from data kindly provided by Allan Rollat.

Examples of recycling with government encouragement are recycling of:

(a) end-of-use Ni-MH batteries
(b) fluorescent lamp phosphors
(c) magnet "swarf" and end-of-use Nd-Fe-B magnets.

Examples of in-house recycling are Japanese robotic extraction of air conditioner, washing machine, and disk drive magnets—for recycle of the magnets *as-is*.

Nonetheless, recycle of rare earths from end-of-use products is still a measly 2% as compared to 90% for iron and steel, so there is considerable room for improvement.

19.2.2 Thrifting

Thrifting, as applied to rare earths, is decreasing the quantities of rare earths that are used to achieve a given objective. An example of this is in petroleum cracking catalyst (Chapter 9) where La and Ce use was cut during the time that La and Ce prices were high. The relative quantities of each were also varied as their prices rose and fell. Recent lower La and Ce prices have restored their use in petroleum cracking catalyst back to previous levels—because they improve gasoline production efficiency and stabilize the catalyst.

Another example is the reduction of polishing powder consumption by 30-50%. This was achieved by eliminating wasteful practices and installing internal company recycling. This decreased consumption freed up ceria for automobile catalytic converter use.

19.2.3 Substitition

The poster child for rare earth use is the Toyota Prius (Fig. 19.2). It uses:

(a) nickel-(rare earth alloy)H rechargeable batteries to power its electric drive motor
(b) rare earth metal-transition metal permanent magnets in its electric drive motor
(c) rare earth zirconate-platinum group metal emission abatement catalyst in its catalytic converters.

Sensing a potential rare earth shortage in 2006 (or before), Toyota began rare earth thrifting and substitution. In 2014, the company now uses slightly less efficient rare earth-free rechargeable batteries and rare earth magnet-free induction motors in some of its new Toyota Priuses. It is also prepared to reduce the quantity of rare earth oxides in its emission abatement catalysts. However, shortages of the cerium oxide used in this last application are unlikely because Ce is usually in excess supply (due to its high concentrations in many rare earth ores). Reduced consumption of ceria polishing powders has also lowered the likelihood of ceria shortages.

Other Japanese automobile manufacturers have followed suit.

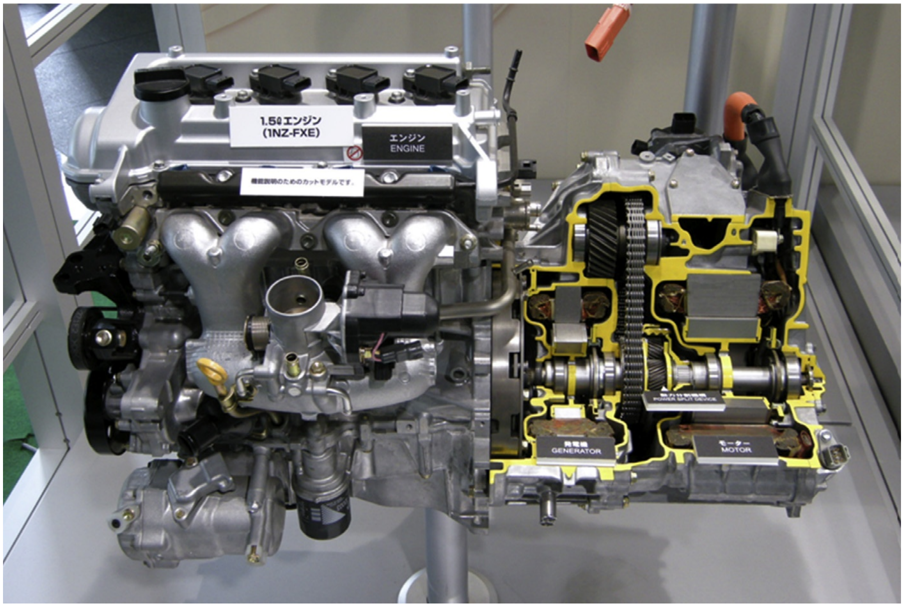

FIG. 19.2

Toyota Prius gasoline engine, generator, and electric motor (public domain photo). The battery pack (Fig. 9.1) is not shown. It is in the rear end of the car, connected to the motor by heavy covered cable. The electric motor usually contains rare earth magnets—but rare earth-free induction motors are also used. Rare earth-free Ni-MH rechargeable batteries have also been developed and used.

19.3 SMUGGLER RESPONSES

China’s rare earth export curtailment has not been leak-proof. Chinese authorities estimate that some 15 kilotonnes of contained rare earth elements are being smuggled out of China each year, mostly from rare earth cation adsorption clay mines (Fig. 19.3) near the Pacific Ocean coast. This smuggling has mitigated the effects of the Chinese government’s rare earth export curtailment.

The recent smuggling record is:

(a) 600 instances of illegal mining have been punished
(b) 14 illegal mines have been shut down
and:
(c) 90 rare earth facilities have been forced to suspend illegal rare earth production and sale.

FIG. 19.3

Rare earth cation adsorption clay mine in southern China (photograph courtesy of Professor Toru Okabe). Mines like these are being used by smugglers to illegally mine and export rare earths. Their ores are relatively concentrated in high atomic number (heavy) rare earths, for example, Tb, Dy, Ho, Er, Tb, Yb—which are high-priced hence perfect for smuggling. They are also in short supply outside China (especially dysprosium, which is needed for rare earth permanent magnets in hot (150-180 °C) electric motors.

Elimination of rare earth smuggling from China is hindered by the fact that:

(a) local governments control mining and are resisting any loss of power
(b) mine regulations are administrative measures rather than central government laws and regulations
(c) there is considerable overlap of law enforcement agencies, weakening their effectiveness.

China also has lengthy borders with Vietnam, Laos, and Burma (Myanmar) (Fig. 19.4). Rare earth cation adsorption clay ores and concentrates are easily

FIG. 19.4

Map of southeast Asia showing lengthy borders between China, Vietnam, Laos, and Burma (Myanmar). Several of these countries have rare earth extraction plants.

Map courtesy Google: Map data © 2014 AutoNavi. Google, Kingway, MapIT, ZENRIN.

smuggled across these borders. Several of these countries have reportedly built rare earth extraction plants.

Hong Kong also hosts rare earth traders who market rare earth products with no indication as to their source.

19.4 GOVERNMENT RESPONSES TO RARE EARTH SHORTAGES

Governments have also responded to perceived rare earth shortages and actual elevated rare earth prices (King and Eggert, 2013). The United States, for example, held numerous Congressional hearings and published several reports as soon as perceived rare earth shortages and high rare earth prices reached the pages of the *New York Times* and the *Wall Street Journal*.

The main consequence of the hearings was provision of U.S. government funds (125 million $) for a *Critical Materials Institute*, which came into being in January, 2013. However, by this time:

(a) Section 19.3's smugglers had increased rare earth production and extraction
(b) Section 19.2's thrifting, substitution and recycle had begun to reduce consumption
(c) a small amount of new non-Chinese rare earth production had come on stream, mainly in Asia
(d) rare earth prices were drifting back to near pre-spike levels.

Korea has also established a similar institute with much the same goals (Kim et al., 2013).

19.5 MANUFACTURING INDUSTRY RESPONSES

It appears that Toyota (and other automobile manufacturers) have efficiently mitigated the world's rare earth *crisis* by:

(a) foreseeing potential rare earth supply/price problems years before they occurred
(b) quickly developing efficient rare earth-free (i) electric motor and (ii) rechargeable battery technology (Tables 19.1 and 19.2).

19.6 MINING/PRODUCTION INDUSTRY RESPONSE

There are currently more than 50 rare earth mining projects outside China (Fig. 19.5). However, only a few are nearing production. They are:

Mountain Pass, California
Mount Weld, Western Australia
Beach sand deposits, India.

Table 19.1 Comparison of Permanent Magnet and Induction Motors for Automobile Use

Characteristic	Permanent Magnet Motor	Induction Motor
Cost, $ per kilowatt	$$$	$$
Power density, kilowatts per liter	Highest	Moderate
Specific power, kilowatts per kg	Highest	Moderate
Efficiency, %	Best	Good
Noise and vibration	Good	Good
Manufacturability	Difficult	Mature
Potential for technical improvement in automobile applications	Significant	Minimal

Table prepared by William Davenport with data from Steve Constantinides.

Table 19.2 Magnets and Their Uses in Modern Motor Vehicles

Device	Devices per Car	Magnets per Device	Total Number of Magnets
Basic Motor/Actuator			
Starter motor	1	8	8
Wiper motor	2	2	4
Seat adjust	4	2	8
Window lift	4	2	8
Fuel pump	1	2	2
Engine fan	1	4	4
Door locks	4	1	4
Heating, ventilation, and air conditioning fan	1	2	2
Trunk release	1	1	1
Mirror positioning	4	1	4
Windshield wash pump	1	2	2
Sophisticated Motor/Actuator			
Alternator	1	8	8
Exhaust gas recirculation valve	1	2	2
Variable valve	4	2	8

Continued

Table 19.2 Magnets and Their Uses in Modern Motor Vehicles—cont'd

Device	Devices per Car	Magnets per Device	Total Number of Magnets
Electronic throttle	1	2	2
Anti-lock braking system	4	1	4
Electronics			
Compact disk player	1	3	3
Speakers	6	1	6
Key sensor	1	1	1
Dash gauges	4	1	4
Sensors			
Anti-lock breaking system	4	1	4
Transmission speed	1	1	1
Throttle position	1	1	1
Brake on/off	1	1	1
Air bag	2	1	2
Seat occupancy	2	1	2
Gas tank level	1	1	1
Transmission shift sensor	1	1	1
Other			
Transmission chip collector	1	1	1
Grand Total = 99			
Other Applications			
Moon roof			
Sliding side doors			
Motorized rear hatch open/close			
Electronic ride control			
Electronic power steering			
Electric brakes			

Hybrid and electric vehicles have an additional major magnet user—the electric drive motor.
Table prepared by William Davenport based on data kindly supplied by Steve Constantinides.

Beach sand projects (Chapter 3) can be developed more quickly than ore-mining deposits. We predict that India will soon be producing 5-10 kilotonnes of monazite concentrate for the world market.

Other than these, significant further rare earth mine production is probably 5-10 years away (Table 19.3).

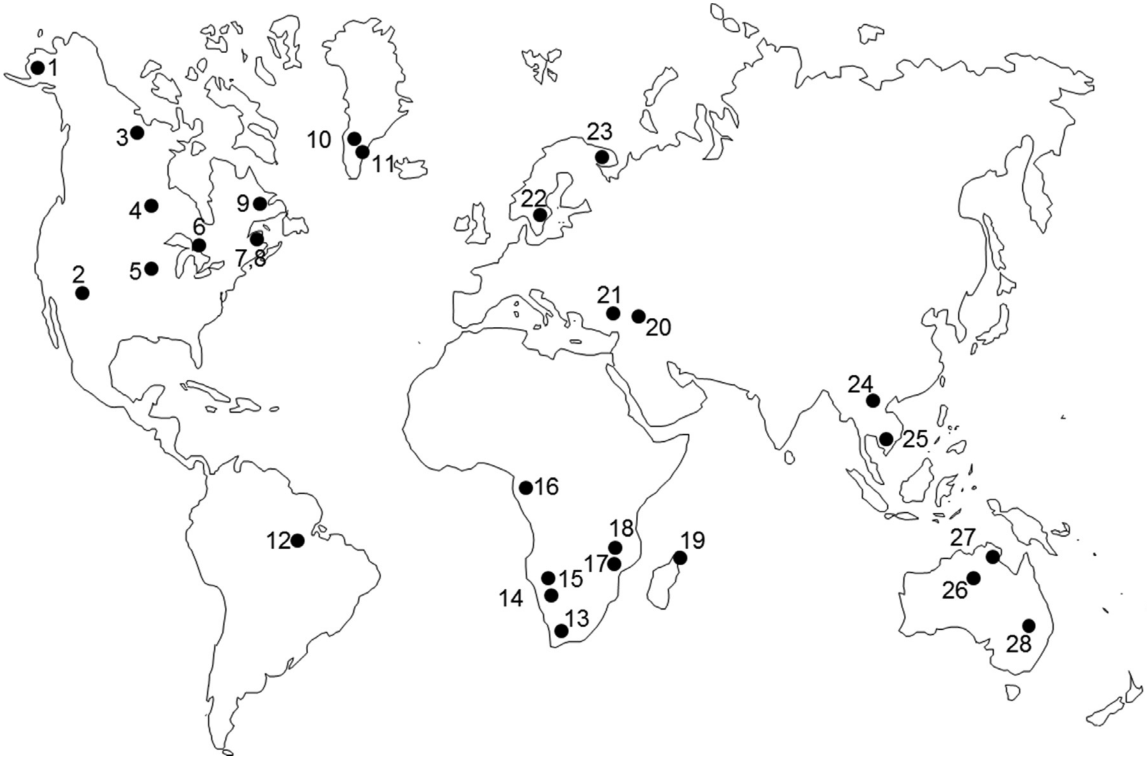

FIG. 19.5

Some of the 50 or so rare earth mine projects outside China. Data kindly provided by Alain Rollat. Table 19.3 gives project name and locality information. It would seem that Siberia and South America deserve more exploration. The search for rare earth cation adsorption clays in the world's semi-tropical regions should also be stepped up—because these ores are concentrated in valuable (and extremely useful) high atomic number (heavy) rare earths, for example, dysprosium.

Table 19.3 Key to Fig. 19.5 Rare Earth Mine Projects

1	Bokan Mountain, USA.
2	Round Mountain, USA.
3	Nechalacho, Canada (2)
4	Hoidas Lake, Canada
5	Bear Lodge, USA.
6	Eco Ridge, Canada
7	Gaspe, Canada
8	Grande-Vallee, Canada
9	Strange Lake, Canada
10	Kringlerne, Greenland
11	Kvanefjeld, Greenland
12	Pitinga, Brazil
13	Steenkampskrall, South Africa
14	Zandkopsdrift, South Africa
15	Lofdal, Namibia
16	Mabounie, Gabon
17	Songwe, Malawi
18	Kagankunde, Malawi
19	Ampasindava Peninsula, Madagascar
20	Kutessay, Kyrgyzstan
21	Aktau, Kazakhstan
22	Norra Karr, Sweden
23	Lvozero, Russia (in production)
24	Nam Xe, Viet Nam
25	Dong Pao, Viet Nam
26	Nolans, Australia
27	Hastings, Australia
28	Dubbo, Australia

Table prepared by William Davenport, checked by Alain Rollat.

19.7 SUMMARY

1. Rare earth elements are used widely around the world.
2. They are greenest option for many technologies, for example, automobiles.
3. China dominates rare earth production. In 2014 it is mining/extracting 90+% of the world's rare earth supply.
4. Until 2006, rare earth supplies from China were sufficient to meet world rare earth requirements.

5. In 2006, and more stringently in 2010, China curtailed rare earth exports to the rest of the world. The official reason for curtailing exports was to reduce the environmental damage being caused by rare earth mining/extraction operations.
6. This curtailment resulted in rare earth shortages and high rare earth prices around the world.
7. Of particular importance was a shortage of dysprosium. This element increases the high-temperature resistance-to-demagnetization strength of Fe-Nd-B permanent magnets—which allows them to be used at hybrid and electric car electric motor operating temperatures (150-180 °C).
8. The dysprosium shortage led Toyota to develop a rare earth-free induction electric motor for its Prius, thereby decreasing rare earth demand and causing lower rare earth prices.
9. This Dy price decrease triggered a general fall in rare earth element prices, which in turn lowered the profitability of some rare earth ores, decreasing mine production.
10. The decrease in rare earth prices also lowered the potential profitability of new rare earth mine projects causing some owners to moth-ball their projects.

19.8 PREDICTIONS

1. With one overwhelmingly dominant rare earth producer, the rare earth industry will be unstable till 2020 at least.
2. New mine projects will eat into this dominance, but slowly. Recycle of end-of-use rare earth products will also help.
3. For many applications (e.g., rare earth permanent magnets, rare earth rechargeable batteries) there are non-rare earth alternatives. However, these are usually less green, hence usually less desirable.
4. For this reason, rare earths will always be wanted for many applications.

An exception to this is light emitting diode illumination, which doesn't use rare earths and which requires less energy than fluorescent (rare earth phosphor) lighting. Light emitting diodes are gradually taking over household and general illumination.

References

King, A.H., Eggert, R.G., 2013. The critical materials institute. In: Rare Earth Elements 2013. Metsoc of CIM, Montreal, QC, pp. 3–9.

Kim, T.-S., Chae, H.J., Kim, B.S., Ott, R.T., Jung, I.-H., 2013. Current Korean R&D and investment strategies in response to REE demand & supply concerns. In: Rare Earth Elements 2013. Metsoc of CIM, Montreal, QC, pp. 11–23.

Further Reading

Constantinides, S., 2013. Rare earth elements in transportation. In: Rare Earth Elements 2013. Metsoc of CIM, Montreal, QC, pp. 47–62.

Goode, J.R., Moloveanu, G., Rayat, M.S., 2012. Rare Earths 2012. Metsoc of CIM, Montreal, QC.

London, I.M., Goode, J.R., Moldoveanu, G., Rayat, M.S., London, I.M., Goode, J.R., Moldoveanu, G., Rayat, M.S., 2013. Rare Earth Elements 2013. Metsoc of CIM, Montreal, QC, Especially the first section: Rare earth element industry overview.

Index

Note: Page numbers followed by *f* indicate figures and *t* indicate tables.